

489304

FTD-TT-63-785

FOREIGN TECHNOLOGY DIVISION



FOUNDATIONS OF A THEORY OF THE WET-STEAM TURBINE

By

Georg Gyarmathy



DISTRIBUTION OF THIS
DOCUMENT IS UNLIMITED



FTD-TT-63-785/1+2+3+4

EDITED TRANSLATION

FOUNDATIONS OF A THEORY OF THE WET-STEAM TURBINE

BY: Georg Gyarmathy

English Pages: 274

Revised Edition of Translation Originally Published

30 April 1964

THIS TRANSLATION IS A RENDITION OF THE ORIGINAL FOREIGN TEXT WITHOUT ANY ANALYTICAL OR EDITORIAL COMMENT. STATEMENTS OR THEORIES ADVOCATED OR IMPLIED ARE THOSE OF THE SOURCE AND DO NOT NECESSARILY REFLECT THE POSITION OR OPINION OF THE FOREIGN TECHNOLOGY DIVISION.

PREPARED BY:

TRANSLATION DIVISION
FOREIGN TECHNOLOGY DIVISION
WP-AFT, OHIO.

FTD-TT-63-785/1+2+3+4

AFLC-WPAFB-SEP 66 102

Date 4 Aug. 1966

S

GRUNDLAGEN EINER THEORIE DER NASSDAMPFTURBINE
Mitteilung Nr. 6 aus dem Institut für Thermische
Turbomaschinen an der Eidgen. Technischen Hoch-
schule in Zürich (Report Nr. 6 from the Insti-
tute of Thermal Turbomachines of the Swiss Fed.
Institute of Technology, Zürich, Switzerland),
Juris-Verlag, Zürich, 1962.

In Memory of György Jendrassik, my uncle,
and
to my dear parents
who sacrificed so much for their children's sake

TABLE OF CONTENTS

Foreword	1
Notation	3
PART ONE: BRIEF SUMMARY OF RESULTS	11
1.1. . The Development of Knowledge Concerning Wet-Steam Turbines	11
1.2. The Physical Picture of the Wet-Steam Turbine	15
1.3. Practical Conclusions	25
PART TWO: THE FORMATION OF STEAM WETNESS AND THE FORMS ASSUMED BY WATER IN THE TURBINE	30
2.1. Layout of Two Turbines as a Basis for Applica- tional Examples	30
2.2. Drag Force and Heat-Transfer Between Droplets and Steam	37
2.3. The Physical Behavior of the Steam in the Wet- Steam Region	47
2.4. The First Appearance of Water in the Turbine: Condensation on the Blades	60
2.5. Spontaneous Condensation of the Steam and the State of the Fog Produced	75
a) Nucleation	77
b) Flow Equations for Condensing Steam	79
c) Application of the Flow Equations to Expansions with Condensation	85
d) Analytical Determination of Onset of Con- densation and the Properties of the Fog Formed	91

e) Certain Conclusions for Wet-Steam Turbines	114
2.6. Flow and Expansion of the Fog	120
a) Fluid-Dynamic Behavior of the Fog . . .	121
b) Thermodynamic Behavior of the Fog . . .	134
2.7. Motion of the Water on the Blades and Casing Walls	143
2.8. Formation, Effect and Fate of Large Drops . .	152
a) Atomization of Detached Drops	153
b) Motion of Detached Drops	156
c) Concerning the Eroding Effect of Detached Drops	159
d) Ricocheting Drops	162
2.9. The Forms the Moisture Appears In, Its Dis- tribution and the Deviation of the Steam State from Thermodynamic Equilibrium	167
a) Calculation Procedure	167
b) Examples	182
PART THREE: MOISTURE-LOSSES	199
3.1. General Remarks	199
3.2. Braking-Losses	203
3.3. Entrainment-Losses	210
a) Entrainment-Losses Due to Fog Droplets .	211
b) Entrainment-Losses Due to Large Drops .	220
3.4. Thermodynamic Losses	222
3.5. Other Moisture-Losses in a Stage	228
3.6. Change of the Exit-Loss	233
3.7. Calculation of Moisture-Losses and Infer- ences	236
a) Summary of the Calculating Procedure . .	236
b) Examples	237
3.8. Concluding Remarks	250

a) Design	250
b) Modelling Laws for the Wet-Steam Turbine	251
Postscript	259
References	262
Appendix	267
Summary	271

FOREWORD

An attempt is made in the present report to give a rigorous theoretical presentation of the processes that take place in wet-steam turbines and from this to derive the outlines of a general theory. The work was prepared at the Institute for Thermal Turbomachines of the Swiss Federal Institute of Technology (ETH).

I have a particular debt to Professor Dr. W. Traupel, who suggested this project to me and made it possible for me to carry it out at his Institute. His comprehensive knowledge, unfailing interest and his many valuable suggestions rendered me considerable assistance during the course of the work.

I am further grateful to Dr. C. Selppel, director of the Brown, Boveri & Company, Ltd., Baden, Switzerland, for permitting to complete the preparations prescribed for the promotion during my activity at Baden and for subsequently and most generously making it possible for me to follow some experimental activities performed by that firm.

I should like to extend sincere thanks to my colleagues, Dipl. Ing. U. La Roche and, above all, to Dipl. Ing. W. Riess for being always ready to discuss problems connected with my work. I profited much by these discussions. I am also indebted to Mr. W. Riess for his meticulous language

editing of the text.

The Swiss Council on Schools approved a contribution toward the printing costs of the presentation copies, for which I should like to express my gratitude here.

Finally, I owe a debt of gratitude and admiration to Miss O. Pallavicini, who managed to complete the manuscript with great care in an incredibly short time.

NOTATION

The numeration of equations, tables and figures begins a new series in each Section. Equations, tables and figures of other sections are referred to as "Eq. 2.3(12)," "Fig. 2.3.1," etc., meaning, respectively, Eq. (12) and Fig. 1 of Section 2.3.

With a few exceptions that are explicitly noted, the MKS system of units is assumed in all formulas. Here we cite briefly the most important conversion formulas (where kg^* = "kilogram-force"): $1 \text{ m} = 39.37 \text{ in}$; $1 \text{ kg} = 0.102 \text{ kg}^* \cdot \text{sec}^2/\text{m} = 2.205 \text{ lb}$; $1 \text{ N} \equiv 1 \text{ kg m/sec}^2 = 0.102 \text{ kg}^* = 0.225 \text{ lb.wt.}$; $1 \text{ bar} \equiv 10^5 \text{ N/m}^2 = 1.02 \text{ atm abs} = 14.51 \text{ psi}$; $1 \text{ kJ} \equiv 10^3 \text{ J} \equiv 10^3 \text{ kg-m}^2/\text{sec}^2 = 0.239 \text{ kcal} = 0.948 \text{ BTU}$.

The large number of physical quantities dealt with made it inevitable that a given letter symbol would have to be used for more than one quantity. In these cases, the distinction is made by means of subscripts, which will understandably be rather long on frequent occasions.

Below we enumerate the most important symbols, i.e., those that appear in several Sections, together with all subscripts that can impart specific significance to the various letter symbols.

SYMBOLS

a	m/sec	Speed of sound
A	m^2	Surface area
b	m	Subtangent in ΔT construction; cf. Sec. 2.6b
b_e	m	Eroded width; cf. Sec. 2.8.2
B	N/m^3	Braking force

c	m/sec	Absolute velocity
c_D	-	Resistance coefficient of sphere
c_F	-	Friction coefficient of wall boundary layer
c_p	J/kgK	Specific heat of steam at constant pressure
c_w	J/kgK	Specific heat of water at constant pressure
D	m	Diameter of bucket ring
D_m	m	Diameter at bucket midsection
E_n	-	Function indicating reduction in number of fog drops, cf. Eq. 2.6(24)
f_{c_D}, f_{c_r}	-	Factors accounting for influence of Kn on c_D and α_r , cf. Eqs. 2.2(27), (28)
F	N/m ³	Field strength
g	-	Functions of quantities G
G	-	Dimensionless quantities that determine the behavior of droplets; specifically, according to subscript, for: Deposition on profile nose (N) or on concave side of profile (H) or on large drops (g); bursting (B); in periodically varying (P) and in turbulent (T) steam flow
h	J/kg	(specific) Total enthalpy
i	J/kg	(specific) Enthalpy
i_*	J/kg	Enthalpy value at zero "Normal enthalpy"; see [20], page 5 (called i_0 there)
i_V	J/kg	Effective loss due to Δq , cf. Eq. 3.1(7)

J	$m^{-3} \text{ sec}^{-1}$	Nucleation rate
k	J/K	Boltzmann's constant ($= 1.380 \cdot 10^{-23}$)
k	—	Scale factor of model (Sec. 3.8b)
K	—	Conversion factor, supersaturation to supercooling (Defined, Eq. 2.3(6))
Kn	—	Knudsen number for sphere. Def. Eq. 2.2(5)
\bar{l}	m	Mean free path of steam molecule
l_{ax}, l_{schfl}	m	cf. Fig. 2.1.4
L	J/kg	Heat of vaporization
m_r	kg	Mass of droplet
\dot{m}_f	kg/m-sec	Water flow rate in moving film
\dot{m}_k, \dot{m}_n	kg/m ² -sec	Condensation rate, or impact rate of fog droplets
M	—	Mach number
\dot{M}	kg/sec	Mass throughput in turbine (with subscript: part-throughput; cf. Eq. 2.9(1))
$\dot{M}_{k, Schfl}$	kg/sec	Mass condensing per second on one bucket
n	kg ⁻¹	No. of Drops per kg of wet steam (without subscript: number of fog drops), except for Section 2.8a
N	kg ⁻¹	Number of molecules in a kilogram of H ₂ O ($= 3.35 \cdot 10^{25}$)
Nu	—	Nusselt number
p	N/m ²	Pressure
p_a	m ⁻¹	Logarithmic axial pressure gradient
\dot{p}	sec ⁻¹	Expansion rate. Defined: Eq. 2.1(4)
Pr	—	Prandtl number
Δq	J/kg	Moisture-loss per stage (with sub-

		script: partial loss, cf. Eq. 3.7(1))
\dot{Q}	J/sec	Heat conduction rate from a droplet
r	m	Droplet radius
\bar{r}	m	Average radius of a given droplet
		species (subscripts as per Sec. 2.9a)
r_{krit}	m	Critical drop radius
$r_{B, max}$	m	Radius of largest nonbursting droplet
R	J/kgK	Gas constant of water vapor ($\equiv p v_d / T_d$)
R_N	m	Radius of curvature of profile nose
Re	—	Reynolds number
s	J/kgK	(specific) Entropy
s_H, s_R	m	Profile contour lengths, cf. Fig. 2.1.4
s_{Sehne}	m	Profile chord length, cf. Fig. 2.1.4
S	m	Linear deflection, cf. Fig. 2.1.4
St	—	Stanton number
t	sec	Time
t_{Schfl}	m	Bucket spacing in midsection circle, cf. Fig. 2.1.4
Δt_{abk}	sec	"Cooling time" of droplet. Def. Eq. 2.2(37)
Δt_{brems}	sec	"Deceleration time" of droplet. Def. Eq. 2.2(33)
T	K	Temperature
T_r	K	"Capillary saturation temperature" (cf. Eq. 2.3(11)), used for the surface tem- perature of a drop
ΔT	K	Undercooling of steam. Def. Eq. 2.3(4)
ΔT^*	K	Maximum undercooling in spontaneous condensation; as $\Delta T^*(\xi_a)$, it signifies

		the "Wilson undercooling" understood in the sense of Section 2.5e
ΔT_{eff}	K	Temperature difference between a surface and the surrounding steam, as governing removal of heat
ΔT_{GS}	K	Adiabatic boundary layer heating ("temperature head")
ΔT_h	K	Locus curve of horizontal tangent in Fig. 2.6.5
ΔT_m	K	Average ΔT in a bucket ring, determining undercooling losses
ΔT_r	K	"Capillary undercooling." Def. Eq. 2.3(10)
u	m/sec	Circumferential velocity; in Sec. 2.7, velocity of water in flowing film
U	m/sec	velocity of steam outside boundary layer
U_r	m/sec	Relative velocity of a droplet with respect to the steam
v	m^3/kg	Specific volume
w	m/sec	Relative velocity with respect to bucket
W	N	Frictional drag on one drop in steam
x	kg/kg	Specific steam content ("steam quality")
y	kg/kg	Specific water content (wetness friction); with subscript (cf. Sec. 2.9a), wetness friction in a particular form
Δy	kg/kg	Specific moisture deficiency. Def. Eq. 2.3(16)

z	—	Number of buckets
Z	N/m^3	Centrifugal field strength
z_0 to z_8	various	Various material quantity groups, cf. Diagrams III and IV in Appendix. For definitions see [45]
α	$J/m^2 \text{ secK}$	Heat-transfer coefficient
α_{Bm}	—	Baumann Moisture-loss coefficient, cf. Sec. 3.1
δ	m	Film thickness (except δ_b in Sec. 2.5d)
ε	—	Transferred mass friction per blade row; for subscripts see Sec. 2.9a
ζ	—	Moisture-loss number
η	m	Coordinate
η_i	—	Internal efficiency of a turbine
η_p	—	Polytropic efficiency of an expansion
κ	—	Ratio of specific heats of steam; used concurrently as isotropic exponent
λ	$J/msecK$	Thermal conductivity
Λ	—	Logarithmic supersaturation ($\equiv \ln p/p_s$)
μ	$kg/msec$	Dynamic viscosity
ν	m^2/sec	Kinematic viscosity
$\nu(\xi_e)$	kg^{-1}	Drop-number distribution function; cf. Eq. 2.5(13)
ξ	m	Coordinate
ξ_a	m	Axial coordinate in turbine ($\xi_a = 0$ at entry)
ξ_e	m	Cf. Sec. 2.5b
$\Delta\xi'_a, \Delta\xi''_a$	m	Cf. Sec. 2.1.4. Also $\Delta\xi_a \equiv \Delta\xi'_a + \Delta\xi''_a$
Π	—	Supersaturation ($\equiv p/p_s$)

Π_r	—	"Capillary supersaturation," cf. Eq. 2.3(9)
ρ	kg/m ³	Density
σ	N/m	Surface tension
σ	m	Streamline ordinate (Secs. 2.6a and 3.3)
τ	N/m ²	Shear stress at wall
χ	—	Reduced logarithmic supersaturation, cf. Eq. 2.5(32)
ω	rad/sec	Angular velocity of shaft
Ω_a	m ²	Flow cross section normal to axis

SUBSCRIPTS, ETC.

a	Axial component
ad	Adiabatic
A	Value at turbine inlet
b	At reference point
d	Vapor phase
E	Value at turbine outlet
f	"Flowing" (cf. Section 2.9a)
g	Large droplet (cf. Section 2.9a)
gg	Recoiling large droplet (cf. Section 2.9a)
gr	Coarse water forms (collective for f, g, gg and h)
GS	Boundary layer
h	Centrifuged out (cf. Sec. 2.9a); Exception: ΔT_h
h, drin	Centrifuged out but not drained away (cf. Sec. 2.9a)
H	Hollow side of profile (pressure side)
K	Condenser
M	Model
n	Fog droplet (cf. Section 2.9a)

nn	Second-generation fog droplet (cf. Sec. 2.9a)
nach	Immediately after a condensation shock
o	For continuum flow
r	Of a drop
R	Rear side of profile (suction side)
s	At saturation (as p_s , T_s , T_s)
t	Tangential components
tr	"Dry," i.e., corresponding to the homogeneous ideal case, cf. Sec. 3.1.
u	Circumferential components
vor	Directly before condensation shock
w	Of the water phase
0	Before guide wheel of stage
1	Between guide wheel and runner of stage
2	After runner of stage
∞	At thermodynamic equilibrium (assuming equal i and s); exception: U_∞
'	For saturated water or for the stator wheel
"	For saturated steam or for the rotor wheel
*	At the locus of the Wilson point
**	At the point where the sudden condensation can be re- garded as complete
o	In the ideal homogeneous case
^	Corresponding to actual expansion line
-	Averaged value

Part One*)

BRIEF SUMMARY OF RESULTS

Following a critical survey of the literature on the subject in Section 1.1, Sections 1.2 and 1.3 give a brief presentation of the information derived on the basis of Parts Two and Three of this study.

The reader who is interested only in the calculation process for determining the distribution of the moisture **between its particular**

forms and the moisture-loss in a turbine, without wishing to gain a more profound insight into the process, should restrict his attention, after perusing Sections 1.2 and 1.3, to Sections 2.1, 2.9a, 3.7a and 3.8a.

1.1. THE DEVELOPMENT OF KNOWLEDGE CONCERNING WET-STEAM TURBINES

In spite of a great deal of effort devoted to it over the last five decades, our understanding of the wet-steam turbine remains imperfect. Although much practical experience has been accumulated and many important problems cleared up satisfactorily, we still lack a self-contained interpretation of the processes. The principal reason for this is the fact that the problem of the very greatest importance — the mode of the condensation — had for the most part eluded investigation for a long time.

In the meantime (and, specifically, as long ago as the late 'Thirties), great progress was made in the study of condensation, in both the theoretical and experimental aspects. These advances were, however, hailed only in meteorology and wind-tunnel design, but not in

*) [Superscripts refer to the footnotes listed on pp. 27-29].

steam-turbine engineering. An attempt will be made in the present study to apply them profitably to steam turbines as well. Here, it will be shown that it is possible, starting out from the laws governing condensation, to obtain an over-all theoretical picture of the physical processes into which empirical observations dovetail nicely, without being forced to resort to arbitrary and unsubstantiated assumptions just at the points of fundamental importance.

The overall picture that can be built upon the basis of individual processes is sketched in Section 1.2, and Section 1.3 draws practical conclusions from it. For the present, however, we shall address ourselves critically to the most important previous studies in this field.

Baumann established on the basis of steam-consumption measurements made on condensation turbines as early as 1910 (the best reference here is (1)) that penetration of expansion into the wet-steam region involves a deterioration of efficiency. (His rule reads as follows: an end moisture content y_E kg/kg results in a deterioration of efficiency in the wet-steam section by a factor of $1 - y_E/2$). This was followed shortly by a theory proposed by Martin (2), in which with support from experiments with nozzles - it was assumed that the expansion in the turbine does not take place at thermodynamic equilibrium, but with consistent severe supercooling. This author succeeded in reproducing the Baumann loss values rather closely, although with recourse to the assumption, not otherwise justified, that only one fifth of the current theoretical moisture is precipitated in all cases. In his book (3) published in 1922, Stodola presents a penetrating treatment of the behavior of water droplets in steam which is of abiding validity and also devotes a great deal of attention to supercooling problems¹). His nozzle experiments provide the first proof of abrupt condensation in flowing

steam. However, since he had no theory at his disposal that was capable of describing spontaneous drop formation in steam, he could not arrive at a self-contained theoretical interpretation of the processes. In 1927, v. Freudenreich (4) presented a moisture-loss formula on the basis of the assumption that the water phase moves slower than the steam but possesses the same type of velocity triangles as the latter. He also made the first efficiency measurements on a steam turbine with marked variation of final moisture content and arrives at a deterioration of efficiency somewhat sharper than that of Baumann. He uses these results to infer the amount by which the water-phase velocity is lower- a procedure that is just as arbitrary as Martin's inference as to the rate of moisture precipitation. On the other hand, his exemplary investigations into the size and motion of the water drops detached from the stator trailing edges have withstood the test of time. In 1928, Zerkowitz (5) formulated the fruitful concept of "inhomogeneous expansion," in which no kinetic motion at all is imparted to the water phase, and drew from this inferences concerning the moisture-loss. In his book on steam turbines (6), Flügel sums up the state of knowledge at the beginning of the 'Thirties. He mentions the initial supercooling after a saturation line has been crossed and the subsequent sudden transition to thermodynamic equilibrium (Wilson line), but stresses that the principal cause of moisture losses must be sought in the braking effect due to the large drops. He assumes without justification that most of the water is present in the form of such large drops even at 3% moisture²⁾. This view was widely held and also served as a basis for the air-turbine experiments of Flatt (8), in which relatively large drops (10^{-6}m) were artificially injected into the flow and their effect on efficiency measured. Let it be stated here with regard to both Freudenreich's investigations con-

cerning the detached drops and Platt's air-turbine experiments that while they provide an extremely valuable insight into the braking effect of the large drops and will be referred to by the present author for this purpose, it is not admissible to draw conclusions from them concerning the over-all effect of the steam moisture content³⁾.

Most of the numerous publications that appeared during the second half of the 'Thirties were concerned with erosion damage and proposals for its elimination⁴⁾. The frequent cases of catastrophic bucket damage obviously strengthened the conviction that the water forms predominantly large drops. While Senger [11] warns against this "erroneous interpretation" of v. Freudenreich's results, the emphasis of his papers is also placed on the behavior of the large-form water, to which he devotes a comprehensive survey.

After the Second World War, it became increasingly fashionable to speak of **drainage** devices of extreme efficiency. Nevertheless, one cannot suppress the suspicion that these statements have, on some occasions, been prompted by wishful thinking and sales psychology rather than by sound measurements.

Very recently, meticulous and highly elaborate measurements have been undertaken on condensation turbines ([12], [13]). An important result was attained in very short order: namely, the efficiency of the low-pressure stages can be raised considerably by improved shaping of the blades. The result is that we now assume the moisture-losses to be somewhat smaller than previously (at most, half to two-thirds of the value indicated by Baumann). It was established by periscopic observations [14] that permitted viewing the interior of a wet-steam turbine that visibility within the turbine was severely affected by a thick fog in cases where the moisture content was considerable. Gigantic water drops could be observed in **separation regions existing**

in the flow.

It is to be hoped that new experimental information on these problems, obtained with the aid of suitably designated experimental turbines and measuring instruments of high accuracy, will be performed in the future and published. Also the theoretical statements made in the present study deserve to be checked empirically through experiments on turbines.

A survey of papers devoted to spontaneous condensation in flowing steam, which are of decisive significance for the wet-steam turbine, will be given in Section 2.5.

1.2. THE PHYSICAL PICTURE OF THE WET-STEAM TURBINE

In this section, we shall give a condensed presentation of the most important physical processes unfolding in a wet-steam turbine. Here we shall use as our point of departure the investigations described in Parts Two and Three of this report and, for the sake of completeness, particularly as concerns the coarse-form water, reiterate conclusions already stated in earlier studies of wet-steam turbines⁵⁾. Proofs and other details will be found in the corresponding sections of Parts Two and Three, which are referred to on occasion in the footnotes.

In practice, a wet-steam turbine can be produced in either of two ways: either a turbine is fed at the very entry with saturated or even wet steam (for example, in nuclear power plants), or the initially superheated steam becomes wet in the course of expansion (condensation turbines); in the latter case, we imply by the term "wet-steam turbine" the part of the turbine beginning with the stage in which the steam reaches saturation. For the sake of simplicity, we shall restrict our discussion to the case in which the steam at the entry into the wet-steam turbine does not entrain any water drops. Further, we shall have

in mind in all calculations the low-pressure wet-steam turbines, i.e., turbines in which the saturation line is crossed at a pressure lower than about 3 bars (44 psia).

At the outset, we must discuss those phenomena that arise immediately after the saturation line has been crossed. It is evident from the i, s -table that immediate condensation would be expected here. Nevertheless, the i, s -table, as usually plotted, is valid only for the so-called "thermodynamic equilibrium," i.e., for the condition to which a mixture of steam and water adjusts itself after a sufficiently long time. In the steam turbine, expansion runs its course in a very short time (only a few milliseconds pass before the steam, beginning at saturation, arrives at a state in which, for example, 15% of water ought to be present!), and we cannot state a priori that thermodynamic equilibrium can be established during this time. Yet another difficulty is encountered at the beginning of condensation: condensate can be deposited only on a surface that is not too sharply curved - a surface that must, moreover, be cooled to prevent it from being heated so severely by the liberated heat of condensation that no further condensation can take place. Now it is found on closer examination⁶⁾ that the blades, walls, dust particles present in the steam, any water drops that may be detached from the blades, etc., present too small and poorly cooled a surface to permit full-scale condensation on them. The amount of water that is actually deposited on these surfaces is at most a few thousandths of the amount that would be deposited at thermodynamic equilibrium. Thus the conditions fall far short of thermodynamic equilibrium: the steam becomes supersaturated or, in other words, supercooled⁷⁾.

Initially, supersaturation increases practically unhindered since the above — mentioned macroscopic condensation (on the blades,

etc) is extremely weak and since the tendency of the steam molecules to combine into microscopic water "clusters" consisting of a few molecules each - a tendency that makes its appearance immediately after saturation - is initially ineffective. That is to say, the tiny aggregates of molecules are unstable in only slightly supercooled steam⁸⁾ and vaporize soon after formation.

However, the greater the supersaturation becomes as expansion progresses, the smaller will be the "critical" drop size that a drop must possess in order to persist. If this critical drop size has become, let us say, so small that even drops containing only 30 to 100 molecules are stable, rapid formation of such stable drop-lets (nuclei) sets in in the steam. Namely, the smaller the size of the nucleus, the higher is the probability that it will accidentally form⁹⁾. These nuclei present a surface of which heavy condensation of the steam can begin¹⁰⁾, so that the nuclei grow very rapidly to become relatively large drops. (The nuclei radius is originally about $6 \cdot 10^{-10}$ to $8 \cdot 10^{-10}$ m, and most of them reach final sizes of 10^{-8} to 10^{-6} m). This process, the so-called spontaneous condensation, takes place, in rapid expansions, in a very short time, and has as a result conversion of the dry steam into a fog¹¹⁾, so that thermodynamic equilibrium is established - at least approximately.

The point at which spontaneous condensation occurs (or, more precisely, the point at which the supersaturation passes its maximum) will be called the Wilson Point and the line joining various Wilson Points (corresponding to a given rate of expansion) in the $1, s$ -chart will be called the Wilson Line¹²⁾. The following statements can be made in regard to the spontaneous condensation of the steam¹³⁾:

- 1) The position of the Wilson Point, the rapidity of spontaneous condensation and the nature of the fog depend primarily on the local

rate of decrease of the pressure ("expansion rate": $P \equiv (-1/p)dp/dt$).

2) Depending on the magnitude of P , a 3- to 6-fold supersaturation is attained as the peak value (which means a maximum supercooling of about 25 to 35°C), so that the Wilson Line lies between the lines representing 2% to 4% theoretical moisture (cf. the i, s -diagram in the Appendix)¹⁴⁾.

3) When fog formation has been terminated, all fog droplets have approximately the same size.

4) The number of fog droplets per unit mass of steam depends very heavily on the expansion rate P , so that their average size also becomes heavily dependent on this quantity¹⁵⁾.

It is found that this sensitivity of the spontaneous condensation process to the rapidity of expansion is a decisive factor for the wet-steam turbine. Namely, the expansion does not take place at constant rate in the stages of the turbine: rapid expansion rates usually occur with the blade wheels ($P_{\max} = 10^3$ to 10^4 sec^{-1}), while in the gaps between the wheels, on the other hand, the pressure may remain constant for a while ($P = 0$) or may even rise slightly in certain regions (negative P). Thus the turbines also offer the possibility of producing fine fog droplets as well as coarse ones, and all arbitrary intermediate cases are conceivable. (For the finest fog encountered in turbines, we may compute the average fog-droplet radius as about $2 \cdot 10^{-8}$, while the coarsest would have about $5 \cdot 10^{-7} \text{ m}$). Even when the layout of a turbine is known, it is not possible to state once and for all what kind of fog droplets will form in it, since the Wilson point can be reached at various values of P , depending on the operating conditions¹⁶⁾. If the position of the Wilson Point in the turbine had no influence on the composition of the fog, or if the fog had no influ-

ence on subsequent processes, this would still be without practical significance. However, it is found on closer investigation that the behavior of the section of the turbine through, which the fog flows is determined first and foremost by the composition of this fog. How large or how small the proportion of the moisture will be that forms harmful drops (erosion!), how widely the state of the steam deviates from thermodynamic equilibrium, and how large or how small the moisture losses are will all depend on it. The finer the fog droplets formed, the better will be the behavior of the fog in the turbine and its consequences.

During the short time spent in the turbine, the fog droplets have virtually no opportunity to coagulate, so that formation of large drops by direct fusion of several fog droplets does not take place¹⁷⁾. On the contrary, immediately after formation of the fog, another mechanism intervenes to convert the water from the fog-drop form to the large-drop form. This mechanism consists in the blades' catching a part of the through-flowing fog in each blade ring and releasing them only in the form of much larger drops. For the most part, the fog drops impinge on the leading edge of the blades - in the neighborhood of the stagnation point - and on the hollow side where a severe diversion of the steam flow is effected¹⁸⁾. In the case of small fog droplets and high steam densities, only a small fraction of the passing drops impinge on the blades in each ring; on the other hand, in the case of coarse fog droplets and low steam densities, this happens to a considerably larger fraction since large drops are less able to keep up with the motion of the steam. Only in rare cases, however, can a ring catch more than 10% of the fog--drop current, and the captured proportion usually ranges from 1 to 5%. The consequence of this is that even at the exit of the wet-steam turbine, where the fog has already passed through sev-

eral blade rings, most of the steam moisture is present in fog-droplet form and only a relatively small portion (5 to 30%) has made the transition to the coarser forms.

The water caught by the blades forms thin liquid sheets (which often contract to form individual water streaks) and flows in a definite direction under the influence of friction with the steam or the centrifugal force¹⁹⁾.

On the stator blades the water is driven only by steam friction, so that it flows in the direction of the steam current. For the most part, it comes to a halt only in the wind-shadow region of the trailing edge and collects there. The result is formation of large water drops that hang on the trailing edge and are kept in constant vibration by the steam flow. From time to time, some of these drops are torn away. These detached drops may still be rather large during the first few instants (say, 1 mm), but are very soon shattered into numerous small pieces by the steam current²⁰⁾. The average size of the drops that are ultimately formed generally runs to $r = 10^{-4}$ to 10^{-5} m (depending on steam density and velocity) so that they are several orders of magnitude larger than the fog drops that form spontaneously in the steam. For this reason, they will be referred to as "large drops." They are practically totally incapable of following the motion of the steam and impinge upon the backs of the next runner blades just behind the leading edge at high velocity²¹⁾; in doing so, they may give rise to the familiar bucket-pitting effect.

Very many original publications and extremely good summaries are available concerning the erosion phenomena. However, the actual mechanism that causes the pitting is still largely a mystery to this day.

It is not our intention to go into this complex of problems in the present study - the more so because erosion does not belong to the core

of the wet-steam problem, but represents a concomitant phenomenon.

The large drops that impinge on a bucket either adhere to it or rebound (perhaps in the form of several smaller drops) to be picked up by the steam again. In doing so, they are suddenly swept into regions where the pressure is lower; the result may be — particularly for the larger individuals among them — that their interior temperature does not drop fast enough, so that they boil and break up into fragments ("bursting")²²⁾. In no event, however, will the large drops be reduced back to fog-droplet size; the difference between the large drops and the fog drops is distinctly maintained throughout.

The water that strikes the rotor blades flows almost radially outward, since the centrifugal-force effect is generally much stronger than that of steam friction²³⁾. The water then sprays away from the tip of the bucket or from the shroud and either strikes the casing or is carried out of the flow channel through the drainage slits. Should the drainage of the water slung off the runner blades be accomplished only partially or not at all, some of it will adhere to the casing to be driven downstream on this casing by steam friction, while part of it will reenter the steam flow, with the result that a zone particularly rich in large drops forms in the vicinity of the casing increasing locally the danger of erosion and causing major losses.

The large drops swirling in the flow space presumably swallow up all fog drops that they encounter. In low-pressure turbines, however, the number of fog drops that go over to the large-drop form in this manner is very small as compared to the number trapped by the blades. This is because there are still no large drops or only very few present in the first stages of the wet-steam section, and in the later stages, where they become numerous, the density of the steam and, consequently, the number density of fog drops, has already become low and the probability of encounter is reduced.

On the other hand, this process is probably important in high-pressure wet-steam turbines and might, for example, make it possible for a considerable portion of the water present in fog-drop form to be separated from the steam by means of a water separator.

The second phenomenon that is most intimately related to the composition of the fog is the deviation of the steam's state from thermodynamic equilibrium, or, in other words, the extent of the supercooling at various places in the turbine. We have already noted that after the saturation line has been passed, supercooling of the steam at first increases without hindrance, until spontaneous condensation intervenes, and that it then collapses very rapidly as a result of fogging. If, however, this fog expands further adiabatically, as is mostly the case in turbines, it can never arrive at perfect thermodynamic equilibrium, since new water must be deposited out continuously in the course of expansion. Practically the only surface available for condensation is that of the fog drops. Thus, heat must be taken away continuously from the fog drops, and this is possible only when the steam surrounding the fog drops is cooler than the fog-drop surface, i.e., when supercooling obtains. The finer the fog, the larger will be the total surface that the drops present and the more favorable will the heat-transfer coefficients become. In this case, therefore, the supercooling need not be strong. If, on the contrary, the fog has coarse drops, strong supercooling is required to permit continuous withdrawal of the liberated heat by the fog drops.

Supercooling has two kinds of practical consequences. Firstly, the interior heat exchange that takes place in the fog with finite temperature differences gives rise to a loss manifested in a drop in the machine's efficiency; secondly, the specific volume of a supercooled

fog is smaller at a given pressure than that of a fog at thermodynamic equilibrium: thus supercooling reduces the volume flow. This effect should be taken into account right when a machine is being designed.

Under certain conditions, large-drop fogs may allow the supercooling to become so large again as to trigger vigorous spontaneous condensation. This means that a second family of fog drops will form in the fog and intermingle with the primary droplets. The second-generation fog drops may naturally have different sizes than the first generation; they are usually much smaller than the latter²⁴⁾.

In low-pressure turbines, the supercooling amounts to 1° to 4°C for an extremely fine fog; if the fog has large drops, it generally ranges between 10° and 25° , but may reach 30°C and even higher, in which event another spontaneous condensation may occur. In all cases, thermodynamic equilibrium is reached very rapidly after exit from the last stage.

On the basis of these insights into the processes of the wet-steam turbine, we can compute those losses that originate from the properties of the wet steam²⁵⁾. It is found that the moisture-losses are of many kinds. There are three processes that result in particularly heavy losses: the impingement of drops - fog drops and large drops - on the buckets ("braking-losses"), the entrainment, acceleration, etc. of drops by the steam as a result of friction ("entrainment-losses") and the previously noted thermodynamic losses, which depend on the extent of supercooling. Apart from these three principal losses, several other less significant losses arise²⁶⁾ (centrifugation, conversion of the kinetic energy of the trapped water drops into heat, disturbance of the profile boundary layers by water drops, etc.), which, taken together, come out about the same as one of the three

principal losses. Usually, there is an exit-loss recovery at the end of the turbine, since the volume of the supercooled steam is somewhat smaller and, consequently, its exit velocity somewhat lower than in the ideal (not supercooled) case.

As regards the magnitude of the moisture-loss, we find²⁷⁾ that the sum of the individually calculated moisture-losses agrees fairly well with the over-all moisture-loss observed in practice. Further, it is found that only a quite small difference can be detected between a reaction-type turbine and an impulse-type turbine effecting the same expansion, but that a larger amount of water will be present in harmful forms in the reaction-type turbine. In no case may we set the moisture loss in one stage proportional to the average wetness. Depending on conditions, the distribution of the losses among the stages may take highly different forms. A further observation is that the moisture-losses depend very heavily on the composition of the fog: they are not even half as large for extremely fine fogs as for the extremely coarse ones.

For the loss in efficiency per 1% average wetness, carrying the calculations through for the turbines used as an example (13% final wetness, 0.035 bar (0.5 psia) final pressure) gives values of 0.4 to 0.65% for the reaction-type model and 0.4 to 0.6% for the impulse-type version²⁸⁾. The very low value of 0.3% can be reached with extremely fine fogs; with extremely coarse fogs and no drainage at all, the approximate values 0.9% (reaction-type) and 0.7% (impulse-type) will prevail²⁹⁾. These last values can be pushed down to about 0.6% and 0.5%, respectively, with the aid of the best conceivable drainage devices, but they will still be almost twice as large as those obtained with a fine fog without benefit of any drainage.

The two hypothetical turbines used in the examples are described in Section 2.1 and shown in Figs. 2.1.2 and 2.1.3; their expansion lines are shown in Fig. 2.1.1. The supercooling plot obtained by calculation and the distribution of the water among the various drop forms, etc., are presented in Figs. 2.9.4 to 2.9.11 (three extreme cases were investigated for each design type, cf. page 183). The moisture-losses in the individual stages are, for the same cases, represented as surfaces in Figs. 3.7.1 and 3.7.2. Finally, Fig. 3.1.1 shows the shape of the expansion line taking moisture-losses into account.

In the following section, we shall attempt to secure certain practical aspects on the basis of this over-all physical picture.

1.3 PRACTICAL CONCLUSIONS

The steam remains practically dry for some time after the saturation line has been passed. Only from the Wilson Point on, i.e., from a point where about 2.5 to 3.5% of wetness should theoretically be present, does the first major quantity of water condense out, doing so in the form of very small fog droplets that can easily follow the flow of the steam.

Even at the end of the turbine, the major portion of the moisture is still present in fog-drop form. Consequently, we may consistently assume that the moisture has almost the same velocity as the steam.

The undesirable large drops that do not follow the motion of the steam and may therefore be deposited incorporate only a smaller fraction of the steam moisture. Thus only a small part of the total moisture can be removed from the flow channel, even with the most effective drainage arrangements.

Thermodynamic equilibrium is not established in the steam as it is expanded in the turbine. Due to supercooling, the steam has a smaller specific volume, which leads to a change in the volume-flow conditions

and consequently, must be taken into account during the design of a wet-steam turbine.

There is no general rule concerning the extent of the moisture-loss in a stage. Apart from the properties of the stage, it depends particularly on the distribution of the water among the various forms which it can assume and may show quite large charges from one set of operating conditions to another.

Both the quantity of water that enters the detrimental forms and the extent of supercooling and moisture-losses depend very heavily on the size of the droplets in the fog formed in the turbine. Since a fine fog behaves much better in all respects than a coarse fog, the principal goal of our efforts must be to configure the wet-steam turbine in such a way that a fine-droplet fog will form. The means to this end is to have the Wilson Point in a region in which the pressure drops sharply.

Securing formation of a fine fog is the most effective measure that can be taken to reduce the danger of erosion and, above all, to reduce moisture-losses.

The blade pitch in the part of the turbine through which the fog flows should be preferably larger rather than too small in order to minimize the number of fog droplets trapped by the blades.

Broad gaps between the wheels behind the runners are pointless as far as reducing the erosion susceptibility is concerned; they would be better placed behind the nozzles, since it is only from these that large drops are detached.

The erosion danger and moisture-loss can be reduced somewhat with the aid of the effective drainage devices, i.e., devices that remove all coarse-form water (indeed, the remainder cannot be removed anyway!),

although the moisture losses cannot be cut to a really incisive degree.

Model experiments are quite feasible on wet-steam turbines, particularly when the average fog-drop diameter is approximately the same as the mean free path of the steam molecules³⁰⁾.

In summary, therefore, we can state that a wet-steam turbine will be the better as regards erosion danger and moisture-losses the more perfect its drainage devices and the smaller (!) the amount of water drawn off by these devices. That is to say that the moisture remains for the most part in the fog-drop form, which presents no hazard. (Unfortunately, however, an apparently identical result, i.e., a low level of water extraction can also be achieved with a coarse fog and inferior dewatering...).

(Footnotes to Part One)

No.

- 1 Here, though, he bases his reasoning on the assumption that during an expansion, the steam remains at all times in (capillary) equilibrium with the uniformly large fog drops present in it, i.e., that the supercooling ΔT at the moment agrees with the capillary supercooling ΔT_r (cf. our Section 2.3) and, consequently, is uniquely determined by the fog-drop size. Since, however, such an equilibrium is unstable and, moreover, the droplet size is not uniform in reality, this assumption is completely out of line with actual conditions.
- 2 The same non-sequitur is also clearly evident, for example, with Goodenough (7).
- 3 Cf. Goerke (9).
- 4 A comprehensive bibliography on this topic can be found in Preiskorn (10). On the whole, his work presents an excellent survey of the erosion problem and contains numerous sound recommendations for control of this effect.
- 5 We shall not go into source citations in this Section.
- 6 Cf. Section 2.4.

- 7 See Section 2.3a.
- 8 Cf. Section 2.3c.
- 9 Cf. Section 2.5a.
- 10 Besides their large number they also possess extraordinarily heat-transfer coefficients.
- 11 In our terminology, "fog" = steam + fog droplets, where the "fog droplets" are water droplets with radii between 10^{-8} and 10^{-6} m, distributed practically uniformly in the flow channel.
- 12 See Section 2.3b and the i, s-diagram (Appendix).
- 13 Cf. Sections 2.5c and d.
- 14 Since the publication of the Swiss original of this report in 1962, the effect of P on the condensation of steam has been studied experimentally (47). These measurements confirmed the influence of P inferred from theory. However, they indicated slightly higher supersaturations than expected on the basis of theoretical calculations. Based on the experiments, the range of peak values occurring in turbines are 4- to 9-fold supersaturation and 30° to 44°C supercooling. These deviations between theory and experiment can be explained by a difference of some 13% between the surface tension of a nucleus and that of a plain water surface. The fog droplet sizes calculated in the present report have been found to agree well with the measured drop sizes. Therefore, the bulk of the conclusions reached in this report are not affected by these corrections.
- 15 A tenfold increase in the expansion rate P increases the number of fog droplets by a factor of 200 to 300 and reduces the average fog-droplets size accordingly by a factor of 6, cf. Fig. 2.5.14.
- 16 Cf. Section 2.5e.
- 17 Cf. Section 2.6a.
- 18 Cf. again Section 2.6a.
- 19 The thickness of this water film or streaks is generally only a small multiple of 10^{-6} m, cf. Section 2.7.
- 20 Cf. Section 2.8a.
- 21 Cf. Section 2.8b.

- 22 Cf. Section 2.8d.
- 23 Cf. Section 2.7.
- 24 Cf. Section 2.9.
- 25 Cf. Sections 3.1 to 3.6
- 26 Called "miscellaneous losses" in this report.
- 27 Cf. Section 3.7.
- 28 Cf. Section 3.7b.
- 29 Let it be noted here that the smaller losses in the impulse-type turbine are not directly related to the low reaction, but to the lower number of stages. This latter, however, is related to the amount of reaction by the fact that stages of low reaction usually can convert more heat drop.
- 30 Cf. Section 3.8b.

Part Two*)

THE FORMATION OF STEAM WETNESS AND THE FORMS
ASSUMED BY WATER IN THE TURBINE

2.1. LAYOUT OF TWO TURBINES AS A BASIS FOR APPLICATIONAL EXAMPLES

The objective of the present study is to investigate the behavior of steam in low-pressure condensation turbines. This behavior may be of different nature depending on the design of the turbine. To be able to judge the influence exerted by design on the processes of the turbine, two turbines were designed on paper to be used as applicational examples, one as a reaction-type and the other as an impulse-type turbine. Both turbines have the same expansion line; it lies almost entirely in the wet-steam region. The reaction-type turbine has twice as many stages as the impulse-type turbine. Both turbines represent extremes of their types. The reaction-type turbine shows an exaggerated axial structural length, with the blade pitch values tending to be larger and the deflections smaller than usual. The impulse-type turbine, on the other hand, is extraordinarily short; its (runner) blades are quite close together and produce large deflections. The exaggerations were intentional so that the differences in behavior between the two turbine designs would be more distinct.

Below we give the data for the two turbines that will be necessary for subsequent calculations, followed by a discussion of how we can use them to determine the plots of certain quantities knowledge of which is presupposed in subsequent Sections.

The turbines were laid out on the basis of the i, s -diagram for

*Superscripts refer to the footnotes listed on pp. 198a and 198b.

thermodynamic equilibrium, and no moisture losses were taken into account in the efficiency figure adopted. Thus the data can be regarded only as a first approximation of reality. How the expansion actually takes place can be determined only at the end of this study, on the basis of the investigations that have been carried through.

For the sake of simplicity, we shall restrict our considerations to the conditions at the blade mean diameter.

The basic data for the two turbines are as follows:

Mass throughput (no bleeding!)	$\dot{M} = 40 \text{ kg/sec (89 lb/sec)}$
Speed 3000 rpm or	$\omega = 314.2 \text{ rad/sec}$
Initial state of steam	$p_A = 1.4 \text{ bar (19.6 psia)}$
	$i_A = 2700 \text{ kJ/kg (1160 BTU/lb)}$

(Initial superheating: about 4.5°C (8°F))

Final pressure (condenser

pressure)

$p_K = 0.035 \text{ bar (0.5 psia)}$

Final wetness

$y_E \approx 13\%$

Percentage reaction,

reaction turbine³¹⁾

50% (40%)

Percentage reaction,

impulse turbine³¹⁾

5% (30%)

The expansion line is shown in Fig. 1. Figures 2 and 3 show meridional sections and blade shapes for the two turbines, as well as certain characteristic velocity triangles.

More explicit data are collected in Table 2.1.1 for the reaction turbine and in Table 2.1.2 for the impulse turbine. The significance of the various symbols will be evident from Fig. 4. The following must be noted regarding the quantities t and \bar{P}_a : The flow time t was determined from the axial-velocity curve, according to the expression

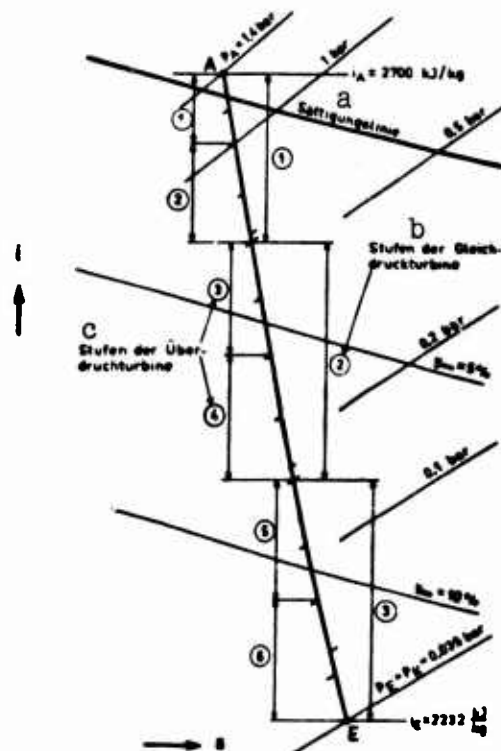


Fig. 2.1.1. Expansion line of turbines used as example (without taking moisture losses into account). a) Saturation line; b) stages of constant-pressure turbine; c) stages of high-pressure turbine.

$$t = \int_0^{t_A} \frac{dt_A}{c_A(t_A)} \quad (1)$$

(we shall return below to the matter of determining the c_A -curve). \bar{P}_A is the average value of the logarithmic axial pressure gradient

$$\bar{P}_A = - \frac{1}{P} \frac{dp}{dt_A} = - \frac{d(\ln p)}{dt_A} \quad (2)$$

in a blade wheel and, for example, in the case of a stator wheel is calculated as

$$\bar{P}_A = \frac{\ln p_0 - \ln p_1}{t_{A1} - t_{A0}} \quad (3)$$

To conduct an exact analysis of the flow process in turbines, we must know the plots of certain quantities along the axial coordinate —

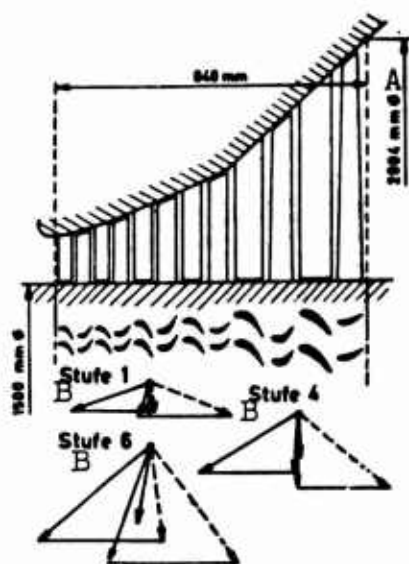


Fig. 2.1.2. Bucket complement and velocity triangles for the high-pressure turbine (cf. also Table 2.1.2). A) Diameter; B) stage.

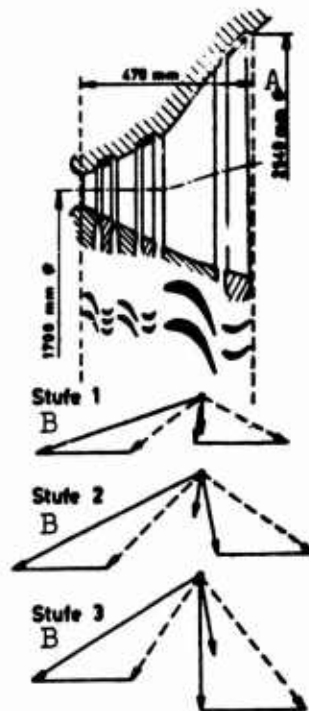


Fig. 2.1.3. Bucket complement and velocity triangles for the constant-pressure turbine (cf. also Table 2.1.2). A) Diameter; B) stage.

particularly those of p , P_a and c_a . Below we shall discuss ways in which these functions can be determined from known design data given for the stations between the blade rings.

Within a stage, the pressure diminishes not approximately linearly, but stepwise. It remains approximately constant in the unbladed intermediate gap, but compensates for this by dropping off the more rapidly at places where the flow experiences the sharpest accelerations. The pressure curve for the bucket surfaces — for which the literature contains numerous measurements — depends heavily on profile shape and is sensitive to changes in the direction of onflow. In the middle of the channel, on the other hand, it should be possible to indicate the nature of the pressure drop in a fairly generally valid form, cf. Fig. 5a. We might arrive at this wavy curve by plotting the pressure on a

logarithmic scale and superimposing a sine curve over the connecting straight lines between the two intermediate pressures before and after the ring in this mode of presentation (Fig. 5b), in such a way that the resultant curve has a horizontal tangent in the intermediate spaces.

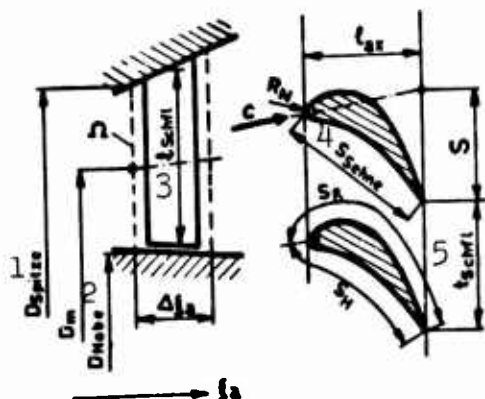


Fig. 2.1.4. Notation for Tables 2.1.1 and 2.1.2. 1) D_{tip} ; 2) D_{hub} ; 3) l_{bucket} ; 4) S_{chord} ; 5) t_{bucket} .

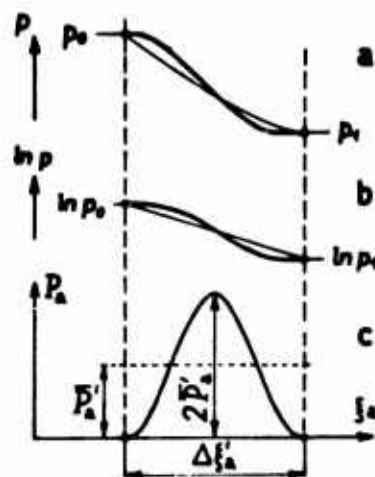


Fig. 2.1.5. Sine-wave approximation for the pressure curve and for the logarithmic axial pressure gradient in a bucket ring (plotted for a guide wheel).

The curve of the logarithmic axial pressure gradient P_a can easily be determined on the basis of this curve for $\ln p(\xi_a)$, as has been done in Fig. 5c. P_a follows a cosine curve, reverts to zero in all intermediate spaces, and has a maximum of height $2\bar{P}_a$ between them (\bar{P}_a is computed from Eq. (2')).

The axial velocity curve $c_a(\xi_a)$ can also be estimated in a similar manner. The values of c_a in the intermediate spaces are known from the layout of the turbine. Between them, c_a would have a uniform curve (line k in Fig. 6) provided that the blades were infinitesimally thin. Since, however, the blades block off part of the flow section, c_a must rise in the ring. This can be estimated approximately by raising the velocity value that would correspond to the uniform curve in

TABLE 2.1.1

(Reaction-type Turbine)

1 Stufe:	1				2				3					
2 Schaufelkranz:	vor 1'	1'	zw. 1', 1"	1"	zw. 1", 2'	2'	zw. 2', 2"	2"	zw. 2", 3'	3'	zw. 3', 3"	3"	zw. 3", 4'	4'
ξ_a m	0		0,05		0,10		0,15		0,20		0,26		0,32	
i kJ/kg	2700		2675		2650		2614,5		2578,5		2538,5		2497	
p bar	1,40		1,20		1,01		0,790		0,612		0,454		0,330	
v m ³ /kg	1,25		1,41		1,635		2,05		2,60		3,36		4,40	
γ_{∞} kg/kg	-		0,003		0,011		0,022		0,033		0,045		0,057	
c_a m/sec	81,8		81,0		83,8		94,5		103,5		114,7		129,4	
c m/sec	81,8		241,2		89,1		281,3		103,6		301,0		130,0	
w m/sec	-		86,4		243,6		94,6		289,0		115,1		314,2	
u m/sec	254,5		256,9		259,3		261,7		265,2		269,4		274,1	
D _{Spitze} 6 m	1,7400		1,7706		1,8012		1,8318		1,8784		1,9344		1,9904	
D _m m	1,6200		1,6353		1,6506		1,6659		1,6892		1,7172		1,7452	
D _{Nabe} 7 m	1,5000		1,5000		1,5000		1,5000		1,5000		1,5000		1,5000	
Ω m ²	0,611		0,697		0,781		0,869		1,004		1,172		1,344	
l _{Schn} 8 m		0,126		0,142		0,157		0,177		0,202		0,232		0,262
s -		121		117		121		130		106		108		106
l _{Schn} 8 m		0,042		0,044		0,043		0,040		0,050		0,050		0,052
s _{Sehne} 9 m		0,054		0,054		0,054		0,054		0,067		0,067		0,067
R _N m		0,0025		0,0025		0,0025		0,0025		0,0030		0,0030		0,0030
l _{ax} m		0,038		0,038		0,038		0,039		0,047		0,049		0,052
s m		0,039		0,024		0,024		0,037		0,049		0,048		0,047
ΔR_a m		0,050		0,050		0,050		0,050		0,060		0,060		0,070
s _H m		0,057		0,057		0,057		0,057		0,069		0,069		0,069
s _R m		0,066		0,066		0,066		0,066		0,096		0,096		0,096
t sec	0		$5,4 \cdot 10^{-4}$		$10,8 \cdot 10^{-4}$		$15,9 \cdot 10^{-4}$		$20,4 \cdot 10^{-4}$		$25,0 \cdot 10^{-4}$		$29,3 \cdot 10^{-4}$	
P _a m ⁻¹		3,1		3,5		4,9		5,1		5,2		5,0		4,8
P _{max} sec ⁻¹		620		730		1070		1270		1530		1580		1690

1) Stage; 2) blade; ring; 3) before; 4) between; 5) after; 6) tip; 7) hub; 8) blade ; 9) chord.

proportion to the cross-sectional reduction (see figure).

The curves obtained in this way for $P_a(\xi_a)$ and $c_a(\xi_a)$ are presented in Fig. 7 for the specified reaction-type turbine and in Fig. 8 for the impulse-type turbine. These c_a -curves were used to calculate the flow times t from Eq. (1) for both Tables 1 and 2.

An additional quantity knowledge of which is presupposed in the

3			4			5			6						
3'	zw. 3', 3"	3"	zw. 3", 4'	4'	zw. 4', 4"	4"	zw. 4", 5'	5'	zw. 5', 5"	5"	zw. 5", 6'	6'	zw. 6', 6"	6"	nach 6"
0, 26			0, 32	0, 39			0, 46	0, 56			0, 64	0, 75			0, 84
2538, 5			2497	2452, 5			2407, 5	2460			2320	2267			2332
0, 454			0, 330	0, 236			0, 168	0, 111			0, 0785	0, 0485			0, 035
3, 36			4, 40	6, 00			8, 30	11, 8			16, 2	25, 5			34, 3
0, 045			0, 057	0, 069			0, 082	0, 095			0, 106	0, 121			0, 130
114, 7			129, 4	155, 6			188, 3	200			222	252			312
→ 301, 0			130, 0	→ 324, 3			188, 3	→ 361			224	→ 395			321
115, 1			→ 314, 2	155, 7			→ 343, 5	200			→ 358	254			→ 390
269, 4			274, 1	279, 1			284, 3	298			310	325			338
1, 9344			1, 9904	2, 0556			2, 1210	2, 3000			2, 444	2, 642			2, 804
1, 7172			1, 7452	1, 7778			1, 8105	1, 9000			1, 972	2, 071			2, 152
1, 5000			1, 5000	1, 5000			1, 5000	1, 5000			1, 500	1, 500			1, 500
1, 172			1, 344	1, 542			1, 765	2, 39			2, 93	3, 72			4, 41
02	0, 232			0, 262	0, 232			0, 356	0, 434			0, 520	0, 608		
	108			108	108			71	94			62	70		
50	0, 050			0, 052	0, 054			0, 080	0, 064			0, 100	0, 093		
67	0, 067			0, 067	0, 066			0, 100	0, 074			0, 109	0, 078		
030	0, 0030			0, 0030	0, 0030			0, 0035	0, 0030			0, 0035	0, 0030		
47	0, 049			0, 052	0, 054			0, 071	0, 060			0, 088	0, 069		
49	0, 048			0, 047	0, 040			0, 064	~0, 044			0, 052	~0, 025		
60	0, 060			0, 070	0, 070			0, 100	0, 080			0, 110	0, 090		
69	0, 069			0, 069	0, 068			0, 103	0, 078			0, 110	0, 079		
96	0, 096			0, 096	0, 082			0, 128	0, 092			0, 127	0, 088		
25, 0 · 10 ⁻⁴			29, 3 · 10 ⁻⁴	33, 7 · 10 ⁻⁴			37, 4 · 10 ⁻⁴	42, 1 · 10 ⁻⁴			45, 6 · 10 ⁻⁴	49, 7 · 10 ⁻⁴			52, 8 · 10 ⁻⁴
5, 0				4, 8	4, 8		4, 1	4, 3		4, 3	3, 7				
1580				1690	1980		1920	2150		2500	2450				

ip; 7)

pre-

Fig. 8

calcu-

n the

B

TABLE 2.1.2

(Impulse-type Turbine)

1 Stufe		1			2			3						
2 Schaufelkranz:		vor 1'	1'	zw. 1', 1"	1"	zw. 1", 2'	2'	zw. 2', 2"	2"	zw. 2", 3'	3'	zw. 3', 3"	3"	nach 3"
ξ_a	m	0		0,05		0,09		0,16		0,21		0,36		0,47
i	kJ/kg	2700		2584,5		2578,5		2412		2407,5		2284,5		2232
p	bar	1,4		0,64		0,612		0,179		0,168		0,0565		0,035
v	m ³ /kg	1,25		2,50		2,60		7,8		8,30		22,1		34,3
γ_m	kg/kg	-		0,031		0,033		0,079		0,082		0,116		0,130
c_a	m/sec	100,0		150		120		254		222		283		359
c	m/sec	100,0		491		123		584		227		544		359
w	m/sec	-		252		271		362		384		334		471
u	m/sec	267		267		267		267		267		289		298
D Spitze	6 m	1,7936		1,8249		1,8623		1,930		1,980		2,380		2,540
D m	m	1,7000		1,7000		1,7000		1,700		1,700		1,840		1,900
D Nabe	7 m	1,6084		1,5751		1,5377		1,470		1,420		1,300		1,260
Ω	m ²	0,220		0,667		0,866		1,229		1,493		3,12		3,82
l_{SchM}	8 m	0,110		0,145				0,200				0,425		0,585
z	-	108		254				108				54		90
l_{SchM}	9 m	0,050		0,021				0,050				0,099		0,064
l_{SchM}	9 m	0,070		0,33				0,081				0,193		0,078
R_N	m	0,0020		0,0013				0,0025				0,0050		0,0035
l_{ax}	m	0,040		0,032				0,053				0,146		0,075
s	m	0,058		-0,030				0,055				0,158		0,068
Δl_a	m	0,050		0,040				0,070				0,170		0,090
a_H	m	0,074		0,040				0,084				0,207		0,083
a_H	m	0,096		0,055				0,097				0,253		0,102
t	sec	0		$3,3 \cdot 10^{-4}$		$5,3 \cdot 10^{-4}$		$8,4 \cdot 10^{-4}$		$10,0 \cdot 10^{-4}$		$15,5 \cdot 10^{-4}$		$18,0 \cdot 10^{-4}$
P_a	m ⁻¹	15,7		1,1				17,6				9,6		5,3
P_{max}	sec ⁻¹	5840		560				10400				7430		4280

1) Stage; 2) blade ring; 3) before; 4) between; 5) after; 6) tip; 7) hub; 8) blade 9) chord.

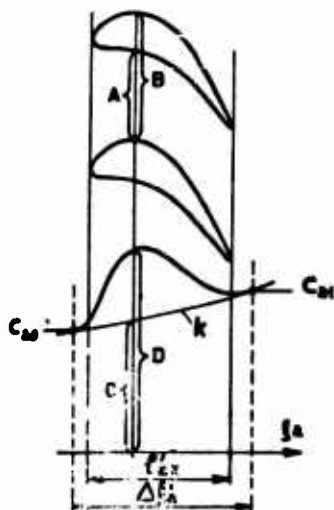


Fig. 2.1.6. Estimated axial-velocity curve for a bucket ring. A:B is to be taken equal to C:D.

following Sections and which is closely related to the logarithmic axial pressure gradient is the "expansion rate"

$$\dot{p} = -\frac{1}{p} \frac{dp}{dt} = P_a c_a. \quad (4)$$

For the most part, we shall approximate the variation of this quantity within the bucket ring by means of a cosine curve that begins and ends at zero (cf., for example, in Fig. 2.9.3). Its amplitude value is

$$\dot{p}_{\max} = (P_a c_a)_{\max}. \quad (5)$$

The \dot{p}_{\max} was determined from the P_a and c_a curves for each ring of the turbines in question and entered in the tables.

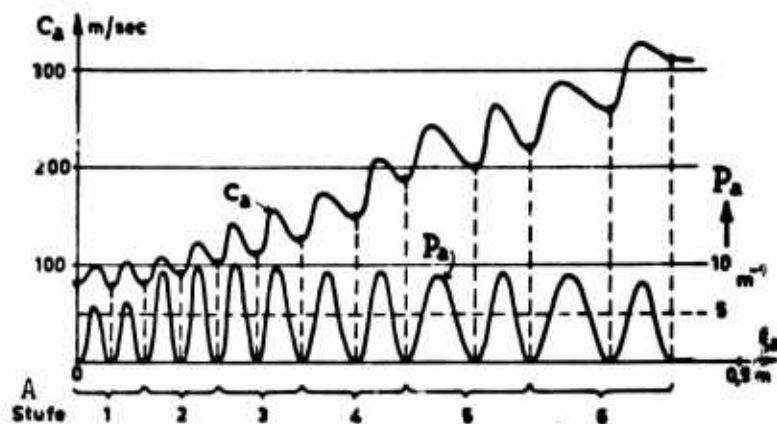


Fig. 2.1.7. Curves of $P_a(\xi_a)$ and $c_a(\xi_a)$ in the reaction-type turbine. A) Stage.

2.2. DRAG FORCE AND HEAT TRANSFER BETWEEN DROPLETS AND STEAM

In the present study, we shall always tacitly assume that the water droplets are spherical unless the contrary is expressly noted. This assumption is notably valid for the most important droplet sizes (diameters $< 1 \mu$). That is to say, such small drops can follow the motion of the steam closely, so that the peripheral pressure-force varia-

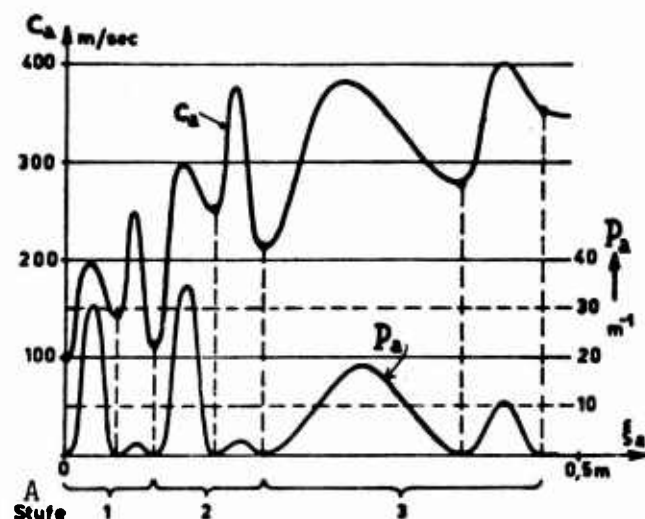


Fig. 2.1.8. Curves of $P_a(\xi_a)$ and $c_a(\xi_a)$ in the impulse-type turbine. A) Stage.

tion that gives rise to distortion remains within narrow limits, being conditioned by the velocity of the droplets relative to the steam; thus the surface tension is in a position to maintain the spherical shape. With larger drops, higher relative velocities arise and the distorting forces can, under certain conditions, become so large that they not only set the droplets into distorting vibration but even shatter them. We shall discuss these problems in greater detail in Section 2.8.

We define the drag coefficient c_D and the heat-transfer coefficient α_r for a sphere in the usual manner, as

$$W = c_D(\pi r^2) \left(\frac{1}{2} \rho_d U_r^2 \right), \quad (1)$$

and

$$\dot{Q} = \alpha_r (4\pi r^2) (T_r - T_{r,ad}), \quad (2)$$

respectively. Here W is the drag force exerted by the steam on the droplets at a relative velocity U_r . \dot{Q} is the quantity of heat transferred from the droplet each second. The "adiabatic drop temperature" $T_{r,ad}$ exceeds the temperature T_d of the surrounding steam by the bound-

ary-layer heating ΔT_{GS} :

$$T_{r,ad} = T_d + \Delta T_{GS} \quad (3)$$

ΔT_{GS} becomes noticeable only at large relative velocities. (In the case of steam, it reaches 1°C at about $U_r = 60$ m/sec.) Frequently, α_r is also expressed in terms of the Nusselt number, which is defined as

$$Nu_r = \frac{2r \cdot \alpha_r}{\lambda_d} \quad (4)$$

Thus the entire problem of drag force and condensation is reduced to the determination of c_D , α_r and ΔT_{GS} . However, before we indicate formulas for their calculation, we must present certain basic arguments concerning flows in general.

The Navier-Stokes equations, which serve as a basis for the usual discussion of flows, presuppose a continuous medium. If this assumption agrees closely with reality, we speak of a continuum flow. If, however, as a result of a very low density of the medium or of very small dimensions of the bodies past which the flow is moving, the free path of the molecules acquires orders of magnitude comparable with the dimensions of the bodies, deviations from continuum flow make their appearance.

The Knudsen number Kn , which indicates the ratio of the mean free path to the principal dimension of the body in question (in our case, to the droplet diameter $2r$), is used as a measure of these deviations:

$$Kn = \frac{l}{2r} \quad (5)$$

For calculation of the mean free path, we have at our disposal the following formula derived from the kinetic theory of gases:

$$l = 1.5 \sqrt{2} \frac{\nu_d}{a_d} = 1.5 \frac{\mu_d}{\rho_d \sqrt{RT_d}} = \frac{(1.5 \mu_d \sqrt{RT_d})}{\rho} \quad (6)$$

where ν_d and μ_d are the kinematic and dynamic viscosities of the steam, respectively, and a_d represents the speed of sound in the steam. The quantity $(1.5 \mu_d \sqrt{RT_d})$ is plotted in Diagram III (Appendix) as a func-

tion of the steam pressure, while Diagram I shows the mean free path \bar{l}_s in saturated steam as a function of pressure. We see that, for example, in saturated steam with $p = 1 \text{ bar} = 10^5 \text{ N/m}^2$ ($T_d = T_s = 99.6^\circ$), the mean free path is about $\bar{l} = 8 \cdot 10^{-8} \text{ m}$. Using Eq. (6), we can also express Kn in terms of the Reynolds number

$$Re_r = \frac{2r \cdot U_r}{\nu_d} = \frac{2r \cdot \rho_d \cdot U_r}{\mu_d} \quad (7)$$

and the Mach number

$$M_r = \frac{U_r}{a_d} \quad (8)$$

as follows:

$$Kn = \frac{1,5}{2r} \frac{\mu_d}{\rho_d \sqrt{RT_d}} = 1,5 \sqrt{\pi} \frac{M_r}{Re_r} \quad (9)$$

If the deviations from continuum flow are not particularly strong, it is possible to set up a theory that gives results in good agreement with experience by retaining the Navier-Stokes equations as valid but dropping the wall-adhesion condition and postulating instead a finite velocity at the wall -- the so-called slip velocity. For this reason, such flows are known as slip flows. In a similar manner in the case of temperature, a discontinuity is also assumed between the wall temperature and the average stream temperature at the wall.

At the very large Knudsen numbers, when the dimensions of the body are small as compared to the free path of the molecules, the processes can be calculated on the basis of the kinetic gas theory, since here we can regard the "flow medium" as a multitude of individual and independent particles. In such cases, we speak of free molecular flow.

A region that has hitherto been inaccessible to theoretical treatment bridges the gap between slip flows and free molecular flows -- the so-called transition flow region. The values of c_D and α_r used for this

region are determined, for want of a better basis, by extrapolation from the two neighboring regions.

There are no sharp boundaries between these flow forms. Nevertheless, we can break up the range approximately as follows:

$Kn < 0.01$: Continuum flow

$0.01 < Kn < 0.18$: Slip flow

$0.18 < Kn < 4.5$: Transition flow

$Kn > 4.5$: Free molecular flow.

An excellent survey of all these problems can be found in [15].

For the continuum flows, it follows from the theory of analogy that c_D and Nu_r depend on Reynolds number. (The subscript 0 will be used to denote values applying for continuum flows.) Thus, we write

$$c_D = c_{D0} = c_{D0}(Re_r), \quad (10)$$

$$Nu_r = Nu_{r0} = Nu_{r0}(Re_r). \quad (11)$$

The form of the dependence has been determined empirically; in this connection, see the representations in [16] and [17], respectively. Strictly speaking, we should also have in Eq. (11) a dependence on the Prandtl number

$$Pr = \frac{c_p \mu_d}{\lambda_d} \quad (12)$$

however, the variation of Pr is so insignificant under our conditions that the effect can be disregarded.

For very small Reynolds numbers, the relationships can also be derived analytically:

$$\left. \begin{aligned} c_{D0} &= \frac{24}{Re_r} = \frac{12 \mu_d}{\rho_d U_r r} \text{ ("Stokes' Law")} \\ Nu_{r0} &= 2 \end{aligned} \right\} \text{ for } Re_r < 1. \quad (13)$$

$$\text{or } \alpha_{r0} = \frac{\lambda_d}{r} \quad (14)$$

For a somewhat higher range of Reynolds numbers, a range important

primarily for the droplets detached from the bucket edges, we have on the basis of experiment (cf. [16] or [17])

$$c_{Do} \approx \frac{13.0}{\sqrt{Re_r}}, \quad (15)$$

$$\left. \begin{aligned} Nu_{ro} \approx 0.66 \sqrt{Re_r} \quad \text{or} \quad \alpha_{ro} \approx 0.33 \sqrt{Re_r} \cdot \frac{\lambda_d}{r} \end{aligned} \right\} \text{for } 20 < Re_r < 800. \quad (16)$$

For the boundary-layer heating we have for (laminar) continuum flows (see, for example, [16])

$$\Delta T_{GSo} = \sqrt{Pr} \frac{U_r^2}{2c_p}. \quad (17)$$

For slip flows we have (cf. [15])

$$c_D = c_{Do} \frac{(1 + 15 Kn)(1 + 4 Kn) + \frac{24}{\pi} Kn^2}{(1 + 15 Kn)(1 + 6 Kn) + \frac{36}{5\pi} Kn^2 (4 + 18 Kn)}, \quad (18)$$

$$\alpha_r = \alpha_{ro} \frac{1}{1 + 3.42 \frac{M_r}{Re_r Pr_o}} = \alpha_{ro} \frac{1}{1 + \frac{3.42 Nu_o}{1.5 \sqrt{Pr} Kn}}, \quad (19)$$

$$\Delta T_{GS} \approx \Delta T_{GSo}. \quad (20)$$

Here c_{Do} and α_{ro} are to be substituted in accordance with the Reynolds number.

For free molecular flows, we find c_D and α_r values that are independent of drop size. They are given in exact form in [15]. Here we shall write them only for the small Mach numbers of interest to us, which simplifies the expressions greatly. We further assume that the recoil of molecules from the droplet surface takes place by reemission. This means that the energy distribution of the rebounded molecules is determined by the Maxwell distribution corresponding to the surface temperature, regardless of the energies that they possessed before impingement, and that the flight directions of the rebounded molecules follow a three-dimensional cosine distribution irrespective of the flight directions before impingement. It has been found through experiment that about 90% of the molecules rebound in this way for various

gas-metal combinations; for droplets and steam, where the surface and the medium consist of identical molecules, we should expect this assumption to be justified to an even much greater degree. We shall assume that it is valid for all molecules. Thus, we obtain the formulas

$$c_D = \frac{35}{8\sqrt{\pi}} \sqrt{\frac{2}{\kappa}} \left(1 + \frac{4\kappa}{35} \sqrt{\frac{T_r}{T_d}} \right) \frac{1}{M_r} \approx \frac{5.50 a_d}{U_r}, \quad (21)$$

$$\alpha_r = \frac{1}{4\sqrt{\pi}} \sqrt{\frac{2}{\kappa}} \frac{\kappa+1}{\kappa} c_p q_d a_d \approx 0.305 c_p q_d a_d, \quad (22)$$

$$\Delta T_{GS} \approx 2.65 \frac{\kappa}{2} \frac{\kappa-1}{\kappa+1} T_d M_r^2 \approx 0.754 \frac{U_r^2}{c_p}, \quad (23)$$

where we have used $\kappa \approx 1.32$ and $T_r \approx T_d$. Applying (7), (9), (12), (13), (14) and (17), these equations can be brought to the form

$$c_D \approx c_{Do} \frac{1.5\sqrt{\kappa} 5.50/24}{Kn} \approx c_{Do} \frac{0.395}{Kn} \quad (24)$$

$$\alpha_r \approx \alpha_{r0} \frac{1.5\sqrt{\kappa} \cdot 0.305 Pr/2}{Kn} \approx \alpha_{r0} \frac{0.315}{Kn} \quad (25)$$

$$\Delta T_{GS} \approx \Delta T_{GS0} \cdot \frac{2.65\kappa}{\kappa+1} \frac{1}{\sqrt{Pr}} \approx \Delta T_{GS0} \cdot \frac{1.51}{\sqrt{Pr}}. \quad (26)$$

Larger Reynolds numbers occur only for larger droplets, and for these the deviations from the continuum flow are negligible anyway.

Although we do not have any formulas at the present time for the transition flows, extrapolation from either adjacent region is made the more possible by the fact that the solutions indicated for slip flows merge rather smoothly with those for free-molecular flows at large Knudsen numbers.

When we compare Formulas (10), (18) and (24) with (11), (19) and (25), respectively, we are struck with the idea of representing the resistance coefficient and the heat-transfer coefficient (for small Reynolds numbers) each in a single formula that embraces all flow types. These would read

$$c_D = c_{Do} \cdot f_{c_D}(Kn), \quad (27)$$

$$\alpha_r = \alpha_{r0} \cdot f_{\alpha_r}(Kn), \quad (28)$$

where c_{D0} and α_{r0} are given by Eqs. (13) and (14), respectively. The functions f_{c_D} and f_{α_r} have unit value for continuum flows and are otherwise given by the factors in Eqs. (18) and (24) or (19) and (25). Figure 1 shows their curves. In the material to follow, we shall always imply the following expressions by f_{c_D} and f_{α_r} :

$$f_{c_D} = \frac{1}{1 + 2,53 \text{ Kn}} \quad (29)$$

$$f_{\alpha_r} = \frac{1}{1 + 3,18 \text{ Kn}} \quad (30)$$

As will be seen from Fig. 1, they permit simple and sufficiently exact reproduction of conditions over the entire range of Kn. In the calculations presented here, the influence of the low steam densities will always be taken into account by means of these formulas.

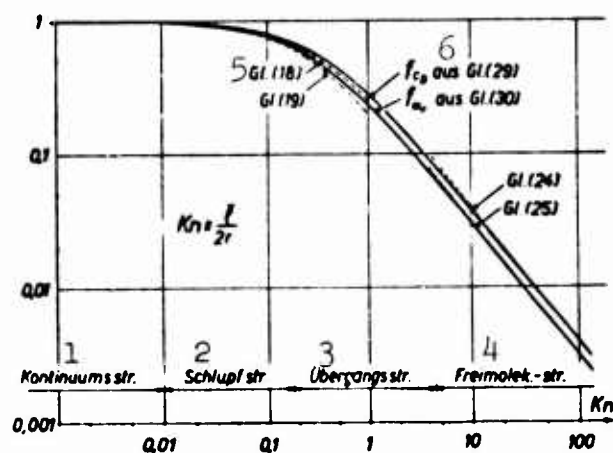


Fig. 2.2.1. The functions $f_{c_D} = c_D/c_{D0}$ and $f_{\alpha_r} = \alpha_r/\alpha_{r0}$ used in accounting for the influence of low steam densities on the resistance coefficient and heat-transfer coefficient of a sphere. 1) Continuum flow; 2) slip flow; 3) transition flow; 4) free molecular flow; 5) Equation; 6) from.

For small Reynolds numbers ($Re_r < 1$), therefore, we calculate with

$$c_D = \frac{24}{Re_r} \frac{1}{1 + 2,53 \text{ Kn}} \quad (31)$$

and

$$\alpha_r = \frac{\lambda_d}{r} \frac{1}{1 + 3,18 Kn} \quad (32)$$

respectively. For large Reynolds numbers, the density effect is generally slight when water droplets are present in the turbine (since the Knudsen numbers are small), so that we can simply employ Eqs. (15) and (16).

In conclusion, we must make reference to yet another effect. All of the formulas just presented apply for the case in which the flow medium is moving past the sphere. Due to condensation at the drop surface, however, a radial sink flow is superimposed on this circumferential flow. A thorough investigation was made to determine whether this disturbance due to condensation would be capable, under our conditions, of producing noteworthy changes in the c_D and α_r values. The result was again found to be negative for the case of small droplets, at which condensation is most vigorous; the influence of condensation never gives a change larger than 1 to 2%. This becomes understandable at once when we consider that the effect can arise only where α_r (and c_D) have already become considerable in magnitude.

We shall now introduce two quantities as a measure for the inertia of a droplet.

The mechanical inertia of the droplet can be characterized by a "deceleration time" Δt_{brems} . This is defined as

$$\Delta t_{\text{brems}} = - \frac{U_r}{\dot{c}_r}, \quad (33)$$

where $U_r = c_r - c$ is the relative velocity of the droplet with respect to the steam and \dot{c}_r is its instantaneous absolute acceleration. When the flow velocity c of the steam is constant, then \dot{c}_r is equal to the relative acceleration \dot{U}_r and, consequently, Δt_{brems} gives the time in which the droplet would reach the velocity of the steam ($U_r = 0$) if

its acceleration were to maintain this constant value. Newton's law for the droplet states that $m_r \dot{c}_r = -W$, where W is given by Eq. (1) and the drop mass m_r can also be expressed in terms of the radius. Thus we have from Eq. (33)

$$\Delta t_{\text{brems}} = \frac{8q_w r}{3q_d c_D U_r}, \quad (34)$$

For small Reynolds numbers, c_D is given by Eq. (31), which yields

$$\Delta t_{\text{brems}} = \frac{1 + \frac{1.271}{r}}{(9\mu_d/2q_w)} r^2 \quad (\text{for } Re_r \lesssim 1) \quad (35)$$

Equation (15) applies for our other important Reynolds-number range, i.e., for detached "large" droplets, and, accordingly,

$$\Delta t_{\text{brems}} = \frac{r^2}{(9\mu_d/2q_w)} \frac{2}{\sqrt{Re_r}} \quad (\text{for } 20 < Re_r < 800), \quad (36)$$

where, of course, we have not taken the influence of Knudsen number into account. The material quantities will be found in Diagram III of the Appendix.

The thermal inertia of the drop can be characterized in a quite similar manner by a "cooling time" Δt_{abk} . We obtain a definition for it by replacing the relative velocity by the excess temperature and the acceleration by the heating rate in Eq. (33). Thus we write

$$\Delta t_{\text{abk}} = - \frac{T_r - T_d}{\dot{T}_r}. \quad (37)$$

Newton's law is supplanted by the cooling formula $c_w m_r \dot{T}_r = \dot{Q}$, where the dissipated heat \dot{Q} is given by Eq. (2). In analogy to Eq. (34), it follows from this that

$$\Delta t_{\text{abk}} = \frac{q_w c_w r}{3\alpha_r}. \quad (38)$$

For small Reynolds numbers, it assumes, with Eq. (32), the form

$$\Delta t_{abk} = \frac{1 + \frac{1.59 I}{r}}{(3\lambda_d / \rho_w c_w)} r^2 \text{ (for } Re_r \lesssim 1) \quad (39)$$

and for somewhat larger Reynolds number, with Eq. (16), the form

$$\Delta t_{abk} = \frac{r^2}{(3\lambda_d / \rho_w c_w)} \frac{1}{3.3 \sqrt{Re_r}} \text{ (for } 20 < Re_r < 800), \quad (40)$$

where the influence of the Knudsen number has again been disregarded. For the material quantities, see Diagram III in the Appendix.

As an example, let us calculate the deceleration and cooling times from Eqs. (35) and (39), respectively, for certain droplet sizes in saturated steam at $p = 0.12$ bar. The values apply for drops that, for all practical purposes, flow with the steam ($U_r \approx 0$). For comparison, we list in parentheses the corresponding values for $U_r = 200$ m/sec, in case this assumption has resulted in Reynolds numbers within the range of validity of Eqs. (36) or (40).

TABLE 2.2.1

r	m	10^{-8}	10^{-7}	10^{-6}	10^{-5}	10^{-4}
Δt_{brems}^1	sec	$1.4 \cdot 10^{-7}$	$1.5 \cdot 10^{-6}$	$3.2 \cdot 10^{-5}$	$2.0 \cdot 10^{-3}$ ($0.7 \cdot 10^{-3}$)	0.190 (0.022)
Δt_{abk}^2	sec	$6.2 \cdot 10^{-7}$	$6.8 \cdot 10^{-6}$	$1.3 \cdot 10^{-4}$	$7.5 \cdot 10^{-3}$ ($3.9 \cdot 10^{-3}$)	0.69 (0.12)

1) Deceleration; 2) cooling.

Inertial effects may be expected for drops whose inertia times are comparable with the flow times. The steam requires about $5 \cdot 10^{-4}$ second to flow through a bucket ring; in rough approximation, therefore, we can state that the inertia effects become significant only at $r \gtrsim 10^{-6}$ m. It will be seen from the data that the thermal inertia of a droplet is somewhat larger than its mechanical inertia.

2.3. THE PHYSICAL BEHAVIOR OF THE STEAM IN THE WET-STEAM REGION

a) Supersaturation and Supercooling

Left to itself, a system containing two phases of the same sub-

stance will tend toward a state of equilibrium. A constant temperature ("saturation temperature") and a constant pressure ("saturation pressure") will prevail everywhere in the system at this so-called thermodynamic equilibrium. A fixed relationship obtains between these two quantities, although it does differ from substance to substance ("vapor-pressure curve"). This can be indicated in the form

$$T_s = T_s(p) \text{ OR } p_s = p_s(T), \quad (1)$$

according to whether we imagine the pressure or the temperature to be given.

In the case of condensation, the heat of condensation that is continuously liberated at those surfaces on which the steam is deposited must also be continuously withdrawn. If that were not the case, heating of the surfaces would occur, so that further condensation would be impeded. If dissipation of the heat to the outside is not possible, it must be taken up by the steam phase, for which purpose the latter must be cooler than the condensation surfaces. The rate of condensation is determined by the efficiency of the heat-transfer process.

If initially superheated steam reaches the saturated state during expansion, say in a turbine or a nozzle, the only surfaces then remaining for condensation are those presented by the fixed linings and any dust particles that may be suspended in the steam. As will be shown in Section 2.4, however, the condensation accomplished here is so slight that no noticeable quantities of water are deposited. In practice, the steam expands further as though no water at all were being condensed and thus enters an unstable state. These unstable states are characterized by failure of the pressure and temperature to follow the fixed relationship given in Eq. (1) even though the saturation point has already been passed. Instead, the steam pressure p is higher than the saturation pressure $p_s(T_d)$ corresponding to the steam temperature T_d

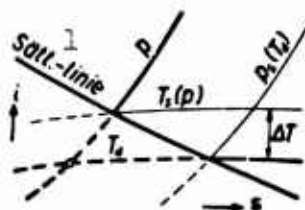


Fig. 2.3.1. Illustrating definition of supersaturation and supercooling. 1) Saturation line.

or, expressed in terms of temperatures, the steam temperature is lower than the saturation temperature $T_s(p)$ corresponding to the steam pressure; cf. Fig. 1.

As a measure of the deviation of such an unstable state from thermodynamic equilibrium, we use the so-called supersaturation Π , which indicates the ratio of the steam pressure to the saturation pressure corresponding to the steam temperature:

$$\Pi = \frac{p}{p_s(T_d)} . \quad (2)$$

We shall also frequently have recourse to its logarithm, the "logarithmic supersaturation" Λ :

$$\Lambda = \ln \Pi = \ln \frac{p}{p_s(T_d)} . \quad (3)$$

However, we might just as well characterize such a state by the supercooling. This is defined as the difference between the saturation temperature and the actual steam temperature:

$$\Delta T = T_s(p) - T_d . \quad (4)$$

The following simple relationship obtains between supersaturation and supercooling. Let us write the Taylor expansion of the pressure curve given by Eq. (1) for the pressure $p = p_b$:

$$T_s(p) = T_s(p_b) + \left. \frac{dT_s}{d \ln p} \right|_{p_b} \cdot \lambda + \frac{1}{2} \left. \frac{d^2 T_s}{(d \ln p)^2} \right|_{p_b} \cdot \lambda^2 + \dots , \quad (5)$$

where

$$\lambda = \ln \frac{p}{p_b} .$$

$T_s(p_b)$ and the other coefficients are material quantities. If we now select the reference pressure such that $p_b = p_s(T_d)$, then $\lambda = \Lambda$, so that

$$T_s(p) = T_d + \left. \frac{dT_s}{d \ln p} \right|_{p_s(T_d)} \cdot \Lambda + \frac{1}{2} \left. \frac{d^2 T_s}{(d \ln p)^2} \right|_{p_s(T_d)} \cdot \Lambda^2 + \dots$$

From this, using the abbreviated notation

$$K = K(T_d, \Lambda) \equiv \frac{1}{T_d} \left(\left. \frac{dT_s}{d \ln p} \right|_{p_s(T_d)} + \frac{1}{2} \left. \frac{d^2 T_s}{(d \ln p)^2} \right|_{p_s(T_d)} \cdot \Lambda + \dots \right), \quad (6)$$

we obtain the relationship that we seek:

$$\Delta T = K T_d \Lambda = K T_d \ln \Pi. \quad (7)$$

This relationship will be used often in the calculations to follow.

The function K is plotted in Diagram II (see Appendix).

By selecting $p_b = p$, we arrive in a quite similar manner at the conversion factor $K(p, \Lambda)$, which is represented in Diagram I. Then it is preferable to calculate ΔT from the formula

$$\Delta T = T_s(p) \frac{K \Lambda}{1 + K \Lambda} \quad (8)$$

which is obtained by elimination of T_d from Eq. (7) by application of Eq. (4).

Whether we use Eq. (7) or Eq. (8) will depend on whether T_d or p is given.

b) i,s-Diagram for Fully Supercooled Steam

The attached i,s-table (see Appendix) represents a supplement to the familiar diagram of Dzung and Rohrbach (see [18]) for the case in which the steam acquires a dry-supercooled state in a certain zone below the saturation line.

Normally, that boundary in an i,s-diagram at which supercooling collapses as a result of spontaneous condensation of the steam is known as the "Wilson line," and drawn approximately parallel to the $x = \text{const}$ lines. It has, however, been widely recognized (cf., for example, [19], [20], [3]) that we are not dealing here with a fixed boundary and that the condensation may take place sooner or later, de-

pending on conditions. Here the rapidity of the pressure drop at the point where condensation intervenes is the governing factor. The method developed in [45] (cf. also Section 2.5d in this connection) offers a means of taking this effect into account mathematically.

The position of the Wilson point was determined mathematically for several parallel-displaced expansion lines as a function of the expansion rate \dot{P} . The Wilson lines sought are then obtained by joining the Wilson points corresponding to the same \dot{P} . For Wilson chambers and the like, we have in approximation $\dot{P} = 10$, for turbine stages $\dot{P} = 500$ to 5000, and for short Laval nozzles 1000 to 10,000 and even higher. The course taken by the lines is in very good agreement with the results of the carefully conducted measurements of Binnie and Woods [21].

Although the thermodynamic equilibrium produced beyond the Wilson point in the expanded steam is not perfect, there is nevertheless an approximate equilibrium. For this reason, the conditions applying for thermodynamic equilibrium in that part of the diagram that lies below the Wilson lines are presented in exactly the same way as is done ordinarily. The two families of curves overlap in the region of the various Wilson lines, since, after all, transition from one to the other takes place at different positions for expansions that occur with different speeds.

c) Behavior of Small Water Droplets in Steam

Thermodynamically, there is an essential difference between a curved water surface, as presented by the surface of a droplet, and a flat surface, such as may be formed on the linings and larger foreign objects. The difference stems from the fact that the sharper the curvature of the surface, the weaker will be the resultant intramolecular attractive force that holds a molecule in the surface layer. The practical consequence of this is that a droplet can persist only in an at-

mosphere of supersaturated steam and, the smaller the droplet, the greater must be the extent of this supersaturation.

The magnitude of this supersaturation necessary for stability of a droplet of radius r , Π_r , is given by the so-called Thomson formula:³²⁾

$$\ln \Pi_r = \frac{2\sigma}{\rho'RT} \cdot \frac{1}{r}. \quad (9)$$

Here, σ is the surface tension and ρ' is the density of the water; R is the specific gas constant of the steam. An everywhere uniform temperature T was assumed in this derivation. The quantity $2\sigma/\rho'RT$ is plotted in Diagram II (Appendix) as a function of temperature.

If we substitute numerical values, we see that this supersaturation becomes pronounced only for very small droplets. For example, the table below applies for $T = 30^\circ\text{C}$.

TABLE 2.3.1

r (Meter)	∞	10^{-3}	10^{-4}	10^{-5}	10^{-6}	10^{-7}	10^{-8}	10^{-9}
Π_r	1	1,00000	1,00001	1,00010	1,00100	1,01005	1,105	2,72
ΔT_r °C	0	0,000	0,000	0,002	0,017	0,17	1,7	17

A) Meters.

It is assumed in deriving the Thomson formula that the surface tension has the same value for quite small water droplets consisting of a few molecules as for a flat water surface. Although this assumption is definitely unjustified, we do not to this day have any definite information concerning the variation of σ with r . There is not even agreement as to whether the value of σ to be inserted in Eq. (9) is smaller or larger for small drops than the value that can be established for flat surfaces. In the present study we shall circumvent this problem — for want of a well-based theory — in the following manner. Spontaneous droplet formation in supercooled steam has been traced carefully by various authors, usually by means of nozzle experiments (see Section 2.5).

Within the framework of the present study, certain experiments of this type were recalculated assuming various $\sigma(r)$ relationships, keeping for subsequent calculations that function $\sigma(r)$ that resulted in the best agreement between calculation and experiment. The assumption of radius-independent surface tension turned out the best. In all cases to follow, therefore, we shall assume that

$$\sigma = \text{independent of } r = \sigma(T).$$

The dependence on temperature is weak; see Diagram II in the Appendix.

We may draw two important conclusions from Eq. (9). Instead of beginning with the temperature and inquiring after supersaturation, we can proceed from the pressure in the surroundings and inquire as to the maximum temperature T_r that a droplet of radius r can acquire and still just be able to exist. This must lie below the saturation temperature. The magnitude of the deviation, which we should like to call the "capillary supercooling" ΔT_r , follows from Eq. (9) and Eq. (7) ³³)

$$\Delta T_r = T_s(p) - T_r = KT_r \left(\frac{2\sigma}{\rho'RT_r} \right)^{\frac{1}{2}}. \quad (10)$$

Certain values of ΔT_r are entered in Table 1. We shall incur no major error if we substitute the numerical values for both K and $2\sigma/\rho'RT_r$ at $T_s(p)$ instead of those at T_r . These can be read from Diagram I at the pressure p .

The temperature

$$T_r = T_s(p) - KT_r \left(\frac{2\sigma}{\rho'RT_r} \right)^{\frac{1}{2}} \approx T_s(p) - KT_s \left(\frac{2\sigma}{\rho'RT_s} \right)^{\frac{1}{2}} \quad (11)$$

has the same meaning for a droplet as the saturation temperature T_s has for a flat water surface. A flat water surface in contact with a steam (vapor) atmosphere at pressure p always tends to the temperature $T_s(p)$, by either condensation or evaporation. In the same manner, a droplet tends to hold its surface temperature at T_r . If this temperature has been reached, further mass exchange between the droplet and

the vapor, such as condensation on the droplet, can take place only provided that the condensation heat liberated is withdrawn from the droplet. If that were not the case, the temperature of the droplet would rise above T_r ; then, however, it is no longer capable of existence in the vapor atmosphere concerned, begins to evaporate, and loses mass until it has been cooled back to T_r by the evaporation heat that has been withdrawn. For this purpose, however, exactly as much must evaporate as had been condensed in excess, i.e., the rate of condensation is dictated by the heat-transfer.

Consequently, in continuous condensation on the droplet, the vapor must have a temperature lower than that of the droplet, so that the temperature distribution represented in Fig. 2 prevails. Here, the effective supercooling

$$\Delta T_{\text{eff}} = T_r - T_d \quad (12)$$

is decisive for heat transfer and, consequently, for the vigor of the condensation.³⁴ Thus the total supercooling of the steam ΔT is

$$\Delta T = \Delta T_r + \Delta T_{\text{eff}}, \quad (13)$$

as will be seen from Fig. 2.

If \dot{m}_r denotes the quantity of vapor that condenses on a droplet per second, then $\dot{m}_r L$ is the heat of condensation liberated each second, and the latter must be equal to the heat \dot{Q} that can be taken away by heat transfer. From this it follows, if we use Eq. 2.2(2) for \dot{Q} , that

$$\dot{m}_r = \frac{\dot{Q}}{L} = \frac{\alpha_r (4\pi r^2) (T_r - T_d)}{L}. \quad (14)$$

The heat-transfer coeff. α_r is given by Eq. 2.2(32). Equation (14) has two omissions: the adiabatic boundary-layer temperature has been replaced by the vapor temperature T_d , and it was tacitly assumed that the entire heat of condensation L is liberated even when the vapor condenses not on a flat surface, but on a small droplet. The former is al-

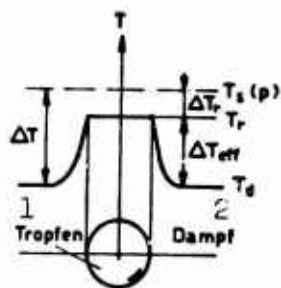


Fig. 2.3.2. Temperature conditions in heat transfer from a water droplet to the surrounding supercooled steam (the pressure p prevails in the vapor space). 1) Droplet; 2) vapor.

ways admissible for small droplets, since their velocities relative to the steam never become too high. As for the latter omission, a somewhat smaller amount of heat is liberated in actuality, since the enlargement of the droplet surface by the newly acquired water appropriates part of the heat of condensation for its own work against surface tension. However, this correction is vanishingly small for all drop sizes with which we shall have to deal.

The second conclusion from Eq. (9) leads us to the concept of critical droplet radius. If a supersaturated vapor atmosphere is assigned, we can use the Thomson formula, Eq. (9), to indicate that droplet size which is just stable in the vapor:

$$r_{\text{crit}} = \frac{2\sigma}{\rho RT_d} \frac{1}{\Delta T} \quad (15)$$

The adjective "critical" stems from the fact that larger droplets are inclined to grow further, while smaller droplets tend to vanish, since their surfaces acquire temperatures higher or lower than T_d and they can therefore give up heat to the vapor continuously or absorb heat from it continuously. The fact that droplets of subcritical sizes can also form ephemerally in the vapor, and some of them even reach supercritical size, is to be attributed solely to the disordered thermal motion of the molecules, which leads to accidental formation of such stuck-together molecule groups or droplets. We shall pursue this further in Section 2.5.

d) Steam with Fog Droplets

Once supercooling has collapsed, small water droplets, distributed uniformly everywhere and owing their existence to spontaneous condensa-

tion, remain suspended in the steam. They are not all of the same size, but have sizes scattered between such narrow limits that it is permissible to regard them as droplets of uniform size. In general, their diameters lie heavily concentrated below $1 \mu = 10^{-6}$ m. We shall refer to them as fog droplets, in contrast to the considerably larger drops that may form by, for example, shattering of collected water masses. This usage reflects both the mode of formation and the external appearance of these steam-water mixtures.

Even though the fog droplets incorporate only a small part (say, 2 to 4%) of the total original quantity of steam, they do present a considerable surface. This is compounded by the fact that the heat-transfer coefficients for such small drops are extraordinarily high. For the most part, therefore, the fog is usually capable, without requiring large temperature differences between the droplets and the steam, to condense onto itself the amount of water that is continuously becoming due for precipitation during the course of further expansion in the turbine or nozzle. The following example can be cited as an illustration.

Let $y = 0.04 = 4\%$ of the steam be in the form of fog droplets with a radius $r = 0.2 \mu = 2 \cdot 10^{-7}$ m. Let us assume the values $p = 0.2$ bar $= 2 \cdot 10^4$ N[Newtons]/m² and $T_d = 60^\circ\text{C}$ for the pressure and steam temperature. The number of droplets in a total quantity of 1 kg is then, with $\rho' = 10^3$ kg/m³, $n = 3y/4\pi r^3 \rho' = 12.0 \cdot 10^{14}$ kg⁻¹ and their total surface area $A = n \cdot 4\pi r^2 = 600$ m²/kg. The heat-transfer coefficient can be determined on the basis provided in Section 2.2. Let us read the mean free path $\bar{l} \approx \bar{l}_g(p)$ from Diagram I and use it to determine the Knudsen number $\text{Kn} = \bar{l}/2r \approx 0.87$; then we shall see that we are concerned with a so-called transition flow past the droplet. α_r is computed from Eq. 2.2(32) (while the relative velocity is very small between such small

drops and the steam): $\alpha_r = \lambda_d / r(1 + 3.18 Kn) = 27,000 \text{ J/m}^2 \text{ } ^\circ\text{K-sec}$. Let us assume further that the expansion proceeds with such rapidity that $\dot{y} = 20 \text{ kg/kg-sec}$ of new water condenses each second, which will be approximately in accordance with conditions in turbines. Thus we obtain the value $\Delta T_{\text{eff}} = \dot{y}L / \alpha_r A = 2.9^\circ\text{C}$ for the effective temperature difference that is necessary to permit surrender of condensation heat by the droplets to the steam. With a supercooling of this magnitude, it is still permissible to treat the steam as though it were at thermodynamic equilibrium. (At most, we could still verify whether the capillary effect causes no essential increase in the required supercooling. According to Eq. (10), with $K = 0.065$, we get $\Delta T_r = (2\sigma / RT_r \rho') KT_d / r \approx 0.09^\circ\text{C}$; thus the more exact supercooling value is $\Delta T = \Delta T_{\text{eff}} + \Delta T_r \approx 3.0^\circ\text{C}$.)

If, in addition to the fog droplets, the expanding steam also contains other bodies that offer condensation surfaces (such as larger water drops, wall linings, etc.), part of the condensation will take place at these surfaces. The product αA is, however, decisive for the effectiveness of a surface of area A ; the secondary condensation surfaces in turbines and the like can at most reach the same order of magnitude as the surface area of the fog droplets. Their heat-transfer coefficients are, however, all of 50 to 100 times smaller than those of the fog droplets. For this reason, we may disregard their share in the condensation, provided that fog droplets are also present in sufficient numbers.

Below we must further discuss how it is possible to treat steam whose supercooling is small but not small enough to be disregarded (i.e., lies between, say, 3 and 15°C) on the basis of an i,s-table for thermodynamic equilibrium.

The deviations of the supercooled steam from the saturated steam at thermodynamic equilibrium arise in part from the fact that less

Suppose that we are given an enthalpy \underline{i} and an entropy \underline{s} that determine a point in the i,s -diagram that lies in the wet-steam region. From the diagram, we can read a moisture value $y_{\infty} \equiv 1 - x_{\infty}$, but this will be valid only when both the steam and the water are at the saturation temperature. If, on the other hand, the steam is supercooled by $\Delta T^{\circ}\text{C}$, then a different moisture content $y < y_{\infty}$ will correspond to the point of the i,s -diagram given by \underline{i} and \underline{s} . To determine the specific moisture deficiency

$$\Delta y = y_m - y \quad (16)$$

let us assume that the pressure lines in the i, s -diagram for super-cooled steam and in the corresponding diagram for steam at equilibrium

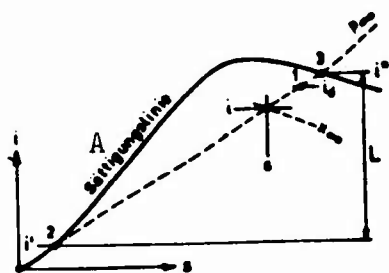


Fig. 2.3.3. Illustrating derivation of moisture deficiency. . A) Saturation line.

coincide, which will be a good approximation

for moderate supercooling values ΔT . Then the supercooled mixture in Fig. 3 is composed of $x = 1 - y$ kg of steam in state 1 and y kg of water in state 2 (saturated).

In the case of thermodynamic equilibrium, the mixture consists of $x_\infty = 1 - y_\infty$ kg of state 3 steam (saturated) and of y_∞ kg of

state 2 water. Both lead us to the same 1 (and, within the framework of the approximation, to the same s as well). Thus we may write

$$(1 - y) i_d + y i' = 1 = (1 - y_{\infty}) i'' + y_{\infty} i' . \quad (17)$$

Now, however,

$$i_d = i'' - c_p \Delta T, \quad (18)$$

so that

$$i'' - y i'' - (1 - y) c_p \Delta T + y i' = i'' - y_{\infty} i'' + y_{\infty} i'.$$

Using Eq. (16) and $i'' - i' = L$, this results in the moisture deficiency

$$\Delta y = \frac{c_p}{L} x \cdot \Delta T, \quad (19)$$

where we set $x \approx x_{\infty}$ for full supercooling $x = 1$ and supercooled wet steam. For pressures below 10 bars, we can take $c_p/L \approx \text{const} = 8 \cdot 10^{-4} \text{ K}^{-1}$. Thus, we can determine how much less moisture there is in the supercooled steam than is indicated by the value $x_{\infty} = 1 - y_{\infty}$ taken from the conventional i, s -diagram. If, for example, $x_{\infty} = 0.90$, $\Delta T = 20^{\circ}$ and the steam is wet, we obtain $\Delta y = 0.014$; instead of 10%, only 8.6% of moisture is present. (An exact derivation of Δy , which would also take into account the difference between the isobars, would result in a formula similar to (19), but the only thing new would be a correction factor that tends to unity for small ΔT . Nevertheless, the exact value of Δy , even for $\Delta T = 20^{\circ}\text{C}$, is larger only by a factor of 1.05 to 1.07 than that calculated from Eq. (19) — 1.05 applying at about 0.2 bar and 1.07 at about 20 bars —, so that the accuracy of Eq. (19) is quite sufficient for our purposes.)

We are now in a position to indicate the specific volume of the steam-water mixture characterized by i, s and ΔT . If the pressure p_{∞} and the specific volume v_{∞} correspond to the state i, s in the case of thermodynamic equilibrium, the following will apply for the volume v at a supercooling ΔT :

$$v = x v_d + y \cdot v'(p) \approx x v_d \approx (x_{\infty} + \Delta y) v'' \frac{T_d}{T_s}. \quad (20)$$

If we apply Eq. (19) and set $T_d = T_s - \Delta T$ and $v_{\infty} \approx x_{\infty} v''$, we get

$$v = v_{\infty} \left[1 - \Delta T \left(\frac{1}{T_s} - \frac{c_p}{L} \right) \right]. \quad (21)$$

The expression in parentheses is presented as a function of pressure in Diagram I; ΔT , \underline{i} and \underline{s} is [sic] assumed given and v_{∞} is read from the i, s -table. At low pressures and $\Delta T = 20^{\circ}\text{C}$, the correction comes to about 5%.

However, even the pressure p_{∞} will require a correction on closer examination. The true pressure p corresponding to the state described by \underline{i} , \underline{s} and ΔT is smaller by an amount Δp than the pressure p_{∞} read from the i, s -diagram for equilibrium:

$$p = p_{\infty} - \Delta p, \quad (22)$$

and we have for Δp

$$\frac{\Delta p}{p_{\infty}} = \frac{\gamma}{2(\gamma-1)} \left[\frac{\Delta T}{T_s(p_{\infty})} \right]^2. \quad (23)$$

This correction rests on the fact that pressure lines other than those entered in the equilibrium diagram apply for supercooled steam. For this reason Formula (23) cannot be derived in the same simple manner as Eq. (19), but only on the basis of more exact assumptions. We shall omit this derivation, the more so because $\Delta p/p_{\infty}$ is small as compared to the other corrections (it comes to about 0.9% with $p_{\infty} = 0.2$ bar and $\Delta T = 20^{\circ}\text{C}$).

Summing up: Eqs. (19), (21) and (23) enable us to compute the moisture content, volume and pressure of the supercooled steam-water mixture whose supercooling ΔT is known, working from its enthalpy \underline{i} and entropy \underline{s} as given in a conventional i, s -diagram.

2.4. THE FIRST APPEARANCE OF WATER IN THE TURBINE: CONDENSATION ON THE BLADES

It is known from experiments with Laval nozzles that if the state of expanded pure steam crosses the saturation line, it is at first supercooled, and that as soon as its supercooling has reached a certain

level (30 to 40°C), it collapses suddenly, since the steam condenses spontaneously in the form of fog droplets. In nozzles, no condensation occurs before the point at which this fog forms, since the boundary layer is superheated everywhere on the nozzle walls. The situation is somewhat different in turbines, since the boundary-layer temperature of the successive **blade** rows becomes progressively lower. It was recognized by Traupel [22] that this makes it possible for water to condense on the surface of turbine buckets before spontaneous condensation sets in in the steam itself. The dust particles present in the flowing steam lead to a similar phenomenon.

We shall refer to this water precipitation that arises prior to fogging as "precondensation" and concern ourselves in this Section with the question as to the surfaces on which it takes place and its intensity. In part, the material to follow is a more explicit repetition of the calculations described in [22], but it does reach the conclusion that precondensation has no noticeable influence on the processes in a wet-steam turbine.

a) Where Can Precondensation Take Place?

As we know, condensation intervenes on all solid surfaces in contact with the steam as soon as the steam's state has crossed the saturation line. To this statement we must, however, append two important remarks: first, the curvature of these surfaces may not be so sharp that they give rise to a noticeable capillary effect. For this, their radius of curvature must, according to Table 2.3.1, be larger than about 10^{-7} m = 0.1 μ ; this condition is satisfied both for the design elements of the machine and for most of the dust particles that may, under certain circumstances, be present in the steam. Secondly, these surfaces must not be so severely heated that their temperature even without condensation is equal to or higher than the saturation tempera-

ture corresponding to the pressure of the surrounding steam. Heating such as this is also presented by boundary-layer friction, by which, as we know, all bodies in stream are heated to an adiabatic boundary-layer temperature T_{GS} higher than the static temperature of the medium flowing past them.

Precondensation is conceivable on two types of foreign surfaces: the surfaces bounding the flow (blades, casing linings) and on the surfaces of the dust and salt particles present in the steam. We shall concern ourselves first with the latter.

As concerns the dust particles, it has been shown by Oswatitsch for the case in which the flow medium is atmospheric air (wind tunnels) that the dust particles do not represent a factor in condensation of the atmospheric humidity. We are still further justified in disregarding them in our discussions of steam turbines, firstly because the steam in modern steam installations is much cleaner than the atmospheric air and, secondly, because the amount of condensation occurring per unit volume in the case of pure steam is much greater than for a lean steam-air mixture.

There is somewhat more to be said concerning the salt dust that today probably represents the only significant impurity encountered in steam installations. In modern installations, the salt content of the steam totals about 1 to 3 mg/kg. At high pressures and temperatures (live steam!), the solubility of the salts in steam is a multiple of this value (the solubility of NaCl in saturated or superheated steam at 150 bars is about 40 mg/kg). We can therefore expect that all salt entering the steam in the boiler - for the most part, in the form of a fine dust - will be completely dissolved on the path to the turbine (in this connection, compare Hömig [23], page 143). Although this salt-steam solution can become supersaturated during subsequent expansion

in the turbine, since its solubility is dropping, the concentration of the salt molecules is nevertheless so infinitesimally small (one salt molecule to 10^6 steam molecules) that formation of salt crystals containing numerous molecules is completely inconceivable. Thus the salt is not at all in a position to present a surface for condensation of the steam. At any rate, the part of the salt precipitated on the bucket surfaces will be small, as is seen on inspection of the salt crust on the buckets of the low-pressure section. The major part of the salt remains in dissolved form all the way to the condenser, where it enters the condensate.

It follows from the above considerations that apart from the surfaces bounding the flow, there is practically no surface available for precondensation. As concerns the effectiveness of the bounding surfaces, this depends on how rapidly they are capable of yielding the liberated heat of condensation. Let us first investigate whether the transfer of heat to the supercooled steam flowing by or heat conduction through the metal to the exterior is more important.

The products of heat-transfer coefficient by temperature difference are decisive for the quantities of heat conducted away from a given surface in various directions. The heat-transfer coefficient α_{inward} [α_{innen}] valid for heat transfer to the flowing steam can be estimated by reference to Eq. (3) and Fig. 5. With the low values $St = 0.002$ and $(c_p \rho_d U) = 1 \cdot 10^5 \text{ J/m}^2 \text{Ksec}$, we get $\alpha_{\text{inward}} \approx 200 \text{ J/m}^2 \text{Ksec}$; further, $\Delta T_{\text{eff}} = T_s - T_{\text{GS}}$ may amount to about 15°K . Thus the product comes at a minimum to $(\alpha_{\text{inward}} \cdot \Delta T_{\text{eff}}) \approx 3000 \text{ J/m}^2 \text{sec}$. The heat-transfer rate outward is primarily determined by what the outer casing surface is in contact with - i.e., it depends on the design of the turbine. If the steam rinsing the outer surface of the channel wall is at a temperature higher than that of the inner-surface boundary layer, or if

approximately the same temperature prevails outside (steam from the next tapping point), practically no heat at all will be conducted outward, and some heat may even flow in. If, on the other hand, the channel liner is in contact with waste steam or — a rarer case — with the external air, we have a temperature gradient worthy of note. In this case, however, the heat-transfer conditions are very poor on the outside, since the density is low in the former case and the flow velocity (free convection!) in the latter. The following may serve as an estimate: outside temperature of the waste steam or air 30°C , with $\Delta T_{\text{total}} = 90 - 30 = 60^{\circ}\text{C}$; outward heat transfer coefficient* $\alpha_{\text{outward}} [\alpha_{\text{aussen}}] \approx 10 \text{ J/m}^2\text{K sec}$ ($\approx 9 \text{ kcal/m}^2\text{-hour}^{\circ}\text{C}$); wall thickness $\delta = 5 \text{ cm} = 0.05 \text{ m}$, heat-transfer coefficient $\lambda_{\text{steel}} [\lambda_{\text{Stahl}}] = 50 \text{ J/mKsec}$, from which we may calculate the resultant heat-passage coefficient α_{res} . We have $1/\alpha_{\text{res}} = 1/\alpha_{\text{outward}} + \delta/\lambda_{\text{steel}} = 0.101$ and $\alpha_{\text{res}} \approx 10$. Thus the determining product will be $(\alpha_{\text{res}} \cdot \Delta T_{\text{total}}) = 10 \cdot 60 = 600 \text{ J/m}^2\text{sec}$.

Thus we find that at least five times as much heat goes over to the steam as flows outward through the wall. For the buckets, there is an additional throttling down of the heat flow in the neck of the bucket, and in the case of the runner buckets, there is no heat conduction outward anyway. Thus we shall incur no major error if we regard the walls of low-pressure turbines as impervious to heat and compute the rate of condensation from the heat transfer to the steam alone.

The adiabatic boundary-layer temperature of a bucket (for example, of a runner bucket) is

$$T_{\text{Gs}} = (T_d)_1 + \sqrt[3]{\text{Pr}} \frac{w_1^2}{2c_p} \quad (1)$$

for detachment-free flow. (For a guide bucket, $(T_d)_1$ is to be replaced accordingly by $(T_d)_0$ and w_1 by c_0 .) Figures 1 and 2 present the steam

states that arise in the bucket boundary layers of the individual rings of the two turbines laid out in Section 2.1 — in much the same way as was done in the cited work of Traupel — and we shall refer to these in our subsequent discussion of conditions.

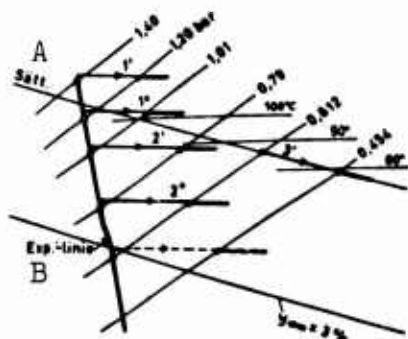


Fig. 2.4.1. States of the steam in various bucket boundary layers of our reaction-type turbine. A) Saturation line; B) expansion line.

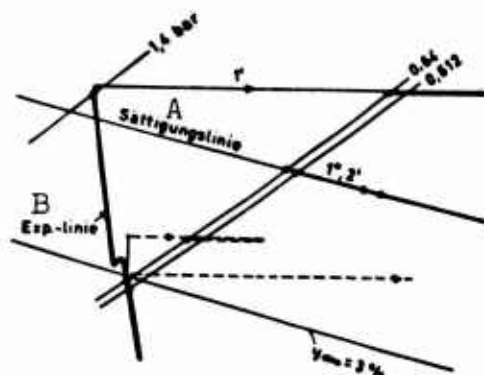


Fig. 2.4.2. States of steam in various bucket boundary layers of our impulse-type turbine. A) Saturation line; B) expansion line.

Let us first discuss the high-pressure turbine with reference to Fig. 1. No condensation occurs in the guide wheel of the first stage (1'), since the entire boundary layer is superheated. In the subsequent runner wheel (1''), some condensation can occur only in the vicinity of the profile leading edge; otherwise, the boundary layer is superheated here as well. In wheels 2' and 2'', condensation takes place all along the length of the bucket contour. It is heavier in 2'' than in 2', since the supercooling of the steam is sharper here. In turbines, the spontaneous condensation mentioned earlier — the factor causing the supercooling to collapse — occurs approximately where the expansion line reaches the line $y_{\infty} = 2.5\%$ of theoretical wetness. In the majority of cases (concerning this, see also Sections 2.5 and 2.9), the steam is almost saturated from here on, so that the state of the steam component follows the saturation line rather closely. Figure 1 shows the state curve of the steam in bucket ring 3' for the ideal case; the state of

all fog in the boundary layer is indicated by the broken line. Practically no steam condenses on the buckets from this point on; the entire precipitated quantity of water is taken up by the fog drops, as has already been demonstrated in Section 2.3d.

In our constant-pressure turbine (cf. Fig. 2), nothing condenses in the first runner (1') because of boundary-layer heating. Nor is there any condensation on the profiles in the following runner 1" or thereafter, but this time because the supercooling has already collapsed as a result of spontaneous steam condensation. (In this case, of course, wide variations of the load on the turbine may change the pressure curve in such a way that spontaneous condensation takes place only farther downstream. Then precondensation may yet take place in ring 1" or perhaps even in 2'.)

To permit accounting for the condensation on a bucket not only in toto, but also in accordance with its local intensity, let us next carry out the boundary-layer calculations. At the same time, these will afford us an insight into the magnitude of the shearing stress that will also be helpful in investigating the motion of the water on the buckets (Section 2.7).

b) Boundary-Layer Calculations

The pressure or velocity curve over the entire profile contour must always be given for boundary-layer calculations. For each profile shape (and for each onflow angle), therefore, we should first determine the pressure curve, by measurement or, for example, with the aid of potential theory, to enable us to begin with calculation of the boundary-layer properties. Since, however, we are not interested here in the general nature of the boundary layers or in the behavior of a certain blade arrangement in a certain operating mode of a certain turbine, we can spare ourselves the first part of the calculation by ac-

cepting a pressure curve as near as possible to typical for use as an example. Here we can find a basis in various theoretical (such as [24]) and experimental (such as [25], [26]) studies. The pressure curve that

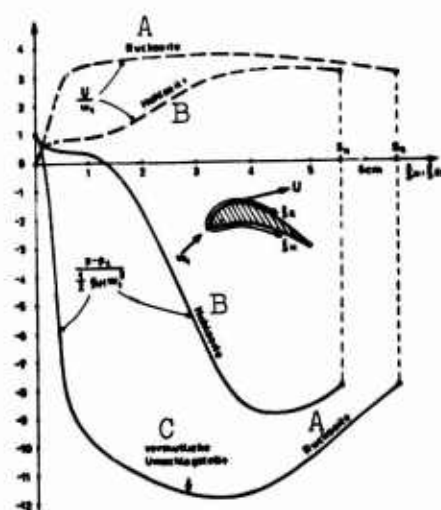


Fig. 2.4.3. Pressure curve over blade contour, taken as a basis for the boundary-layer calculations (cf. also Fig. 2.5.13a). The broken line indicates the corresponding velocity curve. A) Back; B) trough; C) hypothetical transition point.

we have selected for the following calculations is represented in Fig. 3. Its choice was based approximately on the profile shape in the second stage of the high-pressure turbine specified earlier.

The object of these boundary-layer calculations is to determine the curves of the wall shear stress τ and the heat-transfer coefficient α along the profile contour. As usual, we reduce these to dimensionless quantities on the basis of the formulas

$$\tau(\xi) = c_F(\xi) \cdot \frac{1}{2} \rho_{d1} w_1^2 \quad (2)$$

and

$$\alpha(\xi) = St(\xi) \cdot c_p \rho_{d1} w_1 \quad (3)$$

i.e., to the coefficient of friction c_F and the Stanton number St , for which the literature indicates various determination procedures. (Equations (2) and (3) are to be taken simultaneously as those defining c_F and St , respectively. For a stator profile, ρ_{d1} is to be replaced by ρ_{d0} and w_1 by c_0 .)

The calculation of c_F and St proceeds differently for laminar and turbulent boundary layers, and for this reason the nature of the boundary layer at the turbine bucket profiles must be made clear even before the calculation begins. If the flow onto the bucket wheel is only slightly turbulent (grid experiment!), the transition of the initially

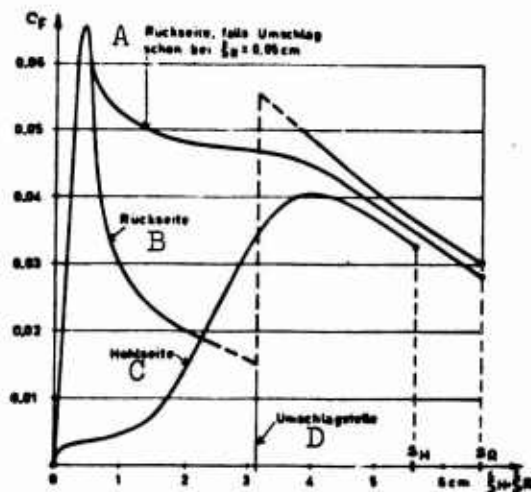


Fig. 2.4.4. Coefficient of friction in profile boundary layer (calculated for the pressure curve of Fig. 3). A) Back, case of transition as early as $\xi_R = 0.05$ cm; B) back; C) trough; D) transition point.

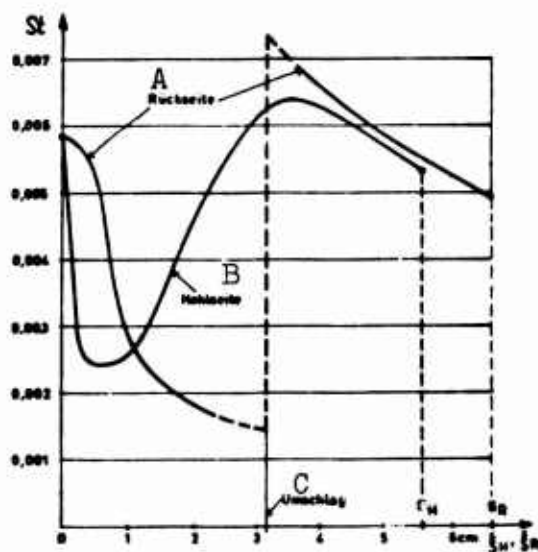


Fig. 2.4.5. Stanton number in profile boundary layer (calculated for the pressure curve of Fig. 3). A) Back; B) trough; C) transition.

laminar boundary layer into a turbulent one would take place only just prior to the point at which the pressure begins to rise again. (Such a case was investigated, for example, by Bammert in [27].) In turbo-

machines, however, the flow is so severely turbulent that the boundary layer has a tendency to make the transition far upstream and premature transition can be avoided only by means of a continuous sharp pressure drop. Figure 3 shows that this is the case on the back (suction side) of the buckets, but not on the trough (pressure) side; consequently, we must assume that the boundary layer on the trough is turbulent practically from the outset. As for the convex side, we assume that the turbulence of the flow is not capable of pushing the transition point far upstream; nevertheless, we shall carry through a calculation for the case in which the transition point lies upstream, since this situation could still come to pass as a result of a brutal disturbance effect (such as continuous impingement and rebounding of vagrant water droplets in bucket rings lying deeper inside the wet-steam region, cf. Section 2.8).

For the laminar part, the calculation procedure of Cohen and Reshotko [28] was followed. In the turbulent part, the c_F curve was computed by the method of Truckenbrodt (cf. [16], page 470ff) and the α -curve from c_F and the Reynolds analogy (cf. v. Kármán, [29]). The results of the calculations are presented in Figs. 4 and 5. Here, it was assumed that

$$Re_{Schl} = \frac{w_1 \varrho d_l \mu_{Schne}}{\mu_d} = 2,5 \cdot 10^5 \quad (4)$$

and

$$Pr_1 = \left(\frac{\mu_d c_p}{\lambda_d} \right)_1 = 1,2 \quad (5)$$

a condition well satisfied in stage 2 of our reaction-type turbine. The St values obtained are somewhat higher than those produced from grid experiments. The reason for this is probably that stronger turbulence was assumed here. While we shall not go into a more detailed interpretation of the shape of these curves, we should like to note that

both c_F and St also incorporate the direct influence of flow velocity U (cf. Fig. 3, velocity curves), since, indeed, the τ and α in Eqs. (2) and (3), respectively, were referred to the entry quantities.

c) Rate of Condensation on the Blades

From the equality of the amount of heat liberated and the amount withdrawn, we obtain the following equation for the amount of steam condensed per unit of area per unit of time on a blade:

$$\dot{m}_k(\xi) = \frac{\alpha(\xi)}{L} (T_{Schfl} - T_{GS}), \quad (6)$$

where L is the heat of evaporation, T_{Schfl} [T_{blade}] is the actual temperature of the blade (or that of the water film encasing it) and T_{GS} is the temperature that the blades would have in the absence of condensation.

The blade temperature adjusts everywhere to the local saturation temperature, i.e., $T_{Schfl} = T_s(\xi)$. Thus, applying Eq. (3), Eq. (6) assumes the form

$$\dot{m}_k(\xi) = \frac{c_p q_{dl} w_l}{L} \cdot St(\xi) [T_s(\xi) - T_{GS}] \quad (7)$$

where T_s can be computed from the pressure curve and T_{GS} from Eq. (1). From this local condensation rate \dot{m}_k we obtain $\dot{M}_{k,Schfl}$, the entire amount of steam condensing on a blade by integration for both sides of the blade:

$$\dot{M}_{k,Schfl} = l_{Schfl} \left[\int_0^{\xi_H} \dot{m}_k(\xi_H) d\xi_H + \int_0^{\xi_R} \dot{m}_k(\xi_R) d\xi_R \right]. \quad (8)$$

Here it has been assumed that the heat-transfer conditions are uniform over the entire length of the blade, an assumption, however, that would probably be met adequately for noncylindrical blades as well.

Let us now compute a "mass-exchange coefficient" that indicates what part of the steam quantity \dot{M}_d entering a given blade ring con-

denses on the blades of this ring. Evidently, this mass-exchange coefficient

$$\varepsilon_{d-f} = \frac{z \cdot \dot{M}_{k, Schl}}{\dot{M}_d}, \quad (9)$$

will differ sharply from ring to ring, primarily because the temperature jump evident in Eq. (7) may have widely different values. (The subscript to ε indicates that we are dealing with a transition from the vapor form to liquid water:) The smaller ε_{d-f} is found to be for turbines, the less significant will be the precondensation on the blades and, consequently, the more accurate will be the statement that the supercooling of the steam is not affected by precondensation.

Now, on the basis of Fig. 5 and Eqs. (7), (8) and (9), we can quickly carry through a rough calculation. We shall proceed from average values whose assumption we qualify with the note that the trailing part of the profile is more important for heat transfer. The temperature jump can be determined in a simple manner from Fig. 1; it is only necessary to read the temperature difference between the boundary-layer state and the saturation line. The average value of St follows from Fig. 5. We find for

$$\text{Ring 2': } \overline{T_s - T_{Gs}} \approx 6^\circ\text{C}, \quad \overline{St_H} \approx 0,005, \quad \overline{St_R} \approx 0,0045;$$

$$\text{Ring 2'': } \overline{T_s - T_{Gs}} \approx 20^\circ\text{C}, \quad \overline{St_H} \approx 0,005, \quad \overline{St_R} \approx 0,0045.$$

With $c_p/L = 8 \cdot 10^{-4} \text{ K}^{-1}$ and Table 2.1.1, we obtain (since $\rho_{dl} \approx 1/v_1$)

$$\frac{c_p \rho_{dl} w_1}{L} = \begin{cases} 0,044 \text{ kg/m}^2 \text{ Ksec} & (\text{for Ring 2'}) \\ 0,037 \text{ kg/m}^2 \text{ Ksec} & (\text{for Ring 2'')}, \end{cases}$$

from which it follows from Eq. (7) for

$$\begin{aligned} \text{Ring 2': } & \begin{cases} (\overline{\dot{m}_k})_H = 0,044 \cdot 0,005 \cdot 6 \approx 1,3 \cdot 10^{-3} \text{ kg/m}^2 \text{ sec} \\ (\overline{\dot{m}_k})_R = 0,044 \cdot 0,0045 \cdot 6 \approx 1,2 \cdot 10^{-3} \text{ kg/m}^2 \text{ sec} \end{cases} \\ \text{Ring 2'': } & \begin{cases} (\overline{\dot{m}_k})_H = 0,037 \cdot 0,005 \cdot 20 \approx 3,7 \cdot 10^{-3} \text{ kg/m}^2 \text{ sec} \\ (\overline{\dot{m}_k})_R = 0,037 \cdot 0,0045 \cdot 20 \approx 3,3 \cdot 10^{-3} \text{ kg/m}^2 \text{ sec} \end{cases} \end{aligned}$$

The integrals in Eq. (8) can now be calculated as \bar{m}_k times the contour length \underline{s} , so that Eqs. (8) and (9) are simplified to the form

$$\epsilon_{d-f} = \frac{z \cdot l_{\text{Schfl}} [(\bar{m}_k)_H \cdot s_H + (\bar{m}_k)_R \cdot s_R]}{\dot{M}_d} \quad (10)$$

The steam throughput is $\dot{M}_d = \dot{M} = 40 \text{ kg/sec}$ for Ring 2', since everything is still in vapor form here; for Ring 2'', we shall be able to determine it only after we find the reduction of the steam throughput as a result of condensation at Ring 2'. With Table 2.1.1, we obtain for the two rings of the reaction turbine, where precondensation occurs, i.e., for Ring 2':

$$\epsilon'_{d-f} = \frac{121 \cdot 0,157 [1,3 \cdot 0,057 + 1,2 \cdot 0,066] \cdot 10^{-3}}{40} = 0,000073 \quad (11)$$

and for Ring 2'':

$$\epsilon''_{d-f} = \frac{130 \cdot 0,177 [3,7 \cdot 0,057 + 3,3 \cdot 0,066] \cdot 10^{-3}}{(1 - 0,000073) \cdot 40} = 0,000247. \quad (12)$$

These mass-exchange coefficients are very small, so that only a vanishingly small part of the steam flowing through settles on the blades. This result can also be expressed by means of the steam content or water content y and compared with the ideal water content y_∞ , that which would have to be present at perfect thermodynamic equilibrium (according to Table 2.1.1):

after Ring 1''

$$x = 1, \quad y = 0; \quad y_\infty = 0,011. \quad (13)$$

after Ring 2'

$$x = (1 - 0,000073) = 0,999927, \quad y = 0,000073; \quad y_\infty = 0,022. \quad (14)$$

after Ring 2''

$$x = 0,999927 (1 - 0,000247) = 0,999680, \quad y = 0,000320; \quad y_\infty = 0,033. \quad (15)$$

According to the above, the amount of water y that actually condenses on the blades behind the second stage of the reaction-type turbine never amounts to more than 1% of the "expectation" y_∞ !

This water forms thin water veils or water filaments on the blades, and these are set in motion by friction with the steam and, on runner buckets, by centrifugal force. It will be shown in Section 2.7 that the flowing water is driven to the trailing edges of stator [guide] blades and strayed off these edges in the form of larger droplets, while on the runner buckets it moves almost entirely to the tip of the bucket and strays off from this point outward. Thus the water condensed on runner buckets is not capable of exerting further influence on condensation processes in the middle of the steam current. The droplets flung off the stator blades, however, remain in the steam flow, and further condensation can take place on their surfaces. Their average size is given by Eq. 2.8(6), which, applied to conditions in Stage 2, would read

$$r_g = \frac{9\sigma}{\epsilon_{dl} c_1^2} = \frac{9 \cdot 62 \cdot 10^{-3}}{0.49 \cdot 281.3^2} \approx 1.5 \cdot 10^{-5} \text{ m}. \quad (16)$$

To be able to calculate the extent of condensation on these droplets, we must know three things: their total surface area, the heat-transfer coefficient between them and the steam, and their time of residence in the steam. For every 1 kilogram of flowing steam, $y = 7.3 \cdot 10^{-5}$ kg of water is torn from Ring 2' according to Eq. (14). The surface area of the detached droplets formed from this water is

$$A_g = (4\pi r_g^2) \frac{3y}{4\pi \cdot r_g^3} = \frac{3y}{r_g} = 0.0146 \text{ m}^2. \quad (17)$$

As regards the heat-transfer coefficient $\alpha_{r,g}$, it is to be noted that the conditions of continuum flow prevail for the droplets (cf. Section 2.1), since $Kn = 1.0 \cdot 10^{-7} / 2 \cdot 1.5 \cdot 10^{-5} = 0.0033$. With a relative velocity $U_r = 220$ m/sec between the droplets and the steam, we obtain $Re_r = 270$ (with $\mu_d = 12 \cdot 10^{-6}$ kg/m·sec), so that Eq. 2.2(16) applies and gives us with $\lambda_d = 0.021$ J/m·Ksec

$$\alpha_{r,g} = 0,33 \sqrt{Re_r} \frac{\lambda_d}{F_g} = 7600 \text{ J/m}^2 \text{ Ksec} \quad (18)$$

The time of residence of a droplet in the steam up to the point at which it strikes a bucket of the next ring can likewise be estimated on the basis of Section 2.8. Figure 2.8.3 serves for estimation of the flight velocity, but first we must compute the value of the inertia parameter for the droplet in question. The "deceleration time" of the drops is found from Eq. 2.2(36) with $(9\mu_d/2\rho_w) = 6.0 \cdot 10^{-8} \text{ m}^2/\text{sec}$ as $\Delta t_{\text{brems}} [\Delta t_{\text{deceleration}}] = 4.6 \cdot 10^{-4} \text{ sec}$, so that the inertia parameter has the value $(\frac{1}{2}U_r \Delta t_{\text{brems}}) = 0.050 \text{ m}$. It will be seen from Fig. 2.8.3 that such droplets are accelerated very rapidly. If they travel a distance $\xi = 3 \text{ cm} = 0.03 \text{ m}$ before striking, they will be accelerated to about $0.5 c_1 \approx 140 \text{ m/sec}$. With 70 m/sec as the average velocity in flight, we obtain for the flight time

$$\Delta t_{\text{Flug}} \approx \frac{0,03}{70} \approx 4,3 \cdot 10^{-4} \text{ sec} . \quad (19)$$

[Flug = flight]. If we still assume that the temperature difference between the droplet surface and the steam is $\Delta T = 25^\circ\text{C}$ during this time, but that of this $\Delta T_{\text{GS,g}} = \sqrt{1,2 \cdot 220^2 / 2 \cdot 2 \cdot 10^3} \approx 13^\circ\text{C}$ is needed to withdraw the heat of friction from the boundary layer, so that only

$$\Delta T_{\text{eff,g}} = \Delta T - \Delta T_{\text{GS,g}} \approx 12^\circ\text{C} \quad (20)$$

is left for withdrawal of the heat of condensation, then we have all data necessary for determining the condensation of the droplets torn from Ring 2'.

We wish to obtain the result in the form of a mass-exchange coefficient ϵ_{d-g} (subscript: "from steam (d) to large (g) drops"), which will indicate the fraction of the steam precipitated on these flying droplets. Obviously this will be

$$\epsilon_{d-g} = \frac{\alpha_{r,g} A_g \Delta T_{\text{eff,g}} \Delta t_{\text{Flug}} / L}{x} , \quad (21)$$

where the numerator is the amount of steam condensed per kilogram of mixture and the denominator is the entire quantity of steam prior to this condensation. Equations (14) and (17) to (20) give

$$\epsilon_{d-t} = \frac{7600 \cdot 0,0146 \cdot 12 \cdot 4,3 \cdot 10^{-4} / 2,28 \cdot 10^6}{0,999927} = 2,5 \cdot 10^{-7} \ll \gamma_{\infty}, \quad (22)$$

so that, in summary, we arrive at the unequivocal conclusion that no noteworthy portion of the steam goes over into the liquid state either as a result of condensation on the blades or as a result of condensation on the droplets sprayed off behind the blades.

For the impulse-type turbine being used as an example, this conclusion is at least just as valid; referring to Fig. 2, we have even concluded that no precondensation at all takes place there under the proper conditions.

The absence of any precondensation worthy of the name has as a consequence that the supercooling of the expanding steam can proceed without restriction, and will soon lead to spontaneous condensation of the steam (fogging). We shall place this process under the magnifying glass in the next Section.

2.5. SPONTANEOUS CONDENSATION OF THE STEAM AND THE STATE OF THE FOG PRODUCED

To the best of our knowledge, the abrupt condensation of the steam that takes place in turbines has never been directly observed. The presence of a dense fog in the last stages of condensation turbines is nevertheless an established fact [14]. That fogging must proceed in turbines in the same way as it does in a single Laval nozzle follows from the fact that the steam being expanded experiences the same fate in either case: saturation is followed by supersaturation and this increases rapidly, since virtually no condensation is possible.

Numerous experiments have been carried out — cf. [19], [21], [30]

and [31] - to investigate the sudden condensation in supersonic nozzles (the so-called "condensation shocks"). It was recognized long ago that the sudden condensation is to be attributed to spontaneous formation of nuclei in the vapor [steam] itself. Later, it became possible to apprehend this nucleation mathematically by thermodynamic-statistical techniques; the clearest presentation of this theory is due to Frenkel [32]. A decisive step - one that brought the theory into agreement with experiments - was taken by Oswatitsch [33], in that he combined the theoretically derived formulas for the frequency of nuclei formation with the conventional flow equations and a growth law for the resulting droplets, forming a complete system of equations that put him in a position to determine the pressure curve in a nozzle with spontaneous condensation by stepwise calculation. The agreement between the calculated pressure curve and the experimental curve was quite good. A very good summary of the entire circle of problems is to be found in Stever [34]; he provides an excellent survey of both theory and experiment.

It is absolutely necessary to know the properties of the fog in order to investigate the processes that unfold in the rear part of a wet-steam turbine as the fog flows through it. Thus this Section forms the pivot point for those that follow. We shall first concern ourselves briefly with nucleation, so that, like Oswatitsch, we shall be able in Section b) to write an equation system permitting us to compute the expansion processes with condensation (in both nozzles and turbines). Proper functioning of the equation system will be checked through simulation of various nozzle experiments. Then we shall calculate the expansion in a low-pressure turbine to obtain certain essential features of the process. These insights will assist us toward a simpler analytical method of calculation for the condensation process - a method that will be sketched out in Section d) and will finally permit us to

draw important conclusions in Section e).

a) Nucleation

By the word small we imply a droplet that is just big enough to grow in a supersaturated atmosphere of steam surrounding it. Making use of the concept of critical drop size introduced in Section 2.3c, we shall use the term nucleus to denote a drop infinitesimally larger (say, by one molecule) than the critical size. We see from Eq. 2.3(15) that the nucleus size is large at a small supersaturation Δ but small at large supersaturations. In practical cases, rapid nucleation sets in when the critical droplet size has gone down to about 30 to 100 molecules.

But how is it at all possible for such water droplets to form in steam? The answer is to be sought in the fact that continuous density fluctuations arise in a vapor — as they do in an ideal gas — as a result of the thermal motion of the molecules. If the steam becomes almost saturated or even supersaturated in the course of expansion, it occurs more and more often that some molecules stick together for a certain time after colliding. This microscopic liquefaction amounts to the same thing as an extremely wide density fluctuation. That it does indeed occur frequently is due — in a thermodynamic sense — to the fact that the liquid form of the substance is approximately equally as "probable" as the vapor form in the neighborhood of the saturated state.

Now, using the Boltzmann law $S = k \ln W$, we can calculate for a certain number of steam molecules the relative probability W/W_0 for finding all of them balled up into a single water drop. We need to know only the amount by which the entropy increases if the drop forms purely from steam molecules. In a large vapor space, containing many molecules, the value of this relative probability will simultaneously indicate the fraction of all molecules present at any time in

the form of such drops.³⁶ Thus, for example, we can determine how many critical droplets will be found simultaneously in a certain amount of steam. We can calculate further how many critical droplets acquire an additional molecule during one second: this will then give the nucleation rate that we seek. The formula reads (see [32] or [34])

$$J = \frac{\sqrt{2\sigma/\pi N}}{q'} \cdot \frac{p^2}{(RT_d)^2} \cdot e^{-\frac{4\pi r_{krit}^2}{3kT_d}} \quad (1)$$

[krit = critical]. J is the number of nuclei formed in 1 m^3 of steam each second and N is the number of molecules in one kilogram of steam. If we substitute the r_{krit} from Eq. 2.3(15) in this equation and note that $Nk = R$, we obtain the following form, which is suitable for practical calculations:

$$J = \left(\frac{\sqrt{2\sigma N^3/\pi}}{q'(RT_d)^2} \right) p^2 \cdot \left(\frac{16\pi\sigma^3 N}{3q'^2(RT_d)^3} \right) \cdot \frac{1}{\Lambda^2} \cdot e^{-\frac{Z_1^2}{\Lambda^2}} = Z_0 p^2 \cdot e^{-\frac{Z_1^2}{\Lambda^2}} \quad (2)$$

here, the logarithmic supersaturation is defined according to Eq. 2.3(3) as

$$\Lambda = \ln \frac{p}{p_s(T_d)} \quad (3)$$

The two quantities denoted by Z_0 and Z_1 depend only on the temperature of the steam and are presented in Diagram IV (see Appendix).

On the basis of various experiments — all of which show sudden condensation, we should expect the nucleation rate to increase very sharply with increasing supersaturation. If we substitute typical values for the quantities in Eq. (2), it might acquire the following form:

$$J = 10^{24} \cdot (0.3 \cdot 10^5)^2 \cdot e^{-45/\Lambda^2} \approx 10^{33} \cdot 10^{-20/\Lambda^2}.$$

It is readily seen that J depends extraordinarily heavily on Λ . That is to say, if the supersaturation p/p_s increases from twofold (corres-

ponds to $\Lambda \approx 0.7$) to fourfold ($\Lambda \approx 1.4$), then J will increase from 10^{-8} to 10^{+23} nucl./m³-sec. Thus, doubling of the supersaturation may result in an increase in nucleation rate by more than thirty powers of ten!

b) Flow Equations for Condensing Steam

The equations of the system that describes the expansion of the steam in a nozzle or turbine may — as in the case of any other medium — be classified into two groups. One group, comprising the continuity equation, the energy equation and the equation of motion, expresses general physical laws and also contains data on particulars of the expansion, for example, channel shape, friction, and the like. The other equations contain only the properties of the flow medium and consist, for example, in the simplest case of the ideal gas, of the thermal equation of state $p v = R T$ and the caloric equation of state $d i = c_p d T$. For condensing steam, this second group of equations becomes much more complicated, but this has no fundamental effect on the state of affairs.

With regard to our flow medium, we shall make two important assumptions, assumptions that are also extensively the case in reality: firstly, that the steam can condense only through nuclei/formation and subsequent condensation on these nuclei, and cannot condense on linings, foreign particles and the like; secondly, that the droplets formed move everywhere with the same velocity as the steam itself.

We shall assume the expansion to be adiabatic but with friction. In cases where a turbine is involved, we shall imagine it to be replaced by a model that effects the same expansion in a more readily represented fashion: this model turbine would consist of an infinite number of stages with infinitesimal pressure ratios, stages capable of extracting the work continuously from the flow medium, i.e., of reducing its total enthalpy continuously (in accordance with any prescribed

law). In the equation of motion, this conception would manifest itself as a field strength directed in opposition to the flow against which work has to be done by the medium. Thus the essential aspect of the expansion in this context - namely, the time sequence of that which is experienced by a flowing steam particle - is extensively retained; on the other hand, the two-dimensional nature of the cascade/flow, which is less important here, is dispensed with entirely. That is to say, we are fully justified in treating the flow in a turbine, which is complicated in itself, one-dimensionally with application of a suitable field strength, just as in the case of a nozzle. We need only concern ourselves with the axial velocity c_a and the annulus cross section Ω_a

normal to the axis. Thus the data by means of which we must specify a turbine or nozzle are the curve of the axis-normal cross section along the axial coordinate $\Omega_a(\xi_a)$, that of the total enthalpy $h(\xi_a)$ and a statement concerning the generation of friction heat (in which all possible losses are conceived of as combined and uniformly distributed over the entire flow cross section), as with the aid of the polytropic efficiency η_p . Thus the following are to be assigned:

$$\Omega_a = \Omega_a(\xi_a), \quad (4)$$

$$h = h(\xi_a) \quad (\text{for nozzle: constant}), \quad (5)$$

$$\eta_p = \eta_p(\xi_a) \quad (\text{approximately constant}). \quad (6)$$

Further necessary data are the mass throughput \dot{M} in kg/sec and the initial state of the steam, p_A and i_A . It is assumed that the steam contains no droplets at entry.

The continuity equation is written

$$c_a = \frac{\dot{M}}{\Omega_a}, \quad (7)$$

and the energy equation

$$1 + \frac{c_a^2}{2} = h. \quad (8)$$

The quantities \underline{y} and \underline{i} refer to the mass unit of the entire flow medium, irrespective of whether it is pure steam or fog.

In the equation of motion, the fact that the flow medium yields work to the outside is taken into account by means of a field-strength term F (force/unit of volume), whose magnitude we shall again refer back to the prescribed total enthalpy curve $h(\xi_a)$. Even the friction can be taken into consideration in a similar manner by means of a decelerating force B . If we refer all terms to the volume unit, the equation of motion will be written

$$\frac{c_a}{v} \frac{dc_a}{d\xi_a} = - \frac{dp}{d\xi_a} - F - B. \quad (9)$$

Now F can be related to $h(\xi_a)$ and B with $\eta_p(\xi_a)$: the field strength vF acts on the mass unit of the flow medium. The work done against the field strength during subsequent flow over the distance $d\xi_a$ is equal to the reduction in the medium's total enthalpy, i.e.,

$$vF d\xi_a = - \frac{dh}{d\xi_a} d\xi_a,$$

from which

$$F = - \frac{1}{v} \frac{dh}{d\xi_a}. \quad (10)$$

The frictional force B must be so large as always to dissipate as much work as corresponds to the local polytropic efficiency. During traversal of $d\xi_a$, the frictional force per unit of mass comes to $vB d\xi_a$ and must be equal to $-(1 - \eta_p)d\bar{i}_s = -(1 - \eta_p)vdp$, from which

$$B = -(1 - \eta_p) \frac{dp}{d\xi_a}. \quad (11)$$

If we insert F and B in Eq. (9), the equation of motion assumes the form

$$c_a \frac{dc_a}{d\xi_a} = - \eta_p v \frac{dp}{d\xi_a} + \frac{dh}{d\xi_a}. \quad (12)$$

Below we shall apply ourselves to the properties of the flow

medium. We have to deal either with pure steam or with fog, i.e., with a mixture of steam and entrained small droplets. These fog droplets are of different sizes depending on whether they formed earlier or later, since the older ones have had more time to grow. In the following discussion, we shall characterize each droplet by the place ξ_e at which it formed as a nucleus.³⁷⁾ All quantities that have reference to individual droplets are thus not only functions of the position ξ_a , but also of the drops to which they refer, i.e., of the place of origin ξ_e . We shall therefore speak of the droplet radius $r(\xi_e, \xi_a)$, the droplet mass $m_r(\xi_e, \xi_a)$, the droplet temperature $T_r(\xi_e, \xi_a)$, etc. Droplets that are smaller than the nucleus size will not be taken into account at all as part of the water content, since their mass and energy contributions are vanishingly small. In other words, we shall be assuming that the steam suddenly produces "ripe" nuclei. The nucleation rate is known from Eq. (2), so that we can calculate the number $v(\xi_e)d\xi_e$ of those droplets that form per kilogram of flow medium between positions ξ_e and $\xi_e + d\xi_e$:

$$v(\xi_e) d\xi_e = v(\xi_e) \frac{d\xi_e}{c_a(\xi_e)}$$

(the volume taken in is thus $v(\xi_e)$ and the residence time of the medium between the two places is $d\xi_e/c_a$). It follows from this that the distribution function of the droplets by place of origin ξ_e is

$$v(\xi_e) = \frac{J(\xi_e) v(\xi_e)}{c_a(\xi_e)} \quad (13)$$

The steam is assumed to be an ideal vapor (cf. Traupel [20]); thus it follows the equations of state

$$pv_d = \frac{M-1}{M} (i_d - i_a) \quad (14)$$

and

$$c_p T_d = i_d - i_a \quad (15)$$

where κ and i_* can be assumed constant within wide limits and $(\kappa - 1)/\kappa \cdot c_p = R$.

Let the water be incompressible with a known temperature curve of density:

$$\rho_w = \rho_w(T_w), \quad (16)$$

and with a known enthalpy-vs-temperature relationship

$$h_w = h_w(T_w). \quad (17)$$

The droplets are so small that we may, without incurring any noticeable error, set their internal temperature T_w equal to the surface temperature T_r . Thus we have

$$T_w = T_r, \quad (18)$$

with which, however, it must be remembered that T_r is always smaller than the local saturation temperature, and, specifically, by an amount that may vary with drop size according to Eq. 2.3(11):

$$T_r(\xi_e, \xi_a) = T_s(p) - \frac{2\sigma}{\rho_w(T_w)} \frac{K T_s}{r(\xi_e, \xi_a)}. \quad (19)$$

(For the factor K , see Eq. 2.3(6).)

The direct influence of surface tension on the enthalpy of the drop, through the surface enthalpy $(5/3)\sigma \cdot 4\pi r^2$ can be disregarded.

The relationship

$$m_r(\xi_e, \xi_a) = \frac{4\pi}{3} \rho_w(T_w) \cdot r(\xi_e, \xi_a)^3. \quad (20)$$

obtains between droplet radius and droplet mass.

The specific water content y of the flow medium at position ξ_a can be calculated by taking together the masses of all droplets that have formed between passage across the saturation line ($\xi_a = \xi_s$) and the position ξ_a currently of interest:

$$y = 1 - x = \int_{\xi_s}^{\xi_a} m_r(\xi_e, \xi_a) \cdot v(\xi_e) d\xi_e. \quad (21)$$

The specific volume of the entire flow medium follows from

$$v = x v_d + \frac{4\pi}{3} \int_{\xi_0}^{\xi_2} r(\xi_e, \xi_2)^3 \cdot v(\xi_e) d\xi_e \approx x v_d \quad (22)$$

(since, indeed, the volume occupied by the water is negligible as compared to the steam volume), and its specific enthalpy from

$$i = x i_d + \int_{\xi_0}^{\xi_2} i_w(\xi_e, \xi_2) \cdot m_r(\xi_e, \xi_2) \cdot v(\xi_e) d\xi_e \quad (23)$$

(i_w is different for each drop size as a consequence of Eqs. (17) through (19).)

Finally, we must still concern ourselves with the mass transfer between the two phases. This is governed by nucleation and by condensation on drops that are already present. For the former, we have the formula of Eq. (2); according to Eq. 2.3(14), the subsequent growth of a droplet as a result of continuous condensation on it amounts to

$$\dot{m}_r = \frac{\alpha_r (4\pi r^2) (T_r - T_d)}{L} \quad (24)$$

The heat-transfer coefficient α_r is given by Eq. 2.2(32). If we sum these \dot{m}_r for all droplets present and add it to the amount that goes over into the liquid form as a result of nucleation, we obtain overall local increase in water content. Thus this is

$$\frac{d\gamma}{d\xi_2} = \frac{J v}{c_a} + \frac{4\pi}{3} \eta_w r_{krit}^3 + \frac{1}{c_a} \int_{\xi_0}^{\xi_2} \dot{m}_r(\xi_e, \xi_2) v(\xi_e) d\xi_e, \quad (25)$$

[krit = critical] since, indeed, $dt = d\xi_a / c_a$ and the seed size is given by the critical radius, which, according to Eq. 2.3(15), is

$$r_{krit} = \frac{2\sigma}{\rho RT_d} \cdot \frac{1}{\Lambda} \quad (26)$$

Together with the equations (13), (14), (15), (16), (17), (18),

(19), (20), (21 or 25), (22), (23), (24), (2), (3), (26) describing the behavior of the flow medium, Eqs. (7), (8) and (12) present a system of differential equations from which the curve of expansion can be determined by stepwise solution. It goes without saying that the calculation is exceedingly time-consuming and suitable only for automatic computers.

In the following Section, we shall report certain applications of this system of equations to expansions and in the next one after that we shall show that the essential conclusions can also be obtained from the equation system quickly and with sufficient accuracy.

c) Application of the Flow Equations to Expansions with Condensation

In setting up the system of equations for expansion, we have been pursuing the goal of calculating the course of expansion in a turbine. Before doing this, however, it would appear necessary first to apply the system of equations to expansions whose courses are exactly known from experiments. Here we would decide not only the question as to whether the equations describe the processes only qualitatively, but we should also be able to find out whether the place of condensation onset can be determined correctly.

Among the nozzle experiments described in the literature, those of Binnie and Woods [21] appear best suited for testing the equation system, since the measurements were taken with great care and the experiments described with explicit numerical material. Among the numerous measurements, in which the intake pressure was always held constant, while the entry temperature (superheating) was varied - four were selected for recalculation; in one of them, the onset of condensation occurred immediately behind the narrowest point, in another near the end of the nozzle, and in between in the two others. The cross-section curve was known from the dimensions of the nozzle; the curve

of polytropic efficiency was determined by trial and error so that the pressure curve without condensation would agree with the measured curve. The material quantities were always regarded as constant.

The calculation was carried out on the ERMETH,³⁸ a digital computer capable of about 60 elementary operations per second. The program was constructed in such a way that the step of the solution could be adjusted manually and that free choice was available between two solution procedures of different accuracy (Euler-Cauchy, Runge-Kutta). This offered an opportunity of checking the mathematical accuracy of the calculation, running certain cases through with two different step widths or with two different solution methods. On the average, the solution time required for one case - with condensation - was $1\frac{1}{2}$ hours.

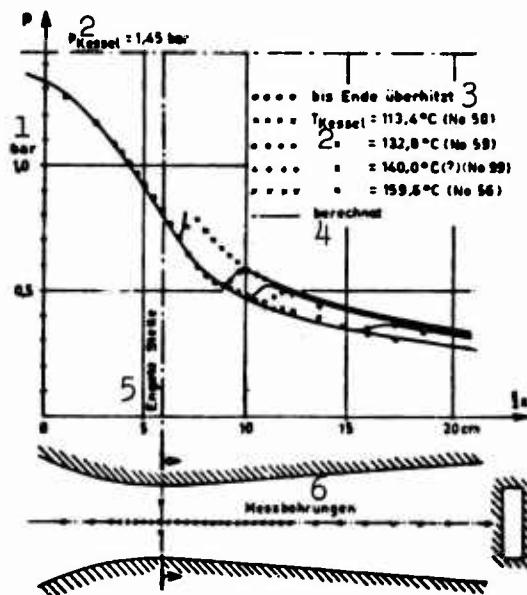


Fig. 2.5.1. Illustrating test of computing process: measured and re-calculated pressure curves in the nozzle of Binnie and Woods [21]. 1) bars; 2) boiler; 3) superheated to the end; 4) calculated; 5) throat; 6) pressure taps.

The pressure curves obtained are compared in Fig. 1 with those measured. The measured pressure shows, at certain places, pronounced waviness, which is to be attributed to two-dimensional effects and was

consequently not reproduced in the calculation. Apart from this side effect, the agreement between the calculation and the experiment is quite good. Both the place of condensation and the pressure rise were reproduced correctly. Only in Test No. 99 is there a marked discrepancy. On closer examination of the data furnished by Binnie and Woods, however, it was found that Measurement No. 99 is not coherent with other measurements taken with adjacent initial states, and must therefore have been burdened by some sort of error.

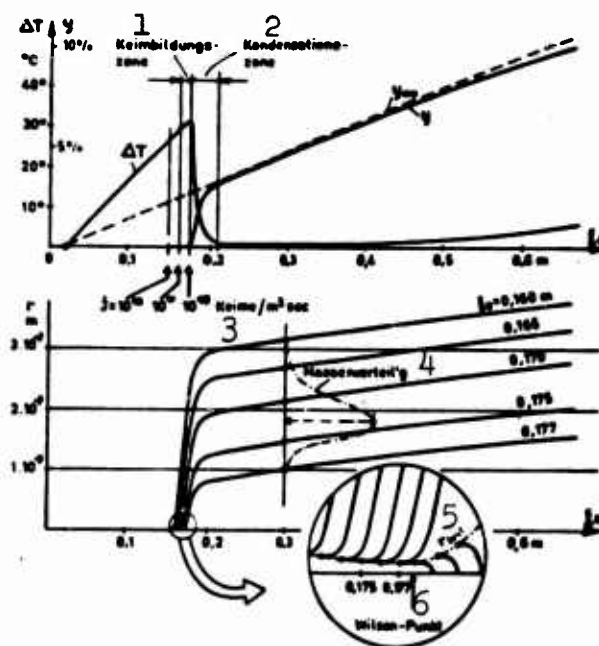


Fig. 2.5.2. Calculated supercooling curve, moisture content and fog-droplet size in a continuous-expansion turbine. 1) nucleation zone; 2) condensation zone; 3) nuclei; 4) mass distribution; 5) r_{critical} ; 6) Wilson point.

When these calculations had shown that the equation system apprehends the condensation process correctly, a turbine expansion was run through the computer.

For this purpose, we replaced the **reaction-type** turbine described in Section 2.1 by a continuous-expansion model turbine, such as was

referred to in Section b).

For the efficiency, we put $\eta_p = \text{const} = 0.87$. The assigned Ω_a and h curves are shown in Fig. 3. The stepwise calculation was carried through twice with the same step length but with different solution processes. The agreement between the two calculations was good. In the range $0 < \xi_a < 0.15$ m, the step length was a uniform 1 cm; in the zone of marked nucleation and rapid droplet growth ($0.15 < \xi_a < 0.225$ m, cf. Fig. 2), we went over to 1 mm. From $\xi_a = 0.225$ on, the calculation was carried to the end with a step of 5 mm. Nucleation was taken into account only where $J > 10^{10}$ (its maximum value came to more than 10^{19} !). The droplets were distributed in as many groups as there were computation steps in the range with $J > 10^{10}$ (31 groups).

The results of the calculation are presented in Figs. 2, 3 and 4. The top part of Fig. 2 shows that the supercooling $\Delta T = T_s - T_d$ first increases undisturbed; the steam expands as though it were still superheated. Only at a supercooling ΔT of about 27°C does nucleation reach a notable intensity. Condensation sets in at this point and continues with subsequent growth of the droplets. The growth of the droplets is seen in the lower part of Fig. 2. Shortly after their formation, the droplets grow exceedingly rapidly; this rapid growth is braked only by the disappearance of supercooling. The curve of the specific water content y shows that almost perfect thermodynamic equilibrium ($y \approx y_\infty$) is reached within a very short time after nucleation has become noticeable. The formation of the water and the disappearance of supercooling go hand in hand.

According to Eq. (13), the number of drops is related to the intensity of nucleation at the position at which these droplets have formed. Later-born droplets are more numerous than the earlier-born ones; nevertheless, they grow only to a smaller size. From this we obtain a dis-

tribution of the mass among the individual droplet groups as shown in Fig. 2. The spectrum of the droplets is rather narrow; this fact will be exploited extensively in the following, since it offers the possibility of regarding the fog droplets as equally large in various subsequent investigations. The nuclei forming in the immediate vicinity of maximum supersaturation (supercooling) or even later cannot grow, since they remain below the critical droplet size, which is increasing steadily from here on. Their size diminishes until they have been completely evaporated (magnified area of Fig. 2). Thus the point of maximum supercooling can be understood as the boundary between two zones: in front of it, droplet formation occurs, but no noticeable quantity of water is condensed ("nucleation zone"); behind it, no further stable droplets form, but it is here that the actual deposition of water takes place, namely through growth of the droplets already present ("condensation zone").

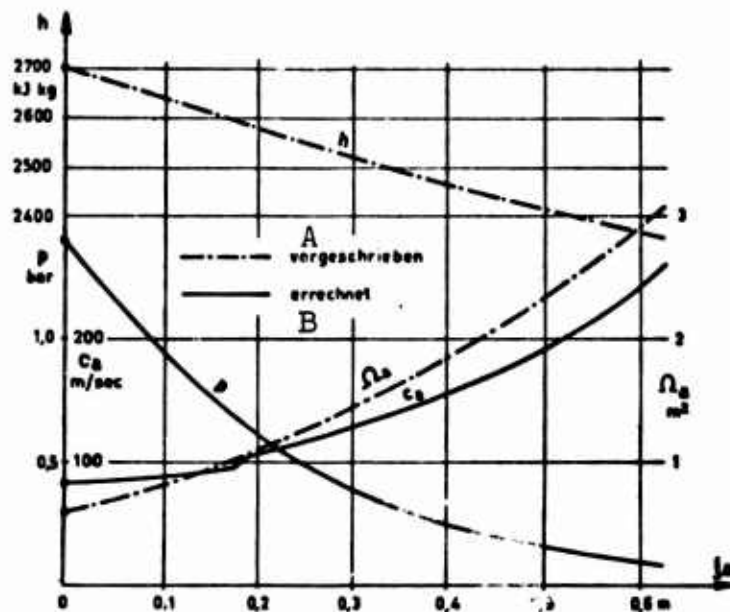


Fig. 2.5.3. Curves of total enthalpy h and axis-normal flow cross section Ω_a taken as the basis for the continuous-expansion turbine, together with computed curves for pressure and axial velocity. A) Assigned; B) calculated.

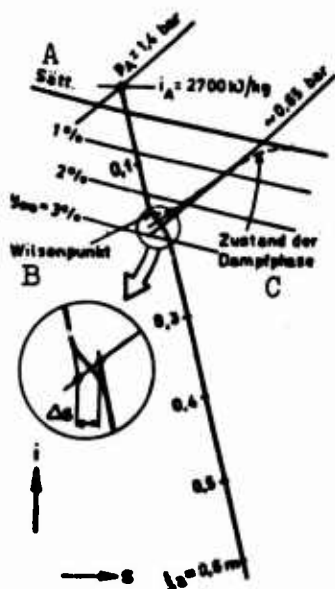


Fig. 2.5.4. Expansion line calculated for the continuous-expansion turbine. A) Saturation; B) Wilson point; C) state of steam [vapor] phase.

Figure 3 shows that the flow velocity increases sharply in the condensation zone. In Section d), we shall show that this is the case with subsonic flows (since the specific volume diminishes suddenly), and that exactly the opposite is the case in supersonic flows. We note no jump on the pressure curves; this is to be ascribed to the fact that the flow velocity is relatively low, so that the impulse change that arises on sudden acceleration also remains modest.

Figure 4 shows the expansion line. (It was determined in such a way as to add additional equations to the equation system to permit continuous determination of the entropy.) It will be seen that the condensation is associated with an increase in entropy. This was found to be $\Delta s = 9.7 \text{ J/kgK}$. In Section d), we shall also make general statements concerning the magnitude of Δs . The Wilson point (in our terminology, the point of maximum supersaturation or supercooling) lies at about 2.6% of theoretical wetness. The state curve of the vapor phase applies itself quickly to the saturation line after condensation has set in.

In the after parts of the turbine, we note that the supercooling rises again and y accordingly lags noticeably behind y_∞ , cf. Fig. 2. This problem involves the deterioration of heat transfer to the fog droplets at low steam densities and will be treated in detail in Section 2.6.

d) Analytical Determination of Onset of Condensation and the Properties of the Fog Formed

Calculation of spontaneous fogging on the basis of the equation system written in Section b), as was done in the examples of Section c), requires a very large outlay of machine time. A question presses itself upon us: is there no simpler way to get a sufficiently exact answer to the essential questions? A closed analytical method — even if only approximate — would also have the great advantage of permitting easy recognition of the importance of individual factors (expansion rapidity, Mach number, etc.). The following questions should be answered here: Where does spontaneous condensation set in (Wilson point)? What does the bend in the expansion line look like? How large are the fog droplets formed?

The examples calculated in the previous section led to recognition of the fact that we can regard the progress of spontaneous condensation as divided into two stages (this thought was first voiced by Oswatitsch [33]): the first step ("nucleation zone") sees formation of the nuclei from which fog drops will grow, but they are at first still so small that only very little water is contained in them, see Fig. 5. (The droplet count \underline{n} increases, but y still $\ll y_{\infty}$). In the second step ("con-

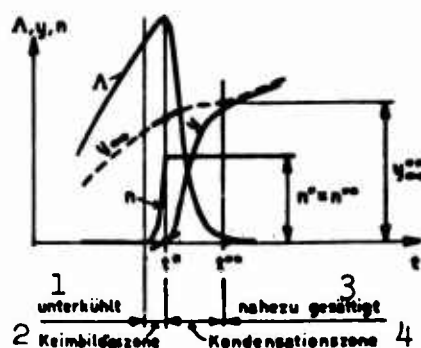


Fig. 2.5.5. Illustrating course of spontaneous condensation in time. 1) Supercooled; 2) nucleation zone; 3) almost saturated; 4) condensation zone.

densation zone"), no new nuclei form,³⁹⁾

i.e., \underline{n} remains constant: the amount of water precipitated is taken up solely by growth of the droplets already present.

Droplet growth ceases only when practically the entire quantity of water y_{∞} due

to precipitate according to thermodynamic equilibrium has actually been precipitated, i.e., when the state $y = y_{\infty}$ has

practically been reached. So much for the physical picture.

Due to this subdivision, simplifications become possible without which analytical calculation would not be feasible: in the first step of the computation, we calculate nucleation and growth, disregarding the effect of condensation on the vapor state: as a result, we obtain the locus of the Wilson point and the number of droplets formed. In the second step, we do not concern ourselves any longer with the condensation mechanism, but seek to find what sort of effect precipitation of the theoretical wetness has on the flow; the state at completion of condensation is obtained from this treatment. Finally, the average size of the full-grown fog droplets follows from the results of the two steps, so that all of the questions posed at the outset have been answered. Let us now discuss these calculation steps one at a time.

Nucleation Zone

The following discussion is based on a computation process derived in [45] under more general assumptions (two-component atmosphere, higher pressure) and tested on numerous sets of experimental results. Here we shall point out only the basic thought behind the process, together with the results and their uses. Here we shall restrict ourselves to pure water vapor [steam] and to the boundary case of low pressures, where droplet growth is governed by molecular laws for the tiny droplets coming under discussion.

We conceive of the physical process unfolding in a vapor element traversing the nucleation zone as follows. New droplets form continuously in all parts of the vapor element and have the critical size at birth in each case (the size corresponding to the instantaneous supersaturation). The frequency of formation of such nuclei in a unit volume increases steadily in the course of time, since the supersaturation is at first increasing steadily. Further condensation starts immediately

on the nuclei so that growth of the old droplets runs concurrently with the birth of new ones. The growth of a droplet is governed by heat-transfer laws, and is therefore primarily a function of droplet radius and the extent of supersaturation (more precisely, of supercooling). If it is now possible to predict the time behavior of all quantities in the nucleation zone that affect nucleation and droplet growth, then 1) the nucleation rate J will become a known function of time and, with it, the number of droplets that have been born up to a certain arbitrary point in time will be known; 2) the curve of droplet growth, i.e., the function $r(t)$, will be determined uniquely for each one of these droplets. (Even then, of course, the latter must be determined for each droplet through solution of a differential equation.) Having $J(t)$ and all $r(t)$, we could then write the intensity of condensation dy/dt as a function of time:

$$\frac{dy}{dt} = m_{krit} \cdot J + \sum_{\substack{\text{for all} \\ \text{droplet groups}}} q \cdot 4\pi r^2 \frac{dr}{dt} \times \begin{matrix} \text{(number of droplets in group)} \\ \text{(in question)} \end{matrix} \quad (28)$$

Here the first term signifies the condensation due to nucleation in accordance with the condition that the droplets formed are counted as part of the condensed phase only from the point at which they have exceeded the critical size. The second term is the condensation as a result of growth (dr/dt) of the supercritical droplets, which we may regard as characterized, for example, by their birthdays and grouped accordingly.

But how can we predict the curves of the state quantities in the nucleation zone without previous knowledge concerning the condensation? This follows from the previously mentioned finding (cf. Fig. 5) that throughout nucleation zone, the amount of moisture precipitated is so small that the state change corresponds practically to dry supersatura-

tion. That is to say, extrapolation of the dry expansion curve is permissible. Further, it was found in Section c) that the nucleation zone is very narrow,⁴⁰ so that most quantities vary only by extremely small percentages. This suggests the further simplification of setting constant all of the quantities that have only a secondary influence on nucleation (pressure, flow velocity, temperature, material quantities, etc.). For the logarithmic supersaturation Λ , which is what really decides nucleation rate, we shall assume a linear increase with time. (The ΔT curve in Fig. 2, which, with a scale distortion, can also be interpreted as the Λ curve, indicates that this is quite permissible. Otherwise, as shown in [45], this assumption is practically equivalent to the assumption of constant expansion rate \dot{P} .)

On the basis of these assumptions, we first derive a formula for $J = J(t)$, and then, solving the differential equation (24), we can determine the function $r(t)$ for the droplets that have formed at various times. It is found that these functions, which are, in themselves, complicated, can be reproduced with sufficient exactness by straight lines that begin their rise from zero only after a certain lapse of time following generation of the droplet as a nucleus. (For droplets with different birthdays, these $r(t)$ lines run parallel, but are shifted in time, like the exact r -curves in Fig. 2.) If these $r(t)$ are inserted in Eq. (28) and the number of droplets determined from the value of nucleation rate at the point in time at which the nuclei are born, we can sum (or integrate) over the droplets. Thus we have now obtained dy/dt as an analytically assigned function of t .

It is quickly seen that the Wilson point (= supersaturation maximum) lies very nearly where

$$\frac{dy}{dt} = \frac{dy_0}{dt} , \quad (29)$$

cf. Fig. 5, since then $(y_\infty - y)$, the amount of water lacking for thermodynamic equilibrium, no longer increases, i.e., the supersaturation also ceases to rise. The quantity dy_∞/dt is naturally given by the rapidity of expansion and can be regarded as constant within the nucleation zone.

If we insert the analytical expression obtained from Eq. (28) as a substitute for dy/dt in Eq. (29), we obtain an algebraic equation of the form

$$f(t) = \text{const}, \quad (30)$$

whose root t^* indicates the flow time ascribed to the Wilson point. From the latter we can then determine the other quantities of state at the Wilson point (Λ^* , p^* , etc.) quite easily.

Once the Wilson point has been established, we can finally also determine the number n^{**} of fog droplets per kilogram of fog by integrating the function $J \cdot v$ up to the Wilson point.

The considerations presented above lead us to the following computation program: we select as the reference point a point on the expansion line slightly in front of the locus of the hypothetical Wilson point — in slower (turbine) expansions, at about 2.5 to 3% of theoretical wetness, and, in fast (nozzle) expansions, at about 3 to 3.5%. From an i, s -table (see Appendix) compiled for supercooled steam, we read the pressure p_b and the steam temperature $T_{d,b}$ at this point. Then we determine the polytropic efficiency $\eta_{p,b}$ from the slope of the expansion line and calculate the local value of expansion rapidity \dot{P}_b from the design data (cf., for example, Section 2.1). Then from $T_{d,b}$, we obtain the corresponding values of supersaturation, using Diagrams II and IV (Appendix):

$$\Lambda_b = \ln \frac{p_b}{p_s(T_{d,b})}, \quad (31)$$

and those of the quantities Z_1, Z_2, \dots, Z_5 , which represent various combinations of material quantities, and, with $T_{d,b}$ and Λ_b , the conversion factor K as well.

It is expedient to introduce the "reduced log supersaturation"

$$\chi = \frac{\Lambda}{(Z_1)_b} \quad (32)$$

whose value at the reference point is found to be

$$\chi_b = \frac{\Lambda_b}{(Z_1)_b} \quad (33)$$

Then we calculate the dimensionless parameters

$$\gamma_b = \frac{(Z_3)_b}{\Lambda_b^3} \cdot \frac{p_b^4}{p_b^4} \quad (34)$$

and

$$\delta_b = \frac{(Z_2)_b}{\Lambda_b^{5/4}} \quad (35)$$

These two parameters appear in the final form of Eq. (30) and thus alone determine the position of the Wilson point. We can present the roots of Eq. (30) in a generally applicable form as a function of these parameters, see Fig. 6, where we have plotted the value of the reduced log supersaturation at the Wilson point, χ^* , instead of the meaningless t^* . When we read χ^* from Fig. 6, we have obtained our first indication as to the Wilson point.

At this point, we can at the same time check whether the choice of the reference point was correct. This is the case if, with the χ^* obtained, the relationship

$$0.92 \leq \frac{\chi_b}{\chi^*} \leq 0.98 \quad (36)$$

is satisfied; then the reference point lies in the middle of the nucleation zone. Otherwise we must assume a more favorable reference state and determine χ^* all over again.

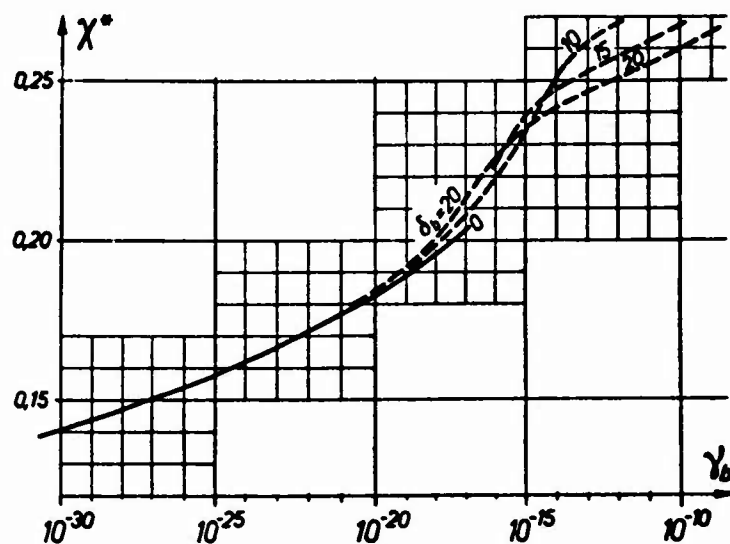


Fig. 2.5.6. Diagram for determining reduced log supersaturation at Wilson point.

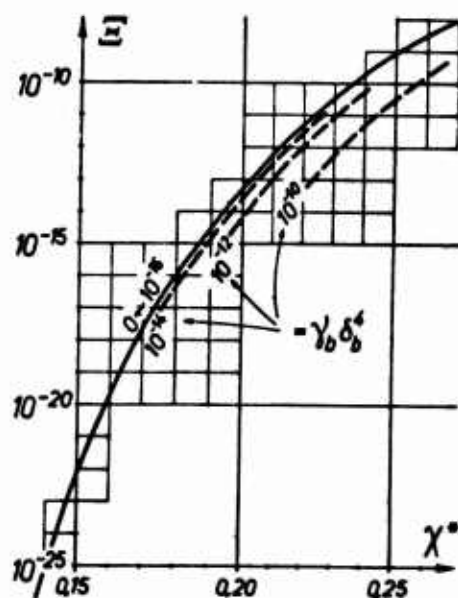


Fig. 2.5.7. Diagram for computing number of droplets.

If χ^* has definitely been determined, then the log supersaturation Λ^* and the supersaturation Π^* at the Wilson point follow:

$$\Lambda^* = \ln \Pi^* = (z_1)_b \chi^*, \quad (37)$$

and the supercooling at the Wilson point is obtained as

$$\Delta T^* = K_b T_{d,b} \Lambda^*. \quad (38)$$

The pressure p^* corresponding to the Wilson point is determined from the expression

$$p^* = p_b [1 - (z_4)_b (\chi^* - \chi_b)] . \quad (39)$$

Finally, we obtain n^{**} , the number of droplets per unit mass of wet steam that result in stable fog droplets and thus permit inferences as to the average droplet size, from

$$n^{**} = (z_5)_b \frac{p_b}{p^*} \cdot \Xi . \quad (40)$$

where Ξ is an abbreviated integral expression and can be stated as a function of χ^* and the quantity $\gamma_b \delta_b^4$ formed from the parameters. Its value can be read from Fig. 7. This concludes the calculation for the first step (nucleation zone).

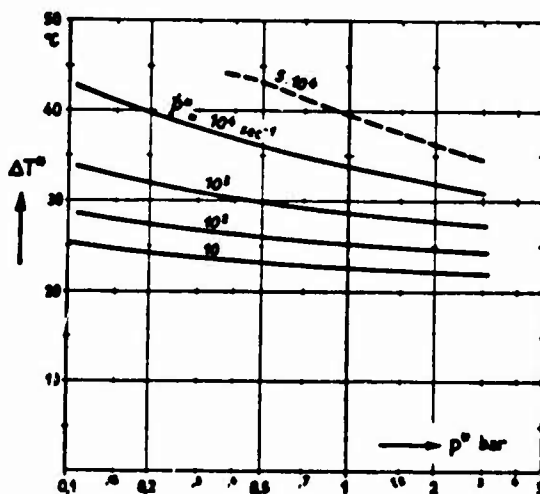


Fig. 2.5.8. Magnitude of Wilson-point supercooling for various expansion rates and various pressures, with expansion isentropic.

The importance of the **expansion rate** is easily appreciated from Fig. 6 and Fig. 7. For example, if in an expansion the same steam states are run through ten times faster than in another, δ_b remains approximately constant, while γ_b becomes larger by a factor of 10^4 . As a result, we obtain a χ^* that is larger by about 15% and a Ξ about 10^4 times as large, which ultimately leads to a thousandfold increase in the number of drops!

For the rest, the equations also indicate that a diminution of

the pressure has an effect similar to that of an increase in \dot{P} .

It follows from the above that different Wilson lines apply for different expansion rates: these are calculated assuming isentropic expansion ($\eta_p = 1$)⁴¹ for steam and entered in our enthalpy-entropy diagram (Appendix). The supercooling peaks ΔT^* that occur have also been calculated (again with $\eta_p = 1$) and plotted as a function of expansion rapidity and pressure in Fig. 8. (For the sake of simplicity, we have referred \dot{P} and p to the Wilson point, since $\dot{P}_b \approx \dot{P}^*$ and $p_b \approx p^*$ anyway if the reference point has been correctly chosen.)

Condensation zone

In this second step of the calculation, we shall concern ourselves with the variation of the quantities of state and the flow velocity in the condensation zone. In order again to avoid a stepwise numerical solution of the system of differential equations written in Section b), we shall make use of the assumption that the transition of the steam from the completely **supercooled** state to thermodynamic equilibrium occurs jumpwise ("condensation shock"). Since the condensation zone has a finite width in actuality, it is best to assume that the jump occurs not immediately at the Wilson point, but somewhat farther back, cf. the representation in Fig. 9 in this context. Then we have as the state before the jump a hypothetical state that can be obtained by extrapolation of the **supercooled** expansion curve. From the laws of the condensation jump, we can obtain from this a likewise hypothetical state behind the jump, from which it will be possible to extend the expansion curve assuming thermodynamic equilibrium. Within the condensation zone this extension has no physical validity, and only beginning at its end (p^{**}) does it present a valid approximation for the actual expansion curve.

Actually, we can place the point of the jump arbitrarily within the condensation zone. We shall place it where half of the water y_{∞}^* due

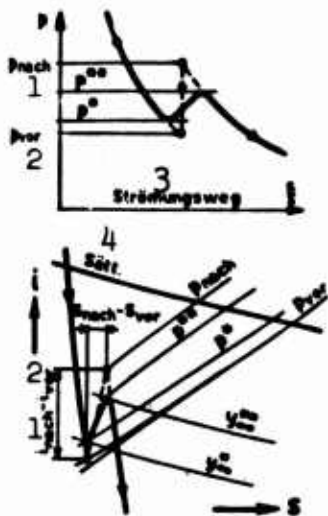


Fig. 2.5.9. Pressure curve and expansion line in spontaneous condensation (solid line: corresponding to solution of differential equation system; broken line: assuming a condensation jump). The case shown arises in supersonic flows. 1) After; 2) before; 3) flow path; 4) saturation.

at the Wilson point has actually condensed. This point can be determined with the aid of the droplet-growth curve that was applied to the seeding zone. According to [45], we get

$$p_{vor} = p^* - \frac{p^*}{Z_6 \cdot \Lambda^*} \cdot \sqrt[3]{\frac{3y_{cd}^*}{8\pi q^* n^*}}, \quad (40)$$

$$\Lambda_{vor} = \Lambda^* + \frac{Z_1}{Z_4} \frac{p^* - p_{vor}}{p^*}, \quad (41)$$

[vor = before] which uniquely defines the state before the jump. We can use an i, s -table to obtain y_{∞}^* , since we already know the Wilson point from the preceding calculation. The material quantities Z_1 , Z_4 and Z_6 are to be taken from Diagram IV (see Appendix) for the steam temperature at the Wilson point. In all practical cases, $p^* - p_{vor}$ will amount to only a few percent of p^* .

In general, the condensation shock is calculated in much the same way as a normal compression shock in a streaming gas: we write the three basic equations (continuity equation, energy equation and equation of motion) in one-dimensional form for the place of the shock and solve them. No difficulty is encountered in this solution, since all of the equations are algebraic. Stever [34] refers to certain similar studies. These are concerned with a sudden influx of heat of known intensity to a streaming ideal gas. It is found that two dimensionless parameters are decisive for the properties of the shock: M_{vor} , the Mach number before the shock, and (Q_{zu}/h_{vor}) [zu = influx], the amount of heat flowing into the streaming medium per unit of mass, referred to its total enthalpy before the shock.

The question is posed somewhat differently in the case of pure steam, primarily because we cannot indicate in advance the amount of heat that will be liberated. (At high Mach numbers, for example, there is even a possibility of compression shocks so severe that the state of the steam goes suddenly into the superheated region, so that in the end nothing condenses at all.) Further, a change in the isentropic exponent κ arises in the case of steam, and part of the volume-occupying mass also vanishes (since the specific volume of the water is, after all, negligibly small). Taking these peculiarities into account, the author has carried through calculations for condensation shocks in water vapor: see [46]. The assigned amount of heat has been replaced by an indication of the supercooling before the shock (referred to a temperature of the vapor) and the condition that thermodynamic equilibrium prevails behind the shock.

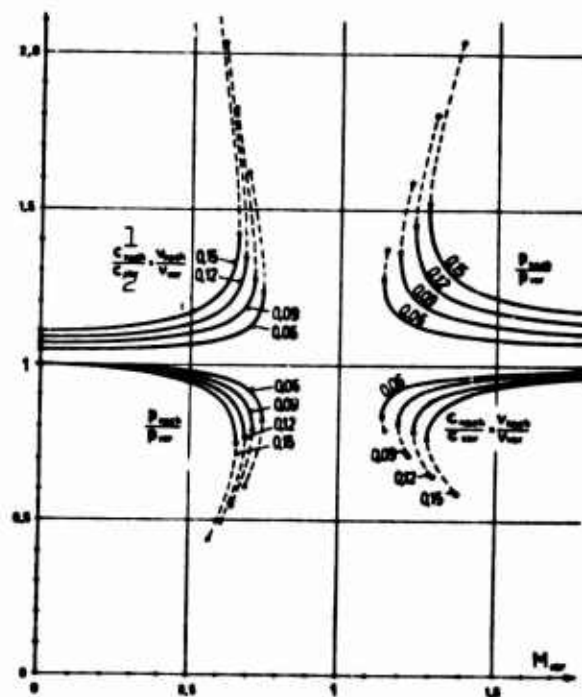


Fig. 2.5.10. Pressure and velocity variations due to a condensation shock as functions of the Mach number before the shock, for various initial supercoolings (concerning the parameter of the curves, see text). 1) After; 2) before.

Accordingly, the two dimensionless parameters that determine the properties of the shock in pure steam are M_{vor} and $(\Delta T/T_d)_{\text{vor}}$. The calculations were carried out for a number of initial pressures and embraced the Mach number range up to about $M_{\text{vor}} = 2$ and individual values of $(\Delta T/T_d)_{\text{vor}}$ lying between 0 and 0.15; see Figs. 10 and 11. It was found that the shock diagrams corresponding to the various initial pressures p_{vor} are not exactly identical - a result that may be ascribed to the peculiar properties of water vapor (shape of vapor-pressure curve, variation of heat of evaporation). Nevertheless, the shapes of the curves remain similar and the change in the initial pressure has about the same effect as a certain change in the curve parameter $(\Delta T/T_d)_{\text{vor}}$. It follows from this fact that the deviations as a result of changes in p_{vor} can be taken into account rather exactly by correcting the $(\Delta T/T_d)_{\text{vor}}$ value. The numerical change in the evaporation heat L is found to be the most suitable correction. These representations result in the following rule: the curves shown in Figs. 10 and 11, which apply originally for $p_{\text{vor}} = 0.5$ bar and with $(\Delta T/T_d)_{\text{vor}}$ as the curve parameter, can also be used for other initial pressures ($0.05 < p_{\text{vor}} < 5$ bars at least), provided that

$$\begin{aligned} \text{in Fig. 10 the quantity } & \left[\left(\frac{\Delta T}{T_d} \right)_{\text{vor}} \cdot \frac{L(p_{\text{vor}})}{L(0.5 \text{ bar})} \right], \\ \text{in Fig. 11 the quantity } & \left[\left(\frac{\Delta T}{T_d} \right)_{\text{vor}} \cdot \frac{L(0.5 \text{ bar})}{L(p_{\text{vor}})} \right] \end{aligned}$$

is used as the curve parameter.

It will be seen from Fig. 10 that the influence exerted by condensation on the flow depends very heavily not only on the extent of the initial undercooling, but also on the stream Mach number. According to Fig. 10, the condensation is associated with a drop in pressure and a rise in velocity at places where subsonic flow prevails and with

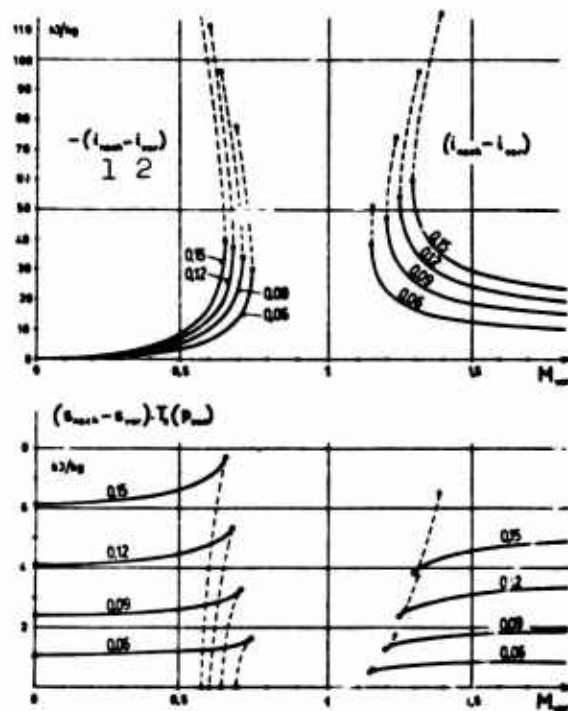


Fig. 2.5.11. Enthalpy- and entropy jump due to a condensation shock as a function of Mach number before the shock, with various initial undercoolings (concerning the curve parameter, see the text). 1) After; 2) before.

a pressure rise and velocity drop where the flow is supersonic. For $M_{vor} = 0$, the process is isobaric; the velocity ratio, which is simultaneously the volume ratio, is greater than unity, while the condensation effects an increase in volume with p remaining the same. For $M_{vor} \rightarrow \infty$, the process will unfold with volume constant.

The most striking feature of Fig. 10 is the absence of condensation shocks in the vicinity of $M_{vor} = 1$. The system of equations given has no solution in this region. What this signifies can be made clear somewhat as follows: the present investigation of the condensation shock was prefaced by two apparently self-evident assumptions: namely, that the shock can be produced at any arbitrary Mach number by appropriate design of a nozzle (for example, by selection of the total pressure), and that the flow behaves stationary. Each steady state must,

however, be introduced by a nonsteady prelude process that merges with it asymptotically. Now it is quite conceivable that under certain conditions, the desired asymptotic transition cannot come to pass at all. In our case, this would be when the condensation shock tended to penetrate into the forbidden Mach number region during the prelude process. If this penetration should occur in the subsonic region, we have a back effect on the state before the nozzle; if a certain pressure is forced here, the mass throughput must become smaller; if the mass throughput is forced, the pressure must pile up; in any event, the set of conditions specified cannot be satisfied and is replaced by another. In the other case, when the prelude process unfolds in such a way that the condensation shock reaches the boundary of the forbidden supersonic Mach-number region, a back effect on the upstream conditions is excluded and the initial conditions thus remain unaffected. Since, on the other hand, according to our equations, such a stationary state is not possible, no asymptotic transition into such a state can take place either. To investigate the processes that unfold in such a case, we should substitute equations of nonstationary behavior for the stationary equations. The solutions of these equations for the state following the prelude process would then be periodic in nature, i.e., the flow state would perform oscillations of some sort. For the rest, these would have to be of relatively high frequency so that the nonstationary acceleration terms would really be considerable as compared to the stationary terms. Thus we would have to deal with a more or less intensely oscillating flow. These conclusions are supported by the sporadic observation of bucket failure in wet-steam turbines under conditions such that it could not be attributed to any of the known causes. This breakage could be eliminated only by changing the cross sections with the concomitant fundamental changes in other flow conditions.

The two boundary Mach numbers at which a condensation shock is still just possible are the farther from unity the stronger the condensation, i.e., the greater the undercooling prevailing before the shock (note the increasing removal of the inflection point of the curves from $M_{vor} = 1$ for increasing parameter values).

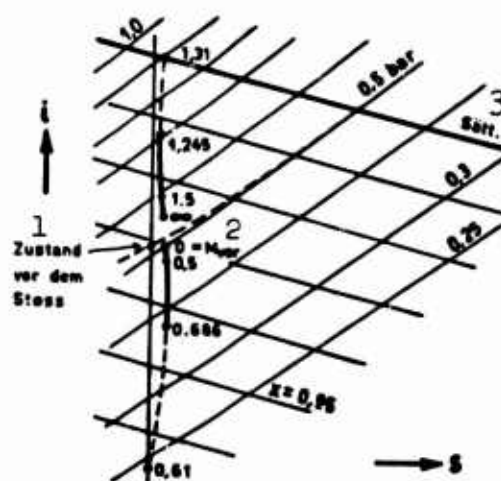


Fig. 2.5.12. Locus curve of steam states after the shock in the i,s -diagram, calculated for $p_{vor} = 0.5$ bar and $(\Delta T/T_d)_{vor} = 0.12$. The jump that occurs is determined by the magnitudes of the Mach number M_{vor} . 1) State before the shock; 2) before; 3) saturation.

Theoretically, two solutions are possible in the neighborhood of the inflection point for a given M_{vor} . The solid curves apply to the "weak" case, in which only the absolutely necessary consequences of a condensation arise, while the broken-line curves have reference to the so-called "strong" condensation shock, which, according to Oswatitsch [35], can be interpreted as the simultaneous occurrence of a (weak) condensation shock and an ordinary normal compression or rarefaction shock. We may conclude on the basis of experience that weak shocks arise in practical cases, since the absolute abruptness of condensation that would be necessary for a strong shock is not at all guaran-

teed in reality. We shall return again to the end points of the broken-line curve branches.

Figure 11 presents a plot of the enthalpy and entropy jumps produced by the shock. The entropy increase was multiplied here by a temperature value so that it would provide a direct point of reference for the work loss due to the shock. Knowing the sizes of the two shocks places us in a position to determine that point of the i,s -diagram beginning at which the expansion continues behind the shock in cases where the point before the shock is known. For example, we obtain for $p_{\text{vor}} = 0.5$ bar, $(\Delta T/T_d)_{\text{vor}} = 0.12$ and various Mach numbers the state points behind the shock as shown in Fig. 12.

Referring to Fig. 12, we shall be in a better position to discuss the curves of Fig. 11 as well. In the case of a vapor at rest ($M_{\text{vor}} = 0$), there is no change in enthalpy; the entropy increase has exactly the value necessary for the transition from the curved (undercooling) isobar to the straight (equilibrium) isobar. According to Fig. 11, the entropy increase will be the greater the greater the supercooling. (And, indeed, almost in a square-law relationship!) For subsonic flows, the jump is downward, i.e., the enthalpy diminishes (after all, acceleration!). With rising Mach number, the entropy increase becomes somewhat larger and reaches its maximum at the highest subsonic Mach number at which a condensation shock is still possible. Cases corresponding to the broken branch of the curve, which, though they do not occur in practice, are still theoretically possible, lead to much smaller increases in entropy, since they are connected with an expansion shock. In the boundary case of constant entropy, the theoretical possibility of the existence of such shocks also falls by the wayside, and this is the reason why Fig. 10 limits the lengths of the broken-line subsonic curve branches.

In the supersonic region, a rather strong positive enthalpy jump arises at the lowest Mach number at which a shock is still at all possible. For larger Mach numbers, the jump becomes increasingly indistinct in the real case (unbroken curve), but is connected with a noticeable enthalpy increase even for $M_{vor} = \infty$. The entropy increase always remains somewhat smaller than in the subsonic case and is minimal at the boundary Mach number. The "strong" shock (broken-line branch) leads to sharp increases in enthalpy, which, in the extreme case, result in dry-saturated states. This is what establishes the strongest theoretically possible condensation shock.

In actuality, the jump is less pronounced, since development of the heat of condensation extends over a finite period of time. In Fig. 9, the sharp-cornered expansion curve computed with the aid of the shock conception is compared with the "exact" curve, which would be obtained by stepwise solution of the system of equations set forth in Section b. Just as the forward salient point (the Wilson point) occurs at a pressure $p^* > p_{vor}$, the rear salient point also lies not at p_{nach} , but at a lower pressure p^{**} , whose magnitude can be estimated from the time required for condensation. If we define p_{vor} by Eq. (40), we can with sufficient accuracy take

$$p^{**} = p_{nach} - 2(p^* - p_{vor}) \quad (42)$$

$(p_{nach} - p^{**})$ will therefore be greater than $(p^* - p_{vor})$, since the condensation proceeds more slowly toward the end because the supercooling has already receded.

We can now summarize the course of the calculation for the condensation zone. Strictly speaking, the calculation applies only for narrow one-dimensional channels in which the condensation shocks are perpendicular to the flow. We shall return at the conclusion to the case of turbine cascades in which extensively two-dimensional flow pre-

vails. After we have found the Wilson point (i.e., p^* and Λ^* have become known), we calculate p_{vor} and Λ_{vor} from Eqs. (40) and (41), respectively, thus locating the jump. The governing parameters of the jump are obtained from

$$M_{vor} = \sqrt{\frac{2}{\kappa + 1} \left[\left(\frac{p_{tot}}{p_{vor}} \right)^{\frac{\kappa - 1}{\kappa}} - 1 \right]} \quad (43)$$

and

$$\left(\frac{\Delta T}{T_d} \right)_{vor} = K(p_{vor}, \Lambda_{vor}) \cdot \Lambda_{vor} \quad (44)$$

Here, p_{tot} is the total pressure of the flow. The coefficient K — introduced in Section 2.3a — is presented in Diagram I (see Appendix). If we skip the calculation of the seeding zone and wish to determine the Wilson point on the basis of the Wilson lines drawn into the i, s -table, it will also be simplest to read ΔT also from the table or from Fig. 8 and connect it with T_d , whereupon Eq. (44) becomes superfluous.


Then, on the basis of M_{vor} , $(\Delta T/T_d)_{vor}$ and p_{vor} , applying Figs. 10 and 11, we determine the properties of the condensation shock, i.e., the quantities


$$\frac{p_{nach}}{p_{vor}}, \quad (i_{nach} - i_{vor}), \quad (s_{nach} - s_{vor})$$

[nach = after; vor = before]. Using them, we can determine the pressure p_{nach} and that point of the i, s -diagram beginning at which the expansion continues. The expansion lines are drawn out from this point with about the same efficiency as before, cf. Fig. 9.

Finally, p^{**} , the pressure actually attained at the end of the condensation zone, can be determined from Eqs. (42) and (40), so that an approximation of the real expansion curve is obtained (solid line in Fig. 9). At the pressure p^{**} , we read from the expansion line the y_w^{**} , which indicates the quantity of suddenly precipitated water and

thus represents an important basis for determination of the average droplet size. This completes our second calculation step.

However, before proceeding farther to our goal, the droplet size, let us first consider briefly the influence exerted on the appearance of condensation shocks by the two-dimensional nature of the turbine-cascade flow. The reason for the deviations that will be found in **turbine cascade** as compared to narrow straight nozzles is the fact that in the cascades, the condensation does not set in simultaneously on all streamlines, so that there is a distortion of the streamline pattern as compared to the condensation-free case. To determine the disposition of the condensation shock in a  cascade, let us pursue the following line of reasoning.

If the condensation had no disturbing effect on flow conditions (i.e., if no shock arose), the streamline and isobar pattern in the  cascade would be exactly the same as without condensation, see Fig. 13a. We would only have to concern ourselves with a fog behind the isobar p^* (p^* is the Wilson pressure, at which condensation intervenes⁴²). In actuality, however, spontaneous condensation is associated with a shock. Let us now imagine that we have replaced the drawn streamlines with thin rigid sheet walls, cf. Fig. b. As a result, the flow has been divided into four separate flow filaments, each of which is so narrow that it may be regarded as one-dimensional. Then normal shocks arise in these channels, staggered in a manner corresponding to the course of the p^* line. If we now take the sheet walls out, the flow field between the two bucket profiles will again be continuous and must naturally be spanned continuously by the shock. Obviously, however, this shock line will not run vertically onto the streamlines. Such a case — that of the so-called "oblique condensation shock," can easily be understood on the basis of the normal shocks by decomposing

the flow velocity into a component perpendicular to the shock and a component parallel to it (Fig. c). The normal component is subject to the shock laws, while the parallel component remains unaffected by the shock. This then results in a knee in the streamline - assuming the shape shown for subsonic flow - since the normal component is, after all, increased by the shock in this case. (The determining Mach number M_{vor} is to be formed with the normal component!) On the basis of this fact, we can conceive of the actual streamline pattern as shown in Fig. d. A result of the knee shape is that the filament right next to the back of the bucket must become somewhat broader before the shock as compared with Fig. a or b. According to Bernoulli, however, the pressure would then diminish more slowly, so that the Wilson pressure p^* is reached somewhat later and thus the shock is displaced a bit downstream. The opposite effect arises in the filament on the concave side of the bucket, so that the shock ultimately has a form deviating less from the perpendicular, such as the line originally assumed for p^* in Fig. a. The shock must be normal in the neighborhood of the profile, since, indeed, no knee can be formed in the streamlines because of the solid wall presented here. Thus we have ascertained the sought shape of the condensation shock in a bucket cascade.

Naturally, the Wilson pressure may occasionally be reached farther forward or farther back in the cascade. If, for example, we modify the state before the cascade in such a way that the pressure p^* is reached farther back in each successive case, the shock will also be shifted in the manner shown in Fig. e. If here the end point of the shock has already reached the exit edge on the concave side of the profile and the entry state is modified still further, the shock line will not separate at all from the exit edge and end in free space, but will remain attached: that is to say, a jet-deflection-like flow will

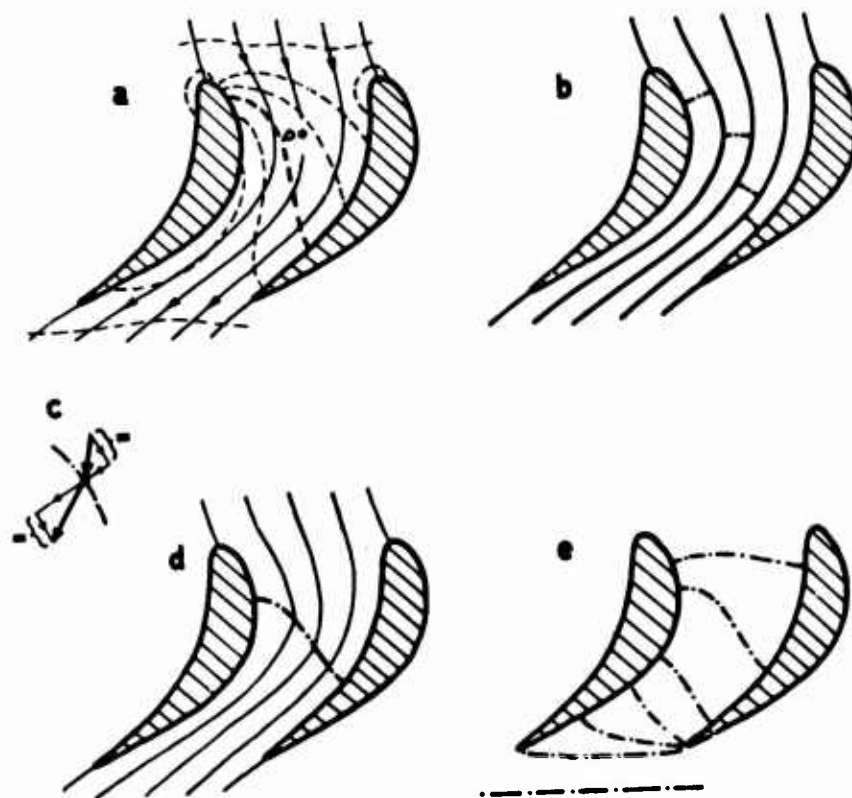


Fig. 2.5.13. Illustrating position of condensation shock in a bucket cascade.

move past the exit edge and result in a local acceleration, i.e., a local pressure drop, one that levels out in exactly such a way that the pressure p^* is reached at the edge. If the pressure level before the cascade rises further, the jet deflection will become steadily more pronounced, until the other end of the shock line has also drifted to the exit edge. Only by a still further increase in the pressure level can the shock line be separated from the cascade. In the case of a turbine, the shock then migrates out into the intermediate axial space or even into the next bucket ring.

Finally, a word on the three-dimensional effects. In turbines, the pressure in the intermediate space in front of a cascade is generally not constant along all radii. Accordingly, different shock lines among those drawn in Fig. 13e apply for different radii, i.e., the shock surface is somewhat canted between the blades.

The stronger the variation of the pressure in the intermediate space as a function of radius, the greater will be the deviation of the shock surface from the cylindrical. Nevertheless, this effect of pressure will generally be partly offset by the variation of the percentage reaction, which determines the extent of the pressure drop in the cascade itself and, through it, likewise influences the shape of the shock surface. Nevertheless, it is conceivable, for example, that the shock surface lies under certain circumstances between rotor buckets at the hub, crosses the intermediate space at the midsection circle, and squeezes in between the next following stator buckets near the casing liner. In Section e, we shall briefly discuss the question as to whether these three-dimensional effects can have substantial consequences for the behavior of a turbine.

Size of fog droplets and remanent supercooling

In the first step of the calculation (nucleation zone), we have, in addition to the locus of the Wilson point, determined the number of fog droplets n^{**} that have formed. The second step of the calculation (condensation zone) resulted in the water content y_{∞}^{**} at the end of the condensation zone at thermodynamic equilibrium, taking the properties of the flow into account. If the specific amount of water y_n^{**} is present in the fog droplets at the end of the condensation zone, these have the average radius

$$r_n^{**} = \sqrt[3]{\frac{y_n^{**}}{(4\pi\rho/3)n^{**}}} \quad (45)$$

where $4\pi\rho/3 \approx 4100 \text{ kg/m}^3$ at moderate pressures. (If almost perfect thermodynamic equilibrium has been established and no water is present other than that in the fog drops, we may set $y_n^{**} \approx y_{\infty}^{**}$.)

On the basis of Eq. (45), using the calculation methods for the seeding and condensation zones, we can determine the influence exerted

by rapidity of expansion, pressure and Mach number on the average fog-droplet size. The result is Fig. 14, from which the overwhelming significance of expansion rate \dot{p} will be seen at once. The reason for this strong influence is the fact that greater supercoolings are reached in rapid expansions — cf. Fig. 8! — so that the nucleation frequency assumes very high values and, even in a very short time, this is manifested in a very large number of droplets. Since, on the other hand, the amount of water precipitated does not change appreciably, the result is a sharp reduction in droplet size.

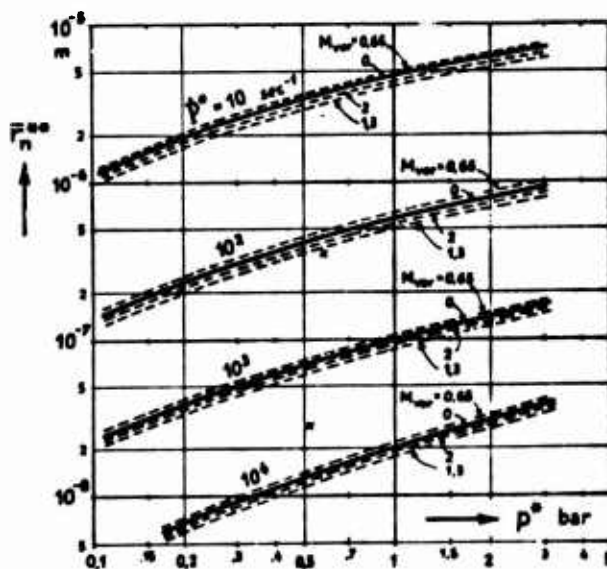


Fig. 2.5.14. Average droplet size in fog for various expansion rapidities and pressures prevailing at the Wilson point and for various Mach numbers, under the assumption that the entire theoretical wetness condenses ($y_n^{**} = y_\infty^{**}$). vor = before.

With this, we have acquired answers to all questions posed at the beginning of this Section d) and now come to the subject of the supercooling ΔT^{**} remaining at the end of the condensation zone. This occurs only because the steam is expanded further and new water must be condensed steadily during this process. The water condenses on the surfaces of the fog droplets and its heat of condensation is given up to

the steam (which is cooler by ΔT^{**}). The heat balance would be written

$$L \frac{dy_{\omega}}{dt} \Big|_{r^{**}} = n^{**} \cdot (4\pi \bar{r}_n^{**2}) \alpha_r^{**} \Delta T^{**}, \quad (46)$$

where the heat transfer coefficient α_r^{**} refers to droplets of size \bar{r}_n^{**} at a pressure p^{**} and is given by Eq. 2.2(32). By transformation and introduction of the expansion rapidity, we obtain

$$\Delta T^{**} = Z_8(p^{**}) \frac{\dot{p}^{**} \bar{r}_n^{**2}}{y_{\omega}^{**}} \left[1 + \frac{1.59 \bar{I}(p^{**})}{\bar{r}_n^{**}} \right]. \quad (47)$$

Here, Z_8 incorporates the material quantities:

$$Z_8(p, \eta_p) = \frac{q' L}{3\lambda_d} \frac{dy_{\omega}}{d(-\ln p)}. \quad (48)$$

Z_8 has somewhat different values for different polytropic efficiencies; these are plotted in Diagram III (see Appendix). We may calculate \bar{I} from Eq. 2.2(6) or read it from Diagram I. In nozzles, ΔT^{**} is usually 1 to 3°C; for turbines, in which the expansion rapidity varies greatly, no general statement can be made, since the magnitude of ΔT^{**} depends very heavily on precisely how large the local expansion rapidity \dot{p}^{**} is. The further progress of supercooling will be treated in Section 2.6b.

e) Certain Conclusions for Wet-Steam Turbines

The investigation of the spontaneous condensation process given in Section d) applies for expansions in which the expansion rapidity \dot{p} is not subject to sharp changes. Unfortunately, expansion in turbines does not present such a simple case, since the rapidity of expansion shows extraordinarily sharp fluctuations. (It is high within the blade rings and drops practically to zero in the intermediate spaces.) Thus the assumption that supersaturation increases linearly with time is no longer justified and the applicability of the methods described in Section d) for determining the Wilson point (where, indeed, this assump-

tion was one of the basic premises!) must be questioned. It can, however, be shown that the methods also give correct results for expansions with \dot{P} variable in time (or, what is the same thing, locally), provided that we determine the *effective* value of \dot{P} in a suitable manner.

Specifically, it is found that for all expansions with constant \dot{P} [45], only those droplets formed in the pressure range

$$1,02 p^* > p > p^* \quad (49)$$

participate heavily in the precipitation of water up to the Wilson point. This gives us a clue to the width of the nucleation zone. Such an expansion is represented in the upper part of Fig. 15. The only thing of importance for the position of the Wilson point and for the number

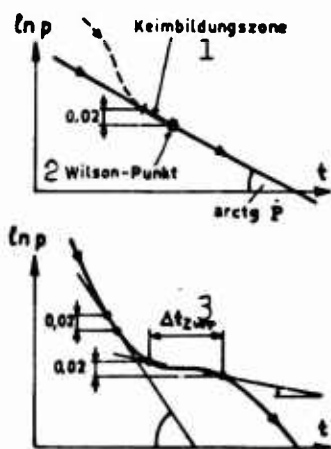


Fig. 2.5.15. Illustrating determination of P^* in a turbine. Top: conditions at $\dot{P} = \text{const}$; bottom: approximation of a turbine expansion through expansion segments with $\dot{P} = \text{const}$. 1) nucleation zone; 2) Wilson point; 3) Z_{wr} = intermediate spaces.

of droplets is how rapidly the expansion unfolds in this zone. What has happened previously makes no difference, since the droplets formed there are not a factor in view of their relatively small number. Thus the condensation process would remain practically unchanged if the expansion were to proceed not along the straight pressure line, but instead along the dashed pressure curve.

Thus we are given the key to calculation of turbine expansions. We must replace the stepwise pressure variation of which a section is shown at the bottom of Fig. 15 by segments with $\dot{P} = \text{const}$, but in such a way that these approximations always embrace a region with a pressure change of at least 2%, see the figure. The slopes of these lines in the $(\ln p), t$ -diagram every-

where indicate the value of \dot{P} governing nuclei formation. Thus we may not set $\dot{P} = 0$ in the intermediate spaces, although this may be the case locally, but must set instead

$$\dot{P}_{\min} = \frac{0,02}{\Delta t_{Zwr}} \approx \frac{0,02 \cdot c_a}{\Delta \xi_{a,Zwr}}, \quad (50)$$

where the significance of Δt_{Zwr} is evident from Fig. 15 and $\Delta \xi_{a,Zwr}$ is the axial width of the intermediate space. With $\Delta \xi_{a,Zwr} = 2$ cm and $c_a = 100$ m/sec, we obtain, for example, $\dot{P}_{\min} \approx 100 \text{ sec}^{-1}$.

Now if we wish to find the Wilson point in a turbine, we draw the curve of \dot{P} on the basis of this rule for those blade rings in the region where we estimate that condensation will set in, cf. Fig. 16, top. (The local values of \dot{P} are indicated by dashed curves; it is seen that the averaging results in substantial deviations only in the axial intermediate spaces.) We then determine the curve of the "Wilson supercooling" $\Delta T^*(\xi_a)$, cf. Fig. 16, bottom,⁴³ from the $\dot{P}(\xi_a)$ curve with the aid of Fig. 8. This curve tells us how great the supercooling at each point ξ_a must become for sudden condensation to set in. For the rest, we can determine the extent of the undercooling $\Delta T = T_s(p) - T_d$ in the intermediate spaces on the basis of the design data (for example, using an i,s-diagram for supercooled steam) and plot it in the diagram set up for ΔT^* . If we connect these points with a wavy ascending line (see Fig. 16), then we have the curve of undercooling within the bucket rings with sufficient accuracy. Now the Wilson point will be situated where the $\Delta T(\xi_a)$ line first reaches the $\Delta T^*(\xi_a)$ curve. We read from this point the value of the expansion rapidity $\dot{P} = \dot{P}^*$ and the pressure $p = p^*$ and thus obtain the two items of data from which the losses, drop size, etc. follow in the manner described earlier.

At this point we should like to make reference to something that provides an explanation for the often inexplicable differences observed

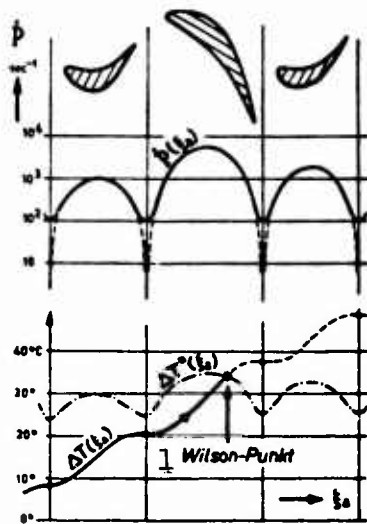


Fig. 2.5.16. Illustrating determination of the Wilson point in a turbine. 1) Wilson point.

unchanged, since its shape depends primarily on \dot{P} and the latter is independent of the absolute pressure value.) If, however, the shape of ΔT changes, the Wilson point will also have a different position: if the saturation line is crossed at, for example, B instead of at S, the Wilson point may easily slide forward, but will still remain in the region where \dot{P} has a high value. Only when saturation intervenes still farther forward (at A) will the condensation be triggered in the intermediate space in front of the ring. Conversely, when the saturation line is reached only later (C), the Wilson point will slide farther back into the ring, until finally (D) it comes out into the intermediate space, thus creating a situation analogous to A, i.e., spontaneous condensation at low \dot{P} .

Thus we find that fogging in a turbine may occur at either large \dot{P} or small \dot{P} , depending on how the state of the steam happens to vary from ring to ring. The consequences that this has for the composition of the fog can be seen from Fig. 14: for $\dot{P}^* = 4000 \text{ sec}^{-1}$, which corresponds approximately to the Wilson point on the heavy curve in Fig. 17,

in the behavior of even quite similarly configured wet-steam turbines. If the saturation line in the turbine for which Fig. 16 was drawn were to be crossed slightly earlier or later, as might easily occur, for example, as a result of a slightly different intermediate-pressure pattern or even as a result of an operational state deviating from design, the entire $\Delta T(\xi_a)$ curve would be shifted somewhat higher or lower, respectively, as shown in Fig. 17 for certain examples. (The ΔT^* curve remains practically

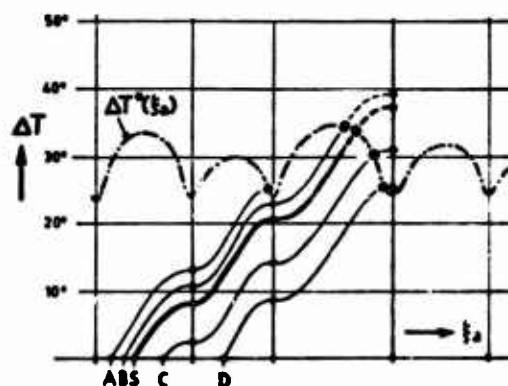


Fig. 2.5.17. Displacement of the Wilson point in a turbine when the pressure curve is changed. (Heavy line: design state).

we read a fog-droplet radius $\bar{r}_n^{**} \approx 3 \cdot 10^{-8}$ m; for $\dot{P}^* \approx 150 \text{ sec}^{-1}$, on the other hand, this corresponds approximately to curves A and D, we read a radius $\bar{r}_n^{**} \approx 3.5 \cdot 10^{-7}$ m! (See crosses in Fig. 14.) Thus when condensation sets in in an intermediate space, the fog droplets are about ten times (!) larger than when condensation intervenes during the sharp pressure drop within a ring. The significance of this finding will come to light in the sections to follow, where it will be shown that fine fog droplets cause smaller moisture losses and present a lesser erosion danger than coarse ones.

Up to this point, we have ignored the fact that not all of the steam particles flowing through a ring experience the same pressure drop. The differences stem on the one hand from the unique nature of cascade flows and, on the other, from the fact that the percentage reaction is not, in general, constant along the turbine buckets. If, however, the condensation takes place under different conditions in parts of the steam that pass through a ring at different points, we can no longer speak of a uniform fog-droplet size in the entire flow space, since different drop sizes will occur in different regions. The influence of the cascade flow can be judged by determining the expan-

sion curve and the Wilson point also, for example, on the two streamlines in the immediate vicinity of the blade profile (pressure and suction sides) in addition to those at the middle streamline (for which Fig. 16, etc., have been drawn). The pressure curves drawn in Fig. 2.4.3 may, for example, be used for this purpose. Nevertheless, it will be found — in spite of the great differences between the pressure curves — that in most cases, condensation takes place under almost identical conditions (with almost identical local \dot{P}) in the entire bucket channel, i.e., that the uniform droplet size is not severely "smeared out" by these effects. The points at which the Wilson points are located are generally in agreement with the condensation-shock lines of Fig. 13e. As concerns the influence of the change in the streamline relationships in the radial direction, this can, under certain circumstances, result in gross differences, in that, for example, coarse fog droplets form in the zone around the rotor and fine ones in the vicinity of the casing liner (or even vice versa), depending on where condensation intervenes at small and large values of \dot{P} . The smaller l_{Schfl}/D_m [$Schfl = \text{blade}$], the more uniform will be the fog droplets throughout the flow space.

From the insights gained from Fig. 17, we may draw two practical conclusions. First, there is a possibility of checking these theoretical statements experimentally: if, using suitable means, we shift the Wilson point in a wet-steam turbine, the related variation of fog-droplet size would necessarily produce, for example, a variation in the moisture loss — one that could be ascertained by efficiency measurement. As we pull the Wilson point through one stage, the moisture-loss variations should run through a period.

Secondly, a basic commandment for the design of wet-steam turbines follows from the above: pains should be taken to have the spontaneous

condensation result in the finest droplets possible. A means to this end is to draw the appropriate pressure curve and hold the stretches with slow pressure drop (intermediate spaces!) short so that, if possible, the Wilson point will always lie within a bucket ring with a steep pressure drop.

2.6. FLOW AND EXPANSION OF THE FOG

Forward in time from the collapse of supersaturation, the flow medium is no longer a pure vapor, but instead a fog, i.e., a mixture of steam and myriad tiny water droplets. (Note that in our usage, the term "fog" also embraces the steam. Only larger water droplets are excluded from it.) If we were to leave this fog at rest, it would come rapidly to thermodynamic equilibrium, with the droplet and steam temperatures approximating one another. If, on the other hand, the fog is subjected to further expansion, more and more water will keep coming due for precipitation, and this must — since otherwise sufficiently large areas would not be available — condense on the fog droplets. This is possible only if the steam is somewhat cooler than the drops. The extent of the "remanent **supercooling**" resulting from this depends on various factors (total surface area of the droplets, heat of condensation to be withdrawn per unit of time, effectiveness of heat transfer) and may vary quite considerably during the course of the subsequent expansion. Since any deviation from thermodynamic equilibrium means a loss, we shall go into greater detail in the second part of this section concerning determination of the remanent **supercooling**.

For the rest, the fog contains a considerable quantity of water, latent in which are an erosion danger and various possibilities for additional losses. The fog droplets are indeed so small ($\bar{r}_n = 0.2 \times 10^{-7}$ to $6 \cdot 10^{-7}$ m) that they can follow the motion of the steam almost perfectly in spite of its continual changes, but nevertheless

some of them skid onto the blade surfaces of each blade ring, with the result that water collects and coarse water droplets detach. It might also be hazarded that fog droplets collide with one another and ball up into larger droplets. Further, fog droplets may strike slower-moving larger water droplets and be swallowed up by them. Below we shall first go into the processes that tend to reduce the number of fog droplets.

a) Fluid-Dynamic Behavior of the Fog

Let us seek answers to the following questions: Do the fog droplets remain distinct during the expansion or do they ball together to form larger droplets? How large is the fraction of the fog droplets precipitated onto the blades during flow through the subsequent blade rings? How large is the fraction swallowed up by large water drops?

In order to form some conception of the droplet distribution in the fog, let us compute the average distance \bar{d} separating two fog droplets from one another. Let us imagine the steam space to be broken up into small cubes of edge length \bar{d} , each containing just one drop. Then let us compute the \bar{d} in a fog that has just formed, i.e., a fog in the state characterized by **: we have $\bar{d}^{**} = (v^{**}/n^{**})^{1/3} = (4\pi\rho_w \bar{r}_n^{**3} v^{**}/3y_n^{**})^{1/3}$, or $\bar{d}^{**}/2\bar{r}_n^{**} = (\pi\rho_w v^{**}/6y_n^{**})^{1/3}$. In a typical case with $y_n^{**} = 0.03$, $v^{**} = 2.5 \text{ m}^3/\text{kg}$, $\rho_w = 1000 \text{ kg/m}^3$ we get $\bar{d}^{**}/2\bar{r}_n^{**} = 35$, which alone indicates that collisions between two fog droplets will tend to be infrequent occurrences. Since, however, the specific steam volume y will still increase sharply to the end of the turbine, the average droplet distance will become still larger and we can therefore figure in general on $\bar{d}/2\bar{r}_n = 30$ to 70 .

A second quantity that can provide an insight into the conditions in the fog is the deceleration time of the fog droplets, which illustrates the ratio of the inertia and friction forces acting on them.

The deceleration time has been calculated for various droplet sizes at the end of Section 2.2 (Table 2.2.1). The fog-droplet radius is of the order of 10^{-7} m, so that their deceleration times are at most a few times 10^{-6} second, which represents a very small value. We can therefore state that the fog droplets are, so to speak, "nailed down" by friction in the steam.

We obtain an insight into the migration of the fog droplet in the steam from another angle if we regard the fog droplets as large molecules that form a "drop gas" mixed with pure steam. We may, in approximation, assume thermodynamic equilibrium between the two "gases." Then the equipartition law will apply and the kinetic gas theory gives for the mean thermal velocity of the droplets (see, for example, [36])

$$\bar{c}_{\text{therm}} = \sqrt{\frac{8KT}{\pi m_r}} = \sqrt{\frac{6KT}{\pi^2 \rho_w r_n^3}}. \quad (1)$$

With the data of the above example, we obtain about $\bar{c}_{\text{therm}} = 2$ cm/sec (while the steam molecules possess an average speed above 600 m/sec!). We may use \bar{c}_{therm} to obtain an estimate of the time that a fog droplet requires on the average in order to collide with another. We shall refer to this time as the mean lifetime of a droplet, since there is a high probability that on collision, the two droplets will combine to form a larger drop. Now on the average, a collision will occur when the droplet, flying hither and thither at \bar{c}_{therm} and with a frontal area $\pi(2\bar{r}_n)^2$ has swept the volume v/n ascribed to one droplet. The reason for calculating the "frontal area" with twice the droplet radius is that a collision occurs even when the centers of the two droplets are separated by a distance $2\bar{r}_n$. Accordingly, $\pi(2\bar{r}_n)^2 \bar{c}_{\text{therm}} \Delta t_{\text{Leben}} = v/n = v4\pi\rho_w \bar{r}_n^3 / 3y_n$, from which

$$\Delta t_{\text{Leben}} = \frac{4\rho_w v \bar{r}_n^3}{3y_n \bar{c}_{\text{therm}}}. \quad (2)$$

[Leben = lifetime]. If we assume the above numerical values, $v = 2.5$ m³/kg and $y_n = 5\%$ wetness, we obtain $\Delta t_{\text{Leben}} = 0.17$ sec - a very large value when we consider that the steam requires only $(2 \text{ to } 4) \cdot 10^{-3}$ sec to flow through the entire low-pressure part of a steam turbine!

Thus we have cast light on the coagulation of the fog droplets from two aspects. Our first train of reasoning showed that the friction in the surrounding medium is large as compared to the inertia of the drops. This excludes the possibility of rapid coagulation as a result of centrifuging, turbulence, etc. The second path of reasoning showed that even gas-kinetic considerations indicate no noteworthy balling together of droplets during such a short time. If we consider further that the fusion of two droplets of radius r_n produces a droplet of radius $\sqrt[3]{2} \cdot r_n = 1.26r_n$, i.e., one that differs only very slightly in size from the original droplets, we may well regard it as having been demonstrated that the properties of the fog are not influenced by coagulation as it flows through the turbine. This gives us the answer to our first question.

Let us next consider how we shall answer the second question - that as to the causes that might effect precipitation of the fog droplets. First to come under consideration as such a factor is the fact that the buckets force the passing steam to follow sharply curved streamlines. The entrained droplets follow these changes in direction only with a certain - if small - delay, and some of them strike the wall in the process. This effect arises in the vicinity of the stagnation point and at the concave (pressure) side of the profile. An additional factor might be found in the Brownian motion of the fog droplets; if a droplet accidentally touches the wall, it remains stuck to it. This gives rise to diffusion of the fog droplets against the wall. This tendency might be further intensified by any electrical forces of

attraction that operate. Below we shall investigate the phenomena cited one by one.

In front of the profile nose, the flow pattern is extensively similar to the flow about a circular cylinder. Thus we may reproduce the motion of the fog droplets in front of the profile nose with sufficient accuracy by computing the droplet orbits in the flow field about the cylinder (which we know from the complex representation), cf. Fig. 1. We obtain the differential equations of the problem from the Newtonian law of motion. The system formed by these two equations cannot

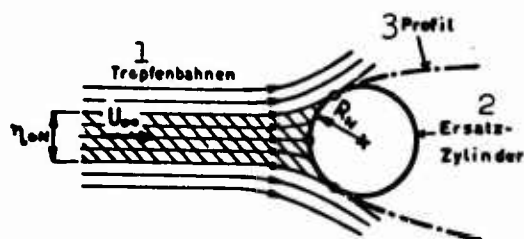


Fig. 2.6.1. Illustrating deposition of fog droplets on profile nose. 1) Drop orbits; 2) equivalent cylinder; 3) profile.

be solved analytically, but it can be solved stepwise without any trouble. The problem was programmed for the ERMETH* on the assumption that the droplets are brought into the flow at a distance of one cylinder diameter in front of the stagnation point but anywhere outside the axis of symmetry and have been endowed with the local flow velocity prevailing there. From the orbit curves obtained in this way, we quickly conclude the case that the droplets are brought into the flow at an infinite distance in front of the cylinder. For various droplet sizes or, more correctly, for various values of the governing dimensionless parameter

$$G_N = \frac{(\rho_d/2\rho_w)}{1 + 2.53Kn} \cdot \frac{R_N}{U_\infty F_n^2} = \frac{R_N}{U_\infty \Delta t_{\text{brems},n}} \quad (3)$$

we computed a number of orbit lines and, from these, picked out the ones that just made contact with the cylinder. There are two such lines, lying symmetrically. All droplets moving between these two lines strike the cylinder, while the others avoid it, see Fig. 1. The original distance of the two tangent orbit lines η_{ON} gives the width of the incident pencil of orbit lines. The following relationship was established:

$$\eta_{ON} = 2 R_N g_N(G_N). \quad (4)$$

The function g_N has the curve shown in Fig. 2. The case $g_N = 1$ (i.e., G_N small, say because the drops are very large) signifies that all droplets whose velocities were directed at the cylinder at infinity strike the cylinder, while $g_N = 0$ corresponds to total avoidance.

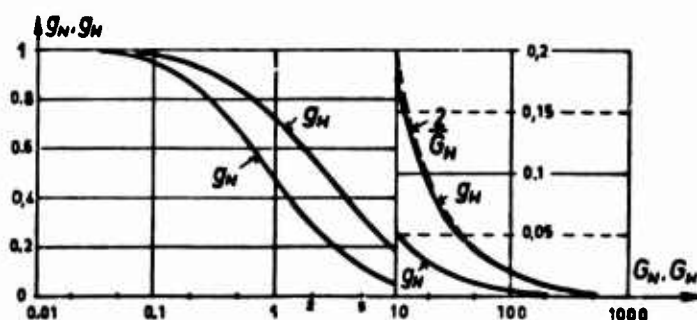


Fig. 2.6.2. Influence of the parameters G_N and G_H on deposition of fog droplets, cf. Eqs. (4) and (17), respectively.

For finer droplets ($\bar{r}_n \approx 2 \cdot 10^{-7}$ m), G_N is of the order of 10. Only very few of such droplets will therefore be deposited at the leading edges of the buckets. If, on the other hand, the fog droplets are coarser (for example, $\bar{r}_n = 6 \cdot 10^{-7}$ m, $\Delta t_{\text{brems},n} = 1.5 \cdot 10^{-5}$ sec), then G_N is about unity and we have $\eta_{ON} \approx R_N$, which is already enough to signify appreciable fog-droplet precipitation.

As concerns the droplets that spin out of the flow against the concave sides of the buckets, the result can be derived by a simple analytical path. The simple assumption that the concave side of the

profile and, with it, the streamlines $\sigma(\xi)$ of the steam in its vicinity are parabolic in shape permits close reproduction of reality. Then, with the notation of Fig. 3, the equation of the streamlines will be written

$$\sigma(\xi) = \text{const} + \gamma_1 \xi + \gamma_2 \xi^2, \quad (5)$$

where

$$\gamma_1 = \frac{s - s_1}{l_{ax}}, \quad (6a), \quad \gamma_2 = \frac{s}{l_{ax}^2}. \quad (6b)$$

Let us assume further that the axial component $c_{r,a}$ of the droplet velocity is always the same as the axial velocity of the steam and that both are constant:

$$c_{r,a} = c_a = \text{const}. \quad (7)$$

Thus we need write the equation of motion of the droplets only for the tangential direction. It is $m_r \dot{c}_{r,t} = W_t$, where the frictional resistance is given by Eqs. 2.2(1) and (31). After transposition, the equation of motion assumes the form

$$\frac{dc_{r,t}}{dt} = \frac{9\pi d^2 \rho_w F^2}{2(1 + 2.33 Kn)} (c_t - c_{r,t}), \quad (8)$$

where $c_t - c_{r,t}$ has been put for the tangential component of the relative velocity between droplets and steam.

To be able to decide which drops will strike the blades and which will not, we must know the trajectories of the droplets. If we represent these as the functions $\eta = \eta(\xi)$, we may write

$$\frac{d\eta}{d\xi} = \frac{c_{r,t}}{c_{r,a}} = \frac{c_{r,t}}{c_a}, \quad (9)$$

since, after all, the velocity of the droplet always traces its orbit in the tangential direction. An analogous relationship obtains between c_t/c_a and the shape of the streamlines:

$$\frac{d\sigma}{d\xi} = \gamma_1 + 2\gamma_2 \xi = \frac{c_t}{c_a}. \quad (10)$$

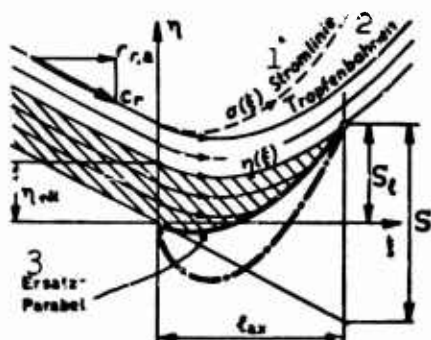


Fig. 2.6.3. Illustrating deposition of fog droplets on the concave side of a bucket profile. 1) Streamline; 2) droplet orbits; 3) equivalent parabola.

where we have used the parabolic streamline shape reproduced in Eq. (5).

Since, in general, the fog droplets are capable of following the motion of the steam quite closely, it would appear convenient to presuppose identical droplet and steam velocities at the entry into the bucket ($\xi = 0$) as an initial condition. The significance of this for the orbit line is that its tangent at

$\xi = 0$ must agree with that of the streamlines, as illustrated in Fig. 3:

$$\left. \frac{d\eta}{d\xi} \right|_{\xi=0} = \left. \frac{d\eta}{d\xi} \right|_{\xi=0} = \gamma_1. \quad (11)$$

From the equation of motion (8), applying Eqs. (9) and (10) and bearing in mind the relationship $dt = d\xi/c_a$, we can derive the following differential equation for the orbit line:

$$l_{ax} \frac{d^2 \eta}{d\xi^2} = \frac{(9\mu_d/2q_w)}{1 + 2.53 Kn} \frac{l_{ax}}{c_a l_n^2} \left(\gamma_1 + 2\gamma_2 \xi - \frac{d\eta}{d\xi} \right). \quad (12)$$

It is linear and of the second order, so that its solution presents no difficulty. Before writing the solution, however, we must formulate a second boundary condition, which, together with Eq. (11), will dictate the solution.

As in the case of the profile nose, we are also interested here primarily in that orbit line that separates the impinging droplets from those that do not impinge. This line is characterized by the fact that it passes through the exit edge. It thus satisfies the equation

$$\eta(l_{ax}) = \eta_1, \quad (13)$$

with which the sought second boundary condition has been found.

The solution of Eq. (12) with the boundary conditions (11) and

(13) will read

$$\eta(\xi) = r_1^2 + r_2^2 + \frac{2r_2^2 l_{ax}^2}{G_H^2} \left(G_H - \frac{G_H \xi}{l_{ax}} + e^{-\frac{G_H \xi}{l_{ax}}} - e^{-\frac{G_H \xi}{l_{ax}}} \right), \quad (14)$$

where, in analogy to Eq. (3), we have set

$$G_H = \frac{(\rho_p/2\rho_w) \cdot l_{ax}}{1 + 2.53 Kn} \cdot \frac{l_{ax}}{c_a F_n^2} = \frac{l_{ax}}{c_a \Delta t_{\text{brems},n}} \quad (15)$$

(The deceleration time $\Delta t_{\text{brems},n}$ was plugged in from Eq. 2.2(35).)

The value of this function at $\xi = 0$ is governing for the width of the impinging pencil of orbit lines, and we shall denote it by η_{OH} , cf. Fig. 3. We obtain from Eq. (14)

$$\eta_{OH} = \frac{2r_2^2 l_{ax}^2}{G_H^2} (G_H + e^{-G_H} - 1), \quad (16)$$

or, after substitution of r_2 from Eq. (6b),

$$\eta_{OH} = S \frac{2(G_H + e^{-G_H} - 1)}{G_H^2} = S \cdot g_H(G_H). \quad (17)$$

Thus the tangential width of the pencil impinging on the concave side of the profile, η_{OH} , referred to the "linear deflection" S (see figure), depends only on the dimensionless parameter G_H , which incorporates the physical quantities. The function g_H is represented in Fig. 2.

As a numerical example, let us again take $\bar{r}_n = 2 \cdot 10^{-7}$ m as the droplet radius and a profile with $l_{ax} = 0.05$ m, $c_a = 130$ m/sec. Depending on the magnitude of the Knudsen number (i.e., depending on the pressure), we then get $G_H = 200$ to 100 . (G_H is smaller for low pressures.) We read g_H from Fig. 2 and obtain with it $\eta_{OH} \approx (0.01-0.02)S$. If the S agrees approximately with the bucket spacing (which is very often the case), this signifies that about 1 to 2% of the fog droplets flowing through each ring glance off the buckets. This is, in itself, a very small amount; nevertheless, this effect is quite substantial for

turbines, since once it has gotten onto the buckets, the water gets back into the flow only in the form of large drops.

The fraction of the fog droplets deposited on the bucket profiles during flow through the ring, according to Eqs. (17) and (4) with t_{Schfl} denoting the bucket spacing, is

$$\epsilon_{n-f} = \frac{s}{t_{Schfl}} \epsilon_H(G_H) + \frac{2R_N}{t_{Schfl}} \epsilon_N(G_N) . \quad (18)$$

The subscript n-f indicates that the water passes here from fog-droplet form to the running-water form.

A second mechanism that can transport droplets to the turbine casing is diffusion. The bucket plates act as sinks that swallow up the fog droplets that reach them. In this process, the diffusion constant plays the same role as the thermal conductivity in heat flow through a body. It can be calculated for a certain droplet size. Its value for fog droplets is very small, since these droplets are enormously large as compared to the steam molecule. Further, the partial differential equation obtained from the law of diffusion for the distribution of the droplets in the space can be solved for the flow through a (geometrically simplified) cascade and we can determine from it how many fog droplets diffuse against the turbine casing per second. We find that fewer than one one-hundred-thousandth of all of the fog droplets flowing through are involved. For this reason, we shall dispense with reiteration of the calculation here and simply record the result - that diffusion is not in a position to bring an appreciable fraction of the fog droplets to the buckets.

Charging of the shaft with static electricity has frequently been noted in steam turbines. Since this observation has been made only on condensation turbines, it has been hazarded that the cause of the charging should be sought in the presence of the water droplets. Valu-

able ideas in this regard may be found in a paper by Gruber and Hansen [37] and in the appended discussion by R. Beach. Strictly speaking, we can hardly make more than qualitative statements concerning such static charging effects. Nevertheless, it appears that while, on the one hand, impingement of statically charged fog droplets might give an explanation for the shaft voltage, on the other hand the electrical forces are much too small to exert any influence on the motion of the droplets.

Finally, we must speak of yet another phenomenon that can, under certain circumstances, also convert noteworthy quantities of water from the fog-droplet form to large drops. The large drops torn from the buckets or rebounding from them require a relatively long time before they have more or less reached the velocity of the steam. During this time, they have a relative velocity - first very high and then diminishing - with respect to the steam. The question arises as to whether the fog droplets flowing with the steam can avoid the large drops or whether they collide with them and are thus swallowed up.

The results that we have obtained for the profile nose can be invoked to clear up this situation. That is to say, if in Eq. (3) we replace the profile-nose radius R_N by r_g , the radius of the large drop in question, we obtain with the calculated G_N from Fig. 2 that fraction of the onflowing fog droplets trapped by a cylinder having the same diameter as our large drop. The difference between a cylinder and a sphere would hardly be so great that the result could not be used for estimation purposes. We therefore now compute the parameter

$$G_g = \frac{(\rho_p/2\rho_w)}{1 + 2.53 Kn} \cdot \frac{r_g}{U_r r_n^2} = \frac{r_g}{U_r \Delta t_{\text{brems},n}} \quad (19)$$

where \bar{r}_n is the radius of the fog drop, r_g is that of the large drop and U_r is the relative velocity of the large drop with respect to the fog. The numerator in the first factor can be read from Diagram III,

or $\Delta t_{\text{brems},n}$ (for the fog drops!) can be taken from Table 2.2.1.

If we take $r_g = 5 \cdot 10^{-5}$ m, $\bar{r}_n = 2 \cdot 10^{-7}$ m and $U_r = 100$ m/sec as typical values, we obtain for low-pressure turbines the order of magnitude $G_g \approx 0.05$. If the function g_N is read from Fig. 2 for this value of G_N , we see that for all practical purposes $g_N = 1$, i.e., that practically all fog droplets moving at a large drop strike it (and are most probably swallowed up as a result).

The large drops that can digest fog droplets in this manner are divided into two groups in accordance with whether they have just been torn from the trailing edge of a (stator) bucket or have rebounded from the flat of a bucket. The drops of the first group (subscript g) are always accelerated from a standstill, while those of the second group (subscript gg) begin their flight with an initial velocity that is often quite high and may be directed at random either upstream or downstream.

Let us first investigate the freshly detached large drops and assume for the purpose that all of them are of approximately the same size,* i.e., that all have the radius \bar{r}_g . If such a drop traverses a relative path s_{rel} with respect to the flowing fog before its next impingement, it will sweep a volume $V_{\text{rel}} = \pi \bar{r}_g^2 s_{\text{rel}}$ and will, in its progress, swallow all of the fog droplets present in that volume. If we denote by y_g the mass present in these freshly detached drops, referred to the mass unit of the entire amount of wet steam flowing through, we have $n_g = 3y_g / 4\pi \rho_w \bar{r}_g^3$ for the number of drops. The ratio $V_{\text{rel}} n_g / v$ indicates that fraction of the steam volume whose fog droplets are swallowed by these drops. It can be assumed in approximation that the detached droplets are accelerated to one-fourth of the steam velocity c_1 by the time they strike the rotor buckets. Then their relative path with respect to the steam will be about $s_{\text{rel}} \approx 0.25 c_1 \Delta t_{\text{brems},g}$,

so that the fraction of the fog droplets swallowed up under these assumptions will be

$$\epsilon_{n-g} = \frac{v_{rel}^2}{v} \approx \frac{3}{4q_w} \frac{0,25 \Delta t_{brems,g}}{F_g} \frac{c_1}{v_1} y_g \quad (20)$$

A quite analogous train of reasoning can be applied to the rebounding large drops, except that here s_{rel} does not have a common value for all drops, but depends on the size of the individual drops and the direction of their initial velocity. It can be shown, however, that the average value of the relative paths of all drops agrees exactly with the relative path of the drops accelerated from a standstill if as many drops are sprayed off upstream as downstream. This is probably secure, since most of the drops strike the backs of the buckets almost perpendicularly, cf., for example, Fig. 2.8.2. We can therefore appropriate Eq. (20) in a corresponding sense; only the influence of drop motion across the steam streamlines must still be taken into account, at least roughly. For this purpose, we attach a factor $\sqrt{2}$ to Eq. (20) and thus obtain for the fraction of fog droplets swallowed by the rebounding large drops in a ring

$$\epsilon_{n-gg} \approx \sqrt{2} \frac{3}{4q_w} \frac{0,25 \Delta t_{brems,gg}}{F_{gg}} \frac{w_1}{v_1} \cdot y_{gg}, \quad (21)$$

where y_{gg} represents the specific mass contained in the ricocheting large drops. This process also unfolds in stator rings, where w_1/v_1 is to be replaced by c_0/v_0 . The average sizes of the two species of large drops, \bar{r}_g and \bar{r}_{gg} , will be accessible on the basis of Section 2.8.

If, for example, the wetness of the steam is $y = 0.05$ and 10% of this is contained in the large drops bounding back and forth between the buckets, i.e., $y_{gg} = 0.10 \cdot 0.05 = 0.005$, and the radius of these drops measures out at $\bar{r}_{gg} = 10^{-5}$ m, then we find with Eq. 2.2(36) and $w_1 = 200$ m/sec, $v_1 = 10$ m³/kg, the value $\epsilon_{n-gg} \approx 0.005$. The number of

fog drops swallowed up by slower-moving large drops from ring to ring is thus roughly comparable to the number caught by the buckets.

In summary, we may state the following: the number of fog droplets present in the flowing steam is reduced during passage through the turbine. This reduction can be traced back for the most part to three effects: centrifuging against the concave side of the bucket plates, deposition on the leading edges, and, to a lesser degree, on the tendency of the slower-moving large drops to aggrandize. The first two effects are in evidence in all rings; the third can become noticeable only where a sufficiently large amount of water is already present in the form of larger (detached) drops. The coefficient that indicates the reduction of fog-droplet count in the steam on passage through a single ring may be written as

$$\epsilon_n = \epsilon_{n-1} + \epsilon_{n-2} + \epsilon_{n-3} \quad (22)$$

Using the ϵ_n factors for the individual rings, we can calculate the change in the number of fog droplets. At the point ξ_a^{**} , where fogging had just been completed, this number was n^{**} per unit mass of steam and it dropped to

$$n_{nach\ k} = n^{**} (1 - \epsilon_n)_1 (1 - \epsilon_n)_{1+1} \dots (1 - \epsilon_n)_k \quad (23)$$

behind the k th ring [$nach$ = after]. The subscript 1 refers to the first ring coming after the point ξ_a^{**} .

Since the various ϵ_n lie between 0.005 and 0.10, depending on the shape of the buckets and the composition of the wet steam, i.e., are rather small, the major part of the water content (about 60-90%) will still be present at the end of the turbine in the form of fine-distributed fog droplets. This statement is confirmed by observations made on condensation turbines. That is to say, visibility into the interior of the turbine is severely impaired by the dense fog.

b) Thermodynamic behavior of the fog

The properties of the fog that forms on collapse of supercooling can be determined with sufficient accuracy on the basis of Section 2.5d. Among other things, we now know the total mass of all fog droplets per kg of steam, y_n^{**} , the average fog-droplet radius \bar{r}_n^{**} and the state point in the i, s -diagram from which the expansion continues — all for the point ξ_a^{**} , i.e., immediately after the collapse of supercooling. The line of subsequent expansion to be expected is known from the design of the turbine and from it we can take the polytropic efficiency η_p . Further, we know the curve of axial velocity $c_a(\xi_a)$ and the pressure curve $p(\xi_a)$. From the latter we can calculate the curve of the axial logarithmic pressure gradient $P_a(\xi_a)$, as was shown in Section 2.1. These data are sufficient for unique physical definition of the subsequent expansion. Here we assume that there is no water present in the steam apart from the fog droplets.

We shall make two simplifying assumptions for our further calculations: firstly, that all fog droplets are of the same size (we denote their radius by \bar{r}_n) and, secondly, that the number n of fog droplets in 1 kg of fog — cf. Eq. (23) — is known at least as an estimate and given, for example, in graphical form, as a function of the axial coordinate:

$$n(\xi_a) = n^{**} \cdot \xi_a(\xi_a). \quad (24)$$

Let us further assume that the fog droplets have the same temperature in their interior as on their surface and that the capillary effect is negligible. Then

$$T_w = T_f = T_g(\vartheta).$$

For the considerations to follow, we may disregard the relative velocity between fog droplets and steam. — These simplifications are admissible in all practical cases that arise in low-pressure expansions.

To formulate the problem mathematically, let us consider, with reference to Fig. 4, a certain quantity \underline{m} of fog containing a droplet of mass m_r and the quantity of steam m_d that accrues to the former. Obviously,

$$m = m_d + m_r \quad (25)$$

or, expressed in terms of the specific fog-droplet content and steam content,

$$\frac{m_r}{m} = y_n, \quad \frac{m_d}{m} = 1 - y_n = x. \quad (26)$$

We can now write the first principal theorem (in the conventional form $dQ = dI - Vdp$); for the steam we shall have

$$dm_r i'' - \dot{Q} dt = d(m_r i') - \frac{m_r}{\rho} dp. \quad (27)$$

and for the droplets

$$\dot{Q} dt - dm_r i'' + m \dot{q}_{rb} dt = d(m_d i_d) - m_d v_d dp \quad (28)$$

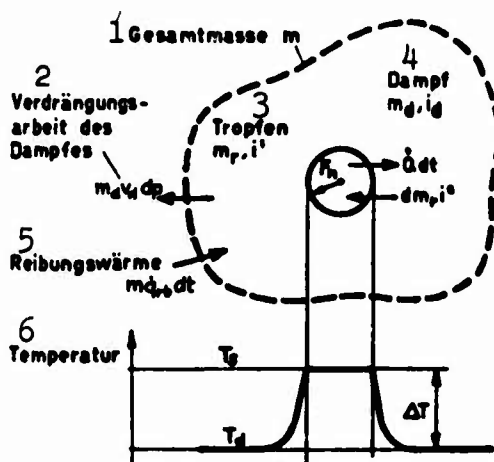


Fig. 2.6.4. Illustrating composition of the balance equations for the fog. 1) Total mass m ; 2) work of compression of the steam; 3) droplet; 4) steam; 5) heat of friction; 6) temperature.

here, \dot{q}_{rb} is the amount of frictional heat evolved in 1 kg of fog per unit time and can be expressed as

$$\dot{q}_{rb} = -(1 - y_p) v dp/dt. \quad (29)$$

This expression immediately becomes plausible when we consider that the "friction" embraces the entire loss stemming from the polytropic

efficiency η_p and that $|dl_s| = -vdp$.

The heat given up by the droplet to the steam is

$$\dot{Q} = 4\pi r_n^2 \alpha_r (T_s - T_d), \quad (30)$$

where, from Eq. 2.2(32),

$$\alpha_r = \frac{\lambda_d}{r_n} \frac{1}{1 + 3,18 Kn}. \quad (31)$$

For the Knudsen number see Eq. 2.2(5) or (9).

Let us further remember that

$$m_r = \frac{4\pi}{3} \rho' r_n^3, \quad (32)$$

and assume that all material properties are known, say as functions of p , then we have a complete system of equations describing the expansion of the fog.

We are interested in the curve of the supercooling $\Delta T \equiv T_s - T_d$ and the specific fog-droplet content y_n in the fog while the latter is flowing through the turbine (or through a certain group of stages). For practical reasons, the axial coordinate ξ_a is used as the independent variable ($dt = d\xi_a/c_a$).

Equations (24) to (33) can be modified in such a way as to leave two simultaneous differential equations for ΔT and y_n . Equation (27) results in

$$\frac{d\Delta T}{d\xi_a} = \frac{1}{c_p} (\eta_p RT_d - \frac{dl''}{d \ln p}) P_a - \frac{3\lambda_d}{\rho' c_p} \frac{y_n^{2/3} E_n^{2/3}}{r_n^{2/3} c_a} \frac{y_n^{1/3}}{(1 + 3,18 Kn)x} \Delta T - \frac{dx}{d\xi_a} \frac{\Delta T}{x} \quad (34)$$

and Eq. (28) in

$$- \frac{dx}{d\xi_a} = \frac{3\lambda_d}{\rho' L} \frac{y_n^{2/3} E_n^{2/3}}{r_n^{2/3} c_a} \frac{y_n^{1/3}}{1 + 3,18 Kn} \Delta T - \frac{1}{L} \frac{dl'}{d \ln p} P_a \cdot y_n + \frac{P}{\rho' L} P_a \cdot y_n. \quad (35)$$

Here we have set $l'' - l' = L$, $l_d = l'' - c_p \Delta T$ and $pv = xpv_d = xRT_d$. The Knudsen number of the droplet can be expressed in the following manner with the aid of y_n and the droplet-count diminution function $E_n(\xi_a)$:

$$Kn = \frac{I}{2r_n} = \frac{I(p)}{F_n^{**}} \left(\frac{y_n^{**} \cdot E_n}{y_n} \right)^{1/3} \quad (36)$$

because, after all, $\bar{r}_n / F_n^{**} = (y_n / y_n^{**} E_n)^{1/3}$.

The last terms of both Eqs. (34) and (35) are substantially smaller than all the others. The error that would be incurred if we dropped them is only as large as the errors that we have already incurred anyway by disregarding the capillary effect and the internal overtemperature of the droplets. Further, it can be shown that

$$x \frac{q'}{3\lambda_d} (\eta_p RT_d' - \frac{di''}{d \ln p}) = \frac{q' L}{3\lambda_d} \frac{dy_\infty}{d(-\ln p)} = Z_\theta(p, \eta_p) \quad (37)$$

- cf. Eq. 2.5(48) - so that we may finally write for Eq. (34)

$$\frac{d\Delta T}{d\xi_a} = \frac{3\lambda_d}{q' c_p} \left[\frac{Z_\theta P_a}{x} - \frac{y_n^{**2/3} E_n^{2/3}}{F_n^{**2} c_a} \cdot \frac{y_n^{1/3}}{(1 + 3.18 Kn)x} \cdot \Delta T \right] \quad (38)$$

and for Eq. (35)

$$- \frac{dx}{d\xi_a} = \frac{3\lambda_d}{q' L} \left(\frac{y_n^{**2/3} E_n^{2/3}}{F_n^{**2} c_a} \right) \frac{y_n^{1/3}}{1 + 3.18 Kn} \Delta T - \left(\frac{1}{L} \frac{di'}{d \ln p} \right) P_a \cdot y_n \quad (39)$$

This is a system of two nonlinear differential equations of the first order. The coefficients are all dependent on pressure or, what amounts to the same thing, on ξ_a . A solution in analytical form is out of the question and even a power-series theorem is found to be fruitless. We shall therefore develop a graphical method that will allow us to determine $\Delta T(\xi_a)$ even for a sharply variable axial logarithmic pressure gradient P_a . A graphical process appears the more appropriate because, after all, $p(\xi_a)$, $P_a(\xi_a)$, $c_a(\xi_a)$, $E_n(\xi_a)$ are also available in graphical form.

We have a first approximation for the solution $x(\xi_a)$; this is the

steam content in the case of thermodynamic equilibrium, $x_\infty(\xi_a)$, which we read from the i, s -diagram along the expansion line and can plot versus the axial coordinate. In the case of supercooling, the values of x will always be greater than the corresponding values in the ideal case. The latter could, in principle, also be obtained from Eqs. (38) and (39) by setting $\Delta T = 0$, $\alpha_r = \lambda_d = \infty$ and $\lambda_d \cdot \Delta T = \text{nonzero}$, but reading directly from the diagram is much simpler.

If, however, we are in possession of a first approximation for $x = 1 - y_n$, then we can for the time being dispense with more exact solution of Eq. (39) and seek a first approximation for $\Delta T(\xi_a)$ by inserting $y_n = 1 - x_\infty(\xi_a) = y_\infty(\xi_a)$ in Eq. (38):

$$\frac{d\Delta T}{d\xi_a} = \frac{3\lambda_d}{q'c_p} \left[\frac{z_a p_a}{x_\infty} \cdot \left(\frac{y_n^{2/3} E_n^{2/3}}{F_n^{2/3} c_a} \right) \frac{y_\infty^{1/3}}{(1 + 3.18 \text{Kn}_\infty) x_\infty} \cdot \Delta T \right]. \quad (40)$$

In this equation, all factors are either constants or known functions of the pressure or of ξ_a . (y_n is also to be replaced by y_∞ in Eq. (36) for the Knudsen number — a circumstance indicated here by means of a subscript.) The material quantities can be read from Diagram III (see Appendix) for each individual pressure.

From Eq. (40), we can define a direction field, calculating the tangents $d\Delta T/d\xi_a$ for various pairs of values ξ_a , ΔT . The result is represented schematically in Fig. 5. As will be seen, the field is so constituted that all solutions running from left to right (i.e., in the direction of declining pressure) must converge in a bundle.

The locus of those points at which the tangents are horizontal is calculated particularly simply in this field. Let us denote this curve by $\Delta T_h(\xi_a)$. Then with $\Delta T = \Delta T_h$, the left side of Eq. (40) must be zero:

$$0 = \frac{3\lambda_d}{q'c_p} \left[\frac{z_a p_a}{x_\infty} \cdot \left(\frac{y_n^{2/3} E_n^{2/3}}{F_n^{2/3} c_a} \right) \frac{y_\infty^{1/3}}{(1 + 3.18 \text{Kn}_\infty) x_\infty} \Delta T_h \right], \quad (41)$$

from which

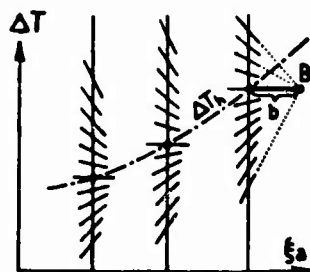


Fig. 2.6.5. Direction field of Eq. (40).

$$\Delta T_h = \frac{Z_8 P_a}{\left(\frac{y_n^{**2/3} E_n^{2/3}}{\bar{r}_n^{**2} c_a} \right) \cdot \frac{y_\infty^{1/3}}{1 + 3.18 Kn_\infty}} \quad (42)$$

or, if we transpose and use Eq. (36) together with Eq. 2.1(4),

$$\Delta T_h = Z_8 \frac{\dot{P}}{E_n} \cdot \frac{\bar{r}_n^{**2}}{y_n^{**}} \left[\left(\frac{y_n^{**} E_n}{y_\infty} \right)^{1/3} + \frac{1.59 I}{\bar{r}_n^{**}} \left(\frac{y_n^{**} E_n}{y_\infty} \right)^{2/3} \right] \quad (43)$$

The factor Z_8 and the quantity $(1.59 I)$ depend only on pressure. Their magnitudes can be determined for each ξ_a with the aid of Diagrams III and I (Appendix), respectively, since the pressure is, after all, known for each ξ_a . y_n^{**} and \bar{r}_n^{**} are given initial properties of the fog; the factor $(\dot{P}/E_n) \cdot (\bar{r}_n^{**2}/y_n^{**})$ is primarily decisive for the depth of supercooling. The expression in square brackets, which is plotted in Fig. 6, is of essential importance only at low pressures. It actually reflects the influence of the increase in total droplet surface and the deterioration of heat transfer at low steam densities.

Thus we can determine the course taken by ΔT_h . Below we shall show that a quick graphical determination of the sought undercooling curve $\Delta T(\xi_a)$ can be made on this basis.

Let us subtract Eq. (41) from Eq. (40). This gives

$$\frac{d\Delta T}{d\xi_a} = \frac{3\lambda_a}{q' c_p} \left(\frac{y_n^{**2/3} E_n^{2/3}}{\bar{r}_n^{**2} c_a} \right) \frac{y_\infty^{1/3}}{(1 + 3.18 Kn_\infty) E_\infty} (\Delta T_h - \Delta T) \quad (44)$$

or, modifying in much the same way as with Eq. (43),

$$\frac{d\Delta T}{d\xi_a} = \frac{\Delta T - \Delta T_h}{\left(\frac{q' c_p}{3\lambda_a} \right) \frac{\bar{r}_n^{**2} c_a}{y_n^{**} E_n} \left[\left(\frac{y_n^{**} E_n}{y_\infty} \right)^{1/3} + \frac{1.59 I}{\bar{r}_n^{**}} \left(\frac{y_n^{**} E_n}{y_\infty} \right)^{2/3} \right] E_\infty} \quad (45)$$

If we now lay off the distance

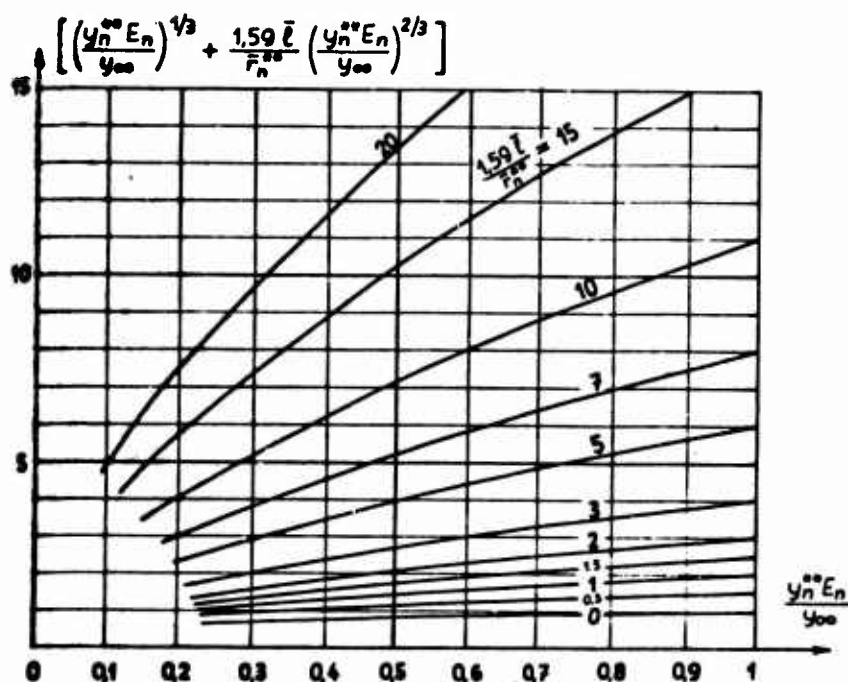


Fig. 2.6.6. Values of the expression in square brackets in Eqs. (43) and (46).

$$b = \Delta(\xi_a) = \left(\frac{q' c_p}{3 \lambda_d} \right) \frac{c_a}{E_n} \frac{\bar{r}_n^{**2}}{y_n^{**}} \left[\left(\frac{y_n^{**} E_n}{y_{\infty}} \right)^{1/3} + \frac{1.59 \bar{r}_n}{\bar{r}_n^{**}} \left(\frac{y_n^{**} E_n}{y_{\infty}} \right)^{2/3} \right] x_{\infty}, \quad (46)$$

which has the dimensions of length, horizontally from the point $(\Delta T_h, \xi_a)$ (cf. Fig. 5), we arrive at a point B possessing the property — as will be seen immediately from Fig. 5 with reference to Eq. (45) — that the tangents at all points corresponding to the ξ_a in question but to different supercoolings are directed toward it.

The fact that knowledge of the two quantities ΔT_h and b is enough to enable us to determine the current tangent of the $\Delta T(\xi_a)$ line is the basis of the graphical method to be described below as a means of determining $\Delta T(\xi_a)$. Let us at once summarize the course of the entire calculation.

Let us determine the course of supercooling in a turbine with fog flowing through it. At the outset ($\xi_a = \xi_g^{**}$), the properties of the fog (characteristic droplet radius \bar{r}_n^{**} , specific moisture content y_n^{**}) and the state point in the i, s -diagram are known. For the expansion

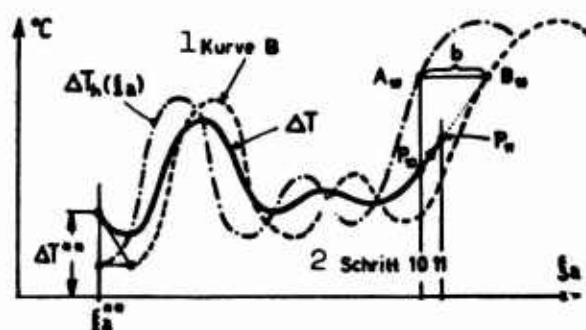


Fig. 2.6.7. Illustrating graphical determination of the supercooling curve $\Delta T(\xi_a)$. Curve B arises as a result of displacement of the points of the curve $\Delta T_h(\xi_a)$ by the corresponding length b to the right; for further explanation, see text. 1) Curve; 2) step.

that follows, we have the polytropic efficiency η_p and the functions $p(\xi_a)$, $c_a(\xi_a)$, $\dot{P}(\xi_a)$, $E_n(\xi_a)$ (pressure, axial velocity, rapidity of expansion, diminution of number of fog droplets). From these, we first use Eqs. (43) and (46) together with the diagrams in the appendix to determine the course of the two quantities ΔT_h and b and plot ΔT_h over ξ_a in a diagram: see Fig. 7. From each point of this curve, we lay off the corresponding value $b(\xi_a)$ in the direction of flow as a horizontal line segment. Thus we obtain a different, displaced curve B, with which we determine the direction of the tangents in the sense of Fig. 5.

If now we have somewhere an initial value given for the supercooling, e.g., the value ΔT^{**} corresponding to ξ_a^{**} , we can proceed from it to determine the course of the ΔT -curve graphically, step by step (see Fig. 7): if, for example, we have gotten the point P_{10} of the sought $\Delta T(\xi_a)$ curve in the 10th step, we seek the corresponding point A_{10} on the ΔT_h curve and with it the point B_{10} on the B curve. We join P_{10} with B_{10} and this gives us the direction in which we must extend the ΔT -curve to get to the point P_{11} . The step lengths can be chosen quite arbitrarily; shorter steps are to be recommended at points where the ΔT line shows sharp curvatures.

Thus we have obtained a supercooling curve based on substitution

of the value x_∞ corresponding to thermodynamic equilibrium for the unknown steam content x in Eq. (38). Thus the ΔT that we have obtained is not an exact solution of the system of equations (38) and (39), but only a first approximation for it. The fact that we can nevertheless dispense with further refinements proceeds alone from the fact [cf. Eq. (43) and Fig. 6] that the moisture-content curve exerts only a secondary influence on the supercooling curve.

For itself, however, the difference between y_n and y_∞ can become quite considerable. For this reason, the ΔT obtained should be plugged into Eq. (38) and the curve of $y_n = y_n(\xi_a) = 1 - x$ determined from it. This would be the consistent approach, but it is superfluous, since the moisture deficiency Δy can be calculated directly from Eq. 2.3(19) from the supercooling. Accordingly,

$$y_n(\xi_a) = y_\infty - \Delta y = y_\infty - \frac{c_p}{L} x_\infty \Delta T. \quad (47)$$

Thus far, everything applies only to the case assumed — namely, that the entire water content of the steam is present in the fog droplets, i.e., that $y = y_n$. In turbines, however, significant quantities of water may occur in other forms (large drops, etc.) under certain conditions. This water is of no significance for the condensation of the steam, since it offers only a small total condensation area and since the boundary-layer heating is generally high on the components of this area. However, its contribution to the water content must be taken into account, so that instead of Eq. (47) we must write

$$y_n = y_\infty - \Delta y - (y_g + y_{ng} + y_h) \quad (48)$$

The same reasoning also applies for the first approximation for y_n , which has been necessary in the course of the calculation to permit determination of the changes in ΔT_n and b from Eqs. (43) and (46), respectively; for the time being, however, we have said $y_n = y_\infty$; however,

to take other water forms into account, y_∞ should be replaced everywhere in Eqs. (43) and (46) by

$$(v_\infty)_{\text{wet}} = y_\infty - (v_g + y_{\text{ss}} + y_N) \quad (49)$$

The quantity in parentheses, which signifies the content of water present in other forms, must be known from other calculations and can therefore be regarded as a given function of ξ_a . More detail concerning this will be found under Heading 2.9.

If now we wish to compute the throughput volume correctly, i.e., taking supercooling into account, we must determine the specific volume of the wet steam. For thermodynamic equilibrium, this is

$$v_\infty = (1 - y_\infty) v''(p), \quad (50)$$

since, after all, we can disregard the volume of the water at lower pressures. If, however, the steam is undercooled, its specific volume will be smaller, and according to Eq. 2.3(21)

$$v = v_\infty \left[1 - \Delta T \left(\frac{1}{T_g} - \frac{c_p}{L} \right) \right]. \quad (51)$$

The quantity $(1/T_g - c_p/L)$ is plotted versus pressure in Diagram I.

The graphical method described here can also be applied to a segment of the turbine section through which the fog flows, say to the last stage. In this case, everything in the calculation remains the same except that the initial undercooling value from which we determine $\Delta T(\xi_a)$ graphically will be different. This is best chosen by trial and error in such a way as best to correspond to the periodic undercooling curve.

2.7. MOTION OF THE WATER ON THE BLADES AND CASING WALLS

On the basis of the considerations set forth under the previous headings, water can find its way onto the walls in considerable quantities in either of two ways: by condensation of the steam flowing through and by impingement of droplets. The former route predominates

before the point at which fogging intervenes and the latter afterward. As regards the impinging droplets, we must distinguish between fog droplets, which do not rebound, since they are very small and, moreover, impinge at an extremely acute angle, and large drops, which can be seen approximately as being torn off the trailing edges of the preceding bucket ring and striking the bucket wall at almost right angles. We should expect some of these drops to rebound, and even to take part of the water film on the wall with them, so that only a small fraction remains clinging to it.

Forces exerted on the water on a wall tend to set it in motion. Friction with the steam and the pressure gradient tend to drive it in the direction of the flow near the wall. The motion of the water is retarded by its viscosity. The surface forces, supported by the inevitable nonuniformities of the wall (grooves, etc.), tend to split the cohering film of water up into individual currents that seek their own routes through the salt crust or even in the metal and erode them away continuously. On the runner buckets, the centrifugal force also comes into play and, as can easily be shown, makes itself the dominant factor. If detachment regions arise on stator blades the water will come to rest there and have time to collect into large drops, which will then — provided that they are large enough — spray off and be atomized by the flow. The trailing edge of a stator blade which is generally from 0.5 to more than 2 mm wide, represents such a detachment region in all cases.

Let us next investigate the conditions in a very thin water film in laminar flow. The reasoning will also apply with sufficient accuracy to individual current filaments, since their extent in width is generally far greater than their thickness. In such cases, one-dimensional flow conditions prevail extensively; that is to say, the velocity com-

ponent perpendicular to the wall is negligible by virtue of the small film thickness and the transverse velocity because we assume — for the time being arbitrarily — that the forces capable of initiating such motion can be disregarded as small compared to the forces operating in the longitudinal direction. (On stationary walls, the governing forces are the pressure gradient and steam friction, while centrifugal force predominates on runner-bucket walls.) Let us denote the flow velocity by $u(\eta, \xi)$ and the field strength acting on a unit volume of the water in the layer by F (assuming it parallel to \underline{u}) and set up the coordinate system as shown in Fig. 1. Most terms of the Navier-Stokes equation can be disregarded under the assumptions that we have made (cf., for example, [16]), so that the flow equation will be

$$\mu_w \frac{\partial^2 u}{\partial \eta^2} = -F = -F(\xi) \quad (1)$$

If $\delta(\xi)$ is the film thickness and \dot{m}_f is the mass throughput in the film per unit of width, which is assumed to be given in advance, the continuity equation assumes the form

$$\rho_w \int_0^{\delta} u \, d\eta = \dot{m}_f = \dot{m}_f(\xi) . \quad (2)$$

Here we have indicated that F and \dot{m}_f need not be constants, but may vary with ξ . We prescribe as boundary conditions that the velocity vanishes at the wall,

$$u(0, \xi) = 0 , \quad (3)$$

and that the shear stress at the surface of the film has the value $\tau(\xi)$ due to the external flow and given in advance, i.e., that

$$\mu_w \left. \frac{\partial u}{\partial \eta} \right|_{\eta=\delta} = \tau(\xi) . \quad (4)$$

Determining the δ and \underline{u} that satisfy Eqs. (1) to (4) presents no difficulty. For the film thickness $\delta(\xi)$, we obtain the equation



Fig. 2.7.1.
Forces and velocities in a water film.

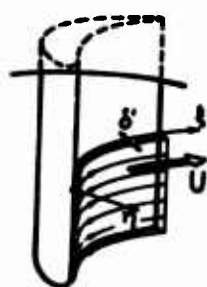


Fig. 2.7.2.
Water film on a stator blade (shown only in part for clarity).

$$\left[\frac{F}{3} \cdot \delta(\xi) + \frac{\tau}{2} \right] \cdot \delta(\xi)^2 = \frac{\mu_w}{\rho_w} \dot{m}_f \quad (5)$$

and, for the velocity profile, a parabola

$$u(\eta, \xi) = - \frac{F}{\mu_w} \cdot \frac{\eta^2}{2} + \left[\frac{\tau}{\mu_w} + \frac{F}{\mu_w} \cdot \delta(\xi) \right] \cdot \eta. \quad (6)$$

We obtain the average velocity in the film from

$$\bar{u}(\xi) = \frac{\dot{m}_f}{\rho_w \delta(\xi)} = \frac{\delta(\xi)}{\mu_w} \left[\frac{F}{3} \cdot \delta(\xi) + \frac{\tau}{2} \right]. \quad (7)$$

let us now apply these equations to the water flow on turbine blades and casing walls.

Blades

No centrifugal force arises in the case of stator blades. The layer is driven forward by the steam friction τ_d , by the momentum current τ_n transferred by the impinging fog droplets and by the pressure gradient $dp/d\xi$. Let us lay the ξ -axis in the direction of the current, cf. Fig. 2. We have

$$\tau(\xi) = \tau_d(\xi) + \tau_n(\xi) = c_F \frac{1}{2} \rho_{d0} c_0^2 + \dot{m}_n U, \quad (8)$$

where τ_d has been substituted from Eq. 2.4(2) (there denoted by τ) and the "shear stress" τ_n produced by the fog droplets calculated as the mass \dot{m}_n arising per unit of time and surface area multiplied by its velocity at impingement U . The field force originates from the pressure drop, but can be disregarded, at least in first approximation, for thin layers such as occur on the buckets:

$$F(\xi) = - \frac{dp}{d\xi} \approx 0. \quad (9)$$

We are interested primarily in the layer thickness. It is found from Eq. (5) as

$$\delta(\xi)' \approx \left(\frac{2\mu_w}{\rho_w} \cdot \frac{\dot{m}_f(\xi)}{c_F \frac{1}{2} \rho_{d0} c_0^2 + \dot{m}_n U} \right)^{1/2} \quad (\text{stator blades}). \quad (10)$$

We shall give a numerical example only later, when we will be able to compare stator and rotor buckets simultaneously.

On a runner blade, the centrifugal force predominates by far (proof follows later), so we lay the coordinate system in such a way that ξ points radially outward, cf. Fig. 3. The field force F is to be set identical to the centrifugal force Z :

$$F = Z \approx \text{const} = \rho_w D_m \omega^2 / 2, \quad (11)$$

where D_m is the diameter of the bucket midpoint circle. Since the steam flows almost axially, there is no shear stress acting radially on the layer, so that

$$\tau(\xi) = 0. \quad (12)$$

Equation (5) gives for the layer thickness

$$\delta(\xi) = \left(\frac{3\mu_w}{\rho_w} \cdot \frac{\dot{m}_f^2(\xi)}{\frac{1}{2}\rho_w D_m \omega^2} \right)^{1/3} \text{ (runner buckets)}. \quad (13)$$

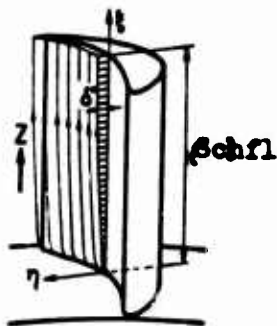


Fig. 2.7.3. Water film on a runner bucket (shown only in part for the sake of clarity); steam friction disregarded.

Let us now compare, as an example, the runner and stator buckets of the next-to-last stage of the reaction turbine described under heading 2.1 (see Table 2.1.1). We insert the following values: $\mu_w = 5.5 \cdot 10^{-4}$ kg/msec, $\rho_w = 10^3$ kg/m³, $\rho_{d0} = 0.12$ kg/m³, $D_m = 1.90$ m, $c_0 = 188.3$ m/sec; $\omega = 314$ sec⁻¹. We calculate the layer thicknesses on the concave sides of both buckets just in front of the trailing edge (where, by estimation, $U = 360$ m/sec, $c_p = 0.035$) or just before the point of the bucket, as appropriate. The fog-droplet content in the flowing steam is assumed to be $y_n = 8\%$, of which $\epsilon_{n-f} = 2\%$ is deposited

on the buckets of a ring.

Since the total amount flowing through is $\dot{M} = 40$ kg/sec, the mass

throughput in all concave-side layers of a ring comes to $\dot{M}_f = \epsilon_{n-f} \times y_n \dot{M} = 0.064 \text{ kg/sec}$. All trailing edges of the stator ring present to the layers a total width $z' l'_{\text{Schf1}}$ [Schf1 = bucket] $\approx 26 \text{ m}$ and all concave-side profile contours of the runner ring offer a total width of $z'' \cdot s''_H \approx 7.3 \text{ m}$. Accordingly, $\dot{m}'_f = 0.064/26 = 2.5 \cdot 10^{-3} \text{ kg/msec}$ and $\dot{m}''_f = 0.064/7.3 = 9 \cdot 10^{-3} \text{ kg/msec}$. If we assume that the incident fog-droplet flow is distributed uniformly over the entire concave side, then \dot{m}_n becomes - with a total impingement area of $A'_{\text{Schf1,H}} = z' s'_H l'_{\text{Schf1}} = 2.6 \text{ m}^2$ - $\dot{m}_n = 0.064/2.6 = 2.5 \cdot 10^{-2} \text{ kg/m}^2\text{sec}$. Thus the layer thicknesses and water velocities near the trailing edges of the stator buckets according to Eq. (10) and (7), respectively, become

$$\delta' = \left(1,1 \cdot 10^{-6} \frac{2,5 \cdot 10^{-3}}{74 + 9} \right)^{1/3} = 0,57 \cdot 10^{-5} \text{ m}, \quad \bar{u}' = 0,44 \text{ m/sec} \quad (14)$$

and those on the runner buckets in the vicinity of the bucket tips, according to Eqs. (13) and (7), respectively,

$$\delta'' = \left(1,65 \cdot 10^{-6} \frac{9 \cdot 10^{-3}}{9,4 \cdot 10^7} \right)^{1/3} = 0,54 \cdot 10^{-5} \text{ m}, \quad \bar{u}'' = 1,7 \text{ m/sec}. \quad (15)$$

Now if the water layers do not cohere to fill out the entire width available to them, but contract to form current filaments that cover a total of, for example, only 5% of the width, then \dot{m}_f increases by a factor of twenty in either case and we obtain

$$\delta' = \sqrt[3]{20} \cdot 0,57 \cdot 10^{-5} \approx 2,5 \cdot 10^{-5} \text{ m}, \quad \bar{u}' \approx 1,0 \text{ m/sec}, \quad (16)$$

$$\delta'' = \sqrt[3]{20} \cdot 0,54 \cdot 10^{-5} \approx 1,5 \cdot 10^{-5} \text{ m}, \quad \bar{u}'' \approx 12 \text{ m/sec}. \quad (17)$$

Thus we see that the thickness of the water layer or water streaks cannot amount to more than a few hundredths of a millimeter.

We still owe a proof that the effect of steam friction can be disregarded in the presence of a centrifugal force. This is the case when the velocity imparted to a given layer by the centrifugal force far exceeds the velocity produced by friction alone. On the basis of Eq.

(7), this would require that $Z\delta/3 \gg \tau/2$. If, for example, we take $\delta = 1.5 \cdot 10^{-5}$ m, leaving other data the same as above, we obtain $Z\delta/3 \approx 470$ and $\tau/2 \approx 42 \text{ kg/m} \cdot \text{sec}^2$; thus the simplification was in fact justified. Only for very thin layers would two-dimensional treatment of the problem become necessary.

An inference can be drawn as to the direction of flow on the rotor buckets from the ratio of the centrifugal and friction forces. We obtain a rough approximation by stating that the axial component of the flow velocity in the layer is as large as though no centrifugal force were in operation and that the radial component is as it would be in the absence of friction. From this we obtain the following estimate for the angle φ indicating the deviation of the flow direction from the radius:

$$\lg \varphi \approx \frac{v_{ax}}{v_{rad}} = \frac{\tau/2}{Z\delta/3} . \quad (18)$$

Using the above data, we obtain for a layer of $\delta = 1.0 \cdot 10^{-5}$ m the angle $\varphi = 7.5^\circ$; for a "thick" layer (or current streak) with $\delta = 2 \cdot 10^{-5}$ m, we get approximately $\varphi = 3.8^\circ$. In the last runner-bucket rings, therefore, we should expect approximately radial flow. This result is in fact in agreement with the erosion tracks (cf. [8]) observed in practice. It follows from this nearly radial flow that only a small part of all the water caught by a runner bucket reaches the trailing edge. Further, some of this water, acted upon by the centrifugal force field, might find its way to the tip of the bucket between the minute nonuniformities on the trailing-edge spine, with the result that only a small residue, which we may disregard with a clear conscience, sprays off the trailing edge. In practice, this result is confirmed by the observation of little or no erosion traces on the leading edges of stator blades (which would, after all, be struck directly by such drops),

while damage of this type can always be detected on the runner buckets.

Casing walls

Conditions on the casing wall are similar to those on the stator buckets, with the following differences. Firstly, more water must, in general, flow through here per unit of width, so that \dot{m}_f is larger. Secondly, the motive friction forces are smaller, since practically no fog droplets strike the casing wall, for which reason τ_n is dropped from Eq. (8), and also because the friction coefficient c_F is smaller than on the buckets due to the larger boundary-layer thicknesses. The secondary flows favor swelling of the water layer in the vicinity of the blade suction sides. Due to the greater layer thicknesses, the influence of the pressure gradient may not be disregarded. With $\tau_n = 0$ (i.e., $\tau = \tau_d$) and $F = -dp/d\xi$, assuming that ξ points in the flow direction of the layer, Eq. (5) becomes

$$\left[-\frac{1}{3} \frac{dp}{d\xi} \cdot \delta(\xi) + c_{F, \text{Gehäuse}} \frac{\rho_{d0} c_0^2}{4} \right] \cdot \delta(\xi)^2 = \frac{\mu_w}{\rho_w} \dot{m}_{f, \text{Gehäuse}}, \quad (19)$$

[Gehäuse = casing] from which we may calculate the layer thickness.

As an example, let us calculate the layer thickness on the wall between two stator buckets. We may assume $c_{F, \text{Gehäuse}} = 0.01$ and, further, that $\dot{M}_{f, \text{Gehäuse}} = 0.4$ kg/sec of water flows circumferentially on the wall (this corresponds to 1% of the total mass throughput, and is thus an exaggeratedly high assumption, as will be shown under heading 2.9). The width available to this flow is of the same order as the casing circumference, i.e., about $2.20 \cdot \pi \approx 7$ m. It would be better, however, to assume that due to rivulet formation and collection of water in the corner at the suction side, only part of this width, let us say only about 2 m, is used by the flow. Then $\dot{m}_{f, \text{Gehäuse}} = 0.4/2 = 0.2$ kg/m·sec. We use the same values as previously for μ_w , ρ_w , ρ_{d0} and c_0 . The pressure gradient can be estimated from Table 2.1.1. The

average axial pressure gradient in ring 5' is $(dp/d\xi_a)_{\text{mittl}} \approx$
 $\approx -p_{\text{mittl}}(-d \ln p/d\xi_a)_{\text{mittl}} = -p_{\text{mittl}} \cdot P_a \approx -0.14 \cdot 10^5 \cdot 4.1 \approx -0.6 \cdot 10^5$
 N/m^3 [mittl = average]; the pressure gradient along the streamlines of
the water layer is, on the one hand, somewhat larger than this, since
the steam flow is sharply accelerated in the ring, and, on the other
hand, somewhat smaller because ξ is not axial. For this reason, we as-
sume $dp/d\xi = -1 \cdot 10^5 \text{ N/m}^3$. Then Eq. (19) reads

$$[0.33 \cdot 10^5 \cdot \delta + 10, 7] \cdot \delta^2 = 1,1 \cdot 10^{-7}, \quad (20)$$

from which

$$\delta_{\text{Gehäuse}} \approx 0,9 \cdot 10^{-4} \text{ m}, \quad U_{\text{Gehäuse}} = \frac{m_{\text{f, Gehäuse}}}{\rho_w \delta_{\text{Gehäuse}}} \approx 2,2 \text{ m/sec.} \quad (21)$$

[Gehäuse = casing]. Thus, while the layer thickness of the rivulets
flowing along the casing wall may be considerably larger than the layer
thicknesses on the buckets, it is nevertheless hardly greater than a
tenth of a millimeter!

The water running around the casing wall is continuously being
driven into regions where the pressure is lower. It is conceivable
that the water layer might boil up in this process, in much the same
way as the water boils in a pressure cooker when the pressure in the
cooker is suddenly reduced. This danger of boiling is the greater the
more rapid the decline in the pressure to which a flowing water par-
ticle is subject. (High flow velocity, steep pressure gradient.) The
layer has two possibilities for reducing its temperature without boil-
ing. It can give up heat at its surface, in which case evaporation
arises there, and it can yield heat to the casing wall, since this is
frequently somewhat cooler. The thinner the layer is, the more effec-
tive will these two processes become.

Now it can be calculated that, with the layer thicknesses and ve-
locities somewhat as they appear in Eq. (21), the excess temperature

that must arise in the interior of the water layer for continuous cooling of the layer to take place by heat conduction in both directions amounts only to a few tenths of a degree Centigrade. Since the temperature of the steam-side surface of the water layer is about the same as the local saturation temperature at all times as a result of suitably vigorous vaporization, this implies that the interior of the layer is overheated by a few tenths of a degree. Now, however, a liquid generally requires several degrees of excess temperature if it is to boil internally. (In much the same way as steam requires about 30°C or more of supercooling for spontaneous condensation.) Otherwise the most that could happen is formation of steam bubbles on the wall side of the layer. — In any event, it can be established that vigorous bumping of the water layer, with the associated slinging of water back into the steam flow in the form of more or less coarse drops is hardly to be expected in turbines.

2.8. FORMATION, EFFECT AND FATE OF LARGE DROPS

Water that has somehow gotten onto the buckets and collected at the trailing edges or in detachment regions is torn away from these places from time to time by the steam current. These spraying clumps of water may initially be of the same order of size as raindrops (diameters of 1 mm or even more); however, due to the high velocity of the steam, they are instantly broken up into many fragments. These small droplets are, however, still very large as compared to the fog droplets that have formed in the steam. As will be calculated below, their radii lie between 10^{-5} and 10^{-4} m. We shall always refer to them as the "large drops" and provide quantities referring to them with the subscript g. If projections and the like are present on the casing wall, the water flow moving by them may be sprayed off to form another contribution to the formation of such large drops.

The fact that the behavior of these "large drops" will differ quite grossly from that of the fog droplets can be seen alone from the fact that their radii are about a hundred times larger and their masses consequently about a million (!) times larger than the mass of the fog droplets. It is these large drops that cause erosion.

a) Atomization of Detached Drops

First we must know the size of the drops formed on fragmentation of a detached clump of water. This problem has been treated in detail by v. Freudenreich [4]. He conducted drop-fall experiments in which large drops of water were blown apart by a vertical current of air. Similar experiments had already been designed earlier for other objectives, compare Lenard [38] and Hochschwender [39].

As a dimensionless stability criterion for a drop, we obtain

$$Kz = \frac{\rho_d \cdot U_r^2 \cdot 2r}{\sigma}, \quad (1)$$

which expresses the ratio of the deforming pressure forces (which are proportional to $\frac{1}{2}\rho_d U_r^2$) to the cohesive surface-tension forces (the latter being proportional to $2\sigma/r$). The value of this criterion for the largest drops that are still stable, Kz_{\max} , can be determined by experiment. Lenard found $Kz_{\max} = 6$, Hochschwender got 9 to 16, and v. Freudenreich about 20. (Concerning Lenard's experiments, we should note that in this case, the drops were kept hovering in the air current, so that much time was available for blowing the individual drops apart.) For our calculations we shall use the value

$$Kz_{\max} = 15, \quad (2)$$

which gives the expression

$$r_{g, \max} = \frac{15}{2} \frac{\sigma}{\rho_d U_r^2} \quad (3)$$

for the radius of the largest still stable drop. Drop-size criteria applying for other forms of liquid disintegration, e.g., for atomiza-

tion, are not useful here, since they are extensively based on the influence of the internal turbulence in the jet of liquid - something that does not exist at all in our case.

The upper limit of drop size is imposed by Eq. (3). There is no corresponding fixed lower limit, and quite small droplets can also form accidentally. On the basis of experience, however, very small droplets occur relatively seldom. Various authors have determined the size distribution of the drops by means of drop counting. An elegant theoretical derivation of the distribution curves can be found in Troesch [40]. From statistical considerations, he obtains the formula

$$dn = \frac{3}{4\pi Q_w} \cdot \frac{r_g e^{-\left(\beta \frac{r_{g, \max}}{r_g}\right)}}{e^{-\beta} + \beta \cdot Ei(-\beta)} \cdot \frac{dr_g}{r_{g, \max}} \quad (4)$$

for the distribution of the drop count over the various radii, and for the distribution of drop masses

$$dm = \frac{e^{-\left(\beta \frac{r_{g, \max}}{r_g}\right)}}{e^{-\beta} + \beta \cdot Ei(-\beta)} \cdot \frac{dr_g}{r_{g, \max}} \quad (5)$$

(dn is the number and dm the mass of the drops per kilogram of total water quantity whose radii fall between r_g and $r_g + dr_g$).

The parameter β characterizes the type of atomization. Its magnitude is obtained by comparing the distribution curves obtained through Eq. (5) with curves determined experimentally. Troesch establishes the order of magnitude $\beta \approx 0.35$ for atomizations. For free-fall experiments, where, after all, a different mechanism provides for the disintegration, the same value of β need not apply. Enumeration curves pertaining to this can be found in Hochschwender; they are reproduced most closely by selecting $\beta = 2$, cf. Fig. 1.

The important thing that these distribution curves tell us is that the average drop size is only a little smaller than $r_{g, \max}$, or, in

other words, that the drop sizes have a narrow spectrum. For this reason, we can consistently treat all large drops on the basis of a representative large-drop radius \bar{r}_g , whose magnitude we select in such a way as to provide the best possible approximation for all drops. If we take $\bar{r}_g = 0.8 r_{g,\max}$, then more than 80% of the total mass is present in the droplets whose radii differ by no more than $\pm 25\%$ from \bar{r}_g .⁴⁶⁾ On the basis of Eq. (3) we then obtain

$$\bar{r}_g = 0.8 r_{g,\max} = 0.8 \frac{\sigma}{\rho_d U_r^2} \quad (6)$$

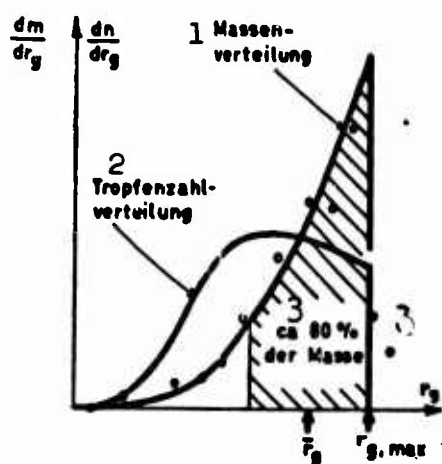


Fig. 2.8.1. Distribution of drop number and mass for blown-apart drops, as calculated from Eqs. (4) and (5), respectively, with $\beta = 2$. Circles indicate experimental values from [39]. 1) Mass distribution; 2) drop-number distribution; 3) about 80% of the mass.

In the case of drops torn from the trailing edge of a stator blade, the governing flow velocity U_r to be inserted here would be equal to the exit velocity from the blading (c_1) if the steam were blown at full speed against the initially still stationary drops. Since, however, a lower steam velocity prevails in the boundary layer and in the wake, we estimate

$$|U_r| \approx 0.8 c_1 \quad (7)$$

for substitution, thus finally obtaining the formula

$$\bar{r}_g = \frac{9\sigma}{\rho_{d1} c_1^2} = \frac{(9\sigma RT_d)_1}{\rho_{d1} c_1^2} \quad (8)$$

for the representative size of the large drops spraying off the stator-bucket trailing edges, where we may set $(9\sigma RT_d) = \text{const} = 8.7 \cdot 10^4$ kg-m/sec for pressures below 10 bars.

With $\sigma = 0.067$ N/m, we obtain, for example, with a steam density $\rho_{d1} = 0.08$ kg/m³ at the exit from the stator ring (which corresponds

to a pressure of about 0.12 bar) and $c_1 = 360$ m/sec, a drop radius

$$r_g = 7 \cdot 10^{-5} \text{ m}, \quad (9)$$

which means a drop diameter of about a tenth of a millimeter. Thus these "large" drops are in fact enormous compared to the fog droplets.

b) Motion of Detached Drops

Given knowledge of the drop size, we can judge of the motion of the drops on the basis of heading 2.2. Let us denote by ξ the path

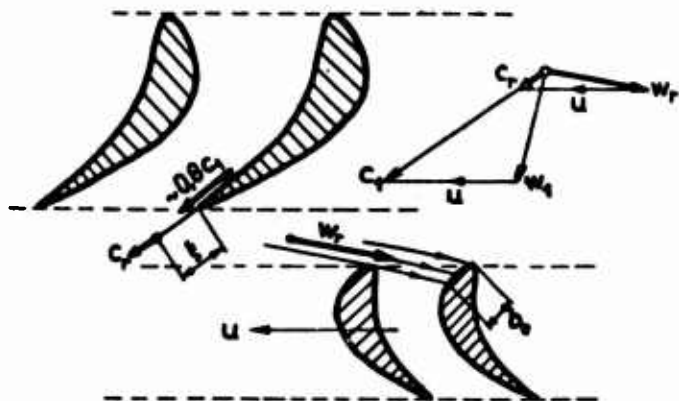


Fig. 2.8.2. Illustrating motion of drops torn from trailing edge of stator blade.

that has been covered by a drop since it was torn away (cf. Fig. 2) and set its initial velocity equal to zero:

$$c_r(0) = 0. \quad (10)$$

The motion of the drop can be calculated on the basis of Newton's law, inserting the steam friction W from Eq. 2.2(1) as the accelerating force. Such a solution of the equation of motion has been carried out, for example, in [4].

Now, however, the major part of the detached drops strikes the next row of runner buckets, as will soon be shown, so that it is sufficient for our purposes to know their motion on a short initial path ($\xi \leq 5$ cm). A simple estimate of their motion can be made if we assume that the force of friction working on a drop does not diminish noticeably on this initial path. This assumption is justified as long as the

relative velocity has not become essentially smaller than it was at the beginning. Then \dot{c}_r , the acceleration of the drop, will also remain constant:

$$\dot{c}_r \approx \dot{c}_r(0), \quad (11)$$

and, according to an elementary formula of mechanics, the drop velocity after the path has been traversed will be

$$c_r(t) = \sqrt{2 \dot{c}_r(0) \cdot t}. \quad (12)$$

The calculation of $\dot{c}_r(0)$ can be made with the aid of the deceleration time defined by Eq. 2.2(33), which represents a measure of the friction force. It follows from Eq. 2.2(36) on substitution of $r = \bar{r}_g$ in that equation and use of $U_r = 0.8c_1$ in the Reynolds number. With introduction of the deceleration time, Eq. (12) assumes the form

$$c_r(t) = \sqrt{2 \frac{-U_r(0)}{\Delta t_{\text{brems}}(0)} \cdot t}. \quad (13)$$

[brems = deceleration]. Since the drops start from a state of rest, $U_r(0) = -c$. We shall again assume the steam velocity c to be constant and set $c \approx 0.8c_1$, since, after all, it appears that the majority of these drops will remain in the downstream depression. Below we shall not concern ourselves any further with the negative sign of U_r , but use that quantity to imply the absolute magnitude of the relative velocity between steam and drops. After transposition, Eq. (13) gives

$$\frac{c_r(t)}{c_1} = \sqrt{\frac{2 \cdot 0.8t}{c_1 \Delta t_{\text{brems}}(0)}} = 0.8 \sqrt{\frac{t}{(\frac{1}{2} U_r \Delta t_{\text{brems}})_{t=0}}}. \quad (14)$$

Thus the curve of drop velocity is a function of the parameter $(\frac{1}{2} U_r \Delta t_{\text{brems}})$. Some curves of this type are shown in Fig. 3.

The inertia parameter is calculated on the basis of Eq. 2.2(36):

$$(\frac{1}{2} U_r \Delta t_{\text{brems}})_{t=0} = \frac{F_g^2}{(9\mu_d/2q_w)} \cdot \frac{U_r(0)}{\sqrt{Re_r(0)}} = \left(\frac{0.14 q_w \sqrt{RT}}{\sqrt{\mu_d}} \right) \frac{F_g^{3/2} \sqrt{c_1}}{p_1}. \quad (15)$$

The material quantity in parentheses varies only slightly with pres-

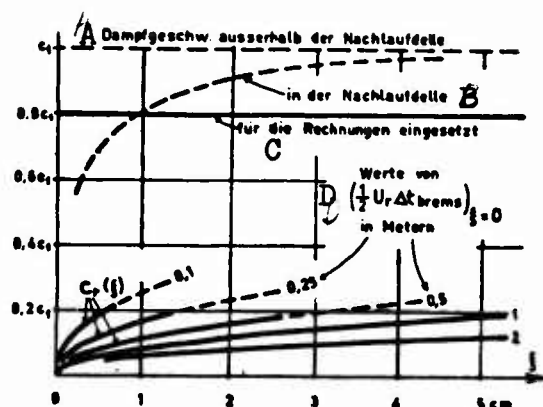


Fig. 2.8.3. Approximate curve of absolute velocity c_r of a detached drop, calculated from Eq. (14). A) Steam velocity outside the downstream depression; B) in the downstream depression; C) used in calculations; D) values of $(\frac{1}{2}U_r \Delta t_{brems})_{\xi=0}$ in meters.

sure; for low-pressure turbines, we can set the value for this quantity at $1.6 \cdot 10^7$, provided that we insert \bar{r}_g , c_1 and p_1 in m, m/sec and N/m^2 , respectively. As an example, let us calculate the values of the inertia parameter for various droplet sizes for $c_1 = 360$ m/sec and $p_1 = 0.15$ bar:

TABLE 2.8.1

r_g m	10^{-5}	$2 \cdot 10^{-5}$	$5 \cdot 10^{-5}$	10^{-4}
$(\frac{1}{2} U_r \Delta t_{brems})_{\xi=0}$ m	0,08	0,22	0,88	2,5

A) brems = deceleration.

These parameter values can easily be extended to other values of pressure and steam velocity by the use of Eq. (15).

A further correction would be necessary due to the deviation of the drops from the spherical shape. For distorted drops, the resistance coefficients are greater than for perfectly round ones, so that their deceleration times become shorter. From Lenard's experiments, we may conclude that the distortion is not perceptible for drops smaller than $0.3 r_{g,max}$. At $0.8 r_{g,max}$, which we shall use as the characteristic

drop size \bar{r}_g , we find the resistance coefficient to be larger by a factor of about 1.9 than the value that would correspond to a spherical shape. This sharp increase in the resistance applies, of course, only for a short instant; with diminishing relative velocity, the drop again assumes the spherical shape. Since the drops therefore experience an increased acceleration for a time as a result of their distortion, the error that we have introduced into our calculation through the assumption of Eq. (11) is partly compensated. Thus we can readily dispense with the curves of Fig. 3, which we only intended to use for rough estimates anyway.

The typical indicated values $p = 0.15$ bar, $c_1 = 360$ m/sec, $\bar{r}_g = 7 \cdot 10^{-5}$ m give $(\frac{1}{2}U_r \Delta t_{\text{brems}})_{\xi=0} \approx 1.5$ m (by interpolation in Table 1). A glance at Fig. 3 shows that these drops are accelerated only sluggishly. For example, after a flight path $\xi = 3$ cm has been traversed, their velocity c_r is only about 10% of c_1 , i.e., $0.10 \cdot 360 = 36$ m/sec!

The result of this is that the forcibly detached drops strike the next runner buckets from quite the wrong direction and with a high relative velocity (see the velocity triangles in Fig. 2). This fact was long ago recognized as the principal cause of erosion. However, it was always assumed here that the entire wetness content of the steam forms large destructive drops of this type.

Since, on the contrary, it develops quite decisively in the present study (cf. under heading 2.9) that only a minor part of the total wetness is involved in this phenomenon — a statement that appears by no means impossible even in the light of practical observations — we present briefly below certain considerations regarding the destructiveness of large water drops.

c) Concerning the Eroding Effect of Detached Drops

Very little can be said concerning the erosion of turbine buckets,

etc. on the basis of theory. It is probably the result of a complicated collaboration between mechanical-metallurgical-chemical and perhaps even electrical effects. In studying it, we have recourse only to experiment. However, it is difficult to simulate conditions in a wet-steam turbine by means of a simple experimental setup. Frequently it is necessary to work exclusively with large drops or even with a stream of water. Nevertheless, such experiments permit only a qualitative insight into the processes and perhaps comparisons between different materials (even this is quite questionable in the water-jet experiment).

We shall now carry through two short calculations by way of illustrating the impact of a drop. First, let us evaluate the local pressure that arises when a drop strikes the bucket. With respect to the rotor, the kinetic energy of the drop on impact is $\frac{1}{2}m_r w_r^2$ (see Fig. 2). Let us assume that the drop strikes the bucket surface vertically and that while it is being brought to a stop its center of gravity moves forward by one radius. Then we can compute the force necessary for deceleration: $\frac{1}{2}m_r w_r^2 / r$, and this force, divided by the frontal area of the drop, gives a point of reference for the instantaneous local pressure rise:

$$\Delta p_{\text{Tropfenschlag}} \approx \frac{\frac{1}{2}m_r w_r^2}{(\pi r^2)r} = \frac{2}{3} \rho_w w_r^2. \quad (16)$$

[Tropfenschlag = drop impact]. This quantity is thus independent of drop size and, for example, at $w_r = 250$ m/sec is about 420 bars or, expressed in technical units, $4.2 \text{ kg}^*/\text{mm}^2$. Thus we see that the pressure arising is rather small from the standpoint of strength.

The second question that we would like to clear up is as follows: how often, on the average, does a point of the target region of the bucket experience such impacts? Suppose that the width of the eroded band (see Fig. 2) is $b_e = 4 \text{ mm} = 4 \cdot 10^{-3} \text{ m}$. Let the total wetness con-

tent be $y = 10\%$, of which only $1/20$ goes into the impinging large drops. With a total throughput of $\dot{M} = 40$ kg/sec, a mass of $\dot{M}_g = 40 \times 0.10/20 = 0.20$ kg/sec will then strike all buckets, or, with a drop radius of $\bar{r}_g = 7 \cdot 10^{-5}$ m, $3\dot{M}_g/4\pi\rho_w\bar{r}_g^3 = 1.4 \cdot 10^8$ drops/sec. If now all bucket leading edges of the ring in question present the total length $z^{11}_{Schfl} = 40$ m, the entire impacted bucket area will be $z^{11}_{Schfl} b_e = 0.16$ m². If we were to cover this surface with close-packed spheres of the same size as a water drop, we would need $z^{11}_{Schfl} b_e / \pi \bar{r}_g^2 = 0.16 / 15 \cdot 10^{-8} = 1.1 \cdot 10^7$ balls. The ratio of the number of drops striking each second to this number indicates how often a drop strikes one and the same point on the surface. We find that $1.4 \cdot 10^8 / 1.1 \cdot 10^7 = 13$ drop impacts occur in each second on each point of the impacted flat strip. During a 5000-hour turbine operating life, therefore, each point on the entry zone of the rotor buckets receives about $5000 \cdot 3600 \times 13 = 2.3 \cdot 10^8$ small impacts.

While the loads imposed by the impacts remain far below the yield point, they affect only a region about the size of a crystal granule. The question arises as to whether such loading of the surface, so often repeated, might not be capable of breaking down the crystalline structure of the metal. However, further pursuit of this question is not the purpose of the present study.

On the basis of the old conception in which all of the water present in the turbine flies around in the form of large drops, it might appear incredible to us at first that in actuality only a small fraction of the water is responsible for the erosion. Where, however, is the difference between the two conceptions? If we were to return to the old system, only the frequency of the impacts would rise (by a factor of twenty in the above example; we should have $4.6 \cdot 10^9$ impacts in 5000 hours instead of $2.3 \cdot 10^8$); their intensity would, however, remain

the same. Thus it would be just as difficult to explain the erosion damage, since, after all, the main problem lies not in the number of impacts necessary, but the manner in which they have their effect.

d) Ricocheting Drops

For lack of observations with a bearing on the matter, we can judge only with uncertainty what the fate of the detached drops will be after their first collision with a bucket. Part of the water that they contain probably bounces off the blade surface immediately, while another part remains clinging to it. The general view is that clinging is favored by the roughening of the leading edges. Under the influence of centrifugal force, this water then begins to move radially outward along the buckets, but probably with part of it spraying off the rough spots and reentering the steam flow. (Spraying back might be inhibited by grooves milled radially in the buckets.) The average size of the returning drops — whether they return by rebounding or are sprayed off later — is obviously somewhat smaller than that of the original impinging drops.

The returned drops are caught by the steam flow and blown through between the buckets. In regions of sharp pressure drop, this may give rise to a phenomenon that we shall refer to as "bursting" (or "flashing"), consisting in the water boiling in the interior of the drop and exploding it into fragments. Wood made reference to this phenomenon in turbines [41].

Since the water boils by itself, it must have a certain excess temperature (according to experiments made in this connection, of the order of about 5°C). This overtemperature arises in turbines as a result of the pressure in the vicinity of the drop falling off suddenly, so that the saturation temperature also declines. The outer surface of the drop can adapt very quickly to the new saturation temperature by

evaporation; the interior, on the other hand, can be cooled only by heat conduction, so that an excess temperature arises in the drop, i.e., it becomes superheated. Since the highest temperature occurs in the middle of the drop, we may write the condition for bursting in the form

$$T_{\text{Mitte}} - T_s = 5^\circ\text{C} \quad (17)$$

[Mitte = center]. Large drops are more susceptible to bursting than small ones, since they have greater thermal inertia. Below we shall derive a formula for the size of the largest drops still just capable of surviving the pressure drop in the bucket ring, using as a basis the criterion of Eq. (17).

The manner in which the saturation temperature drops within a bucket ring (for example, a stator) is linearized as shown in Fig. 4.

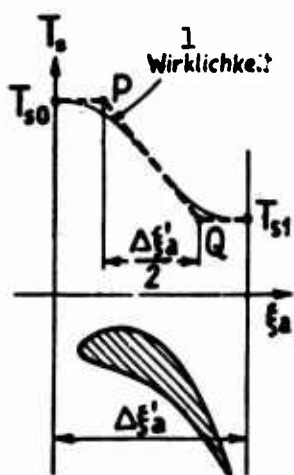


Fig. 2.8.4. Curve of saturation temperature in a bucket ring. 1) Actuality.

If we use point P as the origin of time reckoning, we obtain the simple law

$$T_s(t) = T_{s0} + \left(\frac{dT_s}{dt}\right)t, \quad (18)$$

for the time variation of saturation temperature for a drop moving at constant speed; here, applying Eq. 2.1(2),

$$\frac{dT_s}{dt} = -\frac{dT_s}{d\ln p} \left(\frac{-d\ln p}{d\xi_a}\right) \frac{d\xi_a}{dt} = -\left(\frac{dT_s}{d\ln p}\right) \cdot 2\bar{P}_a \cdot c_{r,a} \quad (19)$$

Here $c_{r,a}$ is the axial component of the drop's velocity.

The influence of the capillary effect can be disregarded for the drop sizes coming under consideration here (about 10^{-5} m; cf. Table 2.3.1), so that T_r , the surface temperature of the drop, is about the same as the current saturation temperature:

$$T_r = T_s(t). \quad (20)$$

The temperature curve for the interior of a sphere whose surface temperature varies linearly in time can be determined by solution of the heat-conduction equation concerned (cf. [42], page 235). Here it is assumed that the drop has the temperature T_{s0} throughout its interior at time zero (point P in Fig. 4), which is probably a very good approximation for both the detached and the rebounded drops. We obtain as a solution

$$T_{\text{Mitte}} - T_s = - \left(\frac{dT_s}{dt} \right) \frac{\rho_w c_w}{\lambda_w} \frac{r^2}{6} \left[1 + \frac{12}{\pi^2} \sum_{k=1}^{\infty} \frac{(-1)^k}{k^2} e^{-\text{konst} \cdot k^2 t} \right]. \quad (21)$$

Here Eq. (20) has also been taken into account. The abbreviation "konst" [const] in the exponent represents $(\pi^2 \lambda_w / r^2 \rho_w c_w)$ and r is the drop radius.

The greatest rise in temperature occurs — provided the drop has not already burst — at point Q, for which $t = \Delta \xi'_a / 2c_{r,a}$. Thus, inserting this value for t and applying Eq.

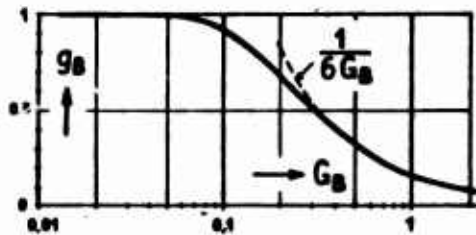


Fig. 2.8.5. The function $g_B(G_B)$.

(19), we obtain from Eq. (21)

$$(T_{\text{Mitte}} - T_s)_Q = - \left(\frac{dT_s}{dt} \right) \rho_a \Delta \xi'_a \left\{ \frac{1}{6G_B} \left[1 + \frac{12}{\pi^2} \sum_{k=1}^{\infty} \frac{(-1)^k}{k^2} e^{-\pi^2 k^2 G_B} \right] \right\}, \quad (22)$$

where the quantity

$$G_B = \left(\frac{\lambda_w}{\rho_w c_w} \right) \cdot \frac{\Delta \xi'_a}{2c_{r,a}} \cdot \frac{1}{r^2} \quad (23)$$

appears as the thermal-inertia parameter for bursting. (For a rotor, we would replace $\Delta \xi'_a$ by $\Delta \xi''_a$.) The first factor is a material quantity (thermal diffusivity) and has the approximately constant value of $1.6 \times 10^{-7} \text{ m}^2/\text{sec}$ for water. The expression in curly brackets in Eq. (22) is a function of G_B alone and is denoted by $g_B(G_B)$. Its value can be

read from Fig. 5. For the quantity $(dT_s/d \ln p)$ we may use about 20°C for low pressures.

Now we can connect Eq. (22) with the bursting criterion, Eq. (17). We find that those drops for which

$$(T_{\text{Mittle}} - T_s)_Q = 20^\circ \bar{P}_a \Delta \xi'_a \epsilon_B(G_B) < 5^\circ,$$

remain insured against bursting, i.e., that

$$\bar{P}_a \Delta \xi'_a \epsilon_B(G_B) < 0.25 \quad (24)$$

From this criterion, we can calculate the radius $r_{B,\text{max}}$ of the largest nonbursting drops. We determine g_B from

$$g_B = \frac{0.25}{\bar{P}_a \Delta \xi'_a} \quad (25)$$

and then read G_B from Fig. 5. (If we find that $g_B > 1$, then no drops at all burst in the ring, since the pressure drop is not sufficient to trigger boiling.) With this G_B , $r_{B,\text{max}}$ then follows from

$$r_{B,\text{max}} = \sqrt{\left(\frac{\lambda_w}{q_w c_w}\right) \frac{\Delta \xi'_a}{2 c_{r,a}} \frac{1}{G_B}}. \quad (26)$$

As an example, let us calculate $r_{B,\text{max}}$ in rotor 5" of the high-pressure turbine laid out under heading 2.1. Here we have $\Delta \xi''_a = 0.64 - 0.56 = 0.08 \text{ m}$, $\bar{P}_a = 4.3 \cdot \text{m}^{-1}$, so that we get $g_B = 0.25/4.3 \cdot 0.08 = 0.73$ and, from Fig. 5, $G_B = 0.18$. The axial velocity $c_{r,a}$ of the drops (and here we imply an average value at which they move between points P and Q in Fig. 4) must next be estimated; Fig. 3 gives us a point of departure for this: about 5 cm past the point of detachment, the drops in question have about reached the velocity $c_r = (0.3 \text{ to } 0.5) \cdot c_1$, i.e., roughly speaking, $c_{r,a} \approx (0.3 \text{ to } 0.5) \cdot c_{a1}$. If we take $c_{r,a} = 80 \text{ m/sec}$, then

$$r_{B,\text{max}} = \sqrt{1.6 \cdot 10^{-7} \cdot \frac{0.08}{2 \cdot 80} \cdot \frac{1}{0.18}} \approx 2.1 \cdot 10^{-5} \text{ m}. \quad (27)$$

The upper limit imposed on the drop size by bursting is thus somewhat

smaller in this example than the $r_{g,max}$ resulting from mechanical division; compare Eqs. (6) and (9).

In conclusion, let us summarize the impression thus formed of the fate of the large drops. The drops torn away from the trailing edge of

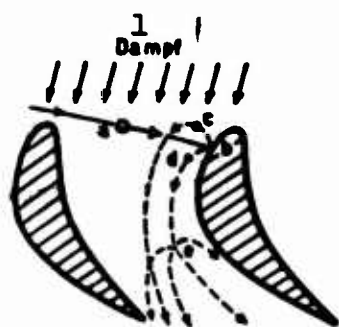


Fig. 2.8.6. Illustrating fate of large drops in a bucket ring (drawn for a rotor). 1) Steam.

the stator buckets (see a in Fig. 6), which, in general, show sizes of $\bar{r}_g = (2 \text{ to } 10) \times 10^{-5} \text{ m}$ - cf. Eq. (6) -, strike the buckets of the next rotor at b. Part of the mass flow that they represent remains clinging here and, under the influence of centrifugal force,

flows radially outward over the surface of the bucket. The rest gets back into the steam flow (either by ricocheting or by subsequently being slung off at rough spots on the surface).

The smaller of these drops are gradually accelerated by the steam current and leave out the back of the ring with their size unchanged (c). On the other hand, those that are accidentally somewhat larger (d) cannot survive the sudden pressure drop in the ring and burst (e). Only a superficial estimate can be made for the size of the rebounded large drops (subscript gg) coming out the back of a bucket ring: they are probably smaller than before their original impingement and at any rate smaller than the $r_{B,max}$ for the ring in question. We can submit the rough estimate

$$r_{gg} \approx \frac{r_{B,max}}{2} \cdot \frac{f}{2} \quad (29)$$

for their average size. In practical cases, we find approximately $\bar{r}_{gg} \approx 1 \cdot 10^{-5} \text{ m}$, which is therefore still much larger than the size of the fog droplets. Even these drops can follow the motion of the steam only very poorly.

2.9. THE FORMS THE MOISTURE APPEARS IN, ITS DISTRIBUTION AND DEVIATION OF THE STEAM STATE FROM THERMODYNAMIC EQUILIBRIUM

Under headings 2.4 to 2.8, we have made a detailed investigation of the processes that figure in connection with turbine wetness. On the basis of the formulas thus obtained, we can now build up a general calculation process by means of which we can investigate the over-all pattern of the physical processes in a wet-steam turbine.

We shall pursue two goals: first, we should like to calculate how much water actually is present and how it is distributed among the various drop sizes; secondly, we should like to know how sharply the state of the steam deviates from thermodynamic equilibrium, i.e., how great the supercooling is. On the basis of the results, we shall be in a position to draw inferences as to the possible effectiveness of de-watering and - in the third part of the study - as to the extent of moisture losses. First let us sketch out the path by which we come to the results and then discuss the results with reference to the two turbines described under heading 2.1.

a) Calculation Procedure

It has been shown that the water assumes various phenomenal forms in turbines (such as, for example, fog droplets, various large drops, flowing water, etc.), and that its behavior varies in accordance with these forms. For this reason, we subdivide the entire throughput quantity \dot{M} of the turbine into part throughputs:

$$\dot{M} = \dot{M}_d + \dot{M}_n + \dot{M}_f + \dot{M}_g + \dot{M}_{gg} + \dot{M}_b + \dot{M}_{m} . \quad (1)$$

The subscripts have the following significance:

- d - steam
- n - fog droplets
- f - water streaming over the blades
- g - large drops, just torn away

- gg - large drops, rebounded
- h - water centrifuged out
- nn - fog droplets from a secondary fogging.

The behavior of the individual forms can be characterized briefly as follows on the basis of earlier results (cf. Fig. 1): "n" follows, on the whole, the flow of the steam; "f" flows to the trailing edge on stator buckets and is there torn away in the form of "g;" on rotor

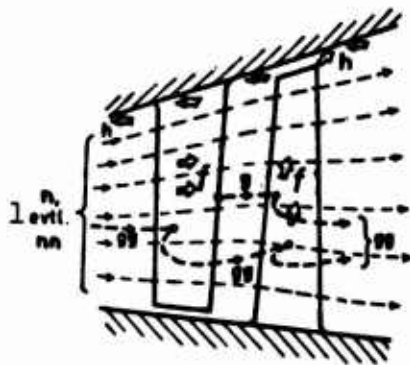


Fig. 2.9.1. The forms of appearance of the water. 1) n and possibly nn.

buckets, "f" flows almost radially outward and contributes to "h;" after its forcible detachment, "g" covers a short flight path and impinges upon the next row of rotor buckets; "gg" bounces back and forth between the buckets; "h" can either be withdrawn from the flow by trap devices or move in the vicinity of the casing wall

(partly as large drops and partly as water flowing on the wall); "nn" will be formed only in special cases (namely, when a coarse-drop "n" is accidentally formed in the first fogging in a turbine in which very rapid pressure drops occur) and generally consists of droplets much finer than those of "n." For the arguments to follow, we shall assume that no second fogging arises ($\dot{M}_{nn} = 0$) and also that no steam is withdrawn from the flow. We shall return later to the allowance to be made for "nn."

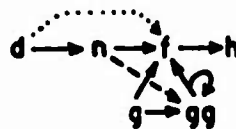
During the flow through the turbine, there is constant transition from one phenomenal form to another. Of the many conceivable conversions, however, only a few are of importance, since most of them do not occur at all or do so only to extremely minor degrees. Figure 2 indicates the more important transitions by means of arrows and requires the following explanation:

- $d \rightarrow f$: by condensation on the blades; this occurs only in those rings in which the supercooling is not compensated by boundary-layer heating (i.e., where $\Delta T > \text{about } 20^{\circ}\text{C}$), and is hardly perceptible even then;
- $d \rightarrow n$: by fog-droplet formation and subsequent condensation on these droplets;
- $n \rightarrow f$: by slinging of fog droplets against the leading edges and concave sides of the buckets;
- $n \rightarrow g$: as a result of fog droplets being swallowed up by large drops;
- $n \rightarrow gg$: as a result of fog droplets being swallowed up by large drops;
- $f \rightarrow g$: by tearing away from the trailing edge (in stator rings);
- $f \rightarrow h$: by spraying off the bucket tips or shroud (in rotor rings);
- $g \rightarrow gg$: by ricocheting after impingement on blades;
- $g \rightarrow f$: by clinging after impingement on blades;
- $gg \rightarrow gg$: as with $g \rightarrow gg$;
- $gg \rightarrow f$: as with $g \rightarrow f$.

1 Leitrad:



2 Laufrad:



\longrightarrow = wichtig 3
 \dashrightarrow = zweitrangig 4
 $\cdots\rightarrow$ = Verkondensation 5

Fig. 2.9.2. Transitions of mass from one phenomenal form into another. 1) Stator; 2) rotor; 3) important; 4) less important; 5) precondensation.

The rates of these transitions can be expressed quite clearly by means of "mass exchange coefficients" ϵ . These indicate what part of a certain mass-flow subdivision entering a ring has gone over into some

other form by the time it comes out of the ring. Below we present a few guidelines:

- ϵ_{d-f} : cf. Eq. 2.4(10);
- ϵ_{d-n} : not introduced, since fogging and growth of the fog drops are calculated directly from headings 2.5 and 2.6b;
- ϵ_{n-f} : cf. Eq. 2.6(18);
- ϵ_{n-g} : cf. Eq. 2.6(20);
- ϵ_{n-gg} : cf. Eq. 2.6(21);
- ϵ_{f-g} = 1 (only for stator rings!)
- ϵ_{f-h} = 1 (only for rotor rings!)
- ϵ_{g-f} : } cf. under heading 2.7;
- ϵ_{gg-f} : } lie between zero and unity (smaller for smooth bucket surfaces and larger for roughened ones), so that we are forced to fall back on arbitrary assumptions;
- ϵ_{g-gg} = 1 - ϵ_{g-f} } since practically no large drops get
- ϵ_{gg-gg} = 1 - ϵ_{gg-f} } through a ring without striking it.

Not all of the phenomenal forms arise simultaneously in the turbine. For example, large drops appear only after water has first been torn away from the stator-blade trailing edges; for this purpose, however, this water must have gotten onto the blades somehow, and so forth. It happens that certain transitions are still lacking primarily in the first stages of the wet-steam section of a turbine, so that the calculation is simplified for such stages.

Below we shall illustrate the calculation procedure for a multi-stage wet-steam turbine. The calculation advances from blade ring to blade ring. It begins with that ring in which the saturation line is passed. It is assumed that the design data of the turbine - in the sense of heading 2.1 - are known and that all necessary material quantities are also known (see Diagrams). The subscripts 0, 1 and 2 refer to the intermediate spaces in and behind a stage, and ' and " refer to

quantities that apply for (or within) the rings. (If quantities that change in a ring are provided with the ' or the ", this indicates their arithmetic mean values in the ring; thus, for example, $p' \equiv (p_0 + p_1)/2$, $T'' = (T_1 + T_2)/2$, etc.)

The blade rings before the Wilson point

The first task is to determine the position of the Wilson point in the turbine. The method of solution was described under heading 2.5e. The Wilson point occurs either inside a blade ring or in an axial intermediate space. Below we devote more detailed discussion to the ring in which or immediately behind which it lies.

In cases where extremely steep gradients occur in a ring (impulse-type turbine), it is conceivable that the Wilson point is reached in the same ring in which the saturation line is exceeded; compare, for example, Fig. 8. If this is not the case, we have one or more rings in which undercooled steam is flowing. (In Fig. 4, for example, the saturation line is crossed in ring 1', the steam is increasingly undercooled in 1'' and 2', until finally the Wilson point is reached in ring 2''). In the rings through which undercooled steam is flowing, precondensation may occur on the blades under certain circumstances; in steam turbines, however, this is so slight that it may be disregarded altogether. We may thus assume that no water at all is present in front of the ring with the Wilson point, i.e., that y remains = 0. The theoretical wetness y_{∞} increases in parallel with the supercooling; it is equal to the moisture deficiency Δy , which can be determined from Eq. 2.3(19).

Moisture losses have not yet occurred in these rings, since supercooling produces a loss only when it is coupled with condensation, i. e., with exchange of heat.

The blade ring with the Wilson point

The ring in which (or in the intermediate space behind which) fogging takes place merits more detailed discussion. point has already been determined, we know the corresponding values of the pressure, the rapidity of expansion and the supercooling (p^* , \dot{P}^* , ΔT^*). From this, we might determine the exact state of the steam at the end of the condensation zone on the basis of heading 2.5d. In general, however, we shall satisfy ourselves with a cursory determination of \bar{r}_n^{**} and y_n^{**} , the more so since even p^* , \dot{P}^* and ΔT^* carry uncertainties. We then proceed as follows: on the basis of p^* we decide approximately at which point of the bucket complement the condensation sets in (cf. Fig. 2.5.13e), so that we shall be able to estimate the Mach number M_{vor} [vor = before]. (In the majority of cases, M_{vor} will be considerably smaller than unity.) With M_{vor} , p^* and \dot{P}^* , we can then read \bar{r}_n^{**} , the average fog-droplet radius at the end of the condensation zone, from Fig. 2.5.14. Roughly speaking, there is as much water present in the fog droplets as there was lacking with reference to thermodynamic equilibrium at the Wilson point, so that we have

$$y_n^{**} \sim \Delta y^* = (1 - y^*) \frac{c_p}{L} \Delta T^*, \quad (2)$$

where Δy^* has been denoted by ΔT^* in accordance with Eq. 2.3(19). In case we are dealing with the first fogging event in the turbine, $y^* = 0$ due to the negligible extent of the precondensation. The composition of the fog is sufficiently described by \bar{r}_n^{**} and y_n^{**} . These data form the point of departure for determination of the subsequent state changes in the turbine.

The course of the supercooling in the stages through which the fog flows is determined by the graphical method set forth under heading 2.6b. The locus ξ_a^{**} at which fogging can be regarded as concluded

and ΔT^{**} , the supercooling value at this point, should be known exactly as a point of departure for this construction. In turbines, however, there is frequently no sharp boundary to be discerned between the "formation" of the fog droplets and the subsequent condensation on them, since supercooling does not collapse suddenly at all under certain circumstances. (In particular, this occurs when the Wilson point lies at a small \dot{P} , i.e., when coarse fog drops form. In such a case, the supercooling falls off only much slower than it would if the fog droplets were fine, cf., for example, the dashed-curve segments in Fig. 5 or 6.) Happily, exact knowledge of ξ_a^{**} and ΔT^{**} is not absolutely necessary for our purposes, since the error incurred by starting construction of the supercooling curve from an arbitrarily selected point has vanished practically completely as soon as the next following stage is reached. For example, the dashed-line segments in Figs. 5 and 9 show the undercooling approximately as it varies in reality behind the Wilson point for these cases. The unbroken curve, on the other hand, was determined with an arbitrarily selected initial point, using the graphical method. It is seen that the deviations are restricted to about one-and-a-half ring widths. Otherwise, even a large error in ΔT has no serious consequences: we shall still be able to calculate the undercooling loss correctly (heading 3.4), and ΔT has only a minor influence on the local fog-droplet size (assuming a supercooling approximately 5°C too small results in calculation of a fog-droplet radius large by about 6%).

Thus we shall dispense with exact determination of the state curve in the condensation zone and perform the calculation as though fogging in the same ring (or in the same axial intermediate space) in which it has begun were excluded, regardless of whether this is the case in reality. At the exit from this ring⁴⁸⁾ we assume an estimated

value ΔT_1 for the supercooling as the point of departure for graphical determination of the supercooling curve (between 0 and 1°C if the fog droplets are fine and larger if they are large). In the tables, these assumed supercooling values have been keyed by underscoring and are readily identified in Figs. 4 to 6 and 8 to 10 as the initial points of the solid ΔT line.

If ΔT_1 has been determined in this manner, the other still lacking quantities can be calculated for the ring exit. The moisture deficiency Δy_1 is determined from Eq. 2.3(19), and then the total precipitated unit amount of water y_1 follows from

$$y_1 = y_{w1} - \Delta y_1. \quad (3)$$

Since no large drops have been produced up to this point — apart from precondensation — we have $y_{g1} = y_{gg1} = y_{h1} = 0$ and, consequently,

$$y_{n1} = y_1. \quad (4)$$

The number of fog droplets has as yet suffered practically no reduction in the ring, i.e., $E_{n1} = 1$, and the size of the fog droplets at the exit from the ring is obtained from

$$r_{n1} = r_n^{**} \left(\frac{y_{n1}}{y_n^{**}} \right)^{1/3}. \quad (5)$$

Calculation of an arbitrarily selected wet-steam stage

Suppose that y_{n0} , y_{gg0} , y_{h0} , E_{n0} , ΔT_0 and \bar{r}_{n0} have become known from the calculation of the preceding ring (y_{g0} is zero, since, after all, the preceding ring is a rotor ring from which practically no drops are torn), and suppose that assumptions have already been arrived at for ϵ_{g-f} , ϵ_{gg-f} , ϵ_{g-gg} , and ϵ_{gg-gg} . We proceed with calculation of the processes in the

Stator

and determine as the first order of business the quantity of fog deposited on the buckets. According to Eq. 2.6(15),

$$G'_H = \frac{(9\mu_d/2q_w)'}{1 + 2.53 Kn'} \cdot \frac{l'_{ax}}{c_{n0} \bar{r}_{n0}^2} \quad (6)$$

and, according to Eq. 2.6(3),

$$G'_N = \frac{(9\mu_d/2q_w)'}{1 + 2.53 Kn'} \cdot \frac{R'_N}{c_0 \bar{r}_{n0}^2} \quad (7)$$

where

$$Kn' = \frac{l'}{2F_{n0}} = \frac{(1, 5\mu_d \sqrt{RT_d})'}{p' \cdot 2F_{n0}} \quad (8)$$

Figure 2.6.2 gives us g'_H and g'_N , and these, in turn, give the fraction of the fog drops captured:

$$\epsilon_{n-f} = \frac{S'}{l'_{SchM}} \cdot \epsilon'_H + \frac{2 R'_N}{l'_{SchM}} \cdot \epsilon'_N \quad (9)$$

In addition to the fog droplets, some of the impinging large drops can also remain stuck to the buckets, so that the water content y'_f represented by the water film on the stator buckets can be determined from the formula

$$y'_f = \epsilon'_{n-f} y'_{n0} + \epsilon'_{g-f} y'_{g0} \quad (10)$$

We shall set the number of forcibly detached drops at the exit from the stator, y'_{g1} , equal to y'_f increased by the amount by which the torn-off drops continue to grow by swallowing up fog droplets during their time of acceleration. This aggrandizement will be described by Eq. 2.6(20):

$$\epsilon'_{n-g} = \frac{3}{4q_w} \cdot \frac{0.25 \Delta t_{brems,g}}{F_g} \cdot \frac{c_1}{v_1} \cdot y'_f \approx \frac{0.25}{2} \left(\frac{\sqrt{g}}{\mu_d} \right)_1 \frac{y'_f}{\sqrt{c_1}} \quad (11)$$

[brems = deceleration] where we use Eq. 2.2(36), Eq. 2.8(8) for the size of the torn-off drops, i.e.,

$$F_g = \frac{(9\mu_d RT_d)_1}{p_1 c_1^2} \quad (12)$$

and set $v_{d1} \approx v_1$. (For low-pressure turbines, we obtain for Eq. (11)

$\epsilon'_{n-g} \approx 12.5 y'_f \sqrt{c_1}$, where c_1 is to be inserted in m/sec.) Thus

$$y_{g1} = y_i' + \epsilon'_{n-g} y_{n0} \quad (13)$$

In a perfectly similar manner, we also increase the mass of water rebounding from the stator buckets ($\epsilon'_{gg-gg} y_{gg0}$) by aggrandizement with fog droplets. From Eq. 2.6(21), we have

$$\epsilon'_{n-gg} \approx \sqrt{2} \frac{3}{4\epsilon_w} \frac{0,25 \Delta t_{\text{brems,gg}}}{\bar{r}_{gg}} \cdot \frac{c_0}{v_0} (\epsilon'_{gg-gg} y_{gg0})$$

or, with the assumption $\bar{r}_{gg} \approx \bar{r}_g/2$, which is sufficiently accurate for these purposes, and transposing in the same way as with Eq. (11):

$$\epsilon'_{n-gg} \approx \frac{0,25}{\sqrt{2}} \left(\sqrt{\frac{\sigma}{\mu_d}} \right)_1 \frac{\sqrt{c_0/c_1}}{\sqrt{c_1}} (\epsilon'_{gg-gg} y_{gg0}) \approx \frac{12,5}{\sqrt{c_1}} \sqrt{c_0/c_1} (\epsilon'_{gg-gg} y_{gg0}) \quad (14)$$

Thus we obtain for the mass of the large drops that have rebounded from the stator, as taken at the exit from the stator,

$$y_{g1} = \epsilon'_{gg-gg} y_{gg0} + \epsilon'_{n-gg} y_{n0} \quad (15)$$

No water is centrifuged out in the stator, so that

$$y_{h1} = y_{h0} \quad (16)$$

remains in force.

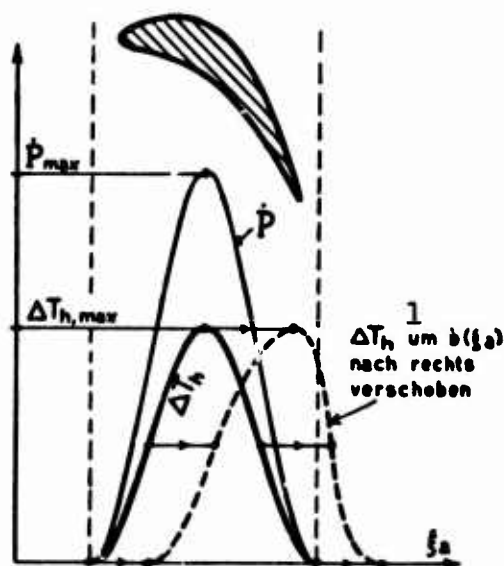


Fig. 2.9.3. Cosine approximation for ΔT_h in a bucket ring.
1) ΔT_h displaced to the right by $b(\xi_a)$.

The loss in number of fog droplets per kilogram of flow medium is described, in accordance with Eq. 2.6(24) - compare also Eqs. 2.6(22) and (23) - by

$$E_{n1} = (1 - \xi'_{n-f} - \xi'_{n-g} - \xi'_{n-gg}) \cdot E_{n0} \quad (17)$$

We must take the following course to determine the total mass of the fog droplets. The fog-droplet content y_{n1} is obviously that part of the total actual condensed water content y_1 , left after subtraction of y_{g1} , y_{gg1} and y_{h1} . Since y_1 is smaller by the moisture deficiency Δy_1 than the $y_{\infty 1}$ known from the specification and Δy_1 can only be calculated from the undercooling, we must first determine the undercooling curve in the stator ring. The graphical method developed under heading 2.6b will serve for this purpose; it requires drawing the function ΔT_h and displacing it by the local sum \underline{b} , compare Eqs. 2.6(43) and (46). Here we can permit ourselves the simplification of setting all quantities constant except for \dot{P} in Eq. 2.6(43) (for example, $x_{\infty} = 1 - y_{\infty 0}$, $T = T'$, etc.) and assuming a cosine approximation for \dot{P} , as indicated in Fig. 3, so that the ΔT_h curve also becomes cosine-shaped and (after determination of the value of $\Delta T_{h, \max}$ from \dot{P}_{\max}) can easily be plotted. Again in Eq. 2.6(46) it is sufficient to regard only c_a as a variable, for which cf. Figs. 2.1.7 and 8. For the quantities $(y_n^{**} E_n / y_{\infty})$ appearing in these equations, we make the estimate

$$\left(\frac{y_n^{**} E_n}{y_{\infty}} \right)' \approx \frac{y_n^{**} E_{n1}}{y_{\infty 0} - y_{gg0} + y_{h0}} \quad (18)$$

in the sense of Eq. 2.6(49). From the ΔT_h curve and its sister curve, which is displaced by \underline{b} , we use stepwise construction, departing from ΔT_0 (see Figs. 2.6.5 and 7), to determine the shape of the undercooling ΔT within the ring. For the control plane behind the ring we finally obtain a value ΔT_1 from which we may use Eq. 2.3(19) to get the moisture deficiency

$$\Delta y_1 = \frac{c_p}{L} (1 - y_{m1}) \Delta T_1 \quad (19)$$

and from this, by the expression

$$y_1 = y_{m1} - \Delta y_1 \quad (20)$$

the moisture effectively present. Finally, we can calculate the fog-droplet content

$$y_{n1} = y_1 - (y_{g1} + y_{gg1} + y_{h1}) \quad (21)$$

together with the average size of the fog droplets behind the stator:

$$r_{n1} = r_n^* \left(\frac{y_{n1}}{y_n^* E_{n1}} \right)^{1/3} \quad (22)$$

Thus we have obtained the end set y_{n1} , y_{g1} , y_{gg1} , y_{h1} , E_{n1} , ΔT_1 and \bar{r}_{n1} and are in a position to take the

Rotor

next in order. Apart from centrifugation, the processes in the rotor are basically the same as those in the stator, so that the calculation procedure remains identical. We shall restrict ourselves to a bare enumeration of the formulas and append explanations only where there is a basic departure from the calculations for the stator.

We have

$$G_H^* = \frac{(9\mu_d/2q_w)^*}{1 + 2.53 Kn^*} \cdot \frac{l_{a1}^*}{c_{a1} F_{n1}^2} \quad (23)$$

$$G_N^* = \frac{(9\mu_d/2q_w)^*}{1 + 2.53 Kn^*} \cdot \frac{R_N^*}{w_1 F_{n1}^2} \quad (24)$$

$$Kn^* = \frac{\gamma^*}{2F_{n1}} = \frac{(1.5 \mu_d \sqrt{RT_d})^*}{p^* \cdot 2F_{n1}} \quad (25)$$

$$\epsilon_{n-f}^* = \frac{s^*}{\epsilon_{Schf1}^*} \cdot \epsilon_H^* + \frac{2R_N^*}{\epsilon_{Schf1}^*} \cdot \epsilon_N^* \quad (26)$$

[Schf1 = bucket]. Since (unlike y_{g0}) y_{g1} is not equal to zero, we get

$$y_i^* = \epsilon_{n-f}^* y_{n1} + \epsilon_{g-f}^* y_{g1} + \epsilon_{gg-f}^* y_{gg1} \quad (27)$$

and since, due to the centrifugation, practically no drops are torn

off from the rotor bucket trailing edges, the quantities ϵ''_{n-g} and \bar{r}_{g2} become meaningless and

$$y_{g2} = 0. \quad (28)$$

Both freshly detached large drops and large drops that have already been bouncing back and forth strike the rotor buckets, and part of each class will rebound, so that

$$\epsilon''_{n-eg} \approx \frac{0.25}{\sqrt{2}} \left(\sqrt{\frac{\sigma}{\mu_d}} \right) \frac{\sqrt{w_1/c_1}}{\sqrt{c_1}} \cdot (\epsilon''_{e-eg} y_{e1} + \epsilon''_{eg-eg} y_{eg1}) \quad (29)$$

where $(0.25/\sqrt{2}) \cdot \sqrt{\sigma/\mu_d} \approx 12.5 \text{ m}^{1/2}/\text{sec}^{1/2}$ for low-pressure turbines.

Thus the following water content is present behind the rotor in the form of large drops that have rebounded again:

$$y_{eg2} = \epsilon''_{e-eg} y_{e1} + \epsilon''_{eg-eg} y_{eg1} + \epsilon''_{n-eg} y_{n1}. \quad (30)$$

All water that has clung to the rotor buckets is centrifuged out, so that

$$y_{h2} = y_{h1} + y_f^*. \quad (31)$$

Further,

$$E_{h2} = (1 - \epsilon''_{n-f} - \epsilon''_{n-eg}) \cdot E_{n1}, \quad (32)$$

which is followed by the graphical determination of ΔT_2 , setting, for one thing,

$$\left(\frac{y_n^{**} E_n}{y_\infty} \right)^2 \approx \frac{y_n^{**} E_{n2}}{y_{\infty 1} - (y_{e1} + y_{eg1} + y_{h1})}. \quad (33)$$

Finally, we have yet to calculate

$$\Delta y_2 = \frac{c_2}{L} (1 - y_{\infty 2}) \Delta T_2, \quad (34)$$

$$y_2 = y_{\infty 2} - \Delta y_2, \quad (35)$$

$$y_{n2} = y_2 - (y_{eg2} + y_{h2}) \quad (36)$$

and

$$\bar{r}_{n2} = \bar{r}_n^{**} \left(\frac{y_{n2}}{y_n^{**} E_{n2}} \right)^{1/3}. \quad (37)$$

Thus we have obtained the quantities y_{n2} , y_{gg2} , y_{h2} , E_{n2} , ΔT_2 , \bar{r}_{n2} ,

which provide the initial data for calculation of the following stage.

Remarks

Equations (14) and (29) are based on a rough assumption for the size of the rebounded large drops (namely, $\bar{r}_{gg1} = \bar{r}_{gg2} = \bar{r}_{g1}/2$), which simplifies the calculation appreciably and gives an approximation sufficiently good for these purposes, since, after all, the processes represented by ϵ'_{n-g} and ϵ''_{n-g} (swallowing up of fog droplets) is only a subordinate factor as compared to the other mass transfers. Nevertheless, more exact knowledge of \bar{r}_{gg} may be necessary — specifically, for calculation of the moisture losses — and for this reason it also becomes necessary to calculate $r'_{B,max}$, the upper limit imposed on drop size by bursting. For a stator ring, we obtain from Eq. 2.8(26) with $c_{r,a} \approx 0.4 c_{a1}$,

$$r'_{B,max} \approx \sqrt{\left(\frac{\lambda_w}{c_w c_a}\right)' \frac{\Delta t_a'}{2.0,4 c_{a1}} \frac{1}{G'_B}}, \quad (38)$$

where G'_B is determined with the aid of Fig. 2.8.5 from

$$\epsilon'_B = \frac{0.25}{F'_B \Delta t_a'} \quad (39)$$

(The procedure for rotor rings is the same, except that we may have $g''_B > 1$ with small percentage reactions, which shows that no bursting at all takes place in the rotor.)

Now the only rebounded drops that will emerge whole from a stator ring are those smaller than $r'_{B,max}$; larger ones burst, i.e., disintegrate into smaller fragments. For the resultant average size of the rebounded drops at the exit from the stator, therefore, we can take as a rough approximation

$$r_{ex1} \approx \frac{r'_{B,max}}{2} \text{ but in any event } \leq r_{ex0} \quad (40)$$

Behind the rotor, "gg" is composed in part of drops that belonged to

y_{g1} before the rotor and in part from drops that belonged to y_{gg1} (but the first component will generally predominate heavily). Incidentally, it is not at all certain that $r''_{B,max}$ exists at all and is sufficiently small. Again as a rough approximation, we set

$$\bar{r}_{gg2} \sim \frac{r''_{B,max}}{2} \text{ but in any event } \leq \frac{\bar{r}_{g1}}{2}. \quad (41)$$

The uncertainty of the \bar{r}_{gg} -values calculated from Eqs. (40) and (41) is, in itself, very large - perhaps a factor of 2 or 3 -; however, it can be accepted without misgiving, since the values are used only to estimate certain unimportant losses.

A second remark applies to the case in which repeated fogging occurs ("nn"). This will most likely take place in impulse-type turbines, but only when a coarse-droplet fog has formed in the first fogging. That is to say, in this case the undercooling may increase to such an extent in spite of the presence of fog droplets (usually in the first stator ring following fogging) that prolific nucleation is again triggered. The point at which this second Wilson point is situated can likewise be determined from the undercooling curve that we have arrived at graphically, using the same method as for the first Wilson point (see Fig. 2.5.16). It is usually inside a stator ring, i.e., P^* is large, so that the second group of fog droplets consists of fine drops. The case in which also the second fogging produces coarse droplets and is followed, under certain circumstances, by yet a third fogging, is not excluded, but it remains highly improbable. We shall not discuss this case.

After these tiny second-edition fog droplets have appeared, they bring down the lion's share of the condensation upon themselves, since, taken together, they possess a much larger surface area and even higher heat-transfer coefficients than the "first-born" drops, which will per-

haps be ten or twenty times as large. We can therefore determine the subsequent course of undercooling solely by reference to the "nn" fog droplets and assume that the "n" fog droplets do not grow any more at all. For the rest, the behavior of the "nn" fog droplets corresponds in principle with that of "n," so that the same formulas will apply, mutatis mutandis, for the mass-transfer coefficients involved here.

b) Examples

Let us now discuss the results that have been obtained from application of the calculation procedure proposed here to the two turbines laid out under Heading 2.1. For reasons to be brought out below, we shall carry out the calculations for several variants of each turbine.

From Section 2.5, we drew the important conclusion that the size of the fog droplets produced on spontaneous condensation in a turbine is extensively determined by an accident: namely, by whether nucleation took place in a region of rapid pressure drop or in a space between two bucket rings, where the pressure remains almost constant for a certain period of time. It was noted that it is generally possible, by varying the pressure curve, to bring both cases about in a given turbine: for this reason, two variants were investigated for each turbine design — one with the finest possible fog droplets and the other with the coarsest possible droplets.⁴⁹⁾

If coarse fog droplets form, a relatively large number of them are caught by the blades. Whether the water caught is centrifuged out and drained or remains in the flow in the form of large drops and bounces back and forth between the buckets would probably have considerable influence on the losses. For this reason, two extreme cases were investigated for the variants with coarse fog: one without drainage, in which "h" remains in the flow channel, and the other with the most ef-

ficient dewatering devices conceivable, which result in the largest possible "h" amount and withdraw it from the flow.

If the fog has fine droplets, the amount of water trapped by the buckets is so small that the difference between no drainage at all and effective drainage is hardly perceptible. For this reason, we omitted the latter variant for the case of a fog consisting of fine droplets.

The three cases for which the calculation was completed carry the following designations (Ub = reaction-type turbine; Gl = impulse-type turbine; specifications see in Sect. 2.1):

- "Ub 1," "Gl 1" : with nucleation in the middle of a ring (i.e., with fine-droplet fog);
- "Ub 2," "Gl 2" : with nucleation in an intermediate axial space (= coarse-droplet fog), without drainage;
- "Ub 3," "Gl 3" : same, with the best drainage conceivable.

If the state curve has been fixed for a turbine — and this has been done for the two turbines of our example, by the specification under Heading 2.1 — then the Wilson point, fog-droplet size, etc. necessarily follow from this curve. To produce the extreme cases with fine-droplet and coarse-droplet fogs, we have in each case modified the pressure curve in our examples in such a way as to place the Wilson point at the desired position. These modifications, which are, in themselves, arbitrary, are restricted for the sake of simplicity to the blade rings up to and including the Wilson point, and the quantities based on this modified state curve have been enclosed in parentheses in the tables. Only in case "Gl 1" was it possible to retain the original specification.

The fine-droplet variants represent nearly absolute extreme cases, since expansion rates higher than those at which fogging occurs in

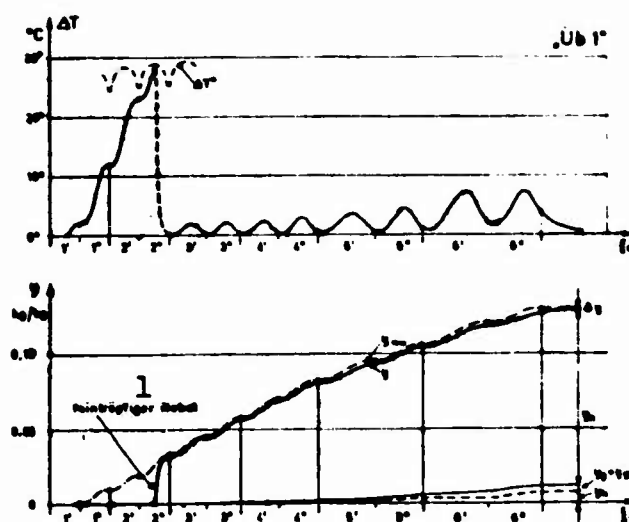


Fig. 2.9.4. Supercooling curve and distribution of water in the reaction-type turbine (variant 1). 1) Fine-droplet fog.

these variants are hardly to be expected in actual turbines. As for the coarse-droplet variants, on the other hand, it is conceivable that in certain turbine models (broad axial intermediate spaces, etc.), it might be possible under certain circumstances for a fog with even coarser droplets to form, since the expansion rate, which governs nucleation, may sink considerably lower than the value assumed here — $\dot{P}^* = 150 \text{ sec}^{-1}$.

It was stated under Heading a) that the precondensation can be disregarded without incurring any noticeable error as a result. In the present calculations, however, it was nevertheless taken into account in all cases in which it occurs according to Section 2.4 (rings 2' and 2'' of the reaction-type turbine), to demonstrate the correctness of this statement for steam turbines.

The results of the calculations are reproduced in Tables 1 to 6 (see pages 193ff) and in Figs. 4 to 11. The assigned quantities were y_∞ and the other data assembled in Tables 2.1.1 or 2.1.2.

The supercooling curve — the upper parts of Figs. 4, 5 and 6 and

8, 9 and 10 – were determined graphically behind the Wilson point; the control-plane values, ΔT , and maxima in the bucket rings, ΔT_{\max} , figuring in the tables were read from the curves. The water distribution – lower parts of the same figures – is obtained from the calculated control-plane values of Δy to y_h by connecting the points with continuous lines.

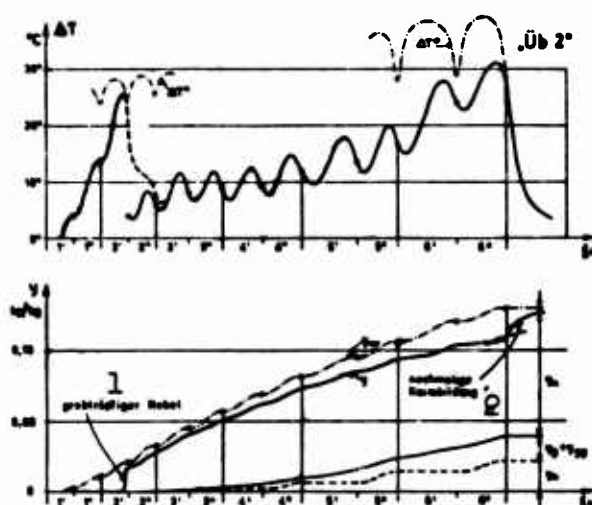


Fig. 2.9.5. Supercooling curve and distribution of water in the reaction type turbine (variant 2). 1) Coarse-droplet fog; 2) secondary nucleation.

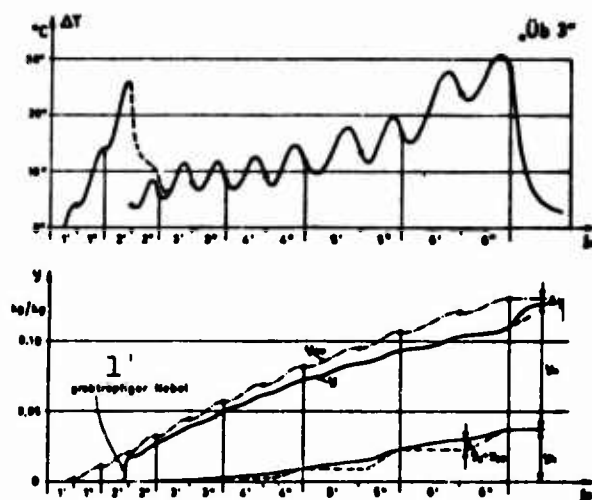


Fig. 2.9.6. Supercooling curve and distribution of water in the reaction type turbine (variant 3). 1) Coarse-droplet fog.

Further, E_n is the numerical proportion of the fog droplets that

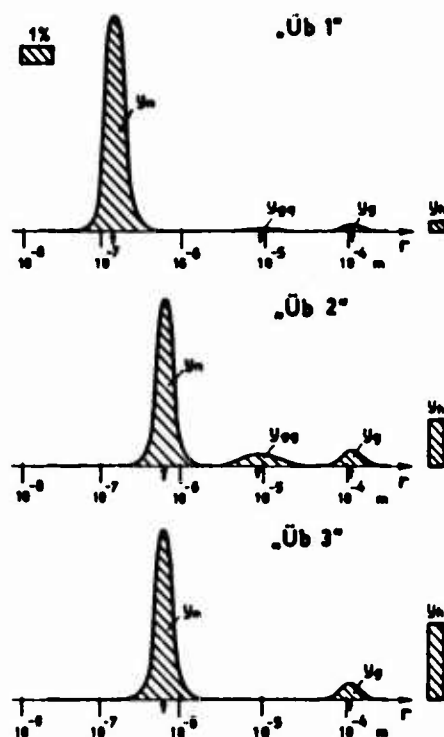


Fig. 2.9.7. Mass distribution of water over droplet radius before the last rotor ring of the reaction-type turbine (the enclosed area is proportional to the mass content; the arrows denote the calculated average radii).

has remained in the flowing steam, i.e., has been able to avoid the blades; E_{nn} is the corresponding proportion for the second-generation fog droplets if any such generation is formed. Through the trapping action of the blades, more and more water goes over into the coarsest forms; the total amount of water in the intermediate spaces, referred to the theoretical water amount is given by the quantity $(y_g + y_{gg} + y_h)/y_\infty$; the next line below indicates, again as a percentage, the amount of water centrifuged out, which simultaneously indicates the upper limit on the amount of water that can be separated by drainage devices.

At the very bottom of the tables we list the average sizes (radii) of the various drop species; in the line just above that, the radius of the largest drop that still does not burst, $r_{B,max}$, is indicated for each ring. It is seen that bursting acquires significance only at

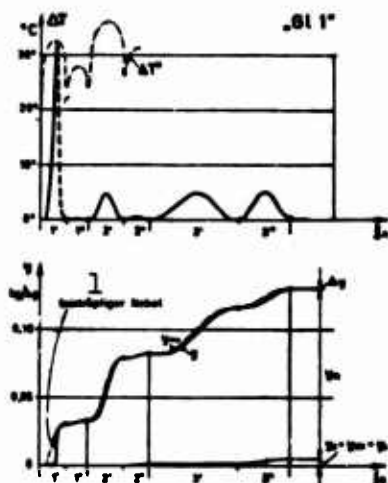


Fig. 2.9.8. Supercooling curve and distribution of water in the impulse-type turbine (variant 1). 1) Fine-droplet fog.

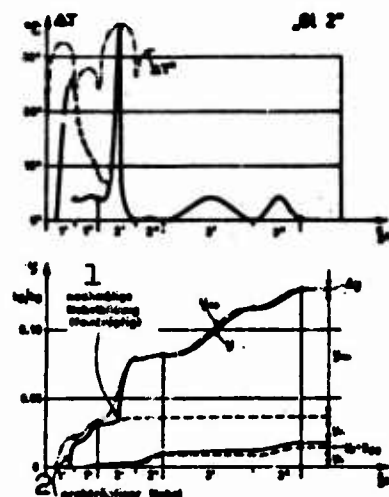


Fig. 2.9.9. Supercooling curve and distribution of water in the impulse-type turbine (variant 2). 1) secondary fogging (fine droplets); 2) coarse-droplet fog.

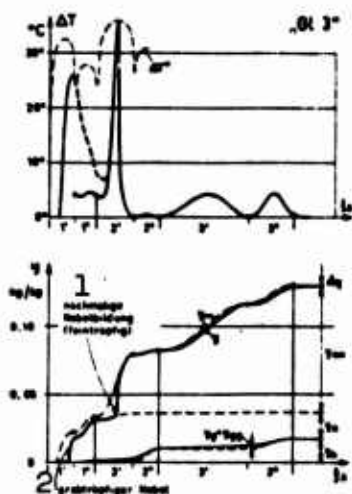


Fig. 2.9.10. Supercooling and distribution of water in the impulse-type turbine (variant 3). 1) secondary fogging (fine droplets); 2) coarse-droplet fog.

low pressures, since with higher steam densities the mechanical size-reduction results from the outset in sufficiently small droplets. The distribution of mass among droplets of various sizes in front of the last rotor ring has been presented in Figs. 7 and 11.

Now these general remarks will be followed by the discussion of results.

We are struck in all cases by the fact that a rather small quantity of mass falls to the lot of the coarse water forms (harm-

ful drops, water centrifuged out). If the fogging produces fine droplets ("Ub 1," "Gl 1"), then the coarse-form water amounts to only 8.6% and 3.8%, respectively, of the water theoretically present, even at the end of the turbine; if a coarse-droplet fog forms, these figures

rise to about 29% and 13%. The fact that about twice as much coarse-form water is produced in the **reaction-type** turbine than in the corresponding case for the **impulse-type** turbine is to be attributed

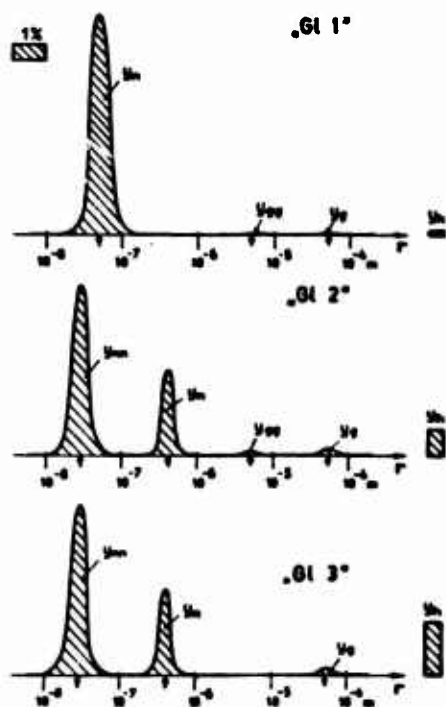


Fig. 2.9.11. Mass distribution of water among drop radii in front of last rotor ring in the **impulse-type** turbine (enclosed area is proportional to mass content; the arrows indicate the calculated average radii).

primarily to the fact that here the fog must flow through twice as many blade rings (deposition!), and not for example, to the differing percentage reactions.

The fog-droplet count in the steam diminishes only slightly; even in the worst possible case there are still more than 50% of the fog droplets present in the steam at the end of the turbine, as indicated by the E_n -values. With a fine fog, of course, E_n will naturally diminish much more slowly; in the "G1 1" case, it sinks from unity only to 0.9469.

For the **drained amount**, this means that even with turbine designs capable of centrifuging out all of the coarse-form water and draining it, only a small fraction of the total theoretical water can be deposited ("Ub 3": 28.6%, "G1 3": 13.1%). If measurements on turbines indicate deposition of more water than this, either an error of measurement or a catastrophically unfavorable fogging should be looked for.

According to the figures, the **supercooling** ΔT is rather large, primarily in the last rings (high vacuums, poor heat transfer between fog droplets and steam!). The size of the fog droplets formed is of prime significance for the **supercooling** curve.

As for the **reaction-type** turbine, we find for "Ub 1" a **supercool-**
ing curve similar to that found under Heading 2.5c for the simplified
turbine model (cf. Fig. 2.5.2): **supercooling** collapses suddenly after
the Wilson point and then remains quite small, regaining levels of 6
to 7°C only toward the end of the turbine. If, on the other hand, a
coarse-droplet fog forms ("Ub 2," "Ub 3"), then ΔT will not vanish
completely behind the Wilson point, but will fluctuate around the 10°C
level and reach peak values in the last ring that even exceed 25°C.
Such a great **remnant supercooling** causes, on the one hand, a con-
siderable thermodynamic loss (see under Heading 3.4) and, on the other
hand, produces a significant wetness deficiency Δy amounting sometimes
to more than 1/10% of the theoretical moisture in the examples. For the
last rings, in which the **supercooling** becomes considerable, we have
plotted the course of the Wilson **supercooling** ΔT^* (see Fig. 5) so that
it will be possible to establish whether a repeated heavy fogging is
triggered here. As is seen, we fall just short of this in the "Ub 2"
example (and likewise in "Ub 3" as well). It should be noted in pass-
ing that nucleation can become perceptible even after the last stage,
since no further expansion is taking place here ($\dot{P} \approx 0$), so that the
supercooling ΔT^* necessary for nucleation drops off sharply. Such nucleation
is, however, of no further significance for the processes in the tur-
bine.

Still higher expansion rates occur in the **impulse-type** tur-
bine, and for this reason the differences due to fog-droplet size
press even more boldly into the foreground. In the event that extremely
fine fog droplets form ("G1 1," Fig. 8), the undercooling remains
small from the Wilson point on; in the rotor rings, where the pressure
maintains a practically constant value, it vanishes almost completely,
while in the stator rings it always increases temporarily, since

rather, sharp expansions are taking place here. If fogging takes place in an intermediate space ("G1 2," "G1 3") and produces coarse fog droplets that present only a relatively limited area for condensation, a totally different picture takes shape: in the rotor wheel behind the Wilson point (1"), the **supercooling** drops only to about 5 to 7°C and shoots up again in the next stator ring as soon as the sharp expansion intervenes there. Here the **curve of the Wilson supercooling, ΔT^*** , is soon attained for a second time and another heavy nucleation takes place in the steam space, and the new-born fog droplets cause another collapse of undercooling. These second-generation fog droplets are much finer than the first ones (formation at high \dot{P}), so that from this point on we have essentially the same undercooling picture as in variant "G1 1." The second flock of fog droplets possesses a much greater surface and far superior heat-transfer coefficients than the first flock, which is still mixed with it, so that practically all of the condensation devolves upon the second group: the quantity of water present in it (y_{nn}) steadily increases, while the mass of the first fog-droplet group (y_n) diminishes considerably, since its droplets show practically no growth, but on the other hand are trapped preferentially by the **blades** due to their relatively high inertia.

It will be seen from Figs. 7 and 11, which plot the "droplet spectra" in the intermediate space between the last stator ring for both turbines, that water drops of widely varying sizes occur in the turbine, but that droplet species of different origins differ clearly from one another as regards size. (The breadth of the frequency curves for y_n and y_{nn} is based on Section 2.5c, and that for y_g on Section 2.8a. It was assumed arbitrarily for y_{gg} .)

It is further seen from Fig. 7, if, for example, we compare the droplet spectra of "Ub 1" and "Ub 2," that the difference between

"fine" and "coarse" fog droplets is never particularly large (orders of magnitude smaller than the difference between fog droplets and detached drops!), but that this slight change of fog-droplet size produces a sharp increase in the mass devolving upon "g," "gg" and "h." In case of absolutely nonreflecting buckets ("Ub 3"), one observes especially an increase of the amount y_h at the expense of the large drops bouncing back and forth ("gg"), which do not occur at all in this case.

The fog droplets forming in the case of "G1 1" (see Fig. 11) are about one-third as large as those of "Ub 1." This on the one hand, and, on the other, the smaller number of stages in the impulse-type turbine are the reasons why such a vanishingly small amount of water goes over into the coarse forms here. In cases "G1 2" and "G1 3," the lion's share of the water quantity is divided between the two fog-droplet species, whose average sizes differ by a factor of more than 10.

In summarizing, we can state that in cases with favorable fogging ("Ub 1," "G1 1"), both turbine designs produce very little water in the coarse forms. If, on the other hand, the fog formed has coarse droplets, the impulse-type turbine clearly performs better than the reaction-type turbine, at least as regards water distribution; this is primarily because, in addition to the coarse drops, fine fog droplets are also subsequently produced. The result is that not only is undercooling kept low, but the transition of too much water into the coarser forms is impeded. Also to be recognized from Figs. 7 and 11 is the fact that a more favorable distribution of the water present in the coarsest forms is also achieved in the impulse-type turbine, namely, most of it can be centrifuged out. This is to be attributed to the fact that the fog droplets are mostly trapped by rotor buckets (compare the y_f values in the tables!),

It must be noted here, however, that examples "G1 2" and "G1 3" do not reproduce the least favorable case that can occur at all in **impulse-type** turbines nearly as well as "Ub 2" and "Ub 3" do this for the **reaction-type** turbine. That is to say, there is a much greater possibility that still much coarser fog droplets may form in an **impulse-type** turbine - due to the small pressure drop in the rotor rings - than was assumed here. Unfavorable intermediate cases are also conceivable, for example, the case in which the first-born fog droplets are only just coarse enough to produce a large supercooling but not big enough to cause a repeated **heavy nucleation**; or - in extremely rare cases - even the second-generation fog droplets may be coarse, so that yet a third fogging occurs.

Further comparison of these examples will be possible only with reference to the moisture losses, in Section 3.7.

TABLE 2.9.1

Example "Ub 1": Reaction-type Turbine, Assuming Fine-Droplet Fog and Poor Dewatering Devices

A Stufe:		1		2	
B Schaufelkranz:		1'	1''	2'	2''
y_{∞}	kg/kg	-	(0,00160)	(0,00960)	(0,01850)
Δy	kg/kg	-	(0,00160)	(0,00960)	(0,01843)
y	kg/kg	-	0	0	0,00007
y_n	kg/kg	-	-	-	-
y_i	kg/kg	-	-	$0,7 \cdot 10^{-4}$	$2,5 \cdot 10^{-4}$
y_g	kg/kg	-	-	$0,7 \cdot 10^{-4}$	-
y_{gs}	kg/kg	-	-	-	$0,7 \cdot 10^{-4}$
y_h	kg/kg	-	-	-	$2,5 \cdot 10^{-4}$
E_n		-	-	-	1
$(y_i + y_{gs} + y_h)/y_{\infty}$		-	-	0,4%	1,0%
y_h/y_{∞}		-	-	-	0,8%
C Bemerkung:		D Der Dampf ist noch überhitzt	E Sättigungslinie wird überschritten	F Spontane Kond. im Kranz bei $p^* \approx 1100 \text{ sec}^{-1}$	
ΔT_{\max}	$^{\circ}\text{C}$	-	-	-	$\Delta T^* = 29^{\circ}$
ΔT	$^{\circ}\text{C}$	-	ca. 2°	ca. 12°	ca. 23°
$r_{B, \max}$	m	-	-	-	$4,0 \cdot 10^{-5}$
\dot{r}_h	m	-	-	-	$0,9 \cdot 10^{-5}$
\dot{r}_g	m	-	-	$1,4 \cdot 10^{-5}$	-
\dot{r}_{gs}	m	-	-	-	$0,7 \cdot 10^{-5}$

A) Stage; B) blade ring; C) remark; D) the steam is still superheated
 E) saturation line crossed F) spontaneous condensation within ring, at $p^* \approx 1100 \text{ sec}^{-1}$.

3		4		5		6	
3'	3"	4'	4"	5'	5"	6'	6"
0,04500 0,00024 0,04476	0,05700 0,00024 0,05676	0,06900 0,00024 0,06876	0,08200 0,00040 0,08160	0,09500 0,00032 0,09468	0,10800 0,00080 0,10520	0,12100 0,00176 0,11924	
0,04432	0,05608	0,06765	0,07972	0,09290	0,09990	0,11165	
10^{-4} 1,2 · 10 ⁻⁴ 0,7 · 10 ⁻⁴ 2,5 · 10 ⁻⁴	2,4 · 10 ⁻⁴ 2,0 · 10 ⁻⁴ 4,8 · 10 ⁻⁴	4,1 · 10 ⁻⁴ 4,3 · 10 ⁻⁴ 2,0 · 10 ⁻⁴ 4,8 · 10 ⁻⁴	7,8 · 10 ⁻⁴ 6,5 · 10 ⁻⁴ 12,3 · 10 ⁻⁴	11,1 · 10 ⁻⁴ 11,6 · 10 ⁻⁴ 6,7 · 10 ⁻⁴ 12,3 · 10 ⁻⁴	21,5 · 10 ⁻⁴ 19,2 · 10 ⁻⁴ 33,8 · 10 ⁻⁴	20,8 · 10 ⁻⁴ 23,1 · 10 ⁻⁴ 20,1 · 10 ⁻⁴ 33,8 · 10 ⁻⁴	32,9
0,9963 1,0% 0,6%	0,9909 1,2% 0,8%	0,9831 1,6% 0,7%	0,9720 2,3% 1,5%	0,9575 3,2% 1,3%	0,9245 5,0% 3,2%	0,9030 6,3% 2,0%	
0,3° 2,1°	0,3° 2,4°	0,3° 3,1°	0,5° 3,7°	0,4° 4,8°	1,0° 7,2°	2,2°	
10^{-5} 2,6 · 10 ⁻⁵	2,3 · 10 ⁻⁵ 2,1 · 10 ⁻⁵		2,0 · 10 ⁻⁵ 2,0 · 10 ⁻⁵		1,7 · 10 ⁻⁵	1,4	
1,0 · 10 ⁻⁷ 2,1 · 10 ⁻⁵ 0,7 · 10 ⁻⁵	1,1 · 10 ⁻⁷ 1,0 · 10 ⁻⁵	1,2 · 10 ⁻⁷ 3,5 · 10 ⁻⁵ 1,0 · 10 ⁻⁵	1,3 · 10 ⁻⁷ 1,0 · 10 ⁻⁵	1,3 · 10 ⁻⁷ 6,0 · 10 ⁻⁵ 1,0 · 10 ⁻⁵	1,4 · 10 ⁻⁷ 1,0 · 10 ⁻⁵	1,5 · 10 ⁻⁷ 11,5 · 10 ⁻⁵ 0,9 · 10 ⁻⁵	

4		5		6	
4''		5'	5''	6'	6''
0,068 00 0,000 24 0,068 78	0,062 08 0,000 40 0,061 68	0,055 00 0,000 32 0,054 68	0,106 00 0,000 80 0,105 20	0,121 00 0,001 76 0,119 24	0,130 00 0,003 12 0,126 88
0,067 65 4,3 · 10 ⁻⁴ 2,0 · 10 ⁻⁴ 4,8 · 10 ⁻⁴	0,079 72 6,5 · 10 ⁻⁴ 12,3 · 10 ⁻⁴	0,092 90 11,1 · 10 ⁻⁴ 11,6 · 10 ⁻⁴ 6,7 · 10 ⁻⁴ 12,3 · 10 ⁻⁴	0,099 90 19,2 · 10 ⁻⁴ 33,8 · 10 ⁻⁴	0,111 65 22,1 · 10 ⁻⁴ 20,1 · 10 ⁻⁴ 33,8 · 10 ⁻⁴	0,115 74 44,5 · 10 ⁻⁴ 66,9 · 10 ⁻⁴
0,063 1 1,6% 0,7%	0,072 0 2,3% 1,5%	0,057 5 3,2% 1,3%	0,024 5 5,0% 3,2%	0,003 0 6,3% 2,8%	0,074 4 8,6% 5,1%
0,3° 3,1°		3,7° 0,4° 4,6°		7,2° 2,2° 7,3°	
0,5°		1,0°		3,9°	
2,1 · 10 ⁻⁵		2,0 · 10 ⁻⁵ 2,0 · 10 ⁻⁵		1,7 · 10 ⁻⁵ 1,8 · 10 ⁻⁵	
1,3 · 10 ⁻⁷ 3,5 · 10 ⁻⁵ 3,0 · 10 ⁻⁵	1,3 · 10 ⁻⁷ - 1,0 · 10 ⁻⁵	1,3 · 10 ⁻⁷ 6,0 · 10 ⁻⁵ 1,0 · 10 ⁻⁵	1,4 · 10 ⁻⁷ - 1,0 · 10 ⁻⁵	1,5 · 10 ⁻⁷ 11,5 · 10 ⁻⁵ 0,9 · 10 ⁻⁵	1,5 · 10 ⁻⁷ - 0,9 · 10 ⁻⁵

TABLE 2.9.2

Example "Ub 2": Reaction-type Turbine, Assuming Coarse-Droplet Fog and Poor Dewatering Devices

A Stufe:		1		2		3	
B Schaufelkranz:		1'	1''	2'	2''	3'	3''
y_{∞}	kg/kg	-	(0,003 20)	(0,011 20)	(0,020 80)	0,033 00	0,045 00
Δy	kg/kg	-	(0,003 20)	(0,011 20)	0,003 20	0,004 80	0,006 50
y	kg/kg	-	0	0	(0,017 60)	0,028 20	0,032 50
y_n	kg/kg	-	-	-	(0,017 53)	0,027 69	0,037 16
y_l	kg/kg	-	-	-	$0,7 \cdot 10^{-4}$	$8,1 \cdot 10^{-4}$	$14,8 \cdot 10^{-4}$
y_g	kg/kg	-	-	-	$0,7 \cdot 10^{-4}$	$8,3 \cdot 10^{-4}$	$8,3 \cdot 10^{-4}$
y_{gg}	kg/kg	-	-	-	-	$0,7 \cdot 10^{-4}$	$0,7 \cdot 10^{-4}$
y_h	kg/kg	-	-	-	-	$4,4 \cdot 10^{-4}$	$4,4 \cdot 10^{-4}$
E_n		-	-	-	1	0,9748	0,9457
$y_l + y_{gg} + y_h / y_{\infty}$		-	-	-	0,4%	1,5%	3,0%
y_h / y_{∞}		-	-	-	-	1,3%	1,0%
C Bemerkung:		Der Dampf ist noch überhitzt D	Sättigungslinie E wird überschritten		F Spont. Kond. im Zw.-raum bei $\dot{p}^* \approx 150 \text{ sec}^{-1}$		
ΔT_{\max}	$^{\circ}\text{C}$	-	-	-	$\Delta T^* \approx 26^{\circ}$	$8,5^{\circ}$	$11,6^{\circ}$
ΔT	$^{\circ}\text{C}$	-	ca. 4°	ca. 14°	4°	$6,0^{\circ}$	$8,1^{\circ}$
$r_{B, \max}$	m	-	-	-	$4,0 \cdot 10^{-5}$	$2,6 \cdot 10^{-5}$	$2,6 \cdot 10^{-5}$
\bar{r}_n	m	-	-	-	$(3,3 \cdot 10^{-7})$	$3,9 \cdot 10^{-7}$	$4,3 \cdot 10^{-7}$
\bar{r}_g	m	-	-	-	$1,4 \cdot 10^{-5}$	-	$2,1 \cdot 10^{-5}$
r_{gg}	m	-	-	-	-	$0,7 \cdot 10^{-5}$	$0,7 \cdot 10^{-5}$

A) Stage; B) blade ring; C) remark; D) the steam is still superheated; E) saturation line is crossed; F) spontaneous condensation in intermediate space, at $\dot{p}^* \approx 150 \text{ sec}^{-1}$.

		4		5		6	
3"		4'	4"	5'	5"	6'	6"
00	0,05700	0,06908	0,06200	0,09500	0,10600	0,12100	0,13000
0	0,00680	0,00690	0,00870	0,00880	0,01200	0,01700	0,02000
0	0,05020	0,06210	0,07330	0,08520	0,09400	0,10400	0,11000
6	0,04737	0,05683	0,06383	0,07028	0,07067	0,07348	0,07157
-4	$14,8 \cdot 10^{-4}$	$25,0 \cdot 10^{-4}$	$39,4 \cdot 10^{-4}$	$51,2 \cdot 10^{-4}$	$81,0 \cdot 10^{-4}$	$85,9 \cdot 10^{-4}$	$73,0 \cdot 10^{-4}$
-4	$9,1 \cdot 10^{-4}$	$28,8 \cdot 10^{-4}$	$36,1 \cdot 10^{-4}$	$53,4 \cdot 10^{-4}$	$93,7 \cdot 10^{-4}$	$68,8 \cdot 10^{-4}$	$171,7 \cdot 10^{-4}$
-4	$19,2 \cdot 10^{-4}$	$9,3 \cdot 10^{-4}$	$58,6 \cdot 10^{-4}$	$37,2 \cdot 10^{-4}$	$139,6 \cdot 10^{-4}$	$96,8 \cdot 10^{-4}$	$212,6 \cdot 10^{-4}$
		$19,2 \cdot 10^{-4}$		$58,6 \cdot 10^{-4}$		$139,6 \cdot 10^{-4}$	
7	0,9087	0,8587	0,7975	0,7295	0,8421	0,5767	0,5145
	5,0%	7,9%	11,6%	15,7%	22,0%	25,2%	29,6%
	3,4%	2,8%	7,1%	6,2%	13,2%	11,5%	16,4%
11,9°	8,7°	12,7°	14,6°	17,9°	19,8°	28,1°	30,9°
		9,2°	11,7°	13,5°	16,8°	24,1°	28,6°
$2,6 \cdot 10^{-5}$		$2,3 \cdot 10^{-5}$	$2,1 \cdot 10^{-5}$	$2,0 \cdot 10^{-5}$	$2,0 \cdot 10^{-5}$	$1,7 \cdot 10^{-5}$	$1,8 \cdot 10^{-5}$
-7	$4,7 \cdot 10^{-7}$	$5,1 \cdot 10^{-7}$	$5,5 \cdot 10^{-7}$	$5,8 \cdot 10^{-7}$	$6,1 \cdot 10^{-7}$	$6,4 \cdot 10^{-7}$	$6,6 \cdot 10^{-7}$
-5	-	$3,5 \cdot 10^{-5}$	-	$6,0 \cdot 10^{-5}$	-	$11,5 \cdot 10^{-5}$	-
-5	$1,0 \cdot 10^{-5}$	$1,0 \cdot 10^{-5}$	$1,0 \cdot 10^{-5}$	$1,0 \cdot 10^{-5}$	$1,0 \cdot 10^{-5}$	$0,9 \cdot 10^{-5}$	$0,9 \cdot 10^{-5}$

TABLE 2.9.3

Example "Ub 3": Reaction-type Turbine, Assuming Coarse-Droplet Fog and Ideal Dewatering Devices

A Stufe:		1		2		3		
B Schaufelkranz:		1'	1''	2'	2''	3'	3''	4'
y_{∞} kg/kg	-		(0,003 20)	(0,011 20)	(0,020 80)	0,033 00	0,045 00	
Δy kg/kg	-		(0,003 20)	(0,011 20)	0,003 20	0,004 80	0,006 50	
y kg/kg	-		0	0	(0,017 60)	0,028 20	0,038 50	
y_m kg/kg	-		-	-	(0,017 53)	0,027 69	0,037 16	
y_f kg/kg	-	-	-	$0,7 \cdot 10^{-4}$	$5,1 \cdot 10^{-4}$	$8,1 \cdot 10^{-4}$	$23,1 \cdot 10^{-4}$	$25,0 \cdot 10^{-4}$
y_g kg/kg	-	-	-	$\rightarrow 0,7 \cdot 10^{-4}$	$\rightarrow 5,1 \cdot 10^{-4}$	-	$\rightarrow 8,3 \cdot 10^{-4}$	$\rightarrow 25,0 \cdot 10^{-4}$
y_{gg} kg/kg	-	-	-	-	-	-	-	-
y_h kg/kg	-	-	-	-	$\rightarrow 5,1 \cdot 10^{-4}$	$5,1 \cdot 10^{-4}$	-	-
E_m	-	-	-	1	0,9748	0,9457		
$(y_g + y_{gg} + y_h)/y_{\infty}$	-	-	-	0,4%	1,5%	3,0%		
y_h/y_{∞}	-	-	-	-	1,5%	1,1%		
C Bemerkung:	Der Dampf ist noch überhitzt D	Sättigungs- linie wird über- schritten E		F Spont. Kond. im Zw.-raum bei $\dot{p}^* \approx 150 \text{ sec}^{-1}$				
ΔT_{\max} °C	-	-	-	$\Delta T^* \approx 26^\circ$	$8,5^\circ$	$11,6^\circ$	$11,9^\circ$	$12,7^\circ$
ΔT °C	-	ca. 4°	ca. 14°	4°	$6,0^\circ$	$8,1^\circ$		
$r_{B, \max}$ m	-	-	-	-	$4,0 \cdot 10^{-5}$	$2,6 \cdot 10^{-5}$	$2,6 \cdot 10^{-5}$	$2,3 \cdot 10^{-5}$
\bar{r}_h m	-	-	-	$(3,3 \cdot 10^{-7})$	$3,9 \cdot 10^{-7}$	$4,3 \cdot 10^{-7}$		
\bar{r}_g m	-	-	-	$1,4 \cdot 10^{-5}$	-	$2,1 \cdot 10^{-5}$		
\bar{r}_{gg} m	-	-	-	-	-	-		

A) Stage; B) blade ring; C) remark; D) the steam is still superheated; E) saturation line is crossed; F) spontaneous condensation in intermediate space, at $\dot{p}^* \approx 150 \text{ sec}^{-1}$.

4			5			6		
3"	4'	4"	5'	5"	6'	6"		
	0,069 00 0,006 90 0,062 10	0,082 00 0,008 70 0,073 30	0,095 00 0,009 80 0,085 20	0,106 00 0,011 90 0,094 10	0,121 00 0,016 80 0,104 20	0,130 00 0,019 50 0,110 50		
	0,056 70	0,063 96	0,070 51	0,071 28	0,074 45	0,073 35		
23,1·10 ⁻⁴	25,0·10 ⁻⁴ 25,8·10 ⁻⁴ 28,2·10 ⁻⁴	65,2·10 ⁻⁴ - 93,4·10 ⁻⁴	51,3·10 ⁻⁴ 53,5·10 ⁻⁴ 93,4·10 ⁻⁴	134,8·10 ⁻⁴ - 228,2·10 ⁻⁴	66,4·10 ⁻⁴ 69,3·10 ⁻⁴ 228,2·10 ⁻⁴	143,3·10 ⁻⁴ - 371,5·10 ⁻⁴		
	0,8595 7,8% 4,1%	0,7997 11,5% 11,5%	0,7328 15,5% 9,8%	0,6484 21,5% 21,5%	0,5853 24,6% 18,9%	0,5271 28,6% 28,6%		
11,9°	12,7° 9,2° 14,6°	11,7°	17,8° 13,4° 19,6°	16,7°	27,7° 23,8° 30,2°	27,9°		
2,6·10 ⁻⁵	2,3·10 ⁻⁵ 2,1·10 ⁻⁵		2,0·10 ⁻⁵ 2,0·10 ⁻⁵		1,7·10 ⁻⁵ 1,8·10 ⁻⁵			
	5,1·10 ⁻⁷ 3,5·10 ⁻⁵ -	5,5·10 ⁻⁷ - -	5,8·10 ⁻⁷ 6,0·10 ⁻⁵ -	6,1·10 ⁻⁷ - -	6,4·10 ⁻⁷ 11,5·10 ⁻⁵ -	6,6·10 ⁻⁷ - -		

B

Example "G1 2":
Impulse-type
Turbine, Assuming Coarse-Droplet Fog
and Poor Dewatering Devices

A) Stage; B) blade ring; C) remark; D) the steam is still superheated; E) saturation line is crossed; F) spontaneous condensation in intermediate space, at $P^* \approx 150 \text{ sec}^{-1}$; G) secondary spontaneous condensation without ring at $P^* \approx 4500 \text{ sec}^{-1}$.

Example "G1 3": Impulse-type and Ideal Dewatering Devices

Turbine, Assuming Coarse-Droplet Fog

[illegible]

A) Stage; B) blade ring; C) remark; D) the steam is still superheated; E) saturation line is crosses; F) spontaneous condensation in intermediate space at $\dot{P}^* \approx 150 \text{ sec}^{-1}$; G) secondary spontaneous condensation in ring, at $\dot{P}^* \approx 4500 \text{ sec}^{-1}$.

[Footnotes to Part Two]

- No.
- 31 The percentage reaction of the last stage at the blade, means diameter is given in parentheses.
- 32 It is also frequently known as the Helmholtz or Kelvin-Helmholtz formula.
- 33 Here it is tacitly assumed that the steam, which surrounds the droplets, possesses the temperature T_r . This condition is automatically satisfied in cases in which the steam can be regarded as a continuum, since a thermal boundary layer (see Fig. 2) whose interior zone actually does have the temperature T_r , forms around the droplets. With long free paths in the steam, however, "colder" steam molecules can also reach the droplets, which is contrary to our assumption. Nevertheless, it follows from the investigations of Stodola ([3], page 562) that Eq. (10) is also valid in close approximation in this case.
- 34 If the droplet were moving with a non-negligible velocity ($U_r > 50\text{m/sec}$) relative to the steam, then T_d would have to be replaced by $T_{r,ad}$ and the quantity ΔT_{GS} would necessarily appear as a third term in Eq. (13); compare Section 2.2. With small droplets ($r < 10^{-6}\text{ m}$), however, this effect does not become noticeable.
- 35 Compare, for example, "Hütte."
- 36 Properly speaking, this equilibrium distribution of the droplets never occurs in reality. Determination of a quasistationary droplet distribution that corresponds more closely to reality was the most difficult point of the theory.
- 37 Strictly speaking, the notation $\xi_{a,e}$ would be the consistent one; for the sake of simplicity, however, we have dropped the subscript a .
- 38 Elektronische Rechenmaschine [Electronic Computer] of the ETH [Swiss Federal Institute of Technology].
- 39 More precisely: no new nuclei that subsequently grow and produce stable droplets.

- 40 In principle, nucleation has already begun immediately on passage over the saturation line. At the outset, however, it is so weak that for all practical purposes, only a narrow region immediately before the Wilson point comes into consideration as a "nucleation zone."
- 41 A 10% deterioration of η_p has approximately the same effect as a \dot{P} smaller by about 15%. (According to Diagram IV, Z_3 is reduced by half and $\sqrt{W/T} \approx 0.85$, which gives the above conclusion on the basis of Eq. (34).)
- 42 Strictly speaking, p^* is not the same for all streamlines, but also depends on the local rate of expansion. We shall disregard this dependence here — it has only a minor influence on the shape of the shocks — but will discuss it explicitly in another context in Section e.
- 43 Since Fig. 8 was determined for the ideal case $\eta_p = 1$, a correction must be introduced when it is applied to real expansions. For $\eta_p < 1$, somewhat smaller ΔT^* -values prevail throughout, and a 10% efficiency deterioration amounts, as we have already noted, to about the same thing as though η_p had remained equal to 1 but \dot{P}^* had become smaller by about 15% as a result.
- 44 Electronic Computer of the **Swiss Federal Institute of Technology**.
- 45 It is proven in Section 2.8a that this assumption is sufficiently well satisfied.
- 46 Such size differences are not sufficient to produce essential changes in the behavior of the droplets.
- 47 With the subscripts, we assume that we happen to be dealing with a stator.
- 48 See footnote 47
- 49 In operational turbines, fogging does not take place under the same circumstances on all radii, since the state **history** is not the same everywhere (variation of the percentage reaction along the buckets). Consequently, these extreme cases never occur in full purity in practice.

Part Three *)

MOISTURE-LOSSES

3.1. GENERAL REMARKS

In making the calculations for a wet-steam turbine, it is assumed at first that even the wet steam represents a homogeneous flow medium, as does the superheated steam, and that the water phase and steam phase are at all times in thermodynamic equilibrium. For this "homogeneous ideal case," the losses in the turbine would be no different from those for superheated steam, and the calculation could be carried out simply, for example, with reference to a conventional i, s -table. The two turbines of Section 2.1 that serve as our example were laid out on this basis.

In reality, however, these assumptions are far from being the case. The wet steam results in additional losses stemming from its deviation from the behavior corresponding to homogeneity and equilibrium. These losses are known as moisture-losses. They are the object of investigation in the sections that follow.

The Baumann rule ([3], page 501), which brings the efficiency deterioration of the wet-steam part of a turbine globally into a simple proportional relationship to the theoretical terminal wetness $y_{\infty E}$, has taken root among engineers as a basis for calculating wetness losses:

$$\eta_1 = \eta_{1, tr} \left(1 - \alpha_{Bm} \frac{y_{\infty E}}{2} \right). \quad (1)$$

Here, α_{Bm} is the proportionality factor introduced by Baumann,⁵⁰ η_1 is the internal efficiency of the wet-steam section and $\eta_{1, tr}$ is the "dry"

*) superscripts refer to footnotes, listed on pp. 258-259.

$$\Delta h_{tr} = \begin{cases} 417,8 \text{ kJ/kg} & (\text{Reaction-type turbine}), \\ 408,5 & (\text{Impulse-type turbine}). \end{cases} \quad (6)$$

Opinions are sharply divergent regarding the numerical value of α_{Bm} . On the basis of observation of numerous operating condensation turbines, Baumann indicated at the time an average value of about 1.0. Later, von Freudenreich [4] found the value 1.18 from experiments made on a condensation turbine. Air-turbine experiments of Flatt [8], where, of course, the work was done not with natural fogging, but by artificial water injection, gave about 1.4. In recent years, practice has begun to adopt the position that the correct value of α_{Bm} is considerably smaller than unity -- probably about 0.5 to 0.7 -- and that the high values hazarded earlier can be attributed only to the unfavorable hydromechanical configuration of the low-pressure stages. These views are supported by experimental results [12], [13], in which considerable improvement of the low-pressure stages was managed by exclusively hydromechanical measures. Accordingly, the losses that must actually be attributed to the peculiarities of the wet steam would be considerably smaller than had been assumed earlier.

A local loss dq , occurring somewhere in the course of expansion, will obviously be partially recovered as expansion continues. The remaining loss, i.e., that which ultimately manifests itself in the deterioration of the over-all expansion, will be obtained (compare [20], page 19) by multiplying the local loss by a factor $[1 - (1 - T_K/T) \times \eta_{s,hint}]$ [hint = behind]. Here, T is the temperature at the point where the loss arises, $T_K = T_s(p_K)$ is the temperature in the condenser and $\eta_{s,hint}$ is the isentropic efficiency of that part of the expansion behind the point of origin of the loss. In the calculations to follow, it will always be the loss in a definite stage (Δq) that will occur as a local loss, so that the actual work loss due to it can be calculated

from

$$\Delta i_v = \Delta q \cdot \left[1 - \left(1 - \frac{T_K}{T_2} \right) \cdot \eta_{s, \text{hint}} \right] \quad (7)$$

(T_2 is the temperature at the end of the stage in question). We modify Eq. (7) somewhat further and, for the sake of simplicity, substitute the prespecified internal efficiency $\eta_{1, \text{tr}}$ for $\eta_{s, \text{hint}}$, by which we incur no appreciable error. Thus we obtain

$$\Delta i_v = \Delta q \left[\frac{T_K}{T_2} + (1 - \eta_{1, \text{tr}}) \cdot \left(1 - \frac{T_K}{T_2} \right) \right]. \quad (8)$$

Since both T_K/T_2 and $\eta_{1, \text{tr}}$ are close to unity, the second term in the brackets is always much smaller than the first.

The individual stage losses Δq can be computed on the basis of Sections 3.2 to 3.5. Then Eq. (4) must be used to calculate Δi_v , the reduced stage loss, and the sum of these Δi_v plus the undercooling loss $\Delta i_{\text{Untk}}^{\text{Stutzen}}$ [Stutzen = exhaust-pipe; Untk = undercooling] (compare Section 3.4) gives the unknown rise in the static exit enthalpy:

$$\Delta i_{v, \text{tot}} = \sum_{\text{Stufen}} \Delta i_v + \Delta i_{\text{Untk}}^{\text{Stutzen}}. \quad (9)$$

[Stufen = stages].

A proposal made on numerous occasions has been to write a formula similar to Eq. (1) also for the efficiency deterioration of a single wet-steam stage. This would then read somewhat as follows:

$$\eta_{su} = \eta_{su, \text{tr}} \left(1 - \alpha_{\text{Bm, St}} \frac{y_{\infty 0} + y_{\infty 2}}{2} \right) \quad (10)$$

where η_{su} and $\eta_{su, \text{tr}} \equiv (i_0 - i_2)/\Delta i_s$ are the "isentropic efficiencies of the stage at the circumference" and $\alpha_{\text{Bm, St}}$ is the Baumann factor applying for the stage. If the over-all wetness loss Δq in the stage is known, we can determine $\alpha_{\text{Bm, St}}$ from the formula

$$\alpha_{\text{Bm, St}} = \frac{\Delta q}{i_0 - i_2} \cdot \frac{2}{y_{\infty 0} + y_{\infty 2}} \quad (11)$$

which is similar to Eq. (4). It should be noted here that the $\alpha_{Bm,St}$ of the individual stages may show very great differences.

For the wetness-loss number ζ defined by Traupel [20] (who referred to it as the "braking-loss number ζ_B "), we write

$$\zeta = \eta_{su,tr} \frac{\Delta q}{t_0 - t_2} \quad (12)$$

There are several physical processes that are responsible for moisture losses. Under subsequent headings, we shall discuss their contribution to the total wetness loss in a stage (Δq) individually. Here we shall everywhere satisfy ourselves with approximation formulas, since the accuracy to be expected from the data calculated on the basis of Section 2.9 and used as a point of departure for the loss determination will not be any too high to begin with. In the last section, we shall determine the losses for the examples calculated under Heading 2.9b and obtain the theoretical values for α_{Bm} for both turbine types from them.

3.2. BRAKING-LOSSES

The heterogeneous nature of the wet steam, noted at the outset of the previous Section, is manifested, for one thing, in the fact that its various components (steam, various sizes of droplets, films of water, etc.) have differing velocities. Further, all of these velocities deviate from the common velocity that they would all share in the homogeneous ideal case.

We shall use the term "braking-losses" to designate those losses that can be stated on the basis of the actual velocity conditions as compared to the homogeneous ideal case, by purely kinematic means.⁵¹ For a long time, it was thought possible to account for the entire wetness loss in this manner (v. Freudenreich [4]), and it was, of course, always assumed that all of the moisture was present in the

form of large drops incapable of following the motion of the steam and therefore impinging upon the blades in each cascade ring. In the light of Part Two of this work and of Section 2.9 in particular, this assumption is untenable. Only a small part of the entire water content devolves upon such destructive drops, so that only a relatively minor significance is to be ascribed to the braking-losses.

It would be possible to conduct an exact determination of the braking-losses in a stage by determining the velocity triangles for each form the moisture appears in, determining from these (knowing the respective masses) the work that they yield in the rotor, and summing over the results. The difference from the work yield of the homogeneous ideal case would then give the braking-loss. In itself, this method would be the exact one; it is, however, highly circumstantial, since the actual velocity vectors would have to be determined individually for each single phenomenal form and also for the steam. It will be found that a good approximation for the braking-losses can be arrived at very simply. For this purpose, we carry the following reasoning through which is based on Zerkovitz [5].

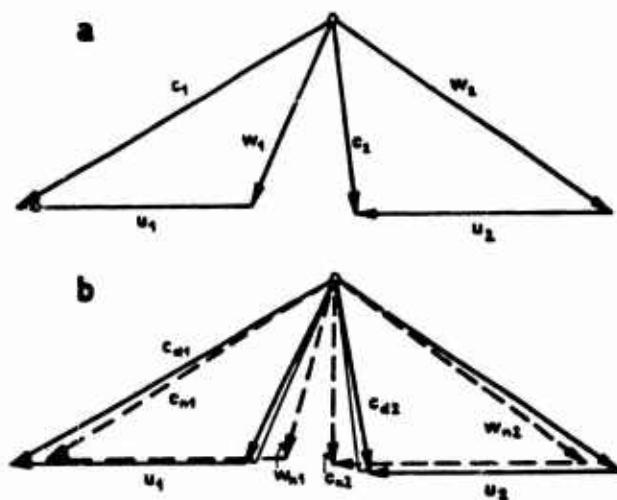


Fig. 3.2.1. Velocity triangles of a stage a) in the homogeneous ideal case and b) for its physical approximation by steam and fog droplets (Light lines represent the homogeneous ideal case; solid lines: steam; dashed lines: fog droplets).

In the homogeneous ideal case, the steam and water have practically equal velocities. The velocity triangles of a stage are drawn in Fig. 1a. This case is approximated very closely in actuality when the water is distributed in the form of fine fog droplets (Fig. 1b), since then the droplet velocities (subscript n) will deviate only slightly from the steam velocities (subscript d).

As the antithesis to the hypothetical homogeneous ideal case, we may define a likewise hypothetical "heterogeneous ideal case," which would be characterized by the water phase always having the absolute velocity zero, or, in other words, the heat drop in each ring being used exclusively to elevate the kinetic energy of the steam phase. Here it is assumed that no additional losses arise and again that thermodynamic equilibrium is maintained. Then, however, the heat drop remains the same everywhere and, roughly speaking, the steam will flow faster by a factor $1/\sqrt{x}$ (see Fig. 2a). Such a case might be brought to reality in a turbine by removing the water from the steam and allowing it to flow slowly along a wall outside the blading (Fig. 2b).

If we write the turbine equations for the homogeneous and heterogeneous ideal cases (compare Traupel, [20], page 328) and compare them, we see that the works L_u and L_u^0 done in the rotors in the two cases differ only by the amount

$$L_u - L_u^0 = \frac{c_0^2 - x_0 c_{d0}^2}{2} - \frac{c_2^2 - x_2 c_{d2}^2}{2} \quad (1)$$

which, due to the relationship $c_d^0 \approx c/\sqrt{x}$ which is satisfied approximately everywhere, becomes almost exactly zero. Thus we find that no braking-loss occurs in the heterogeneous ideal case.

If a real case can be arrived at from these two extreme cases (for which purpose we imagine that a suitably large part of the mass flow belongs to one extreme case and the rest to

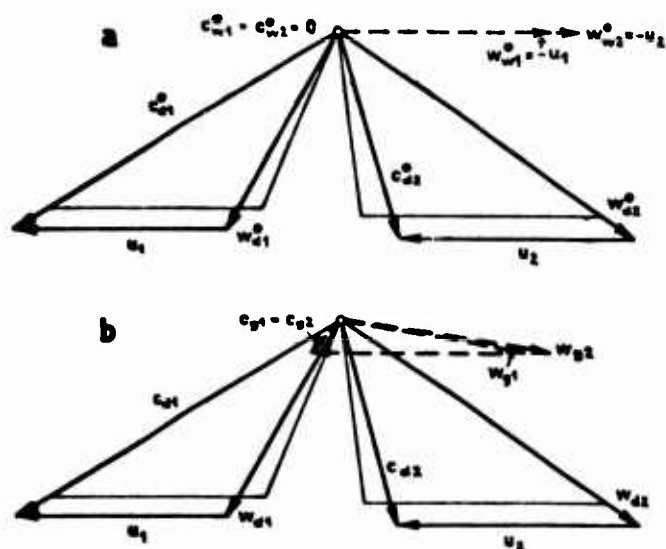


Fig. 3.2.2. Velocity triangles of a stage a) in the heterogeneous ideal case and b) for its physical approximation by steam and slow-moving water. (Light lines represent the homogeneous ideal case; solid lines: steam; dashed lines: water.)

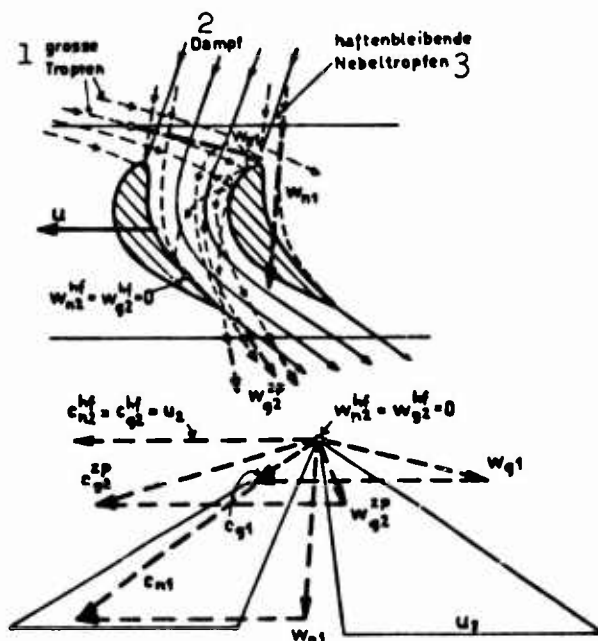


Fig. 3.2.3. Illustrating motion of large drops and depositing fog droplets in a rotor. 1) Large drops; 2) steam; 3) clinging fog droplets.

other), this composite case will again not develop any braking-loss. The compositeness condition is almost satisfied in the cases represented in Figs. 1b and 2b, so that we may state that because of the fog droplets remaining in the steam and because of the water that has been taken out of the steam and, say, is flowing along the casing

wall, no braking- loss occurs. That is to say, the smaller (or non-existent) work done by the water phase is made good by the increase in the work done by the steam phase. (The fact that the thermal contact between the two phases is never perfect either, since the water is not distributed with infinitesimal fineness, prevents any such sharp increase in the work done by the steam in real cases; however, this loss is not governed by the kinematic heterogeneity of the steam and is therefore not covered here. The same applies for the friction losses between the drops and the steam. They are due to be dealt with only in later Sections.)

Now let us turn to those cases in which such "composing" is not possible even in approximation and which, as a result, lead to large braking- losses. Here we are concerned with those water drops that impinge upon the rotor buckets: in part, these are fog droplets that are flung against the concave sides of the buckets and remain stuck there (indices $_{n}^{hf}$), and in part they are large drops striking the rotor buckets with an oblique relative velocity w_{g1} . Part of their mass may ricochet on impingement (indices $_{g}^{zp}$), while the rest remains clinging to the surface of the bucket (indices $_{g}^{hf}$). The relationships are represented graphically in Fig. 3. Here, for the sake of ready comprehension, only the large drops torn off the back of the preceding stator ("g") have been taken into account, and those rebounding from the stator ring ("gg") have been left out of consideration. For these latter drops, we have qualitatively exactly the same considerations as for "g," but their velocities are somewhat more axial and higher at entry into the rotor.

All clinging drops have the absolute exit velocity u_2 , and even the rebounding drops leave the rotor - due to their relatively small and not particularly oblique relative velocity w_{g2}^{zp} - at an absolute

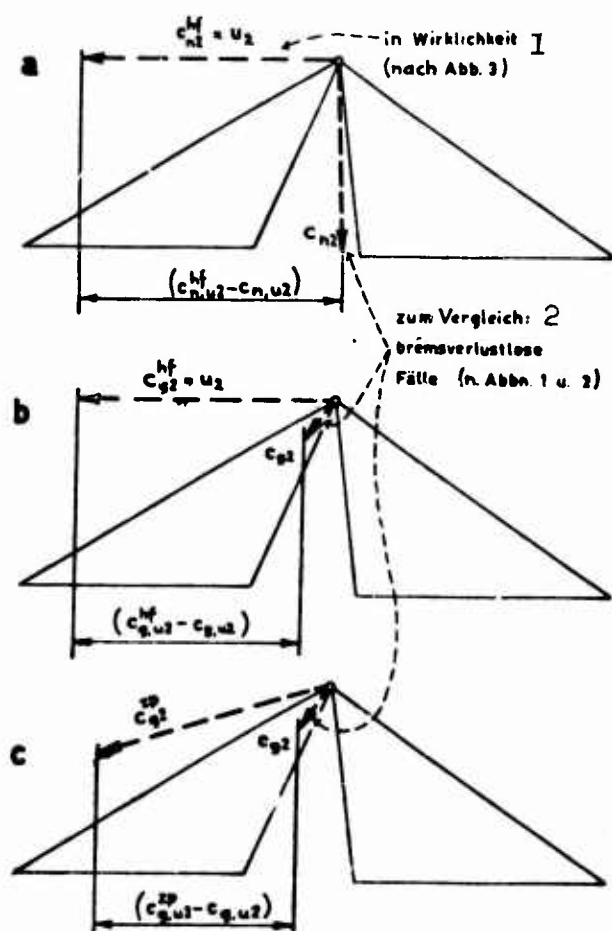


Fig. 3.2.4. Illustrating calculation of braking-losses: a) due to clinging fog droplets; b) due to clinging large drops; c) due to the rebounding part of the impinging large drops. 1) In actuality (after Fig. 3); 2) for comparison: cases without braking-loss (after Figs. 1 and 2).

velocity c_{g2}^{zp} whose circumferential component differs only slightly from u_2 . Now it follows from our earlier statements that there ought to be no braking-losses only provided that these drops also had the exit velocities c_{n2} and c_{g2} , respectively, represented in Figs. 1b and 2b. Since their actual exit velocities always possess circumferential components larger than these (compare Fig. 4), a braking loss must occur. Due to the momentum law, their magnitudes – in each case referred to the unit mass of the drops involved – will be

$$\Delta L_{u,n} = (c_{n,u2}^H - c_{n,u2}) \cdot u_2. \quad (2)$$

for the clinging fog droplets,

$$\Delta L_{u,g}^M = (c_{g,u2}^M - c_{g,u2}) \cdot u_2 \quad (3)$$

for the clinging portion of the large drops, and

$$\Delta L_{u,g}^{SP} = (c_{g,u2}^{SP} - c_{g,u2}) \cdot u_2 \quad (4)$$

for the rebounding portion of the latter. The three quantities in parentheses are represented in Figs. 4a, 4b and 4c. Since in the cases without braking- losses, the exit velocity has only a very small circumferential component, and the actual exit velocity, on the other hand, is either identical to or very close to the circumferential velocity u_2 , we can adopt the approximation $(c_{n,u2}^M - c_{n,u2}) \approx (c_{g,u2}^M - c_{g,u2}) \approx (c_{g,u2}^{SP} - c_{g,u2}) \approx u_2$, which leads us to the very simple formula

$$\Delta L_{u,n} \approx \Delta L_{u,g}^M \approx \Delta L_{u,g}^{SP} \approx u_2^2 \quad (5)$$

In most practical cases, this gives a value high by about 10 to 20% for the braking work.

Since the losses are always referred to the unit mass of the entire flow medium, we must multiply the works ΔL_u by the mass of drops concerned in unit mass of wet steam. Thus we obtain for the

braking- losses caused by clinging fog droplets, per stage per kilogram of flow medium,

$$\Delta q_{Brems,n} = \epsilon_{n-1}^n \gamma_{n1} \Delta L_{u,n} \approx \epsilon_{n-1}^n \gamma_{n1} \cdot u_2^2 \quad (6)$$

[Brems = braking], and for the braking- loss due to large drops

$$\Delta q_{Brems,g} = \gamma_{g1} (\epsilon_{g-1}^g \Delta L_{u,g}^M + \epsilon_{g-gg}^g \Delta L_{u,g}^{SP}) \approx \gamma_{g1} u_2^2 \quad (7)$$

Since we again find a velocity triangle about the same as that drawn in Fig. 3 for "g," for the large drops that have already rebounded once ("gg") and for the portion of the centrifuged-out water that re-

mains in the flow channel ("h,drin"), the braking- losses due to the latter can be calculated in the same way as $\Delta q_{\text{Brems},g}$:

$$\Delta q_{\text{Brems},g} \approx \gamma_{g1} \cdot u_2^2, \quad (8)$$

$$\Delta q_{\text{Brems},h} \approx \gamma_{h1, \text{drin}} \cdot u_2^2. \quad (9)$$

The total braking- loss in this stage, referred to the mass unit of the wet steam, thus becomes

$$\Delta q_{\text{Brems}} = \Delta q_{\text{Brems},a} + \Delta q_{\text{Brems},g} + \Delta q_{\text{Brems},gk} + \Delta q_{\text{Brems},h} \quad (10)$$

where the individual terms can be calculated from Eqs. (6) through (9).

By way of an example, let us consider the next-to-last stage of the reaction-type turbine designed in Section 2.1. Here, according to Table 2.2.1, $u_2 = 310$ m/sec and the specific masses can be read from Tables 2.9.1, 2 and 3, respectively, for the three cases for which the calculation was carried through under Heading 2.9. We obtain for the three cases

$$\Delta q_{\text{Brems}} = \begin{cases} 0,21 + 0,31 + 0,06 + 0,12 = 0,50 \text{ kJ/kg ("Üb 1")} \\ 0,78 + 0,37 + 0,36 + 0,56 = 2,21 \text{ " ("Üb 2")} \\ 0,78 + 0,52 + 0 + 0 = 1,30 \text{ " ("Üb 3")} \end{cases} \quad (11)$$

Since, according to Table 2.1.1, the stage heat drop in this example, without taking the moisture-losses into account, is $2407.5 - 2320 = 87.5$ kJ/kg, the braking- losses reduce the stage outputs by 0.6%, 2.5% and 1.5% for the respective cases. If we wished to express the

braking- losses in terms of a Baumann factor for the stage, this factor would have the values 0.06, 0.27 and 0.16, respectively, on the basis of Eq. 3.1(11). The losses that can be accounted for by the

braking effect alone thus remain far below the total moisture-loss to be expected on the basis of experience.

3.3. ENTRAINMENT-LOSSES

Entrainment of water drops takes place through the frictional forces operating between the water drops and the steam. Since the fric-

tional forces can be produced only by a relative motion between the drops and the steam, the steam keeps dissipating a certain amount of work on the drops, so that part of the kinetic energy of the flow is converted into heat. These losses are referred to for the sake of brevity as "entrainment-losses." They express the fact that even the production of the imperfect (nonhomogeneous) flow state involves losses.

The entrainment-losses can be calculated only by analysis of the droplet motions. It is recommended that the motion of the fog droplets and that of the large drops be handled in quite different ways, since they exhibit gross differences: the fog droplets are capable of following the motion of the steam rather closely (compare Section 2.6), while the large drops, on the other hand, are quite sluggish and keep bumping into the buckets (compare Section 2.8), requiring new acceleration in each ring.

a) Entrainment-Losses on the Fog Droplets -

Resulting from the velocity field imposed by the blading

The motion of the steam and the fog droplets through a stage is represented in Fig. 1a. It can be described in a particularly simple fashion if we select for the purpose a coordinate system that revolves fast enough so that the line connecting the entry and exit points of a

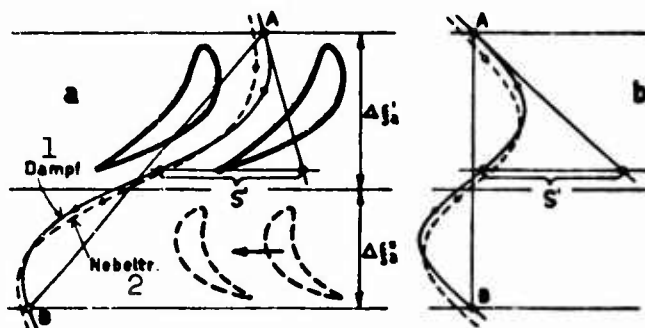


Fig. 3.3.1. Motion of the steam and the fog droplets in a stage: a) as seen by a stationary observer; b) as seen by an observer revolving at an appropriate speed. 1) Steam; 2) fog droplets.

streamline - i.e., points A and B in Fig. 1a - becomes parallel to the axis for a revolving observer, compare Fig. 1b (for example, in the case of identical geometries on the stator and rotor buckets, the coordinate system would have to revolve at half the rpm of the machine). The entire investigation to follow presupposes such a coordinate system.

Figure 1b suggests approximating the streamline shape $\sigma(\xi)$ of the steam in the above coordinate system by a simple sine curve having a period

$$\Delta \xi_a = \Delta \xi_a' + \Delta \xi_a'' \quad (1)$$

whose equation would be written

$$\sigma = \frac{S'}{\pi} \sin\left(\frac{2\pi}{\Delta \xi_a} \xi\right) . \quad (2)$$

Here, ξ is the axial coordinate (with $\xi = 0$ for the control plane in front of the stage), and the amplitude S'/π corresponds to the reversal in the stator, as will be realized at once.

As a further simplification, we put for the axial velocity of the steam

$$c_a = \text{constant} = \bar{c}_a . \quad (3)$$

Thus we obtain the following formula for the tangential component of the steam velocity:

$$c_t = c_a \frac{d\sigma}{d\xi} = \frac{2S'}{\Delta \xi_a} \bar{c}_a \cos\left(\frac{2\pi}{\Delta \xi_a} \xi\right) . \quad (4)$$

These last two equations fully define our model for the steam flow.

Let us now investigate the motion of the fog droplets in such a flow. Here again, as under Heading 2.6a, let us assume for the sake of simplicity that $c_{r,a}$, the axial component of the droplet velocity, is always the same as c_a :

$$c_{r,a} = c_a = \bar{c}_a . \quad (5)$$

Then the axial component of the relative velocity between the droplets

and steam, which is defined by

$$U_r = c_r - c \quad (6)$$

is identically zero:

$$U_{r,a} = 0. \quad (7)$$

Under Heading 2.6a, we have already derived the equation of motion under these assumptions; compare Eq. 2.6(8). If, for the sake of brevity, we simultaneously introduce $\Delta t_{\text{brems},n}$ from Eq. 2.2(35), it will be written

$$\frac{dc_{r,t}}{dt} = \frac{1}{\Delta t_{\text{brems},n}} (c_t - c_{r,t}). \quad (8)$$

Since, in contrast to Section 2.6, our first interest here lies not in the absolute motion of the fog droplets, but in the magnitude of the relative velocity U_r , let us pass from $c_{r,t}$ to

$$U_{r,t} = c_{r,t} - c_t. \quad (9)$$

Further, since $d\xi = dt/c_a$, ξ may be introduced as an independent variable and the equation reduced to dimensionless form with the aid of the quantity $\Delta\xi_a$:

$$\frac{d}{d(\xi/\Delta\xi_a)} \left(\frac{U_{r,t}}{\bar{c}_a} \right) = - \frac{\Delta\xi_a}{\bar{c}_a \Delta t_{\text{brems},n}} \left(\frac{U_{r,t}}{\bar{c}_a} \right) - \frac{d}{d(\xi/\Delta\xi_a)} \left(\frac{c_t}{\bar{c}_a} \right). \quad (10)$$

The last term is given as a function of ξ by Eq. (4), so that there is no further obstacle to the determination of $(U_{r,t}/\bar{c}_a)$.

Let us now seek the purely periodic solution of Eq. (10), i.e., that droplet motion that would be arrived at in reality after passage through a large number of sine-wave periods. This case could probably be approximated closely in a turbine, since several more or less similar stages occur one after the other and the initial incidence phenomena decay quite quickly. This last assertion is justified on the one hand by the fact that the deviations from the asymptotic curve are small from the very outset (indeed, the fog droplets have the same

velocity as the steam when they are born), and, on the other hand, by the fact that the deceleration times for the fog droplets (see Table 2.2.1) are generally much shorter than the time required to pass through a stage.

From a simple sine-wave formula, we find for the purely periodic solution of Eq. (10)

$$U_{r,t} = \bar{c}_a \cdot \frac{4\pi}{\sqrt{4\pi^2 + G_p^2}} \cdot \frac{S'}{\Delta \xi_a} \cdot \sin \left[2\pi \left(\frac{t}{\Delta \xi_a} - \frac{1}{2\pi} \arctg \frac{2\pi}{G_p} \right) \right], \quad (11)$$

where we have introduced the abbreviation

$$G_p = \frac{\Delta \xi_a}{\bar{c}_a \Delta t_{\text{brems},n}} \quad (12)$$

for the dimensionless group characterizing the behavior of the fog droplets in such a periodic steam flow.

As for the liberation of frictional heat, the work of friction done on a fog droplet during the time dt is $WU_r dt$, where W is the entrainment force. The work of friction ΔL_{rb} done on all fog droplets in a kilogram of wet steam during the time required to flow through a stage is

$$\Delta L_{rb} = n \int_0^{\Delta \xi_a} W U_r d\xi. \quad (13)$$

if n is the number of droplets. Using the Newtonian law and Eq. 2.2(33), we can write $W = -m_r \dot{c}_r = m_r U_r / \Delta t_{\text{brems},n}$; m_r is the mass of a fog droplet, i.e., $n \cdot m_r = y_n$. Since, furthermore, $dt = d\xi / \bar{c}_a$, we get

$$\Delta L_{rb} = \frac{y_n}{\bar{c}_a \Delta t_{\text{brems},n}} \int_0^{\Delta \xi_a} U_r^2 d\xi = \frac{y_n}{\bar{c}_a \Delta t_{\text{brems},n}} \left[\int_0^{\Delta \xi_a} U_{r,t}^2 d\xi + \int_0^{\Delta \xi_a} U_{r,a}^2 d\xi \right] \quad (14)$$

This formula can be evaluated in first approximation on the basis of the simplified flow model given above. For the first integral, we obtain from Eq. (11)

$$\int_0^{\Delta \xi_a} u_{r,t}^2 d\xi = \frac{8\pi^2}{4\pi^2 + G_P^2} \left(\frac{s'}{\Delta \xi_a} \right)^2 \xi_a^2 \Delta \xi_a, \quad (15)$$

and the second vanishes by virtue of Eq. (7). Thus we find for the work of friction in such a case (in which only tangential variations of the velocity are taken into account):

$$\Delta L_{r,t} = 2\gamma_n \frac{4\pi^2 G_P}{4\pi^2 + G_P^2} \left(\frac{s'}{\Delta \xi_a} \right)^2 \xi_a^2 = 2\gamma_n \left(\frac{s'}{\Delta \xi_a} \right)^2 \xi_a^2 \cdot \epsilon_P(G_P). \quad (16)$$

The function

$$\epsilon_P = \epsilon_P(G_P) = \frac{4\pi^2 G_P}{4\pi^2 + G_P^2} \quad (17)$$

expresses the influence of fog-droplet inertia and has been represented in Fig. 2. Its shape indicates that the work of friction done on the fog droplets depends very heavily on the size of the droplets, all other conditions the same, and that it has a maximum for a certain

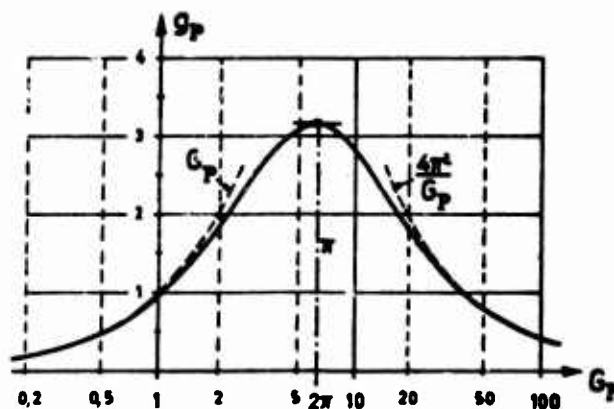


Fig. 3.3.2. The function $g_P(G_P)$.

drop size. The point of inflection of g_P occurs at $G_P = 2\pi$, which, with the typical value of $(\Delta \xi'_a + \Delta \xi''_a)/\bar{c}_a = 8 \cdot 10^{-4}$ sec corresponds to a deceleration time of $t_{\text{brems},n} = 1.3 \cdot 10^{-4}$ sec. According to Table 2.2.1, this deceleration time corresponds at a pressure of $p = 0.12$ bar to the drop size $r_n = 2.5 \cdot 10^{-6}$ m. The size of the fog droplets that actually occur in turbines (cf. Section 2.9) is thus substantially

smaller than this most undesirable drop size.

If the model used thus far fully defined the flow in a turbine blading system, Eq. (16) would give an exact expression for the entrainment losses $\Delta q_{Schlp,n}^{Gitter}$ [$Gitter = cascade$ $Schlp = entrainment$] governed by the *cascade* flow. In reality, however, the axial velocity of the steam is also subject to wide variations; see, for example, Fig. 2.1.7 or 8. As a result, $U_{r,a}$ is also nonzero. Since $c_a(\xi)$ is essentially periodic in nature, $U_{r,a}$ will also vary periodically and therefore could be investigated in much the same way as $U_{r,t}$. For the sake of brevity, we shall restrict ourselves to quick estimation of the second integral in Eq. (14).

The tangential fluctuations of the steam velocity — compare Eq. (4) — had the amplitude $2S'\bar{c}_a/\Delta\xi_a$, which, as regards order of magnitude, is about $(0.5 \sim 0.7) \cdot c_a$ (N.B. Tables 2.1.1 and 2). The fluctuations in axial velocity are smaller; according to Figs. 2.1.7 and 8, their amplitude is only about $(0.2 \sim 0.3) \cdot c_a$, i.e., about half that of c_t . On the other hand, c_a has twice the frequency, since a full variation unfolds in each ring. The fog droplets are somewhat harder put to follow such a fluctuation, and this is manifested in the fact that G_p , whose numerator actually contains the period length of the fluctuations, becomes smaller, and, specifically, half as large as previously. — Since $G_p \gg 4\pi$ at all times for practical cases, we see from Eq. (11) that the fluctuation amplitude of the relative velocity is proportional to the fluctuation amplitude of the steam velocity divided by G_p . In the case of axial fluctuations, these two quantities will be about half as large, so that the amplitude of $U_{r,a}$ must be approximately the same as that of $U_{r,t}$. A consequence of this is that the second integral in Eq. (14) is of about the same magnitude as the first.

Thus the entrainment-losses caused in reality by *cascade* flow ef-

fects are about twice as large as the figure calculated in Eq. (16):⁵²⁾

$$\Delta q_{\text{Schlp},n}^{\text{Gitter}} \approx 2\Delta L_{\text{rb},t} = 4 y_n \left(\frac{s'}{\Delta \xi_a} \right)^2 \bar{c}_a^2 \cdot g_p(G_p) \quad (18)$$

G_p is calculated from Eq. (12) and g_p can be read from Fig. 2. It is best to substitute y_{n1} for y_n .

Let us again take as an example the next-to-last stage of our reaction-type turbine. According to Table 2.1.1, $\Delta \xi_a = 0.180$ m, $s' = 0.064$ m; further, $\bar{c}_a = 220$ m/sec (by estimation from Fig. 2.1.7). The water-distribution calculation made under Heading 2.9 gave for the variant "Üb 1" $y_{n1} = 0.09290$ and $\bar{r}_{n1} = 1.3 \cdot 10^{-7}$ m and for the variants "Üb 2" and "Üb 3" $y_{n1} = 0.07028$ and 0.07051 and $\bar{r}_{n1} = 5.8 \cdot 10^{-7}$ m. From Eq. 2.2(35), we find for these drop sizes $\Delta t_{\text{brems},n} = 10^{-6}$ and 1.44×10^{-5} sec, respectively, giving for "Üb 1" $G_p = 373$ and for "Üb 2" and "Üb 3" $G_p = 57$. From this (compare Fig. 2), we calculate $g_p \approx 4\pi^2/373 = 0.106$ and $g_p \approx 4\pi^2/57 = 0.69$, respectively. Finally, we substitute everything into Eq. (18) and get

$$\Delta q_{\text{Schlp},n}^{\text{Gitter}} = \begin{cases} 0.25 \cdot 10^3 \text{ J/kg} & (\text{"Üb 1"}, \text{bzw.}) \\ 1.25 \cdot 10^3 & (\text{"Üb 2", "Üb 3"}) \end{cases} \quad (19)$$

Thus the entrainment-losses due to cascade flow are of about the same magnitude in this stage as the braking-losses, compare Eq. 3.2(11).

Resulting from turbulence

Small high-frequency fluctuations due to turbulence are superimposed on the steam-velocity fluctuations caused by cascade effects. Here we must keep one thing in view: if we measure the time variation of the velocity fluctuations in a turbine with a fast response probe, we will indeed obtain a certain amount of information on the turbulence, but not the information that is decisive for the entrained drops. Rather, one ought to perform a measurement in which the probe moves with the steam and registers only the velocity fluctuations ex-

perienced by one and the same steam particle. Lacking such devices, we satisfy ourselves with a plausible assumption that at least allows us to obtain some general idea as to the entrainment losses resulting from turbulence.

We assume that the velocity of a steam particle in a stage passes through ten fluctuation periods. The fluctuations are to affect all spatial components, and their amplitudes will be assumed to amount to, for example, 1% of the average axial velocity \bar{c}_a in all directions. The assumption of ten fluctuation periods per stage corresponds approximately to a fluctuation frequency of 10^4 sec^{-1} , since with, for example, $\bar{c}_a = 150 \text{ m/sec}$, $\Delta\xi'_a + \Delta\xi''_a = 0.15 \text{ m}$, the time to flow through a stage is $0.15/150 = 1 \cdot 10^{-3} \text{ sec}$, so that the duration of a fluctuation becomes $1 \cdot 10^{-3}/10 = 10^{-4} \text{ sec}$. Turbulence measurements on flow machines have shown [43] that the frequency of 10^4 sec^{-1} is at the upper limit of the range in which the fluctuations have appreciable intensity. If, however, we assume a frequency that tends to be high, we shall obtain excessively high loss values,⁵³⁾ so that the results obtained from them should be viewed as upper limits. Concerning the choice of the amplitude, it should be noted that the high turbulence levels (10 to 15%) measured with stationary probes cannot be transferred to the relative motion between drops and steam for the reasons noted above.

With these assumptions for the turbulent fluctuations of the steam velocity, we can calculate the entrainment losses for each one of the three fluctuation directions in basically the same way as was done earlier for the tangential fluctuations. The behavior of the fog droplets in the turbulence will be characterized by the parameter

$$G_T = \frac{(\Delta\xi_a/10)}{\bar{c}_a \Delta t_{\text{brems},a}} \quad (20)$$

which is analogous to G_p . For the over-all entrainment loss due to

turbulence in a stage we find (after summation for the three directions in space)

$$\Delta q_{\text{Schlp},n}^{\text{Turb}} = \frac{3}{2} y_n 0,01^2 \bar{\epsilon}_n^2 \cdot 10 g_T(G_T) \quad (21)$$

[Schlp = entrainment] where the function $g_T(G_T)$ is formed entirely by the analogy to $g_P(G_P)$ and can therefore likewise be read from Fig. 2.

For our example, the next-to-last stage of the **reaction-type** turbine, the data already mentioned and $G_T = G_P/10 = 373/10 = 37.3$ ("Üb 1") and $57/10 = 5.7$ ("Üb 2" and "Üb 3") can be used to get the following entrainment losses resulting from turbulence:

$$\Delta q_{\text{Schlp},n}^{\text{Turb}} = \begin{cases} 7 \text{ J/kg} = 0,007 \text{ kJ/kg} & (\text{"Üb 1"}) , \\ 16 \text{ " } = 0,016 \text{ " } & (\text{"Üb 2", "Üb 3"}) . \end{cases} \quad (22)$$

The entrainment losses on fog droplets due to turbulence are therefore vanishingly small compared to those caused by **cascade** flow. We shall therefore ignore them completely and compute the total entrainment losses on the fog droplets simply as

$$\Delta q_{\text{Schlp},n} \approx \Delta q_{\text{Schlp},n}^{\text{Gitter}} = 4 y_n \left(\frac{s'}{\Delta \xi_n} \right)^2 \bar{\epsilon}_n^2 g_P(G_P) \quad (23)$$

G_P can be calculated from Eq. (12) and g_P can be read from Fig. 2. y_{n1} should be substituted for y_n . For the stage in which the fog droplets form, the loss is only a part of the value calculated from Eq. (23), depending on where in the stage the fog forms.

In our illustrative stage, we obtain for the over-all entrainment losses on fog droplets

$$\Delta q_{\text{Schlp},n} = \begin{cases} 0,25 \text{ kJ/kg} & (\text{"Üb 1"}) \\ 1,25 \text{ " } & (\text{"Üb 2", "Üb 3"}) . \end{cases} \quad (24)$$

Yet another type of entrainment loss should be noted in connection with the fog droplets — that which occurs when the fog droplets suddenly enter a space in which a much lower steam velocity prevails and

are decelerated by friction (profile boundary layer, downstream trough, detachment regions). However, this would affect only a minor part of the fog-droplet flow, so that we can probably disregard this loss.

b) Entrainment-Losses on Large Drops

The acceleration of the large drops by the steam flow, such as occurs after each tearing-away or rebounding event, costs friction losses whose magnitude can be calculated very simply after Traupel [20]. For a steam flow of constant velocity c_d , he demonstrates that the work loss occurring in acceleration of a drop is independent of the type of resistance law to which the drop is subject and is a function only of the final velocity c_r reached by the drop. The loss referred to the mass of the accelerated drop is

$$\Delta L_r = c_d c_r - \frac{c_r^2}{2} . \quad (25)$$

In a stage, such drops would include the drops torn away from the trailing edges of the stator blades (y_{g1}), the drops rebounding from both rows of buckets (y_{gg1} and y_{gg2}), and the part of the water centrifuged out that remains in the blading space ($y_{h1,drin}$ and $y_{h2,drin}$). For the decisive steam velocity c_d , we can set $c_d = 0.8 c_1$ for the torn-away drops ("g"), as was also done under Heading 2.6. The rebounding drops ("gg") generally incorporate a smaller total amount of water than the torn-off drops. They are also smaller than the latter and travel longer distances in the steam, since, after all, they enter the flow quite far upstream, in the vicinity of the entry edges of the buckets (see Fig. 2.8.6). For this reason, their ultimate velocity, that with which they strike the next row of buckets, will certainly be considerably higher than that of the drops torn off the trailing edges. For them, we shall satisfy ourselves with a rough estimate of the losses. Let us assume that the steam velocity has remained the same dur-

ing the entire acceleration as it is at the exit from the blading screen (i.e., c_1 and w_2 , respectively), and that the drops have reached half of this velocity - assumptions that should not be too far off. We shall treat the mass proportion "h" in much the same way as "gg."

On the basis of Eq. (25), therefore, we may write for the entrainment losses resulting from the acceleration of the various large drops in the stage, referred to the mass unit of the wet steam,

$$\Delta q_{\text{Schlp, gr}} = y_{g1} \left(0,8 c_1 c_g - \frac{c_g^2}{2} \right) + (y_{gg1} + y_{h1, \text{drin}}) 0,75 \frac{c_1^2}{2} + \dot{v}_{gg2} + y_{h2, \text{drin}} \cdot 0,75 \frac{w_2^2}{2} \quad (26)$$

The only quantity not known here is c_g , the velocity of the large drops torn off the trailing edges when they strike the stator buckets. If, however, we know the drop size \bar{r}_g (compare, for example, Section 2.9) and the path that these drops traverse from the trailing edge to impingement on the next row of rotor buckets, it can be determined in a simple fashion by reference to Fig. 2.8.3.

Let us again use the next-to-last stage of our reaction-type turbine as an example; here, $c_1 = 361$ m/sec and $w_2 = 358$ m/sec. According to Table 2.9.1, $\bar{r}_{g1} = 6.0 \cdot 10^{-5}$ m, for which we get $t_{\text{brems, g}} = 7.6 \times 10^{-3}$ sec, so that the curve parameter in Fig. 2.8.3 becomes $(\frac{1}{2} U_r \Delta t_{\text{brems}})_{\xi=0} = \frac{1}{2} 0.8 \cdot 361 \cdot 7.6 \cdot 10^{-3} = 1.1$ m. The total path comes to about 4 cm (to be taken from the blading drawing), so that we read $c_g = 0.16 c_1 = 0.16 \cdot 361 = 58$ m/sec for the final velocity c_g from Fig. 2.8.3. With the specific mass allotments calculated in Section 2.9, we then obtain from Eq. (26)

$$\Delta q_{\text{Schlp, gr}} = \begin{cases} 0,02 + 0,09 + 0,26 = 0,37 \text{ kJ/kg für "Üb 1",} \\ 0,08 + 0,47 + 1,12 = 1,67 \text{ " " "Üb 2",} \\ 0,08 + 0 + 0 = 0,08 \text{ " " "Üb 3".} \end{cases} \quad (27)$$

These large differences are due to the fact that the quantity of

coarse-form water present in the flow canal is quite different for each of the three cases. In general, the entrainment losses on the large drops are comparable to those on the fog droplets; compare Eq. (24).

In summary, we obtain for all entrainment losses in the stage

$$\Delta q_{\text{Schlp}} = \Delta q_{\text{Schlp},n} + \Delta q_{\text{Schlp},gr} \quad (28)$$

where the first term can be calculated from Eq. (23) and the second from Eq. (26).

For our example, the next-to-last stage of the reaction-type turbine, we find the numerical values

$$\Delta q_{\text{Schlp}} = \begin{cases} 0,25 + 0,37 = 0,62 \text{ kJ/kg für "Üb 1"} \\ 1,25 + 1,67 = 2,92 \text{ " " "Üb 2"} \\ 1,25 + 0,08 = 1,33 \text{ " " "Üb 3"} \end{cases} \quad (29)$$

which correspond to about 0.8 to 3.6% of the stage heat drop (calculated without wetness losses) and are somewhat larger than the braking-losses calculated in Section 3.2.

3.4. THERMODYNAMIC LOSSES

Thermodynamic losses arise in the course of heat exchange processes between the two phases, since these are not exactly at the same temperature. Internal heat exchange is an inevitable concomitant phenomenon to any condensation process unless the heat of evaporation being liberated is somehow withdrawn at once to the outside.

No loss occurs if either the state change occurs at thermodynamic equilibrium (no temperature jump between steam phase and water phase) or if, in spite of supercooling no condensation takes place ("perfect supercooling").

The magnitude of the loss can be obtained from the following reasoning. Let a quantity of steam \underline{dm} condense on the surfaces of drops having a temperature T_r , so that the heat of evaporation $L \cdot \underline{dm}$ liberated in the process is transferred to the surrounding steam, whose tempera-

ture T_d is lower than T_r . This is an irreversible process; it could be made reversible by allowing a Carnot machine to work between the temperatures T_r and T_d and produce a work $L \cdot dm \cdot (1 - T_d/T_r)$. This work gives the loss that occurs during the actual process. If we refer its magnitude to 1 kg of wet steam, then dm is to be replaced by dy and the resultant dq will be

$$dq = L dy \left(1 - \frac{T_d}{T_r}\right) . \quad (1)$$

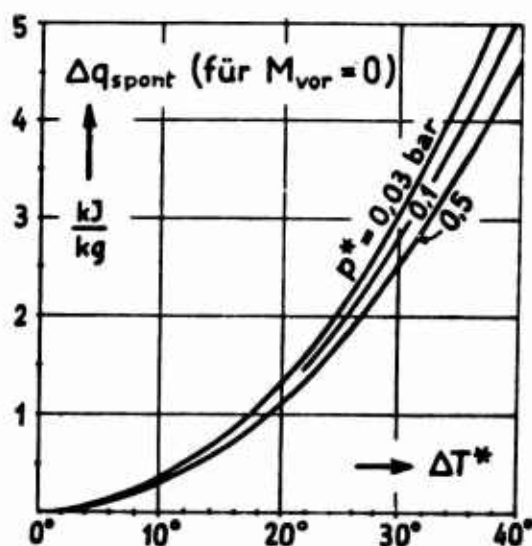


Fig. 3.4.1. Purely thermodynamic loss in spontaneous condensation of steam as a function of peak undercooling for various pressures. für = for.

With the thermodynamic losses in the course of an expansion, it is convenient to treat those losses that arise on the sudden collapse of supercooling (fogging) separately from those that occur during subsequent condensation on fog droplets as a result of continuing supercooling. Strictly speaking, there is no physical difference between the two, but the thermodynamic loss that takes place during a sudden condensation is always connected with an aerodynamically governed positive or negative additional loss, which increases or decreases it further. (The purely thermodynamic loss would take place at the Mach num-

ber zero.) The resultant loss in the condensation shock has already been calculated under Heading 2.5 and represented in Fig. 2.5.11. We shall use this consistently as our source for its value in loss calculations; thus we set

$$\Delta q_{\text{Spont}} = (s_{\text{nach}} - s_{\text{vor}}) \cdot T_s(p_{\text{vor}}) \quad \text{laut Abb. 2.5.11} \quad (2)$$

[nach = after; vor = before] and consistently burden that stage with it in which (or in the axial intermediate space immediately following which) the Wilson point lies. — For Δq_{Spont} , we may always insert the loss read from Fig. 2.5.11 for the Mach number $M_{\text{vor}} = 0$, except in the case in which the Wilson point is reached at a point at which the flow through closely spaced buckets is bounded rigidly on both sides and a rather high Mach number (> 0.6) prevails simultaneously. Since the reading from Fig. 2.5.11 is not accurate enough, the loss values arising at $M_{\text{vor}} = 0$ are plotted in Fig. 1 for various pressures as functions of the undercooling at the Wilson point (ΔT^*). (Strictly speaking, it would be more correct to write ΔT_{vor} instead of ΔT^* , and to denote the curve parameter by p_{vor} instead of p^* , but we incur no major error with this simplification in the cases that occur in practice.) In those cases in which the influence of Mach number cannot be disregarded, it is advantageous first to read the total loss for $M_{\text{vor}} = 0$ from Fig. 1 and then use Fig. 2.5.11 simply for correction.

On the other hand, those losses that occur due to continuing undercooling are determined on the basis of Eq. (1). We determine their extent in a stage by integrating Eq. (1) for the stage:

$$\Delta q_{\text{Unk}} = \int_{l_{a0}}^{l_{a2}} L \frac{dy}{dl_a} \frac{T_r - T_d}{T_r} dl_a \quad (3)$$

Since the capillary effect is no longer an appreciable factor for grown-up fog droplets, we have $T_r - T_d = T_s - T_d = \Delta T$; moreover, $T_r =$

$= T_s$ varies only slightly and can be taken out of the integrand as T_s ("average saturation temperature in the stage"). Then we get

$$\Delta q_{\text{Unth}} = \frac{L}{T_s} \int_{\xi_{a0}}^{\xi_{a2}} \frac{dy}{d\xi_a} \Delta T d\xi_a. \quad (4)$$

If the curves of $\Delta T(\xi_a)$ and $y(\xi_a)$ are known for the stage in question — as they have been plotted for the examples calculated in Figs. 2.9.4, etc. — then Δq_{Unth} can, in principle, be determined immediately from Eq. (4) by graphical integration. However, the curve of $y(\xi_a)$ that we have at our disposal is highly inaccurate, since the calculation by Section 2.9 gives the values of y only for the axial intermediate space. A curve of $dy/d\xi_a$ obtained from this $y(\xi_a)$ would become the more inaccurate. It is therefore indicated that Formula (4) should be replaced at the outset by an approximation, which then also becomes much simpler to calculate. We set

$$\Delta q_{\text{Unth}} = \frac{L}{T_s} [(\nu_1 - \nu_0) \Delta T_m + (\nu_2 - \nu_1) \Delta T_m^*] \quad (5)$$

and thus shift all uncertainties into the determination of suitable values for the decisive supercooling ΔT_m . Since $dy/d\xi_a$ is approximately proportional to dy/dt and the latter is, in turn, about proportional to ΔT (heat-transfer law!), we obtain the following approximation for ΔT_m :

$$\Delta T_m = \frac{\overline{\Delta T^3}}{\overline{\Delta T}}, \quad (6)$$

where $\overline{\Delta T}$ and $\overline{\Delta T^2}$ are defined by

$$\overline{\Delta T^n} = \frac{1}{\xi_{a2} - \xi_{a0}} \int_{\xi_{a0}}^{\xi_{a2}} \Delta T^n d\xi_a \quad (n = 1, 2) \quad (7)$$

and can easily be determined, at least in approximation, from the $\Delta T(\xi_a)$ curve available in graphic form on the basis of Section 2.9. If

ΔT has a wave-form variation in a ring, the formula

$$\Delta T_m = \overline{\Delta T} + \frac{(\Delta T_{\max} - \Delta T_{\min})^2}{8 \overline{\Delta T}} \quad (8)$$

gives a very good approximate value for the unknown ΔT_m . ΔT_{\max} and ΔT_{\min} denote the extreme values that occur in the ring. (The formula would apply rigorously if the ΔT curve had the form of a sine wave elevated by $\overline{\Delta T}$.)

An additional thermodynamic loss takes place in the exhaust-manifold, since the steam is frequently still considerably supercooled at the exit from the last stage. The magnitude of the loss is unaffected by whether the supercooling is made to vanish solely by condensation on fog droplets already present or whether yet another fresh nucleation occurs, as may be the case with large supercoolings at the exit. The specific quantity of the supercooled steam is $(1 - y_E)$, so that the loss can be calculated⁵⁴⁾ from

$$\Delta i_{\text{Unth}}^{\text{Stutzen}} = (1 - y_E) \Delta q_{\text{Spont}} \quad (9)$$

with Δq_{Spont} determined from Fig. 1. Here we must set $p^* = p_K$ and $\Delta T^* = \Delta T_E$. (ΔT_E is the supercooling at the exit from the last stage.) Since nothing more can be recovered from this loss in low-pressure turbines anyway, it has been denoted by Δi and not by Δq .

As a numerical example, let us consider a rather long expansion, in which the specific water content $y_{\text{end}} - y_{\text{anfg}} = 0.10$ [anfg = initial] is deposited on the fog droplets, while the supercooling always remains constant in the process. (For example, let $\Delta T = 1^\circ, 5^\circ$ and 20°C , respectively.) Thus (since $\overline{\Delta T^2} = \Delta T^2$ and $\overline{\Delta T} = \Delta T$) $\Delta T_m = \Delta T$ and, with $L = 2.3 \cdot 10^3 \text{ kJ/kg}$ and $T_s = 350^\circ\text{K}$, this gives the following loss:

$$\left. \begin{aligned} \Delta q_{\text{Unlk}} &= \frac{2300}{350} 0,1 \cdot 1 = 0,66 \text{ kJ/kg für } \Delta T = 1^\circ\text{C}, \\ \Delta q_{\text{Unlk}} &= \frac{2300}{350} 0,1 \cdot 5 = 3,3 \quad \quad \Delta T = 5^\circ\text{C}, \\ \Delta q_{\text{Unlk}} &= \frac{2300}{350} 0,1 \cdot 20 = 13,2 \quad \quad \Delta T = 20^\circ\text{C}. \end{aligned} \right\} \quad (10)$$

The isentropic heat drop in this expansion is about 330 kJ/kg, so that the losses correspond to an efficiency deterioration of about 0.2%, 1% or 4%.

As a different example, let us take the next-to-last stage of the reaction-type turbine specified in Section 2.1. At $p = 0.11$ bar, we have $L = 2.39 \cdot 10^3$ kJ/kg, $\bar{T}_s = 48^\circ\text{C} = 321^\circ\text{K}$, and we get the following amounts of condensation for the three variants under investigation (compare Tables 2.9.1 to 3) from the calculation carried through in Section 2.9:

$$\begin{aligned} \text{for "Üb 1": } y_1 - y_0 &= 0,01308 \text{ and } y_2 - y_1 = 0,01052 \text{ kg/kg,} \\ \text{"Üb 2": } & \quad \quad \quad = 0,01190 \quad \quad \quad = 0,00890 \quad \quad \quad , \\ \text{"Üb 3": } & \quad \quad \quad = 0,01190 \quad \quad \quad = 0,00890 \quad \quad \quad . \end{aligned}$$

On the basis of the graphical supercooling variation (Figs. 2.9.4 to 6), we get

$$\begin{aligned} \text{for "Üb 1": } \Delta T_m' &= 2,2^\circ\text{C}, & \Delta T_m'' &= 2,8^\circ\text{C}, \\ \text{"Üb 2": } \Delta T_m' &= 14,2^\circ\text{C}, & \Delta T_m'' &= 16,2^\circ\text{C}, \\ \text{"Üb 3": } \Delta T_m' &= 14,1^\circ\text{C}, & \Delta T_m'' &= 16,0^\circ\text{C}. \end{aligned}$$

so that the following supercooling losses result from Eq. (5):

$$\Delta q_{\text{Unlk}} = \begin{cases} 0,21 + 0,22 = 0,43 \text{ kJ/kg} & (\text{"Üb 1"}), \\ 1,25 + 1,06 = 2,31 \quad \quad & (\text{"Üb 2"}), \\ 1,24 + 1,06 = 2,30 \quad \quad & (\text{"Üb 3"}). \end{cases} \quad (11)$$

Thus the supercooling losses in a stage are of approximately the same order of magnitude as the braking- or entrainment-losses.

3.5. OTHER MOISTURE-LOSSES IN A STAGE

In addition to the three main types of moisture loss treated in Sections 3.2 to 3.4, there are still numerous less consequential sources of loss, which we should now like to investigate one after the other. In our search for further losses, we must always be on guard against "discovering" something that has already been taken into account once in some other manner.

Centrifugation losses on the rotor buckets: The water that remains clinging to the rotor buckets is centrifuged out, i.e., it flows radially outward on the surfaces of the buckets and then sprays off the tip of the bucket (or from the shroud). During their displacement toward the blade tips, the water particles acquire increasingly high circumferential velocities, i.e., the rotor must expend a pumping work on them. This work qualifies as a loss, since the kinetic energy of the water being sprayed off is all converted back into heat on impingement on the housing wall, etc. If we again refer everything to the unit mass of the wet steam flowing through the turbine, then the amount of water that has clung to the rotor buckets will be given by y''_f and, according to the Euler moment equation the loss will be

$$\Delta q_{Zfg} = y''_f (u_{2, Spitze}^2 - u_2^2). \quad (1)$$

[Zfg = centrifugation; Spitze = tip]. Here the use of u_2 corresponds to the concept in which all of the water at the pitch circle gets onto the buckets. This is a plausible assumption; more than that, it is the only tolerable assumption, since, after all, the braking-losses were calculated in Section 2.2 under the assumption that the water clinging to the rotor is endowed with the circumferential velocity u_2 .

In the next-to-last stage of our reaction-type turbine, $u_2 = 310$ m/sec, $u_{2, Spitze} = 384$ m/sec and $y''_f = 21.5 \cdot 10^{-4}$ ("Üb 1"), $81.0 \cdot 10^{-4}$

("Üb 2") and $134.8 \cdot 10^{-4}$ ("Üb 3"), respectively. From this we obtain

$$\Delta q_{Zfg} = \begin{cases} 111 \text{ J/kg} = 0,11 \text{ kJ/kg} & (\text{"Üb 1"}), \\ 420 & = 0,42 & (\text{"Üb 2"}), \\ 696 & = 0,70 & (\text{"Üb 3"}), \end{cases} \quad (2)$$

which represents less than about one-tenth of the sum of the three main loss sources; cf. Eqs. 3.2(11), 3.3(29) and 3.4(11).

Centrifugation losses on fog droplets: If $c_{n,u}$, the circumferential component of the absolute fog-droplet velocity is different from zero, a centrifugal force Z_r is exerted on each individual droplet and displaces it radially outward. Its magnitude in the line of bucket centers (diameter D_m) is given by $Z_r = 2m_r c_{n,u}^2 / D_m$. If Z_r remains constant, we arrive at a radially outward-directed, constant relative droplet velocity U_r with respect to the steam that is just large enough so that the frictional resistance W exactly offsets the centrifugal force Z_r . Since $W = m_r U_r / \Delta t_{\text{brems},n}$ (compare Section 2.2), the formula

$$U_r = 2 \frac{c_{n,u}^2}{D_m} \Delta t_{\text{brems},n} \quad (3)$$

follows from the condition $W = Z_r$ for the relative velocity. With the estimate $c_{n,u}^2 \approx u_1^2$, we shall certainly be above the average value of $c_{n,u}^2$ in a stage. Thus, for example, we obtain for the next-to-last stage of the reaction-type turbine

$$U_r \approx 2 \cdot \frac{298^2}{1,900} \Delta t_{\text{brems},n} = \begin{cases} 0,19 \text{ m/sec} & (\text{"Üb 1"}), \\ 1,3 \text{ m/sec} & (\text{"Üb 2", "Üb 3"}). \end{cases} \quad (4)$$

[brems = deceleration]. (The deceleration times have already been calculated for the example of Eq. 3.3(19).) The velocity with which the fog droplets travel radially outward is thus very low. This is the reason why fog droplets are not simply **centrifuged out**. In fact, $\Delta \xi_r$, the radial displacement of the drops relative to the steam within this stage is (since the **residence time** in the stage according to Table 2.1.1 is approximately $t_2 - t_0 = (45.6 - 37.4) \cdot 10^{-4} = 8.2 \cdot 10^{-4}$ sec) only

$$\Delta \xi_r = U_r (t_2 - t_0) = \begin{cases} 1,6 \cdot 10^{-4} \text{ m} & (\text{"Üb 1"}), \\ 1,1 \cdot 10^{-3} \text{ m} & (\text{"Üb 2", "Üb 3"}), \end{cases} \quad (5)$$

i.e., at most a millimeter! The frictional loss is equal to the work done by the friction forces on all n fog droplets in the mass unit of the wet steam, or

$$n W \Delta \xi_r = n m_r \frac{z_r}{m_r} \Delta \xi_r \approx \gamma_{n1} \frac{2u_1^2}{D_{m1}} \Delta \xi_r = \begin{cases} 1,4 \text{ J/kg} & (\text{"Üb 1"}), \\ 7,6 & (\text{"Üb 2", "Üb 3"}). \end{cases} \quad (6)$$

Compared with the other losses, these losses are vanishingly small, so that we shall disregard them altogether.

Frictional losses in the flowing water films: The layers or veins of water are kept in motion by friction against the steam and (on rotor buckets) by the field of centrifugal forces. The internal friction losses that arise in a water layer driven by steam friction do not constitute an additional loss, since the losses in the steam boundary layer may be considered correspondingly reduced. (That is to say, the steam flow is bounded not by a stationary wall but by a moving surface.) On the other hand, not even the frictional losses that arise when the water layer is driven by centrifugal force may be regarded as additional losses, since they actually represent part of the pumping work necessary for centrifugation, and the latter has already been regarded in toto as a loss. (The remainder of the pumping work is expended to overcome an — insignificant — radial pressure gradient and, first and foremost, to raise the kinetic energy of the water. In the absolute system, the circumferential components of the water's velocity at the ends of the buckets must be $u_{2, \text{Spitze}}$, but the magnitude of the radial component is free and can adjust itself to conform to the friction.)

Increase in steam friction on the buckets: An increase in the profile losses as a direct result of increased surface roughness of the buckets will hardly be a matter for consideration, at least in a tur-

bine where the erosion remains tolerable, since roughening of the buckets always remains restricted to narrow strips. The appearance of unevenness in excess of the fabrication roughness of the bucket surfaces as a result of waviness on the surface of the water films is excluded at the outset, since the water veils are very thin ($\sim 10^{-5}$ m).

The boundary layer on the suction side (back side) of the bucket profile is normally laminar in the first half (compare Fig. 2.4.4 and [20], page 277), and becomes turbulent only toward the middle. But now the erosion roughening of the leading-edge zone may be capable in some cases of effecting this transition of the boundary layer prematurely, and thus raise the profile losses directly. (The conclusion that the roughening common in wet-steam turbines is sufficient to produce this transition, even when it is only minor in extent, is based on [44].) The transition to the turbulent is probably favored by the disturbing effect implicit in heavy bombardment of the leading edges by the large drops. On stator blades, where the clinging water is driven in the direction of the steam flow, sudden boiling of the water film may occur at that point on the profile contour where the pressure drops sharply (compare Fig. 2.4.3), likewise manifesting as a disturbance of the boundary layer and promoting premature laminar-to-turbulent transition. For this reason it is recommended that the amount by which the profile losses increase be regarded as a moisture-loss in the event that the suction-side boundary layer is also turbulent practically from the outset.

A rough estimate of these additional losses, but one that will be adequate to our purposes, is possible on the basis of experimental profile-loss data (compare [20], page 287) and the boundary-layer calculations made in Section 2.4b for both variants, making the rather obvious assumption that the profile losses increase in the same propor-

tion as the shear stress integrated over the entire profile contour. The shear-stress increase can be determined with the aid of the friction coefficient c_F defined in Eq. 2.4(2), whose variation is shown in Fig. 2.4.4 for the profile used there. By integration we find that the integrated shear stress, i.e., the c_F integrated over the entire contour, increases by about 16%, even if the boundary layer is turbulent over its entire length on the back side.

Since the profile losses due to boundary-layer friction alone in turbine grids represent about 3 to 4% losses (compare [20], page 287), the premature transition to turbulence is accompanied by an increase in losses by about $0.16(3 \text{ to } 4\%) = (0.48 \text{ to } 0.64)\%$. If a great deal of coarse-form water is present, the premature transition takes place in both bucket rings, while when the quantity of coarse water is small, this occurs only in the rotor. For this reason, we shall use the formula

$$\Delta q_{GS} = (0,003 \sim 0,006) \cdot (l_0 - l_2), \quad (7)$$

[GS = boundary layer] for estimation of the losses in the stage to be attributed to the increase in boundary-layer friction; here, the smaller values of the coefficients would tend to apply for cases in which relatively little coarse water strikes the stator blades (small y_{gg}), and the larger values for cases in which y_{gg} tends to be relatively larger. For the next-to-last stage of our reaction-type turbine, this means a loss of

$$\Delta q_{GS} = \begin{cases} 0,003 \cdot 87,5 = 0,26 \text{ kJ/kg} & (\text{"Üb 1"}), \\ 0,006 \cdot 87,5 = 0,5 & (\text{"Üb 2"}), \\ 0,004 \cdot 87,5 = 0,3 & (\text{"Üb 3"}), \end{cases} \quad (8)$$

where it has been taken into account that much coarse-form water is present in the bladed space only in case "Üb 2."

Capture losses: Wherever rapidly moving water particles strike walls, a loss, similar to the exit loss, arises as a result of the

fact that the kinetic energy of these particles is transformed into heat. Naturally, we need regard only the kinetic energy of the fog droplets striking buckets as a loss of this type, since the other similar losses have already been taken into account elsewhere (deceleration losses, centrifugation loss) or are negligibly small. The amounts of water in the fog droplets caught by the two rings per kilogram of wet steam are $\varepsilon'_{n-f} y_{n0}$ and $\varepsilon''_{n-f} y_{n1}$ so that the capture loss is about

$$\Delta q_{\text{Auffg}} = \varepsilon'_{n-f} y_{n0} \frac{c_{a0}^2}{2} + \varepsilon''_{n-f} y_{n1} \frac{c_{a1}^2}{2} \quad (9)$$

[Auffg = capture]. For example, we obtain for the next-to-last stage of the **reaction-type** turbine

$$\Delta q_{\text{Auffg}} = \begin{cases} 0,06 \text{ kJ/kg} & (\text{"Üb 1"}), \\ 0,25 & (\text{"Üb 2", "Üb 3"}). \end{cases} \quad (10)$$

Summary: The less important losses in the stage are grouped together under the heading "miscellaneous moisture-losses" Δq_{Sonst} :

$$\Delta q_{\text{Sonst}} = \Delta q_{\text{Zfg}} + \Delta q_{\text{GS}} + \Delta q_{\text{Auffg}}. \quad (11)$$

[Sonst = miscellaneous; Zfg = centrifugation; GS = boundary layer; Auffg = capture]. The individual terms can be calculated from Eqs. (1), (7) and (9), respectively. For our example, the next-to-last stage of the **reaction-type** turbine, they come to

$$\Delta q_{\text{Sonst}} = \begin{cases} 0,11 + 0,26 + 0,06 = 0,43 \text{ kJ/kg} & (\text{"Üb 1"}), \\ 0,42 + 0,50 + 0,25 = 1,17 & (\text{"Üb 2"}), \\ 0,70 + 0,30 + 0,25 = 1,25 & (\text{"Üb 3"}), \end{cases} \quad (12)$$

or about the same as one of the three principal losses.

3.6. CHANGE OF THE EXIT LOSS

The kinetic energy that the steam still possesses after leaving the last stage is generally transformed practically to completion into heat as a result of friction. In the homogeneous ideal case, this exit loss, referred to a unit mass of the steam, is $c_E^2/2$, where c_E denotes the (absolute) exit velocity from the last rotor, i.e., is identical

with the c_2 for the last stage as presented in Table 2.1.1 or 2.1.2.

In real cases, the exit loss is something else, since, as will be shown below, the exit velocity is not the same and since, moreover, part of the mass flow is led out of the last stage or diverted even earlier with only a low velocity.

Let us now calculate the amount Δi_{Aus} [Aus = exit] by which the real exit loss exceeds the exit loss in the homogeneous ideal case, making two simplifying assumptions for the purpose. First, let us assume that the flow direction of the steam is nearly axial, so that its kinetic energy is practically equal to $c_a^2/2$; secondly, let us equate the velocity of the fog droplets to that of the steam. The two errors that we shall incur with this cancel one another to some degree. If we take into account further that the part of the mass contained in the coarse water forms ("gg," "h") at the end of the turbine possesses practically no axial velocity, we may write for the increase in exit losses

$$\Delta i_{\text{Aus}} \approx (1 - \gamma_{\text{gg}} - \gamma_{\text{h}})_E \cdot \frac{c_{aE}^2}{2} - \frac{c_{aE}^2}{2} \quad (1)$$

The subscript E refers to conditions at the end of the turbine, i.e., at the exit from the last stage. The quantities embellished with the ^ refer to the real conditions, which deviate from those of the homogeneous ideal case.

If we write the continuity equation for the exit cross section Ω_{aE} , it will read $\dot{M}v_E = \Omega_{aE}c_{aE}$ or $\dot{M}\hat{v}_E = \Omega_{aE}\hat{c}_{aE}$, so that (necessarily) $\hat{c}_{aE}/c_{aE} = \hat{v}_E/v_E$ and, consequently, Eq. (1) will assume the form

$$\Delta i_{\text{Aus}} \approx - \frac{c_{aE}^2}{2} \left[1 - (1 - \gamma_{\text{gg}} - \gamma_{\text{h}})_E \frac{\hat{v}_E^2}{v_E^2} \right] \quad (2)$$

The only unknown in this formula is \hat{v}_E/v_E , the ratio of the specific steam volume in actuality to that in the homogeneous ideal case. The

difference between \hat{v}_E and v_E stems from two causes. Firstly, from the fact that the terminal point of the expansion is different for the two cases (see points \hat{E} and E in Fig. 3.1.1), and secondly from the fact that thermodynamic equilibrium does not prevail in the real case ($\Delta T_E \neq 0$). If we denote by $\hat{v}_{\infty E}$ the specific volume that the steam would have at point \hat{E} (Fig. 3.1.1) at thermodynamic equilibrium, we should have — since, after all, the volume of the water phase can be disregarded —

$$\frac{v_{\infty E}}{v_E} = \frac{x_{\infty E}}{x_E} = 1 + \frac{x_{\infty E} - x_E}{x_E} \quad (3)$$

The heat of vaporization L is equal to the enthalpy difference between the points corresponding to $x_{\infty} = 1$ and $x_{\infty} = 0$, and $\Delta i_{V, \text{tot}}$ is the enthalpy difference between points \hat{E} and E . Accordingly, $(\hat{x}_{\infty E} - x_{\infty E}) : 1 = \Delta i_{V, \text{tot}} : L$, and Eq. (3) reads

$$\frac{v_{\infty E}}{v_E} = 1 + \frac{\Delta i_{V, \text{tot}}}{x_{\infty E} \cdot L} \quad (4)$$

The difference between $\hat{v}_{\infty E}$ and \hat{v}_E can, for its part, be calculated from the prevailing supercooling ΔT_E with the aid of Eq. 2.3(21):

$$\frac{v_E}{v_{\infty E}} = 1 - \left(\frac{1}{T_E} - \frac{c_p}{L} \right)_E \cdot \Delta T_E \quad (5)$$

If we substitute Eqs. (4) and (5) in Eq. (2), transpose, and drop products of two or more small quantities, we finally obtain the formula

$$\Delta i_{\text{Aus}} \approx - \frac{c_{aE}^2}{2} \left[(v_{\text{gg}} - v_h)_E - \frac{2 \Delta i_{V, \text{tot}}}{x_{\infty E} \cdot L} + 2 \left(\frac{1}{T_E} - \frac{c_p}{L} \right)_E \cdot \Delta T_E \right], \quad (6)$$

from which we can calculate the change in the exit loss. The material quantities can be read from Diagram I (see Appendix).

If, for example, $c_{aE} = 330$ m/sec, $(y_{\text{gg}} + y_h)_E = 0.020$ kg/kg, $\Delta i_{V, \text{tot}} = 20$ kJ/kg, $x_{\infty E} = 0.87$ kg/kg, $\Delta T_E = 20^\circ\text{C}$ and $p_E = 0.035$ bar, we get

$$\Delta i_{\text{Aus}} \approx -54,5 \cdot 10^3 [0,020 - 0,019 + 0,103] = -5,67 \cdot 10^3 \text{ J/kg.}$$

Δi_{Aus} is also negative, or, in other words, part of the moisture loss $\Delta i_{\text{V,tot}}$ is regained through the change in exit loss! How much is regained depends primarily on the magnitude of ΔT_E , the supercooling at the end of the turbine. In the example given above, Δi_{Aus} represents 29% of $\Delta i_{\text{V,tot}}$; if, however, ΔT_E had been only 1°C , we should have regained only 1.5% of the moisture losses.

3.7. CALCULATION OF MOISTURE LOSSES AND INFERENCES

Under Heading 3.2 to 3.6, we have presented formulas that indicate the magnitudes of moisture losses of various origins. Now these can be used to calculate the total moisture loss in a stage and, from this, the efficiency deterioration of the entire turbine. Under Heading a) below, we shall present a brief treatment of the calculating procedure, while Section b) will present and discuss the results for the examples handled under Heading 2.9.

a) Summary of the Calculating Procedure

The total moisture loss in a stage, Δq , is composed of

$$\Delta q = \Delta q_{\text{Brems}} + \Delta q_{\text{Schlp}} + \Delta q_{\text{Sprnt}} + \Delta q_{\text{Unlk}} + \Delta q_{\text{Sonsl}} \quad (1)$$

[braking- entrainment, spontaneous, supercooling miscellaneous]
where the individual terms can be calculated from Eqs. 3.2(10), 3.3(28), 3.4(2), 3.4(5) and 3.5(11), respectively. The third term has a nonzero value only in that stage in which spontaneous fogging occurs. Apart from the design specifications of the turbine (velocities, material quantities, etc.), calculation of the individual part-losses will naturally require the data to be determined on the basis of Section 2.9a (for example, quantities of water in the individual phenomenal forms, undercooling, drop sizes, etc.). With the aid of the Δq obtained from Eq. (1), we can then determine the Baumann factor or the moisture-loss number of the stage in question from Eq. 3.1(11) or (12).

We take the following approach to the determination of the moisture losses in the over-all turbine. After we have determined Δq for each wet-steam stage, we use Eq. 3.1(8) to calculate the individual Δi_V , i.e., that part of the stage loss that can no longer be recovered during the subsequent expansion ("reduced stage-loss"). If we sum these Δi_V for all stages and add to them the $\Delta i_{Untk}^{Stutzen}$ [Stutzen = manifold] obtained from Eq. 3.4(9), we obtain $\Delta i_{V,tot}$ - compare Eq. 3.1(9) -, which indicates the increase in static enthalpy due to the moisture loss at the exit from the last rotor. Thereupon, we can determine the (usually negative) change in the exit loss, Δi_{Aus} , from Eq. 3.6(6). The sum $\Delta i_{V,tot} + \Delta i_{Aus}$ signifies the total reduction of the total-enthalpy drop in the turbine due to the moisture losses, i.e., plainly the over-all moisture loss. Thereafter, we use Eq. 3.1(4) to determine α_{Bm} , the Baumann factor for the entire turbine, which provides an over-all judgment as to the losses and thus permits comparison with the empirical observations. Thus the loss calculation is complete.

The losses can be calculated rather rapidly once the data obtained from Section 2.9 are at hand. The formulas for the losses are generally very simple; only for the entrainment losses is a preparatory calculation necessary (for determination of g_p , which differs for different stages and fog-droplet sizes, and that of c_g , which has a different value in each stage). Even if a second fogging takes place, Δq_{Spont} also has a value other than zero in a second stage. The losses due to the second generation of fog droplets ("nn") can be treated with the same formulas as those resulting from "n."

b) Examples

Tables 3.7.1 to 6 summarize the moisture losses obtained for the examples investigated in Section 2.9. The numerical values have been

graphed for the **reaction-type** turbine in Fig. 1 and for the **impulse-type** turbine in Fig. 2.

Let us first discuss the **reaction-type turbine**. We remind the reader that "Üb 1" represents that extreme case in which fine fog droplets form in the entire flow cross section on spontaneous condensation. (It was shown in Section 2.9 that this results in a **small remanent supercooling** on the one hand and, on the other, causes most of the water to remain in the fog-droplet form.) The other two cases "Üb 2" and "Üb 3," on the other hand, presuppose that the fog droplets are coarse and differ from one another only in the quality of the **drainage** devices. (In "Üb 2" no water at all is removed, and even y_h remains in the flow channel; in "Üb 3" all water that has gotten onto the buckets is removed.) In both of these cases, we established a large **remanent supercooling**, and it was found that a relatively large amount of water goes over into the large-drop form.

Let us regard Fig. 1. Instead of the axial widths of the stages, the axis of abscissas carries the corresponding $(i_0 - i_2)$, the stage **heat drop** calculated for the homogeneous ideal case, since this permits a similar but more rational representation of the results. The moisture losses have been drawn as areas above these stage gradients, and the contribution of the individual partial losses indicated by shading. The height of the loss rectangle has the significance $\zeta/\eta_{su, tr}$, and is therefore equal to the moisture-loss number ζ divided by the isentropic efficiency at the circumference for the stage in question without taking moisture losses into account (dry). For this latter, we have, in approximation, assumed the value 0.88 in our calculations (Section 2.1).

As for the extent of the moisture losses, we are struck primarily by the fact that they differ very sharply among the three cases. Nevertheless, certain fundamental similarities can be discerned: in the

first stage, there is no moisture loss (since, after all, no water is present); approximately equal thermodynamic losses occur in the second stage in all cases (as a result of passage beyond the Wilson point); from the third stage on, the losses increase rapidly from stage to stage, an observation to be attributed on the one hand to the increase in remanent supercooling and, on the other, to the (almost exponential) increase in the amount of coarse-form water. — In the case of "Üb 1," the remanent supercooling is much smaller than in "Üb 2" or "Üb 3," as is clearly manifested in the magnitude of the stage-3 thermodynamic losses; even the deposition of fog droplets on the blades remains within modest limits in the case of "Üb 1": this is why the braking- and entrainment-losses are so small. On the other hand, the relatively small supercooling at the exit results in an insignificant saving as regards exit losses. — In case "Üb 3," the coarse-form water is removed from the flow channel this results in a sharp drop in the braking- and entrainment-losses as compared to case "Üb 2," but, on the other hand, in an — admittedly small — increase in the "miscellaneous losses" as a result of the enhanced centrifugation. In both cases, we have much larger thermodynamic and fluid-dynamic losses from stage 3 on than in case "Üb 1."

For the first three cases, we obtain the values 0.31, 0.91 and 0.57 for the over-all Baumann factor of the turbine. In order to arrive at the actual conditions in turbines from these values, obtained as they have been under extreme assumptions, we must first remember that in practice, drainage will neither be zero, as was assumed in the case "Üb 2," nor as perfect as was supposed for "Üb 3." Reality will be more likely to lie somewhere in between, so that we may take in approximation $\alpha_{Bm} = (0.91 + 0.57)/2 = 0.74$ as a guideline value for the extreme case with coarse-drop fog. Thus we come to the conclusion that

α_{Bm} will have a value between 0.31 and 0.74 in our reaction-type turbine, depending on how fine or how coarse the fog droplets generated are. Since the size of the fog droplets may be changed very sharply on a change in the flow history in the turbine, we must expect wide scattering of the wetness losses for various operational states.

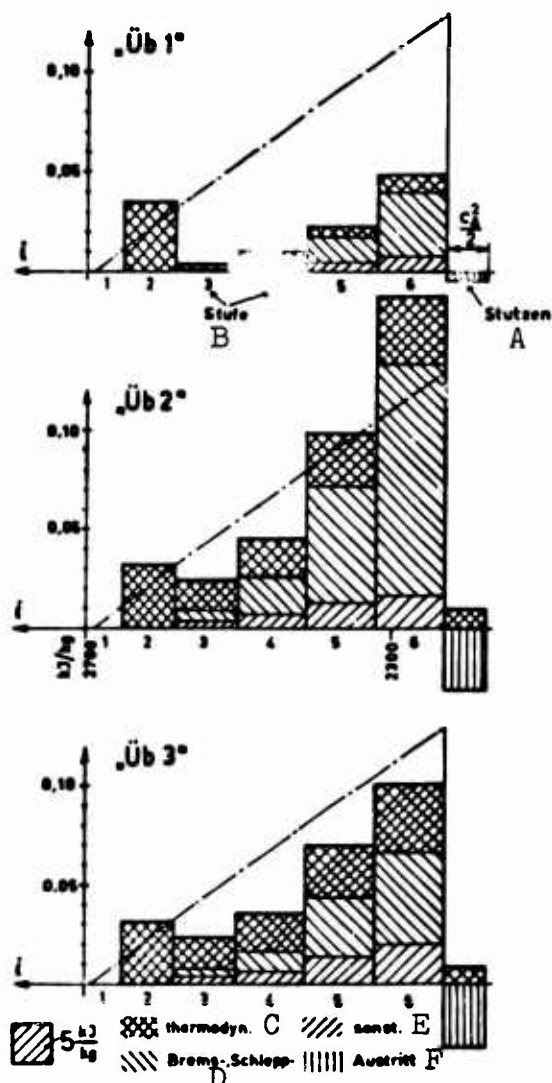


Fig. 3.7.1. Distribution of moisture losses among the stages in the reaction-type turbine; loss = area. --- according to Baumann's rule, with $\alpha_{Bm,St} = \text{const} = 1.0$. A) manifold; B) stage; C) thermodynamic; D) braking- and entrainment; E) miscellaneous; F) exit. $\ddot{u}_b = \text{reaction-type}$.

In operational turbines, the state history of the steam at the rotor is not the same as at the blade tips; thus the fog formed will not be

uniform over the entire flow cross section: in the vicinity of the rotor, for example, it will have coarser droplets, while near the casing the droplets will be finer or vice versa, and a continuous transition will occur between the two extremes. Thus, the extreme cases do not appear at all in their pure forms, and the range of variation of α_{BM}

TABLE 3.7.1

Moisture Losses in Reaction-Type Turbine in Case "Ub 1"

A Stufe	1	2	3	4	5	6
$\Delta q_{Brems,n}^B$ J/kg	-	-	18	60	206	378
$\Delta q_{Brems,g}$ "	-	5	9	34	112	252
$\Delta q_{Brems,gg}$ "	-	-	6	17	65	230
$\Delta q_{Brems,h}$ "	-	-	18	39	116	386
Δq_{Brems} kJ/kg	-	0,01	0,05	0,15	0,50	1,25
$\Delta q_{Schlp,n}^C$ J/kg	-	-	15	52	253	632
$\Delta q_{Schlp,gr}$ "	-	12	40	117	366	967
Δq_{Schlp} kJ/kg	-	0,01	0,06	0,17	0,62	1,60
Δq_{Spont}^D "	-	2,46	-	-	-	-
Δq_{Unlk}^E "	-	-	0,21	0,30	0,43	0,76
Δq_{Zlg}^F J/kg	-	4	5	22	111	263
Δq_{GB}^G "	-	-	-	270	260	260
Δq_{Auslg}^H "	-	-	3	12	63	156
Δq_{SOnst}^I kJ/kg	-	0,00	0,01	0,30	0,43	0,68
Δq "	0	2,46	0,33	0,92	1,98	4,29
$\alpha_{Bm,Et}$ -	0	1,58	0,09	0,15	0,24	0,41
Δi_V kJ/kg	0	2,15	0,29	0,86	1,91	4,29
$\Sigma \Delta i_V J = 9,50 \text{ kJ/kg}$ $\Delta i_{Unlk}^{Stutzen E} = 0,04 \text{ "}$ $\Delta i_{V,tot} = 9,54 \text{ "}$ $\Delta i_{Aus}^K = -1,19 \text{ "}$ $(\Delta i_{V,tot} + \Delta i_{Aus}) = 8,35 \text{ "}$						
$\alpha_{Bm} = 0,31$						

A) Stage; B) braking; C) entrainment; D) spontaneous; E) supercooling; F) centrifugation; G) boundary-layer; H) capture; I) miscellaneous; J) manifold; K) exit.

is to some degree restricted. If we bear this in mind, we can make the following summarizing statement: on the basis of our calculations, we may conclude for the reaction-type turbine used as an example that α_{BM} will have a value between 0.4 and 0.65, depending on the operating regime.

TABLE 3.7.2.

Moisture-Losses in the Reaction Type Turbine in Case "Ub 2"

A Stufe	1	2	3	4	5	6
$\Delta q_{Brems, n}^B$ J/kg	-	31	111	319	779	834
$\Delta q_{Brems, g}^B$ "	-	5	62	209	513	786
$\Delta q_{Brems, gg}^B$ "	-	-	5	75	358	1106
$\Delta q_{Brems, h}^B$ "	-	-	33	155	563	1595
Δq_{Brems}^B kJ/kg	-	0,04	0,21	0,76	2,21	4,32
$\Delta q_{Schlp, n}^C$ J/kg	-	3	103	333	1250	2324
$\Delta q_{Schlp, gr}^C$ "	-	17	106	538	1670	3623
Δq_{Schlp}^C kJ/kg	-	0,02	0,21	0,87	2,92	5,95
Δq_{Spont}^D "	-	1,81	-	-	-	-
Δq_{Unk}^E "	-	0,42	1,32	1,76	2,31	3,02
Δq_{Zig}^F J/kg	-	7	33	118	420	581
Δq_{CG}^G "	-	-	250	500	500	500
Δq_{Aufg}^H "	-	2	14	69	253	394
Δq_{Const}^I kJ/kg	-	0,01	0,30	0,69	1,17	1,48
Δq "	0	2,30	2,04	4,08	8,61	14,77
$\alpha_{Bm, St}$ -	0	1,46	0,56	0,65	1,05	1,42
Δi_V kJ/kg	0	1,99	1,83	3,79	8,29	14,77
$\Sigma \Delta i_V$ J = 30,67 kJ/kg $\Delta i_{Unk}^{Stutzen E}$ = 2,46 " $\Delta i_{V, tot}$ = 33,13 " Δi_{Aus}^K = -8,28 " $(\Delta i_{V, tot} + \Delta i_{Aus})$ = 24,85 "						

$$\alpha_{Bm} = 0,91$$

A) Stage; B) braking; C) entrainment; D) spontaneous; E) supercooling; F) centrifugation; G) boundary-layer; H) capture; I) miscellaneous; J) manifold; K) exit.

Although these numerical values apply only for these particular turbines, it is easy to judge the consequences that would have resulted from a somewhat different turbine design. If, for example, the turbine had effected the same expansion with a larger number of stages, more fog droplets would have been caught on the blades; in the last stages,

TABLE 3.7.3
Moisture Losses in Reaction-Type Turbine in Case "Up 3"

A Stufe	1	2	3	4	5	6
$\Delta q_{\text{Brems},n}^B$ J/kg	-	31	111	319	783	845
$\Delta q_{\text{Brems},g}^B$ "	-	5	62	206	514	792
$\Delta q_{\text{Brems},gg}^B$ "	-	-	-	-	-	-
$\Delta q_{\text{Brems},h}^B$ "	-	-	-	-	-	-
$\Delta q_{\text{Brems}}^B$ kJ/kg	-	0,04	0,17	0,53	1,30	1,64
$\Delta q_{\text{Schlp},n}^C$ J/kg	-	3	103	333	1250	2360
$\Delta q_{\text{Schlp},gr}^C$ "	-	2	21	45	81	50
$\Delta q_{\text{Schlp}}^C$ kJ/kg	-	0,01	0,12	0,38	1,33	2,41
$\Delta q_{\text{Spont}}^D$ "	-	1,81	-	-	-	-
Δq_{Unth}^E "	-	0,42	1,32	1,76	2,30	3,04
Δq_{Zig}^F J/kg	-	8	52	195	696	1140
Δq_{GG}^G "	-	-	250	300	300	300
Δq_{Aufg}^H "	-	2	14	69	254	399
$\Delta q_{\text{Sonst}}^I$ kJ/kg	-	0,01	0,32	0,56	1,25	1,84
Δq "	0	2,29	1,93	3,23	6,18	8,93
$\alpha_{\text{Bm},st}$ -	0	1,45	0,53	0,52	0,75	0,86
Δi_v kJ/kg	0	1,98	1,74	3,00	5,95	8,93
$\Sigma \Delta i_v^J = 21,60 \text{ kJ/kg}$ $\Delta i_{\text{Unth}}^E = 2,33 \text{ "}$ $\Delta i_{v,tot} = 23,93 \text{ "}$ $\Delta i_{\text{Aus}}^K = -8,49 \text{ "}$ $(\Delta i_{v,tot} + \Delta i_{\text{Aus}}) = 15,44 \text{ "}$						
$\alpha_{\text{Bm}} = 0,57$						

A) Stage; B) braking; C) entrainment; D) spontaneous; E) supercooling; F) centrifugation; G) boundary-layer; H) capture; I) miscellaneous; J) manifold; K) exit.

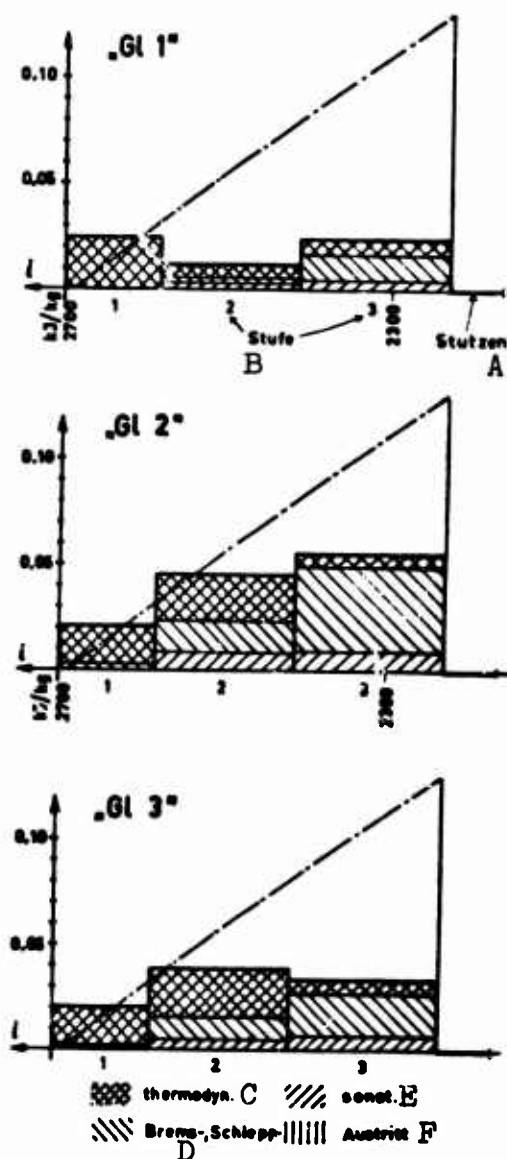
therefore, we should have had more water in the coarse phenomenal forms. This would have resulted in an increase in the moisture losses, since the same quantity of water does more damage when it forms large drops than when it remains in fog-droplet form. - As another example, let us conceive of an expansion line that does not penetrate as deep into the wet-steam region, e.g., by dropping the last stage of our turbine. The α_{BM} obtained for the shortened turbine would certainly be smaller than that of the original turbine, since the last stage is burdened with a disproportionately large wetness loss. At any rate, α_{BM} cannot be reduced indefinitely in this manner, since if the expansion line is made too short, the thermodynamic loss taking place on fogging would become a major load for the entire turbine.

Next in order, let us now take our impulse-type turbine, cf. Tables 4 to 5 and, first and foremost, Figure 2 (which has the same structure as Figure 1).

In case "G1 1" (very fine fog), we have a large thermodynamic loss in the first stage, since fogging takes place here (and at a high peak value of supercooling, $\Delta T^* = 330^\circ$)⁵⁵). In stages 2 and 3, the losses are relatively small, particularly when we remember that a rather large quantity of water is already present here. The increase in the losses from the second to the third stage is to be attributed to the increase in the braking and entrainment losses, as with the reaction-type turbine (increasing mass in coarse drops). - Another spontaneous condensation occurs in the second stage in cases "G1 - 2" and "G1 - 3", and is manifested in the form of large thermodynamic losses. Only in the last stage is the thermodynamic loss lower, because here the second-generation, fine-droplet fog component

secures a small undercooling. The braking and entrainment losses are about twice as large in case "G1 2" as in "G1 3", but in both cases they are

Figure 3.7.2. Distribution of moisture-losses among stages in impulse-type turbine (for legend see Fig. 3.7.1). A) manifold; B) stage; C) thermodynamic; D) braking and entrainment; E) miscellaneous; F) Exit; G1 = impulse type.



considerably larger than in "G1 1", and rise sharply toward the end of the turbine. The large thermodynamic loss in the second stage is to be held responsible for the largest loss occurring in this stage in case "G1 3." Since the supercooling at the exit is very small in all three cases, no loss reduction is achieved in the nozzle.

For the Baumann factor of the entire turbine, we find the values 0.33, 0.72, and 0.53, respectively. Since in practical cases the quality of drainage will probably lie about midway between the two extreme cases in an impulse-type turbine as well, we can assume the tentative value $\alpha_{BM} = 0.72 + 0.53/2 = 0.63$ for the case with coarse droplet fog. - As concerns those cases which were not investigated here and represent a transition between the cases with extremely fine and extremely coarse fog droplets, it must be noted that many of these intermediate cases are likely to be unfavorable in an impulse-type turbine, since as soon as the fog droplets have become somewhat larger than they are in the fine-drop extreme case, large supercooling peaks arise in the nozzle rings, resulting in major thermodynamic losses. (The fog droplets need not become very large at all even to trigger a second spontaneous condensation.) For this reason, we may conclude for the conditions actually to be expected in the impulse-type turbine that α_{BM} will be between 0.4 and 0.6, depending on operating regime⁵⁶).

Thus we find that the moisture-losses in the two turbines used as examples are of about the same size. This statement can probably be applied to reaction-type turbines and impulse-type turbines quite in general, since in specifying our turbines (Section 2.1), we took pains to bring the differences between the two types of design as strongly as possible into evidence.

Even though no substantial difference has been found between the reaction-type and impulse-type turbines as regards magnitude of the losses, a certain difference between the origins of the losses can nevertheless be discerned. The fluid-dynamic losses (braking, entrainment and "miscellaneous") clearly predominate in the reaction-type turbine, while fluid-dynamic

and thermodynamic losses are approximately in balance in the impulse-type turbine. This is on the one hand related to the large number of large drops in the reaction-type turbine, which tend to increase the braking and entrainment losses, and on the other hand, to the shorter flow time in the impulse-type turbine, which requires a greater supercooling for a given precipitation of water.

TABLE 3.7.4. Moisture Losses in the Impulse-Type Turbine in Case "Gl 1."

A Stufe	1	2	3
$\Delta q_{\text{Brems},a}^B$ J/kg	8	100	256
$\Delta q_{\text{Brems},g}$ "	-	4	40
$\Delta q_{\text{Brems},gg}$ "	-	-	4
$\Delta q_{\text{Brems},h}$ "	-	8	134
Δq_{Brems} kJ/kg	0,01	0,11	0,43
$\Delta q_{\text{Schlp},a}^C$ J/kg	10	129	1008
$\Delta q_{\text{Schlp},gr}$ "	3	104	592
Δq_{Schlp} kJ/kg	0,01	0,23	1,60
$\Delta q_{\text{Spont}}^D$ "	2,95	-	-
Δq_{Unk}^E "	0,00	1,11	1,37
Δq_{Zig}^F J/kg	2	36	201
Δq_{GS}^G "	-	500	500
Δq_{Aus}^H "	1	46	126
$\Delta q_{\text{Sonst}}^I$ kJ/kg	0,00	0,58	0,83
Δq "	2,97	2,03	4,23
$\alpha_{\text{Bm},st}$ -	1,63	0,21	0,23
Δi_V kJ/kg	2,57	1,89	4,23
$\Sigma \Delta i_V^J = 8,69 \text{ kJ/kg}$ $\Delta i_{\text{Stutzen}}^{\text{Unk} E} = 0,00 \text{ "}$ $\Delta i_{V,tot} = 8,69 \text{ "}$ $\Delta i_{\text{Aus} K} = +0,00 \text{ "}$ $(\Delta i_{V,tot} + \Delta i_{\text{Aus}}) = 8,69 \text{ "}$			
$\alpha_{\text{Bm}} = 0,33$			

A) Stage; B) Braking; C) Entrainment; D) Spontaneous; E) Supercooling;
F) Centrifugation; G) Boundary-layer; H) Capture; I) Miscellaneous; J) Manifold;
K) Exit.

TABLE 3.7.5

Moisture- Losses in the impulse-type Tur-
bine in Case "G1 2"

A Stufe	1	2	3
$\Delta q_{\text{Brems},a}^B$ J/kg	98	494	381
$\Delta q_{\text{Brems},am}^B$ "	-	27	79
$\Delta q_{\text{Brems},g}^B$ "	-	85	177
$\Delta q_{\text{Brems},gg}^B$ "	-	-	112
$\Delta q_{\text{Brems},h}^B$ "	-	98	770
Δq_{Brems} kJ/kg	0,10	0,70	1,32
$\Delta q_{\text{Schlp},a}^C$ J/kg	140	1028	2470
$\Delta q_{\text{Schlp},am}^C$ "	-	40	390
$\Delta q_{\text{Schlp},gr}^C$ "	38	819	2585
Δq_{Schlp} kJ/kg	0,18	1,89	5,48
$\Delta q_{\text{Spont}}^D$ "	1,81	3,20	-
Δq_{Umk}^E "	0,38	0,68	1,13
Δq_{Zlg}^F J/kg	20	186	362
Δq_{G}^G "	-	1000	1000
Δq_{Aufg}^H "	15	244	255
$\Delta q_{\text{Schst}}^I$ kJ/kg	0,04	1,43	1,62
Δq "	2,51	7,90	9,72
$\alpha_{\text{Bm},St}$ -	1,29	0,80	0,52
Δi_v kJ/kg	2,17	7,35	9,72
$\Sigma \Delta i_v^J = 19,24 \text{ kJ/kg}$ $\Delta i_{\text{Stutzen}}^J = 0,00 \text{ "}$ $\Delta i_{\text{Umk}}^E = 0,00 \text{ "}$ $\Delta i_{v,tot} = 19,24 \text{ "}$ $\Delta i_{\text{Aus}}^K = -0,00 \text{ "}$ $(\Delta i_{v,tot} + \Delta i_{\text{Aus}}) = 19,24 \text{ "}$			
$\alpha_{\text{Bm}} = 0,72$			

A) Stage; B) braking; C) entrainment; D) spontaneous; E) super-cooling; F) centrifugation; G) boundary-layer; H) capture; I) miscellaneous; J) manifold; K) exit.

out and hence precipitable water calculated in Section 2.9 (see y_h in Figs. 2.9.7 and 11) shows that the wetness losses are far from minimized when the maximum of water can be drained from the turbine. It is though true that the losses can be reduced by efficient drainage for a given fog-droplet size (" \bar{u}_b 3" versus " \bar{u}_b 2," "G1 3" versus "G1 2"),

TABLE 3.7.6

Moisture- Losses in the Impulse-Type
Turbine in Case "Gl 3"

A Stufe	1	2	3
$\Delta q_{\text{Brems, a}}^{\text{B}}$ J/kg	98	494	381
$\Delta q_{\text{Brems, m}}^{\text{B}}$ "	-	27	79
$\Delta q_{\text{Brems, g}}^{\text{B}}$ "	-	85	177
$\Delta q_{\text{Brems, s}}^{\text{B}}$ "	-	-	-
$\Delta q_{\text{Brems, h}}^{\text{B}}$ "	-	-	-
Δq_{Brems} kJ/kg	0,10	0,61	0,64
$\Delta q_{\text{Schlp, a}}^{\text{C}}$ J/kg	140	1028	2470
$\Delta q_{\text{Schlp, m}}^{\text{C}}$ "	-	40	390
$\Delta q_{\text{Schlp, gr}}^{\text{C}}$ "	-	96	44
Δq_{Schlp} kJ/kg	0,14	1,16	2,90
$\Delta q_{\text{Spont}}^{\text{D}}$ "	1,61	3,20	-
$\Delta q_{\text{Unth}}^{\text{E}}$ "	0,38	0,68	1,13
$\Delta q_{\text{ZfG}}^{\text{F}}$ J/kg	20	216	501
$\Delta q_{\text{GB}}^{\text{G}}$ "	-	500	500
$\Delta q_{\text{AufE}}^{\text{H}}$ "	15	244	265
$\Delta q_{\text{sonst}}^{\text{I}}$ kJ/kg	0,04	0,96	1,38
Δq "	2,47	6,61	5,83
$\alpha_{\text{Bm, St}}$ "	1,27	0,67	0,32
Δi_{v} kJ/kg	2,14	6,15	5,83
$\Sigma \Delta i_{\text{v}}^{\text{J}} = 14,22 \text{ kJ/kg}$ $\Delta i_{\text{Unth}}^{\text{Stutzen E}} = 0,00 \text{ "}$ $\Delta i_{\text{v, tot}} = 14,22 \text{ "}$ $\Delta i_{\text{Aus}}^{\text{K}} = -0,04 \text{ "}$ $(\Delta i_{\text{v, tot}} + \Delta i_{\text{Aus}}) = 14,18 \text{ "}$			
$\alpha_{\text{Bm}} = 0,53$			

A) Stage; B) braking C) entrainment; D) spontaneous; E) super-cooling; F) centrifugation; G) boundary-layer; H) capture; I) miscellaneous; J) manifold; K) exit.

but the decisive point for the losses is the size of the fog droplets. To produce the finest possible fog droplets over a broad range of operational regimes - this is the goal that must be aimed at in designing wet-steam turbines. Then it will be possible to withdraw only a relatively small amount of water from the turbine, but this is only a con-

sequence of the fact that only a very small amount of water collects on the blades in the first place, going over as a result into the harmful forms. If it is possible to produce a uniform fine-droplet fogging, it also becomes possible to raise the allowable exit wetness without increasing the erosion danger. A development of wet-steam turbines in this direction would have its prime economic significance if it were made possible as a result to dispense with **re-heating**.

3.8. CONCLUDING REMARKS

a) Design

Having determined, on the basis of the provisional design (Section 2.1), the state curve of the steam (from Section 2.9) and, from Section 3.7, the extent of the moisture losses in the individual stages, we can carry out the final design of a turbine.

In the provisional designs, we always presuppose the "homogeneous ideal case," i.e., that the wet steam behaves in a manner corresponding to thermodynamic equilibrium, that its two phases are inseparable and that, consequently, the losses are exactly as large as though the turbine had superheated steam flowing through it.

Now this design must be corrected to take moisture losses and **supercooling** into account. Here, in addition to the other losses, we also subtract the appropriate moisture loss Δq from the **isentropic** stage heat drop; this changes the expansion line, the velocity triangles, etc. The new expansion line will have approximately the form indicated by the broken lines in Fig. 3.1.1. If we retain the original intermediate pressures, the state points will be shifted in the manner indicated by points Q and \hat{Q} in the intermediate-space control-planes. In calculating the axial flow cross section (i.e., the **bladlengths**), we must take into account that the specific volume (\hat{v}_∞) read at point \hat{Q} from the **i,s**-diagram requires, as a result of **supercooling**, a correction whose

magnitude can be calculated from Eq. 2.3(21).

The only fundamental difficulty in this correction consists in the fact that we do not know in advance what loss and supercooling values to use as a basis: those calculated for fine fogs or for coarse fogs. As long as the statements of the present work can be supported only by purely theoretical considerations, a certain amount of healthy mistrust is in order anyway; for this reason, we shall not wrack our brains excessively, but shall assume values for Δq and ΔT about midway between those of the investigated extreme cases. Two essential aspects will nevertheless be retained: that we are, after all, considering a **supercooling**, and that we do not simply assume the moisture losses to increase in proportion to the average wetness in the stages.

If we had once obtained an experimental confirmation of our theoretical conclusions, it would immediately be appropriate to devote attention to realization of optimum fogging, and then the design would also be directed toward this case: that is to say, smaller wetness losses and smaller **supercooling** would be used.

Once this second design of the turbine had been carried through, it would, in principle, be possible to perform another iteration, re-determining the loss values and the **supercooling** curve and using them as a basis for further correction of the turbine design. However, our loss formulas, etc. are too inexact from the outset to make such an iteration rational.

b) Modeling Laws for the Wet-Steam Turbine

In conclusion, let us seek an answer to the following question: is it possible for wet-steam turbines to draw inferences as to the behavior of the **full-size turbine** from measurements made on a scaled-down model?

Let us consider a model that has been scaled down by a factor of

k from the prototype. By raising the rpm of the model by the factor k , we can achieve velocity triangles identical to those of the prototype, so that the stage heat drop and (apart from a change in the losses) the expansion line also remain unchanged. For our considerations, we wish to separate those factors that occur in all turbines (and not only in wet-steam turbines) from those that originate only from the properties of the wet steam and from the wetness losses, and restrict our train of reasoning to the latter.

First and foremost, we shall expect the model experiments to deliver information on the optimum fluid-dynamic configuration of the turbine and on the efficiency that can be achieved with it.

As regards the configuration of the turbine, we shall be able to draw exact conclusions on the basis of the model only provided that the flow medium behaves in exactly the same manner in the model as in the prototype. However, it can by no means be stated a priori that this will be the case, since — in spite of the equal heat drops and equal pressures — other throughput volumes may occur simply because the supercooling curve is not the same in the model. — As for the second question, that of the efficiency, we must know the differences between the moisture losses, which requires, in addition to the supercooling, the distribution of the water among the individual phenomenal forms as it occurs in the model.

Our daydream represents the case in which neither the supercooling curve nor the water distribution differ between the model and the prototype, so that exactly corresponding throughput volumes and moisture losses will occur everywhere.

Since both the supercooling and the deposition of fog droplets on the buckets are determined primarily by the size of the fog droplets, the key to solution of the problem lies in the answer to the question

as to how the fog-droplet size behaves in the model as compared to that in the prototype. Naturally, the fog-droplet size is not the same in all operating states, but depends, as was shown in Section 2.5e, on the position at which the Wilson point is reached. Thus we must formulate the problem as follows: what is the ratio between the fog-droplet sizes in the model and the prototype in the case in which the Wilson point occurs at positions that are in exact geometric correspondence?

However, this question can be answered very simply on the basis of Fig. 2.5.14. Namely, the pressure at the Wilson point and the corresponding Mach number agree for the model and the prototype (assuming identical operating states); only the expansion rapidity \dot{P}^* is different, being determined for the model (subscript M) by

$$\dot{P}_M^* = k \dot{P}^* \quad (1)$$

since, after all, the same expansion takes place here in a span of time shorter by a factor of k . From Fig. 2.5.14 (at constant pressure and Mach number), we may read the relationship

$$\bar{r}_n^{**} \approx \text{konst} \cdot (\dot{P}^*)^{-0,8} \quad (2)$$

for the range of \dot{P}^* that occurs in turbines (between about 10^2 and $3 \times 10^3 \text{ sec}^{-1}$). We may then write for the average fog-droplet size in the model

$$\bar{r}_{n,M} \approx \frac{\bar{r}_{n,M}^{**}}{\bar{r}_n^{**}} \cdot \bar{r}_n \approx \left(\frac{\dot{P}_M^*}{\dot{P}^*} \right)^{-0,8} \cdot \bar{r}_n \approx k^{-0,8} \cdot \bar{r}_n \quad (3)$$

This gives us the point of departure for the subsequent investigations.

Let us first consider the sense in which ϵ_{n-f} , the proportion of fog droplets that sticks to the buckets in the given ring, changes. It is given by Eq. 2.6(18); here the quantities S/t_{Schfl} and $2R_N/t_{\text{Schfl}}$ remain unchanged and, for the conditions that occur in practice, we may always set for g_H (and similarly for g_N , too) $g_H \approx 1/G_H =$

$= c_a \Delta T_{\text{brems},n} / l_{ax}$. Since, according to Eq. 2.2(35), $\Delta T_{\text{brems},n}$ is proportional to \bar{r}_n^2 at small Knudsen numbers ($Kn \equiv 1/2\bar{r}_n < 0.01$) and proportional to \bar{r}_n for large Knudsen numbers (> 5) — see Eq. 2.2(35) and Fig. 2.2.1 —, we find

$$\epsilon_{n-f,M} \approx \frac{\epsilon_{n,M}}{\epsilon_n} \cdot \epsilon_{n-f} \approx \frac{c_{a,M}}{c_a} \cdot \frac{\Delta T_{\text{brems},n,M}}{\Delta T_{\text{brems},n}} \cdot \frac{l_{ax}}{l_{ax,M}} \cdot \epsilon_{n-f} \approx 1 \cdot k^{-(1,6 \sim 0,8)} \cdot \epsilon_{n-f}$$

i.e.,

$$\epsilon_{n-f,M} \approx k^{-0,6 \sim k^{0,2}} \epsilon_{n-f} \quad (4)$$

Here the first coefficient applies for small and the second for large Kn . Since the fog-droplet precipitation always takes place at very low pressures in a low-pressure turbine, in a region where the Knudsen numbers are rather large even for coarse fog droplets (in any event greater than 0.5), we shall not go too far astray if we figure with the exponent zero, i.e., if we take

$$\epsilon_{n-f,M} \approx \epsilon_{n-f} \quad (5)$$

From this we may conclude for low-pressure turbines that fog-droplet precipitation and, consequently, the distribution of the water among the individual phenomenal forms is approximately the same in the model as in the prototype.

Let us first concern ourselves with the extent of the supercooling ΔT . According to Section 2.6b, the supercooling curve is obtained from the curve of the quantities ΔT_h and b . Due to Eqs. 2.6(43) and (46) and the above, we get

$$\Delta T_{h,M} \approx \left[\frac{\dot{p}_M}{\dot{p}} \left(\frac{\bar{r}_{n,M}^{**}}{\bar{r}_n^{**}} \right)^2 \sim \frac{\dot{p}_M}{\dot{p}} \left(\frac{\bar{r}_{n,M}}{\bar{r}_n} \right) \right] \cdot \Delta T_h,$$

$$b_M \approx \left[\left(\frac{\bar{r}_{n,M}^{**}}{\bar{r}_n^{**}} \right)^2 \sim \left(\frac{\bar{r}_{n,M}}{\bar{r}_n} \right) \right] \cdot b,$$

since the quantities c_a , E_n , y_n^{**} , x_∞ , etc. remain practically unaf-

fect. The first coefficients given apply for small Knudsen numbers and the last ones for large ones. With Eqs. (2) and (3), we obtain

$$\Delta T_{h,M} \approx (k^{-0.6} \sim k^{0.2}) \cdot \Delta T_h \quad (5)$$

and

$$b_M \approx (k^{-1.6} \sim k^{-0.8}) b. \quad (7)$$

The quantity b has the significance of a length characterizing the rapidity with which the fog droplets are in a position to bring about thermal equilibrium in the fog. The ratio $b/\Delta \xi_a$, where $\Delta \xi_a$ is some length dimension, e.g., the axial width of the stage in question, is of importance for the **supercooling** curve. We find for it

$$\left(\frac{b}{\Delta \xi_a} \right)_M \approx (k^{-0.6} \sim k^{0.2}) \cdot \frac{b}{\Delta \xi_a}. \quad (8)$$

At those points in the turbine where the Knudsen number of the fog droplets is approximately the same as the mean free path of the steam molecules, the exponent zero⁵⁷ applies for Formulas (6) and (8), so that we shall have $\Delta T_{h,M} \approx \Delta T_h$ and $(b/\Delta \xi_a)_M \approx b/\Delta \xi_a$. It will be realized on the basis of Eqs. 2.6(45) and (46) that in this case the **supercooling** assumes the same values at corresponding points in the model and the prototype. For Knudsen numbers deviating considerably from unity (> 3 or < 0.3), a marked difference arises between the undercooling curves of the model and the prototype, and not only in the absolute **supercooling** values, but also in the shape of the curves, i.e., in the ratio of the largest to the smallest supercooling in the individual stages. However, these deviations will be substantial only in extreme cases, so that we may regard the formula

$$\Delta T_M \approx (k^{-0.6} \sim k^{0.2}) \cdot \Delta T \quad (9)$$

as a guideline also for the extent of the actual **supercooling**, with

the exponent zero for $Kn \equiv \Gamma/2\bar{r}_n \approx 1$ with -0.6 for very small Kn (< 0.01) and with $+0.2$ for large Kn (> 5).

It should be noted here that the smallest value found to occur for Kn in the turbines for which we have made our calculations was $Kn = 0.16$ (in the case of coarse fog droplets and at a point at which the pressure is relatively high, $p = 0.7$ bar); for this case, we have approximately the relationship $\Delta T_M \approx k^{-0.35} \Delta T$. As the largest value occurring, we found $Kn = 25$ (in the case of very small fog droplets and at a minimum pressure, $p = 0.035$ bar), for which $\Delta T_M \approx k^{0.2} \Delta T$. Thus we find that the extent of the supercooling will not differ too greatly between the model and the prototype, even in extreme cases. (With $k = 3$, the supercooling in the model will always be greater than $2/3$ of the value that it would have in the corresponding case in the prototype even in the case of coarse fog droplets and high pressure, and no more than $5/4$ of that value even in the case of the finest fog droplets and lowest pressures. In a broad region of operating states where fog droplets of average size form, we shall have approximately equal supercooling, i.e., we may expect the flow-through behavior to be simulated with perfect fidelity.)

Finally, as regards the wetness losses in the model, we may state the following. The braking- losses remain approximately the same, since they depend only on the circumferential velocity and the water distribution. For the entrainment losses on the fog drops, we find (in much the same way as for ϵ_{n-f}) the formula

$$\Delta q_{Schlp, n, M} \approx (k^{-0.6} \sim k^{0.2}) \Delta q_{Schlp, n}, \quad (10)$$

where the same remarks apply for the exponent as in the case of Eq. (9). The entrainment losses on the large drops remain roughly the same, since the water distribution is practically the same. Since, as was

shown with Eq. (9), the factor in Eq. (10) never deviates sharply from unity and since, furthermore, $\Delta q_{Schlp,n}$ is usually only half of the total entrainment losses, the entrainment losses will also remain almost equal.

The supercooling-losses are related to the decisive supercooling value, so that, due to Eq. (9), we get

$$\Delta q_{Unlk,M} \approx (k^{-0.6} \sim k^{0.2}) \cdot \Delta q_{Unlk} \quad (11)$$

In the turbine model, therefore, we shall obtain somewhat smaller supercooling losses in the cases in which coarse fog forms and somewhat larger losses when the fog has fine droplets. The loss on spontaneous condensation will be a bit larger in the model, since somewhat higher peak supercoolings ΔT^* are reached as a result of the higher expansion rate. The miscellaneous losses are small and we shall therefore disregard their changes. The exit-loss recovery depends primarily on the supercooling so that we may write

$$\Delta i_{Aus} \approx (k^{-0.6} \sim k^{0.2}) \cdot \Delta i_{Aus} \quad (12)$$

Since Δi_{Aus} is almost always negative, its change will work counter to the change in the other losses.

On the basis of this reasoning, we may state that the total moisture-losses in corresponding stages differ only very slightly. With coarse fog droplets, i.e., in cases where large losses actually occur, the model shows losses that are somewhat on the low side, and, conversely, the model losses are somewhat high in the case of fine fog droplets. The result of this is that the model only gives somewhat narrower scattering of the α_{Bm} values than the prototype. The average value of α_{Bm} , however, remains about the same, since the moisture losses are transferable for average-sized fog droplets ($Kn \approx 1$).

In summary, we can state that model experiments on low-pressure

wet-steam turbines are quite feasible, due to a fortunate interplay between the factors that affect the behavior of the fog. The water distribution, the volume flow rate, and the moisture losses deviate only slightly from those in the prototype. The agreement between model and prototype is particularly good in those cases in which the Knudsen number is approximately unity for the fog droplets, especially in the last stages of the turbine.

(Footnotes to Part Three)

No.

- 50 It is referred to frequently as "Baumann's coefficient" or "braking-loss coefficient."
- 51 In the specialized literature, they are also frequently known as "direct braking—losses," following Traupel (20), to distinguish them from "indirect braking losses." The latter have been termed "entrainment-losses" in the present work (Section 3.3).
- 52 Due to spacial flow effects, a radial velocity fluctuation also occurs in turbine stages. However, it produces no essential rise in the entrainment losses, since its amplitude is small compared to its period.
- 53 This statement applies for the case $G_T > 2$, which is always satisfied in practical instances. For $G_T > 10$, the loss even increases quadratically with increasing frequency.
- 54 The influence of Mach number can be disregarded at the outset, since here there is generally no longer any fixed boundary on the flow.
- 55 In the light of experiments - cf. Footnote 14 on p. 28 - the value is cited too low.
- 56 Here, of course, the basic question arises as to whether the high Mach numbers commonly encountered with the stators of impulse-type turbines permit the formation of a fine-droplet fog at all. That is to say, between $M = 0.7$ and 1.2 , no condensation shock is possible, at least in a confined, rectilinear flow (compare Section 2.5d), and since the rapid pressure drops are generally paired with high Mach numbers, the suspicion arises that condensation may perhaps not be able to occur at all at really high

expansion rates. Thus the fine fog assumed here would never be formed in impulse-type turbines (even in the second fogging), and a situation might arise in which fresh, coarse fog droplets are formed again and again behind each stator, with the correspondingly high losses.

57

This can be shown on the basis of Fig. 2.2.1.

POSTSCRIPT

To conclude, let us take a critical standpoint with regard to certain aspects of the present theory. The crucial point of our arguments has been the size of the fog droplets; it has been calculated on the basis of spontaneous condensation theory. As regards prediction of the Wilson point, this theory is well substantiated experimentally, but it is not as regards the calculated fog-droplet sizes. If there were also exact experimental confirmation for the latter, we could place a rather high degree of confidence in the subsequent conclusions - water distribution, losses, etc. -, since these are almost without exception based on experimentally verified foundations (for example, the friction and heat-transfer conditions on a sphere, sizes of the slung-off drops, etc.) or in agreement with observations made on operating turbines (erosion and flow tracks, etc.)

In reality, however, we have no reliable experimental clue concerning the size of the fog droplets.⁵⁸ Although measurements of drop size previously carried out by diffraction of light (for example, [19]) have given drop sizes similar to those that we have calculated, this measurement technique was not accurate. Unfortunately also, the conventional trapping methods are no longer useful for very small drops ($< 10^{-6}$ m). Until it is possible to find a measurement technique that permits sufficiently accurate determination of the fog-droplet size, the fog-droplet sizes determined mathematically on the basis of the spontaneous condensation process must be followed by a question mark.

The great unknown in these calculations is the dependence of the

surface tension σ on drop radius. Since no information at all has as yet been acquired on this subject, there appears to be no other approach available than to "calibrate" the nucleation theory on the basis of nozzle experiments, as was done in Section 2.5b. For lack of more suitable measurements, those of Binnie and Woods were used here, although they are not in full agreement, for example, with the measurements of Yellot and Holland. (These latter authors determined the spontaneous condensation at somewhat higher theoretical wetnesses, and the difference cannot be completely explained away solely on the basis of the somewhat higher expansion rate under the latter conditions.) It would therefore be urgently necessary to conduct exact nozzle experiments and devote greater attention to the influence of expansion rate.

If strong influence of the latter on the position of the Wilson line were indicated, one of the most important conclusions of our theory would be confirmed.⁵⁹ Further, such measurements would provide a basis for recalibration of certain formulas, i.e., it would be possible, for example, to find a more suitable surface-tension value. Here, under certain circumstances, a marked shift of the Wilson lines might occur, but the new σ value would affect the size of the fog droplets only slightly. We do not, of course, mean to imply that this would constitute any direct proof of the correctness of this fog-droplet size.

For practical purposes, however, it is not the fog-droplet size itself that is important, but only its consequences for the turbine; these, however, can be investigated directly with an experimental turbine. In addition to the absolute magnitude of the moisture loss, these experiments would also be concerned with its variation on displacement of the state curve. The turbine most suitable for this purpose would be one in which the fogging proceeds under uniform conditions through-

out the entire flow cross section.

[Footnotes to Postscript]

- 58 Since the publishing of the original of this translation, this point has been verified experimentally, see Footnote 14, on p. 28 and Reference [47].
- 59 This confirmation has been brought about by the experiments described in [47].

REFERENCES

1. Baumann, K.: Some Recent Developments in Large Steam Turbine Practice. Engrg. Vol. 111 (1921) page 435.
2. Martin, H.M.: A New Theory of the Steam Turbine. Engrg. Vol. 106 (1918) pages 1, 53, 107, 161, 189, 245.
3. Stodola, A.: Dampf- und Gasturbinen [Steam and Gas Turbines], 5th Ed. Berlin: Springer, 1922.
4. Freudenreich, J.v.: Der schädliche Einfluss der Dampfnässe in Dampfturbinen [Detrimental Effect of Wet Steam in Steam Turbines]. Brown Boveri Mitt [Brown-Boveri Bulletin]. Vol. 14 (1927) page 119. (Also in Z. VDI [Journal of the Society of German Engineers], Vol. 71 (1927), page 664.)
5. Zerkowitz, G.: Die Entspannung von Nassdampf in der Dampfturbine [Expansion of Wet Steam in the Steam Turbine]. Arch. f. Wärmewirtschaft und Dampfkesselwesen [Archives for Thermal and Steam-Boiler Engineering] Vol. 10 (1929), page 271.
6. Flügel, G.: Die Dampfturbinen [Steam Turbines]. Leipzig: Joh. Ambr. Barth, 1931.
7. Goodenough, G.A.: Supersaturation and the Flow of Wet Steam. Power Vol. 66 (1927), pages 466, 511.
8. Flatt, F.: Untersuchungen über Wasserausscheidung bei Dampfturbinen [Investigations of Water Precipitation in Steam Turbines]. Escher-Wyss-Mitt. [Escher-Wyss Bulletins] Vol. XII (1939), No. 1-2.
9. Goerke, H.: Neues aus der Dampfturbinenforschung [News from Steam-Turbine Research]. Elektrizitätswirtschaft [The Electric Power

- Industry] Vol. 38 (1939), page 686.
10. Preiskorn, G.: Erosionsschäden an Endstufen von Kondensations-Dampfturbinen und Massnahmen zu ihrer Minderung [Erosion Damage to Terminal Stages of Condensation Steam Turbines and Measures to Reduce it]. Maschinenbautechnik [Machinery Engineering] Vol. 7 (1958), page 593.
 11. Senger, U.: Die Dampfstände in den letzten Stufen von Kondensations-turbinen [Steam Wetness in the Last Stages of Condensation Tur-bines]. Elektrizitätswirtschaft Vol. 38 (1939), page 354.
 12. Downs, J.E. and Cotton, K.C.: Low-Pressure Turbine Testing. Mech. Engrg. Vol. 80/2 (1958), page 63.
 13. Meyler, Seglem and Wagner: A Turbine Testing Facility. Mech. Engrg. Vol. 82 (1960), page 47.
 14. Seippel, C.: Brown Boveri Mitt. Vol. 40 (1953), page 271.
 15. Schaaf, S.A. and Chambre, P.L.: Flow of Rarefied Gases. Section H in Emmons, H.W.: Fundamentals of Gas Dynamics. Princeton: Princ. Univ. Press, 1958.
 16. Schlichting, H.: Boundary Layer Theory. London: Pergamon, 1955.
 17. McAdams, W.H.: Heat Transmission. London: McGraw-Hill, 1954.
 18. Dzung, L.S. and Rohrbach, W.: Enthalpie-Entropie-Diagramme für Wasserdampf und Wasser [Enthalpy-Entropy Diagrams for Wet Steam and Water]. Berlin: Springer, 1955.
 19. Yellot, J.I. and Holland, C.K.: The Condensation of Flowing Steam: Condensation in Diverging Nozzles. Engrg. Vol. 143 (1937), page 703.
 20. Traupel, W.: Thermische Turbomaschinen [Thermal Turbine Machinery], Vol. I, 1st Ed. Berlin: Springer, 1958.
 21. Binnie, A.M. and Woods, M.W.: The Pressure Distribution in a Con-vergent-Divergent Steam Nozzle. Proc. I. Mech. Engrs, London, Vol.

138 (1938) I., page 229.

22. Traupel, W.: Zur Theorie der Nassdampfturbine [Toward a Theory of the Wet-Steam Turbine]. Schweiz. Bauzeitung [Swiss Construction Journal] Vol. 77 (1959), No. 20, page 24.
23. Hömig, H.E.: Physikochemische Grundlagen der Speisewasserchemie [Physicochemical Foundations of Feed-Water Chemistry]. Essen: Vulkan, 1959.
24. Schlichting, H.: Berechnung der reibungslosen inkompressiblen Strömung für ein vorgegebenes ebenes Schaufelgitter [Calculation of Inviscid Incompressible Flow for a Given Plane Row of Blades]. VDI-Forschungsheft [Research Periodical of the Society of German Engineers] 447 (1955).
25. Leist, K.: Beitrag zur Untersuchung von stehenden geraden Turbinengittern mit Hilfe von Druckverteilungsmessungen [Contribution to Research on Straight Stationary Turbine Rows by Means of Pressure-Distribution Measurements]. Cologne: Westdeutscher Verlag [West German Press], 1954.
26. Scholz, N.: Strömungsuntersuchungen an Schaufelgittern [Flow Investigations on Bucket Rows]. VDI-Forschungsheft 442 (1954).
27. Bammert, K.: Der Wärmeübergang bei Umströmung von innengekühlten Ueberdruckschaufeln [Heat Transfer in Flow Past Internally Cooled High-Pressure Buckets]. Forsch. Ing.-Wes. [Research in Engineering] Vol. 18 (1952), page 81.
28. Cohen, C.B. and Reshotko, E.: Similar Solutions for the Compressible Laminar Boundary Layer with Heat Transfer and Pressure Gradient, NACA TN 3325, and: The Compressible Laminar Boundary Layer with Heat Transfer and Arbitrary Pressure Gradient, NACA TN 3326 (1955).
29. Karman, Th.v.: The Analogy between Fluid Friction and Heat Trans-

- fer. Trans. ASME Vol. 61 (1939), page 705.
30. Wegener, P.P.: Water Vapor Condensation Process in Supersonic Nozzles. J. Appl. Phys. Vol. 25 (1954), page 1485.
 31. Stever, H.G. and Rathbun, K.C.: Theoretical and Experimental Investigation of Condensation of Air in Hypersonic Wind Tunnels. NACA TN 2559 (1951).
 32. Frenkel, J.: Kinetic Theory of Liquids. Oxford: Clarendon, 1946.
 33. Oswatitsch, K.: Kondensationserscheinungen in Ueberschalldüsen [Condensation Phenomena in Supersonic Nozzles]. ZAMM [Journal of Applied Mathematics and Mechanics] Vol. 22 (1942), page 1.
 34. Stever, H.G.: Condensation Phenomena in High-Speed Flows. Section F in Emmons, H.W.: Fundamentals of Gas Dynamics. Princeton: Princ. Univ. Press, 1958.
 35. Oswatitsch, K.: Gasdynamik [Gasdynamics]. Vienna: Springer, 1952.
 36. Joos, G.: Lehrbuch der theoretischen Physik [Textbook of Theoretical Physics], 7th Ed. Leipzig: Akad. Verlagsges. [Academic Publishing Company], 1950.
 37. Gruber, J.M. and Hansen, E.F.: Electrostatic Shaft Voltage on Steam-Turbine Rotors. Trans. ASME, Ser. A, Vol. 85 (1959), page 97.
 38. Lenard, P.: Meteorolog. Z. [Journal of Meteorology] (1904), page 249.
 39. Hochschwender, E.: Dissertation, Heidelberg, 1919.
 40. Troesch, H.-A.: Die Zerstäubung von Flüssigkeiten [Atomization of Liquids]. Diss. ETH [Dissertation, Confederation Technical High School], Zürich, 1954.
 41. Wood, B.: Wetness in Steam Cycles. Proc. I. Mech. Engrs., London, Vol. 174 (1960), page 491.
 42. Carslaw, H.S. and Jaeger, J.C.: Conduction of Heat in Solids, 2nd Ed. Oxford: Clarendon, 1959.

43. de Haller, P.: Das Verhalten von Tragflügelgittern in Axialverdichtern und im Windkanal (Behavior of Airfoil Rows in Axial Compressors and in the Wind Tunnel). Brennstoff-Wärme-Kraft (Fuel, Heat and Power) Vol. 5 (1953), page 333.
44. Smith, A. M. O. and Clutter, D. W.: The Smallest Height of Roughness Capable of Affecting Boundary-Layer Transition. J. Aero/Space Sci. Vol. 26 (1959), page 229.
45. Gyarmathy, G.: Eine analytische Berechnungsmethode für spontane Kondensationsvorgänge (An Analytical Method to Calculate Spontaneous Condensation Processes). Part 1 of VDI-Forschungsheft No. 508, 1965.
46. Gyarmathy, G.: Kondensationsstossdiagramme für Wasserdampfströmungen (Condensation-Shock Diagrams for Wet-Steam Flows). Forsch. Ing.-Wes. Vol. 29 (1963), No. 4, pp. 105-114.
47. Gyarmathy, G. and Meyer, H.: Versuche über den Einfluss der Entspannungsgeschwindigkeit auf die Nebelbildung in übersättigtem Wasserdampf (Experimental Investigations on the Influence of the Expansion Rate on the Fog Formation in Supersaturated Steam). Part 2 of VDI-Forschungsheft No. 508 (1965). Short version: Brown Overl Review, Vol. 51 (1964), No. 12, pp. 777-783.

APPENDIX

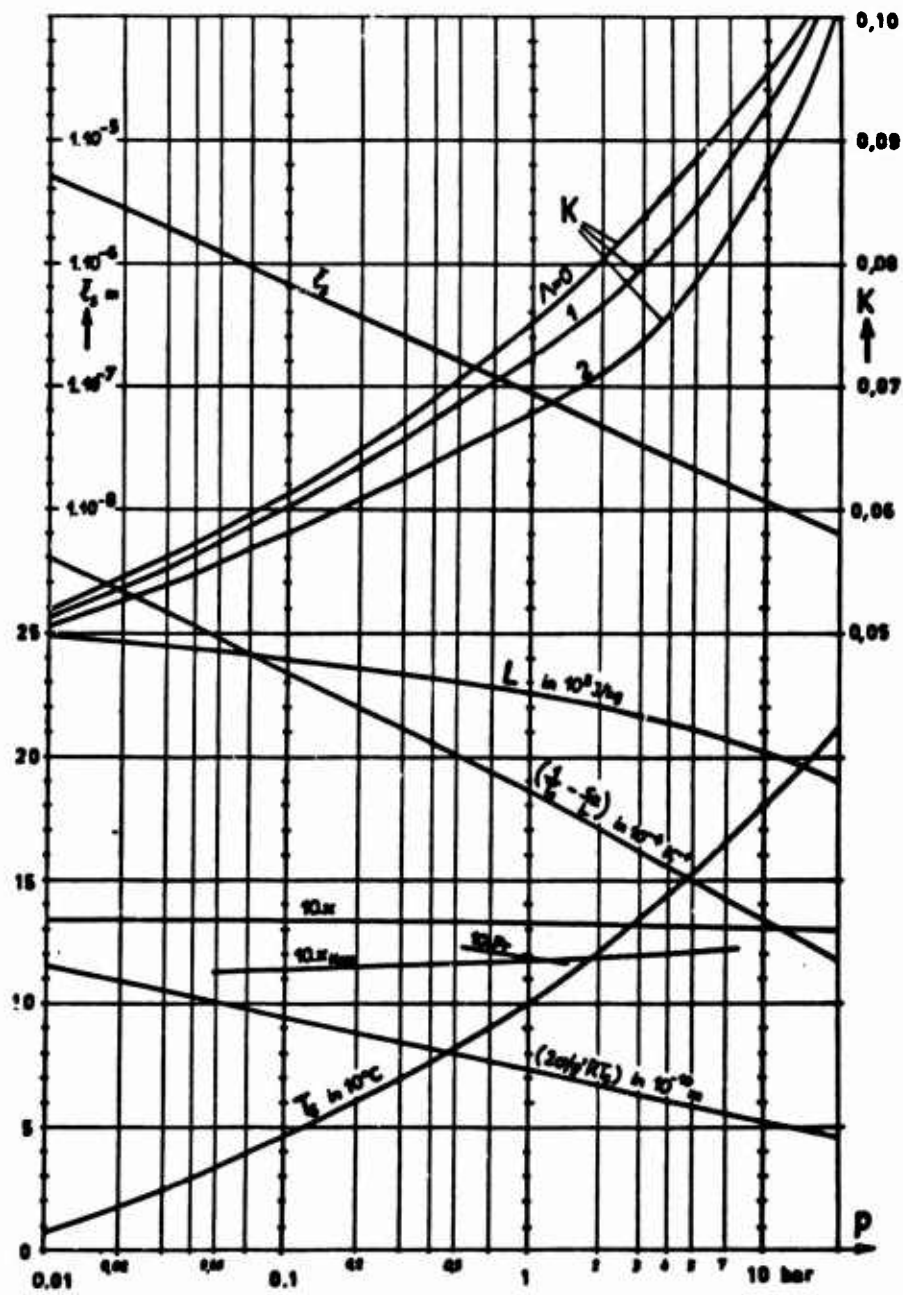


Diagram I. Nass = wet.

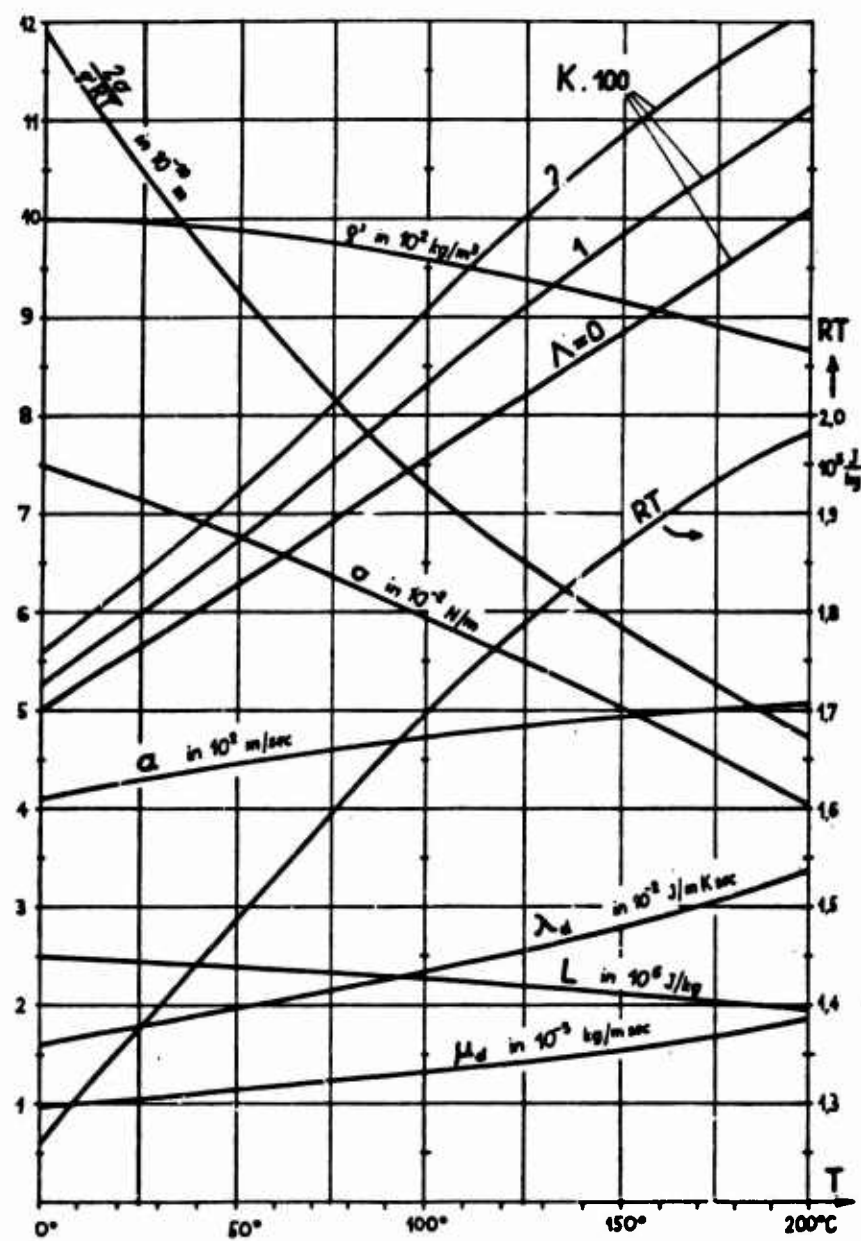


Diagram II

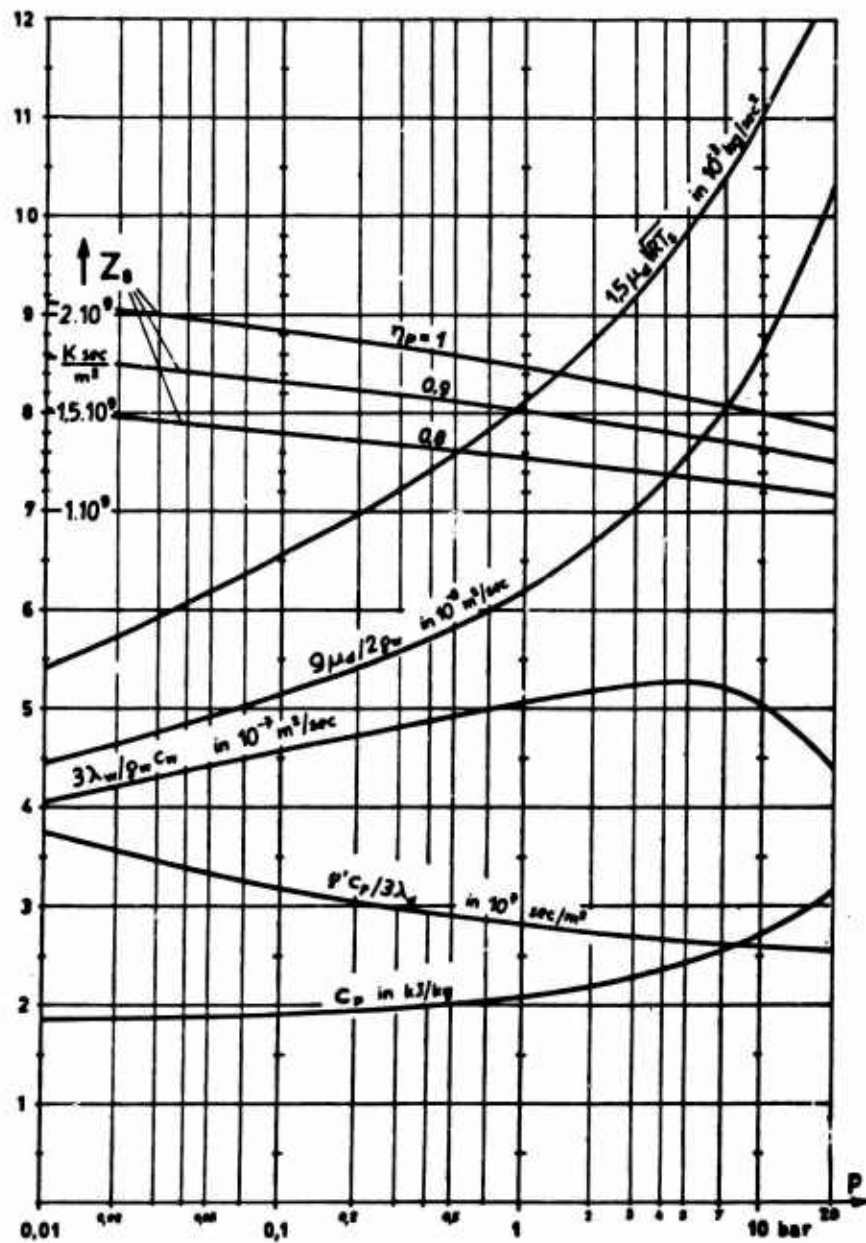


Diagram III

SUMMARY

A satisfactory analysis of the phenomena caused in low-pressure steam turbines by the presence of wetness and by the nonequilibrium behavior of wet steam is possible only if the arbitrary assumptions on droplet size, a common characteristic of most earlier publications on this topic, are replaced by more reliable information. In the present work an attempt is made to derive an initial average droplet size by analyzing the nucleation process, and to use this for a theoretical analysis of the processes the moisture is involved in while passing through the stages of the turbine.

Concerning the onset of moisture formation, there is only an utterly insignificant condensation on the surface of the blades and the walls after passing the saturation line. As a matter of fact, supersaturation increases rapidly and brings about spontaneous nucleation of the steam ("Wilson line"). The exact position of the Wilson line and particularly the size of the "fog" droplets produced depend strongly on the expansion rate that prevails in the region where the nucleation takes place. If the nucleation zone is within a blade row where a considerable expansion takes place, the average fog-droplet diameter is of the order of $2\bar{r}_n^{**} = 5 \cdot 10^{-8} \text{ m} = 0.05 \mu$ (see Fig. 2.5.14); if, however, nucleation happens to take place in a region where the pressure is almost constant, relatively large fog droplets ($2\bar{r}_n^{**} \approx 10^{-6} \text{ m} = 1 \mu$) are produced. A fraction of these fog droplets impinges on and is captured by the blades in the following stages (other types of coagulation turn out to be unimportant), thus giving rise to water films or brook-

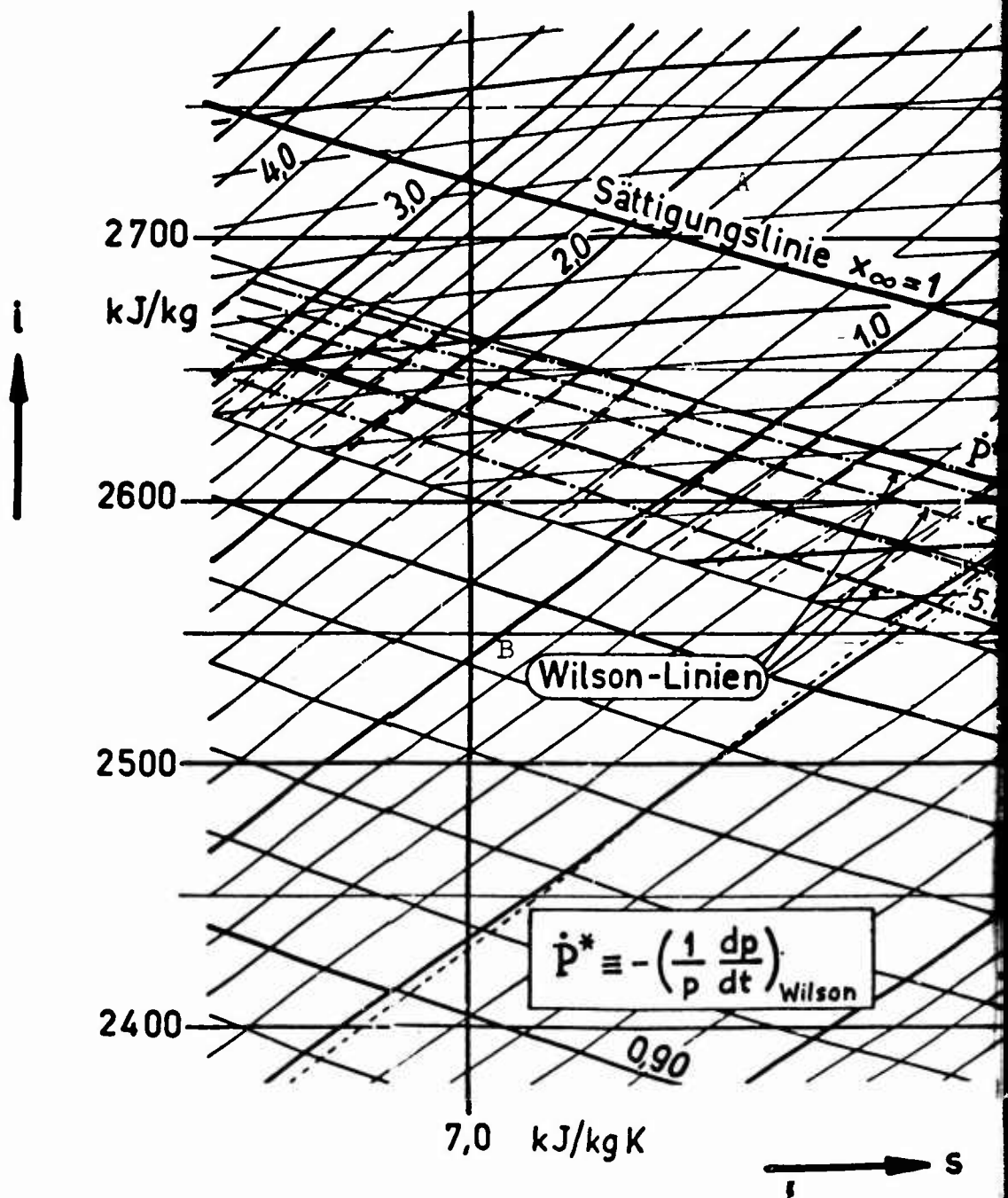
lets which flow toward the trailing edge (on stator blades) or toward the blade tip (on rotor blades) and spray off as relatively large, erosive drops. (Drop sizes of the order of $2r_g = 10^{-4} \text{ m} = 100 \text{ } \mu\text{.}$)

Droplet sizes and the distribution of moisture mass among the various droplet classes along the stages of the turbine have been calculated for several representative examples (Chapter 2.9). Depending on the initial fog-droplet size and the number of stages the fog has to pass through, the mass of water transferred to the "dangerous" (erosive) forms amounts to 5% to 30% of the total wetness present at the end of the turbine. The rest prevails in the form of a finely distributed fog (see y-charts in Figs. 2.9.4, etc.). The amount of undercooling necessary to keep condensation going on at the surface of the droplets is largely dependent on the fog-droplet size (see ΔT -charts in Figs. 2.9.4, etc.).

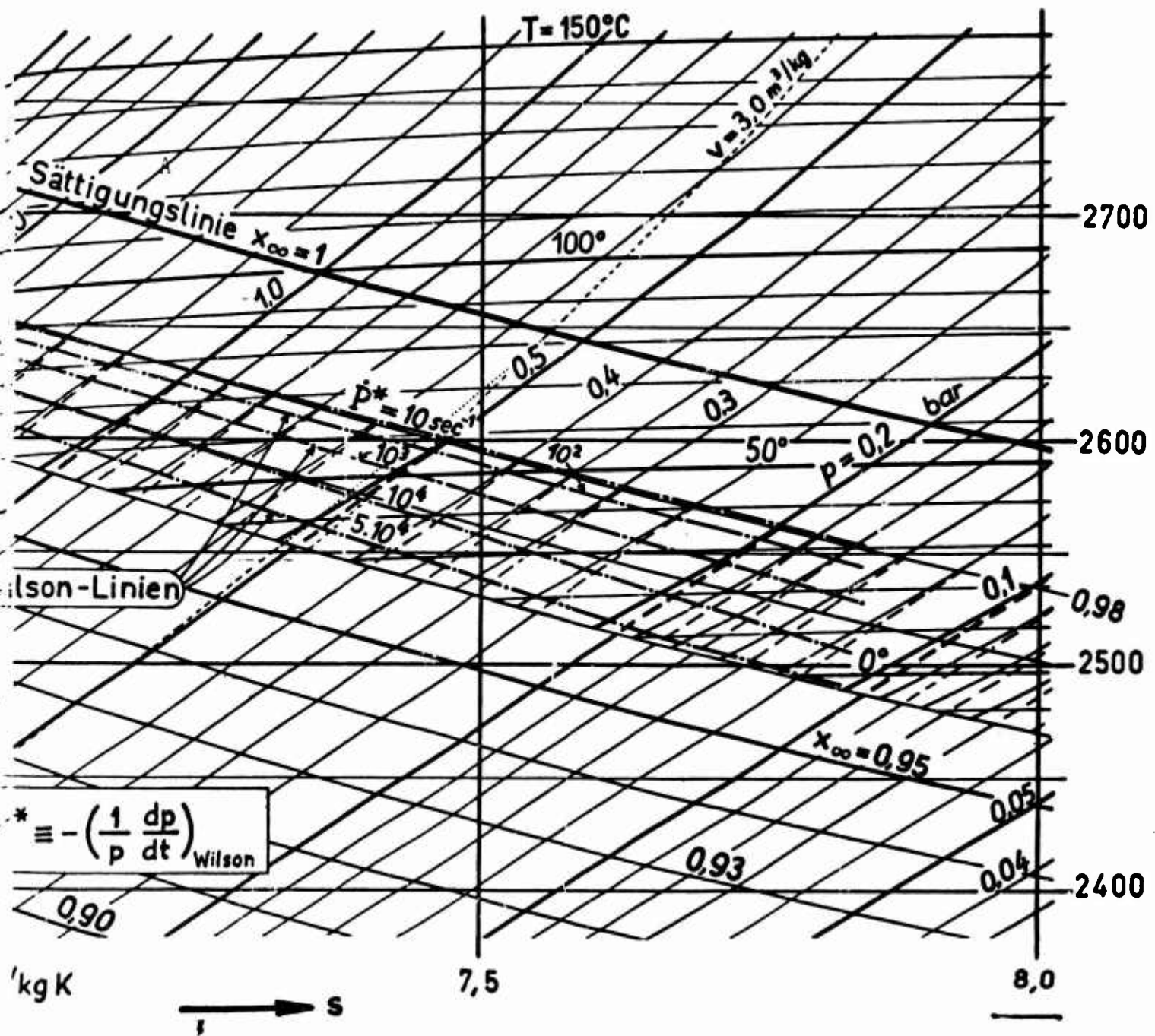
The various efficiency losses resulting from the presence of wetness and from nonequilibrium states of the steam have been calculated. One finds, rather independently of the kind of turbine, a worsening of the total efficiency of the wet stages by 0.3% referred to 1% average wetness for extremely small and by 0.7% for extremely large initial fog-droplet sizes. Meanwhile, the loss in the individual stages is shown to be far from proportional to the average wetness of the stage; see Figs. 3.7.1 and 3.7.2.

On the basis of these results several conclusions of practical interest can be drawn, e.g.: A high degree of drainage indicates that the turbine is running under unfavorable conditions (large fog droplets are being produced). Since only the "dangerous" drops can be removed from the steam, no really high degree of drainage can ever be expected. The most promising way to improve the efficiency and to reduce the danger of erosion consists in assuring a fine fog quality, i.e., in

keeping the nucleation zone within a region where the pressure is sinking rapidly.



i,s -Diagram for water vapor (with supercooling taken into account)
 A) Saturation line; B) Wilson lines.



SUPPLEMENTARY

INFORMATION

TAB No. 70-3

1 February 1970

IDENTIFICATION	FORMER STATEMENT	NEW STATEMENT	AUTHORITY
AD-489 324 Foreign Technology Div., Wright-Patterson AFB, Ohio. Edited Translation. Rept. no. FTD-TT-63- 785 4 Aug 66	No Foreign without approval of Foreign Technology Div., Attn: Translation Div., Wright- Patterson AFB, Ohio.	No limitation	FTD, USAF ltr, 14 Aug 69